APPLICATION OF THE LAPLACE TRANSFORM TO DISCRETE TIME-RATE DATA FOR THE ANALYSIS AND FORECASTING OF WELL PERFORMANCE BEHAVIOR IN UNCONVENTIONAL RESERVOIRS

A Thesis

by

NAT CHINGULPRASAN

Submitted to the Office of Graduate and Professional Studies of
Texas A&M University
in partial fulfillment of the requirements for the degree of

MASTER OF SCIENCE

Chair of Committee,	Thomas A. Blasingame
Committee Members,	Maria A. Barrufet
	Peter Valko
Head of Department,	Jeff Spath

May 2019

Major Subject: Petroleum Engineering

ABSTRACT

The numerical Laplace transformation of discrete data has been discussed extensively in the petroleum literature in applications related to well-test analysis. This approach has been shown to be a useful tool for the deconvolution of variable-rate pressure responses, although the success of this method heavily relies on the algorithms used to transform the discretely sampled data into the Laplace domain and then to invert these results (numerically) back into the time domain (Onur and Reynolds, 1998). Onur and Reynolds [1998] note that the major limitation for the numerical Laplace transformation of discrete data is the need for an "extrapolation" of the data function in the real domain (both for "early" (near zero) times and "late" times (beyond existing data)).

The most important distinction of the present work is that it focuses on rate functions, which are inherently *decreasing* and *positive* functions. The fact that the function of interest is *decreasing* and *positive* is not an issue in terms of the mathematics of this scenario, but there are several challenges — *e.g.*, the applicability of various extrapolation schemes. Simply stated, the primary objective of this research is to examine the application of existing algorithms for discrete-data Laplace Transforms, and to develop an appropriate workflow utilizing the numerical Laplace transform of discrete data for the analysis and forecasting of well performance behavior.

The concept of this research is both simple and straightforward — for a given discrete data set of time and rate values, we use the *Laplace transformation* to generate the following:

- The Laplace transform smoothed rate function: $\hat{q}(t)$
- The Laplace transform smoothed cumulative function: $\hat{Q}(t)$
- The Laplace transform smoothed rate derivative function: $\hat{q}'(t) = \frac{d}{dt}\hat{q}(t)$
- A Laplace transform smoothed *D*-parameter function: $\hat{D}(t) \equiv \frac{-1}{\hat{q}(t)}\frac{d}{dt}\hat{q}(t)$
- A Laplace transform smoothed *b*-parameter function: $\hat{b}(t) \equiv \frac{d}{dt}\left[\frac{1}{\hat{D}(t)}\right]$

The traditional approach to this problem is to use numerical integration (most typically, the Trapezoidal Rule) and numerical differentiation (most typically, the Bourdet (weighted difference) Algorithm). We believe that the Laplace transform has the potential to generate smoother and more mathematically rigorous integration and differentiation. We know that this approach has been used on occasion for such analyses, but neither systematically nor exhaustively as we propose in this work.

ACKNOWLEDGEMENTS

I would like to thank my advisor and the committee chair, Dr. Tom Blasingame, for his tremendous support, understanding, and leadership throughout my time at Texas A&M university. I would not be able to complete this work without his dedicated guidance and advice in both my academic and my personal life. I would also like to thank Dr. Maria Barrufet and Dr. Peter Valko for their time serving as my committee members, for their guidance and support throughout the course of this research.

I would also like to thank my employer and my sponsor, PTT Exploration and Production Public Company Limited (also known as PTTEP).

I also thank my friends and colleagues as well as the department faculty and staff for making my time at Texas A&M University a truly great experience.

Finally, I give thanks to my mother and father for their encouragement and to my girlfriend for her patience and love.

CONTRIBUTORS AND FUNDING SOURCES

This work was supervised by a thesis committee consisting of Dr. Thomas A. Blasingame and Dr. Peter Valko of the Department of Petroleum Engineering and Dr. Maria A. Barrufet of the Departments of Petroleum Engineering and Chemical Engineering.

All work for the thesis was carried out by the student, under the supervision of Dr. Thomas A. Blasingame of the Department of Petroleum Engineering.

Graduate study was sponsored by PTT Exploration and Production Public Company Limited, Bangkok, Thailand (also known as PTTEP).

TABLE OF CONTENTS

LIST OF FIGURES

LIST OF TABLES

1. INTRODUCTION

1.1 Statement of the Problem

In the last decade, unconventional reservoirs — specifically tight and ultra-tight (shale) reservoirs, have emerged as one of most significant petroleum resources in the world. The time-rate relations of the wells producing from these types of reservoirs are characterized by an extended early transient period and a transitional period, rarely (if ever) is there a traditional boundary-dominated flow period. Theoretically, these flow characteristics prevent the use of the conventional Arps hyperbolic time-rate decline model for performance forecasting. We comment "theoretically" because the Arps hyperbolic model is regularly used for forecasting and reserves predictions of cases in unconventional reservoirs — despite its limitations.

Several authors (*e.g.*, Rushing [2007], Lee and Sidle [2010], and Yu [2013]) suggest that the Arps hyperbolic model will highly overestimate the EUR for wells in tight gas sands and shales. To address the "overestimation" issue, several empirical time-rate decline models have been proposed to capture the characteristic time-rate behavior of wells in shale and tight reservoirs. A sampling of the more popular of these time-rate models are:

- Modified Hyperbolic Model (early hyperbolic, late exponential)
- Power-Law Exponential Model (Ilk et al, 2008)
- Logistic Growth Model (Clark, 2011)
- Duong Model (Duong, 2011)

All the models presented above can generally be matched quite well (in general) to time-rate data from wells in unconventional reservoirs — however, these relations yield a high variation in the production forecasts and in the predicted EUR values. In other words, each of these relations can provide a very good, perhaps even excellent, match for a given set of time-rate data, but the subsequent extrapolations are highly variable due to the long-term behavior of a given relation. Ilk et al [2008] introduced a diagnostic plot known as the "*qDb*" plot where the analyst matches not only the rate [$q(t)$], but also the Arps $D(t)$ and $b(t)$ functions — simultaneously. The *qDb* plot aids in flow regime identification (specific features can be observed), as well as in the model selection process (and model parameter identification) *by observing the characteristics which are unique to a given model*.

Relative to this work, the computation of the Arps $D(t)$ and $b(t)$ functions requires numerical differentiation of the discrete time-rate data. Time-rate data typically exhibit random noise and unfortunately, sometimes systematic noise, as well as features due to major changes in production operations. Historically, the petroleum industry has relied on the "weighted difference" derivative algorithm proposed by Bourdet et al [1989]. The "Bourdet" algorithm is used primarily because of its simplicity (and hence, reliability), and it is worth noting that there are many other derivative algorithms that have been used as well (*e.g.*, moving polynomial regressions, spline regressions, collocation formulae, etc.).

When working with data function that contains significant random noise, the resulting derivatives often exhibit oscillations as well as "tail" or "end-point" effects (*i.e.*, erroneous features caused by the first or last point being significantly off-trend). Such features lead to difficulties in interpretations, and in many cases such features can render a given data set uninterpretable.

In this study, our overall goal is to develop a workflow using the Laplace transform of discrete data to improve the analysis of production performance for unconventional wells. One goal is to provide smooth and accurate $q(t)$, $D(t)$, and $b(t)$ functions to enhance the diagnostic analysis of a given set of time-rate data. We refer to the functions derived using our new workflow as the *Laplace transform-smoothed* functions. To produce the Laplace transform smoothed rate function, the principle is as simple as to take the Laplace transform of discrete time-rate data using a piecewise data series, then to numerically invert this series back into the real time domain. For the computation of the Laplace transform smoothed $D(t)$ and $b(t)$ functions, we have adapted the Laplace transform based differentiation algorithm proposed by Onur and Reynolds [1998]. In fact, Onur and Reynolds also proposed an approach that computes the integral function, which is also the basis for computing the Laplace transform smoothed cumulative production function in our work.

The challenge of this work involves taking the Laplace transform of discrete data (*i.e.*, production rate data). Recall that the Laplace transform formula is an integral from $t = 0$ to $t = \infty$, thus the knowledge of the function to be transformed is required across this

interval (*i.e.*, 0 to ∞). As for a discrete data set, interpolation and extrapolation of data are mandatory to obtain a *proper* approximating/represenative function to be transformed into the Laplace domain. Although, there are several existing algorithms for the Laplace transformation of discrete data in petroleum literature, most of these methods were developed for use with well test data (*i.e.*, pressure (drop) and sandface rate data) for well test analysis purposes, these methods might not be applicable for similar applications to production data. For example, the algorithm proposed by Roumboutsos and Stewart [1988] assumes a zero-initial value and a straight-line interpolating function from $t = 0$ to $t = t_1$ as a representative function on the left-hand side of discrete data set. These assumptions are true for the pressure drop function but may not be true for the declining rate function.

Moreover, well test data are typically acquired on a high frequency basis (*e.g.*, minutes and hours), but production data are typically low frequency data (*e.g.*, days or months). As such, we studied the effect of different data frequencies on Laplace transform smoothed functions. In addition, we also consider:

- Data extrapolation techniques for the Laplace transform computation.
- The duration/history of the data (*i.e.*, 3 years, 5 years, and 10 years).
- Magnitude of data noise (*i.e.*, Gaussian noise with 1 and 5 percent standard deviation).
- Type of data function (*i.e.*, increasing and decreasing data functions).

Our expectation is that the proposed Laplace transform smoothing technique must produce results which are at least comparable — and at best, significantly better than the traditional differentiation and integration algorithms applied to this type of problem. To confirm that

expectation we will test the Laplace transform smoothing technique against synthetic data created using the time-rate models previously mentioned (with and without data noise) and actual field production data.

1.2 Objectives

The primary objectives of this work are:

- To *investigate* the characteristic behavior of the Laplace transform of selected time-rate decline models (this is to develop a preliminary understanding of the nature of the "modern" time-rate (decline) curve models used for analysis of data from wells in unconventional reservoirs).
- To *develop* and *validate* a methodology for utilizing the Laplace transform of discrete "time-rate" data sets to generate the smoothed rate, cumulative production, and associated derivative functions.

The **expected deliverables** of this work are:

- A workflow for using the numerical Laplace transformation of discrete "time-rate" data for the following tasks:
  - To provide a visualization of the rate function in the Laplace domain.
  - To generate the smoothed rate, cumulative, and associated derivative functions.
  - To utilize these functions in traditional diagnostic analyses (*e.g.*, the *qDb* plot).
- To provide clear demonstrations and exhaustive validation of the numerical Laplace transformation of discrete "time-rate" data.

1.3 Validation and Application

We validated the workflow using synthetic data sets generated from seven different types of empirical time-rate decline models. Two synthetic data sets for each model were generated — a "perfect data set" (without data noise) and a noisy data set (with Gaussian

noise — 5% standard deviation). We also validated the proposed method using field data from four anonymous wells in unconventional reservoirs using the same methods as for the synthetic data cases.

In each case, we compare the Laplace transform smoothed flowrate, $D(t)$ function, $b(t)$ function, and cumulative production to the model and/or the functions computed from conventional approaches (*i.e.*, the Bourdet differentiation algorithm and the Trapezoidal-rule integration algorithm) to analyze the accuracy and smoothness of the results.

1.4 Summary and Conclusions

We successfully developed a workflow utilizing the numerical Laplace transform of discrete "time-rate" data to produce accurate smoothed rate, rate derivative, $D(t)$ function, $b(t)$ function, and cumulative production functions. The workflow involves a process to select a proper data extrapolation technique for the Laplace transformation process as well as the Stehfest "n" parameter for Laplace inversion. As may be expected, the extrapolation technique and the selection of the Stehfest "n" parameter will be critical factors for this work.

From tests using both synthetic and field data, we have observed that the Laplace transform method can produce more accurate and smoother rate derivative and cumulative production functions as compared to the conventional approaches (*i.e.*, the Bourdet algorithm [1989] and the Trapezoidal based integration algorithm). We also compared the use of rate and reciprocal of rate as the basis-functions to produce the required Laplace transform smoothed functions on a variety of data sets and found that the reciprocal of rate

approach is superior in most cases. As noted above, the critical factors influencing the success of this method are the chosen extrapolation technique and the selection of the Stehfest "*n*" parameter utilized in Laplace inversion process.

2. LITERATURE REVIEW

In this work, we study an application for the Laplace transformation of discrete data to be used for well performance analysis in unconventional reservoirs. We first present an overview of the time-rate decline curve analysis models for both conventional and unconventional reservoirs. The Laplace transformation of discrete data is then introduced as a mean to improve the analysis of unconventional well performance analysis (*i.e.*, improving the computation and resolution of the data functions used on the *qDb* plot). Previous applications of the application of the Laplace transformation to discrete data as well as the algorithms typically used in reservoir engineering applications are summarized and discussed. Lastly, some comments regarding the process of numerical Laplace inversion are provided.

2.1 Time-Rate Decline Curve Analysis

Time-rate data have been used extensively for over a century in the petroleum industry for decline curve analysis as a means of well production performance and reserves. The main assumption for decline curve analysis is that the producing conditions do not change, hence the future behavior of the well will be governed by whatever trend or mathematical relationship is apparent in its past performance. First comprehensive summary of decline curve analysis was given by Arps [1945], but as noted, there were a number of reference articles on extrapolation methods for production rates in the 1910s and 1920s. In the Arps reference [1945], several types of decline curves were discussed and compared, and the well-known "loss-ratio" method was highlighted as a best practice.

The definitions of the loss-ratio and its derivative was first proposed by Johnson and Bollens [1927] as shown in Eqs. 2.1 and 2.2, respectively.

$$\frac{1}{D(t)} \equiv -\frac{q(t)}{dq(t)/dt} \quad \text{.....(2.1)}$$

$$b(t) \equiv \frac{d}{dt}\left[\frac{1}{D(t)}\right] \equiv -\frac{d}{dt}\left[\frac{q(t)}{dq(t)/dt}\right] \quad \text{.....(2.2)}$$

Arps [1945] also suggested the *classification* of decline curves based on their loss-ratio characteristics. A constant loss-ratio yields an exponential decline and a constant derivative of the reciprocal of the loss-ratio (*i.e.*, the *b*-parameter is constant) yields the basic hyperbolic decline relation. Consequently, the *b*-parameter can also be used for categorizing relations — b=0 yields the exponential decline relation and b=1 yields the harmonic type decline relation. Cases where $0 \leq b \leq 1$ are simply labelled as a hyperbolic decline relation.

For conventional reservoirs, petroleum engineers have been using the hyperbolic decline curve model as an essential tool for predicting future well performance and estimating reserves for over 90 years due to its robustness and simplicity. Petroleum engineers often deal with wells producing from various types of reservoirs and production scenarios which yield various declining characteristics. To select an appropriate model, evaluators typically rely on *statistical analyses* to determine the value of *b*-parameter. Despite the simplicity of the method, in many instances, due to poor quality or limited extent of time-

rate data, statistical method can (and often do) lead to non-uniqueness of in the selected *b*-parameter, which results in unreliable forecasts and reserves estimates.

Several authors such as Arps [1945] and Fetkovich [1990, 1996] attempted to determine the distribution of *b*-values for a specific reservoir type to provide guidelines that could yield fast and accurate forecasts. Arps [1945] studied the *b*-value distribution of 149 oil fields and suggested that for 90 percent of the cases, the *b*-parameter is less than 0.5 (*i.e.*, $b < 0.5$). Fetkovich [1990, 1996] suggested using *b*-value less than 0.5 for a single-phase flow in homogeneous reservoir and using a range of $0.5 < b < 1$ for a two-layer gas reservoir with no crossflow.

Fetkovich also mentioned that by using statistical methods, $b > 1$ could be estimated from early-transient production rate data, and it is important to note for conventional reservoirs, this will lead to a significant overestimation of reserves. In fact, Fetkovich specifically mentioned that $b > 1$ cases must be in transient flow, and by implication, we should not be using such relations for extrapolation. However; for tight oil and shale reservoirs (so-called "unconventional" reservoirs), *transient flow behavior will dominate for decades*. The question arises as to how to make production forecasts and estimate reserves in such cases, and the simple answer has been to apply a "terminal decline" to the traditional Arps hyperbolic decline relation. There is nothing inherently wrong with using a terminal decline, actually just the opposite, this must be done — however; a terminal decline is largely empirical, and hence, subjective.

Consequently, several time-rate decline models have been developed in the last 10 or so years to better capture the production behavior of wells in unconventional reservoirs. As noted, the most popular case is the "modified hyperbolic" model (*i.e.*, the original Arps hyperbolic model with an exponential terminal decline).

Returning to the discussion of traditional methods, a direct (graphical) approach to estimate the *b*-parameter was presented by Fetkovich [1980] where he proposed the use of a dimensionless type curve generated using *b*-values from 0 to 1. Matching a field data set onto this type curve would provide the initial rate, the initial decline constant, and the *b*-parameter using the "best-fit" type curve. For conventional reservoirs, this methodology dominated the practice in the 1970s and 1980s, but additional work was required as the methodology was augmented into "rate transient analysis" (*i.e.*, fractured well models, horizontal well models, auxiliary functions, etc.).

For unconventional reservoirs, a different approach should be used to predict well performance. As mentioned earlier, wells in unconventional reservoirs exhibit extended (log-term) transient and transitional periods. As a result, the time-rate data has "non-hyperbolic" behavior (*i.e.*, non-constant *b*-values) which prevents the use of the Arps hyperbolic models.

Rushing [2007] tested the applicability of using Arps hyperbolic decline model with tight gas reservoirs. He generated several time-rate data sets by varying the parameters in the tight-gas reservoir models. Then, for each data set, he applied the Arps hyperbolic model and predicted EURs using various data intervals (*e.g.*, 1, 5, 10, 20, and 50 years). The

EURs were computed using the best fit *b*-value and then were compared to the true EUR obtained from the reservoir model. The study suggests that *b*-values will decrease with time in low/ultra-low permeability reservoirs — in other words, reserves could be (and actually always will be) significantly overestimated using early-time production data. This study emphasizes the non-constant nature of the *b*-value for wells in unconventional reservoirs and that a thorough diagnostic process be used to determine an appropriate model. Lee and Sidle [2010] and Yu [2013] also had similar comments on the issue of using high *b*-values to predict well performance of wells in unconventional reservoirs and that the error of the predicted EURs could be as much as 100 percent.

Ilk [2008] studied the behavior of *b*-values over time [*i.e.*, $b(t)$ behavior] in tight gas sands. The study also suggests a "non-hyperbolic" behavior of these wells and Ilk commented that such behaviors could be derived from various sources — *i.e.*, multilayer effects, extended transient flow behavior, and increasing contacted gas-in-place with time. The diagnostic plot used in the study is the so-called "*qDb*" plot — which is a log-log plot of $q(t)$ on the left axis plotted simultaneously with $D(t)$ and $b(t)$ on the right axis. This "simultaneous" matching of $q(t)$, $D(t)$, and $b(t)$ has an analog the pressure drop and pressure drop derivative plots from pressure transient analysis, and the use of multiple matching functions significantly reduces the non-uniqueness in this diagnostic-based analysis approach.

Using the *qDb* plot, Ilk [2008] developed "rules" — for example; a constant *b*-parameter trend in the plot suggests a constant hyperbolic decline and a (power law) straight-line

declining trend of the $D(t)$ function became the "power-law exponential" (or stretched exponential) type decline. In addition, the *qDb* plot can be used to diagnostically estimate the model parameters for a given model (*e.g.*, the modified-hyperbolic and the power-law/stretched exponential models — and other models to be discussed later). Okouma [2012] showed the application of this plot to determine an appropriate rate-decline relation for a broad selection of wells in unconventional (shale) reservoir systems.

$$\frac{df}{dt} = \frac{(\Delta f_L / \Delta t_L)\Delta t_R + (\Delta f_R / \Delta t_R)\Delta t_L}{\Delta t_R + \Delta t_L} \quad \text{.....(2.3)}$$

Regarding the computation of $D(t)$ and $b(t)$ functions, we use the definitions of the loss-ratio and its derivative in Eqs. 2.1 and 2.2 (respectively), both of which involve the derivative of $q(t)$ function. As mentioned earlier, typically, we use the differentiation algorithm proposed by Bourdet [1989] (Eq. 2.3). The "Bourdet" algorithm is essentially a weighted finite-difference approach. The Bourdet Algorithm does provide a level of smoothness to the computed derivative functions — however, many times the rate data are very noisy such that the results exhibit oscillations. The level of smoothness can be manipulated by adjusting the smoothing parameter "L." However, higher L-values lead to less accurate derivatives and larger end-point effects.

Mattar et al [2008] showed an example that the $b(t)$ function calculation can be severely affected by the Bourdet differentiation algorithm (as could be expected since the $b(t)$ function is the time derivative of the $1/D(t)$ function). Ilk [2008] presented one technique to address (but not resolve) the issue of oscillating $D(t)$ and $b(t)$ functions when they

reformulated these calculations in terms of the rate-cumulative production behavior (as opposed to using the "rate-time" derivative formulations). Collins [2016] showed that the smoothing cubic spline algorithm (proposed by Pollock) provides an alternative approach that produces smooth $D(t)$ and $b(t)$ functions — however; being based on a cubic spline, this method will under-smooth (yielding oscillations) as well as over-smooth (removing small-scale features), depending on the selection of the spline smoothing criteria.

2.2 Numerical Laplace Transform of Discrete Data

As mentioned earlier, we are applying the existing Laplace transform algorithms to discrete time-rate data to generate various smoothed data functions using the Laplace transform smoothing methodology. One goal is to provide an alternative computation method for rate derivative functions in order to produce smooth and accurate $D(t)$ and $b(t)$ functions. We began by studying the literature related to the Laplace transformation of discrete data that will be discussed below.

In reservoir engineering applications, the numerical Laplace transformation of discrete data has historically been used for deconvolution of well-test data, where this approach has been proven useful in the deconvolution of variable-rate pressure responses. Recall that the convolution integral becomes a functional multiplication in the Laplace domain, hence the desire to use the Laplace transform as a deconvolution mechanism. However, the success of the process relies on the algorithms to transform discrete data into the Laplace domain and to invert it back into real time space (Onur and Reynolds [1998]).

In addition to the deconvolution application, the Laplace transform of discrete data can be used to compute accurate and smooth pressure (drop) derivative for well-test analysis as proposed by Onur and Reynolds [1998].

Lastly, the Laplace transform of discrete data have been used to build type curves in the Laplace domain. Bourgeois and Horne [1993] introduced a concept to perform model recognition and reservoir parameter identification in the Laplace domain using a series of Laplace transform type curves. They introduced a new expression in the Laplace domain called the "Laplace pressure." The type curves of the dimensionless Laplace pressure and the reciprocal of the Laplace variable have characteristics similar to the dimensionless pressure type curves in the real time domain — however; the Laplace domain functions tend to be smoother as the integration of data is involved. The "Laplace pressure" can be used in the same manner as the ordinary pressure type curves and can be used to address issues with noisy data (Bourgeois and Horne [1993]). For reference, the "Laplace pressure" function is defined as:

$$s\mathcal{L}\{p(t)\} = s\overline{p}(s) \quad \text{.....} \quad (2.4)$$

Recall that the Laplace transform is an integral defined from 0 to ∞, hence the function being integrated must be known (or represented) at those limits. Thus, to transform a discrete data into the Laplace domain, we require an approximating or a representative function for the data set across the positive semi-infinite interval. Generally, in all three applications mentioned earlier, we are transforming sampled pressure and rate data sets acquired from well testing which are available from t_1 to t_N (where $t_1 > 0$ and $t_N < \infty$).

Thus, to represent this type of data, *interpolation* techniques are used to approximate the function from t_1 to t_N, while *extrapolation* techniques are used to represent the functions from $t = 0$ to t_1 and from t_N to ∞.

Kuchuk and Ayestaran [1985] tried several approximating functions for time-rate data to be used for the deconvolution based on the Laplace transform method (*i.e.*, rational functions, power series, and exponential functions). For pressure transient applications, specifically the analysis of radial flow data affected by wellbore storage effects, Kuchuk and Ayestaran concluded that an exponential function gives the best representation of the time-rate data, which is also in agreement with the work by van Everdingen and Hurst [1953].

Based on some of the work proposed by Kuchuk and Ayestaran [1985], Roumboutsos and Stewart [1988] developed a robust technique using the Laplace transform for the deconvolution in well test analysis. It is worth mentioning that the Roumboutsos and Stewart algorithm has also been used for the estimation of cumulatives and derivatives. They proposed using a piecewise linear data function to approximate the discrete data, as well as linear extrapolation to represent the data function after the sampled data interval. The algorithm assumes a zero-initial value for the function to be transformed, as a result, an extrapolation prior to the sampled data interval is not required in this algorithm. The Roumboutsos and Stewart Laplace transform expression is shown in Eq. 2.5 below.

$$\overline{f}(s) = \frac{1}{s^2}\sum_{i=1}^{N} m_i\left(e^{-st_{i-1}} - e^{-st_i}\right) + \frac{1}{s^2} m_{ext} e^{-st_N} \quad \text{.....(2.5)}$$

It is noted that some symbolic expressions used in the Laplace transform formulations in this thesis report are altered from those in the original equations in literature such that they could be standardized across this document (*e.g.*, in Eq. 2.5, m_{ext} is used instead of $\dot{f}_N$ in the original document). The constant, m_{ext}, shown in the second term on the right-hand side of Eq. 2.5 represents the slope of the extrapolated straight-line on the right end of discrete data set. However; the means to acquire this slope was not specified in the Roumboutsos and Stewart work.

In 1993, Bourgeois and Horne proposed an algorithm to transform pressure (loss) data into the Laplace domain for the purpose of model recognition in the Laplace domain using type curves. For the early-time period (*i.e.*, the time before the pressure measurement), Bourgeois and Horne suggest that the pressure data could be extrapolated linearly if wellbore storage is present. For evaluations required within the measured data, linear interpolation is suggested. Lastly, for the late-time period, Bourgeois and Horne suggest that the extrapolation model should follow the *probable* behavior of data as closely as possible. In case of a closed outer boundary, then linear extrapolation can be used, just as proposed by Roumboutsos and Stewart [1988]. However, in most cases, a semi-log extrapolation is recommended (as an assumption of radial flow would prescribe). A modification of the Roumboutsos and Stewart algorithm by considering this new extrapolation scheme (*i.e.*, semi-log extrapolation for large times) is shown in Eq. 2.6. This relation assumes a stabilized derivative with respect to natural logarithmic of time as

the extrapolating slope of pressure response to infinite time. The constant, m_{ext}, in Eq. 2.6 represents that slope.

$$\overline{f}(s) = \frac{1}{s^2}\sum_{i=1}^{N} m_i(e^{-st_{i-1}} - e^{-st_i}) + \frac{m_{ext}}{s}E_1(st_N) \quad \text{.....(2.6)}$$

For the case of a build-up test, a semi-log extrapolation with respect to Horner time could be used instead (Bourgeois and Horne, 1993). However, it was highlighted that even with a good extrapolation, there is a range for which the calculated Laplace transform is just simply the transform of the extrapolation. The limit where the Laplace transform remains meaningful could be estimated from the rule:

$$s > 1/t_N \quad \text{.....(2.7)}$$

Moreover, Bourgeois and Horne [1993] recommended a method to acquire the semi-log slope when working with field data (where field data always contains data noise). The slope should be computed using an expression which is less sensitive to the last measurement. A centered logarithmic finite-difference (*e.g.*, a modification of the Bourdet algorithm) which computes the slope on the last 0.2 or even 0.4 log-cycle of data was recommended by Bourgeois and Horne [1993]. It is important to note that this approach is recommend for both flowrate and pressure measurements.

Onur and Reynolds [1998] suggests using a log-linear extrapolation instead of a simple Cartesian straight-line trend as suggested by Roumboutsos and Stewart [1988]. For reference, Onur and Reynolds proposed the application of the numerical Laplace

transform for the calculation of pressure drop derivative (and pressure drop integral) functions. As investigated extensively by Onur and Reynolds, the accuracy of the pressure derivative function is highly influenced by the extrapolation strategy used at both ends of data. In addition, the "smoothness" of the derivative is a feature of the Gaver-Stehfest numerical Laplace inversion algorithm used to invert (or recover) the Laplace domain solution back to the real domain (Onur and Reynolds [1998]).

Several algorithms were tested in the Onur and Reynolds study, including various types of interpolation and extrapolation schemes. The interpolation functions tested are: piecewise linear, quadratic, and log-linear functions. The extrapolation functions include linear, semi-log, and log-linear extrapolation functions. In the case of the semi-log and log-linear extrapolations, two separate methods to estimate the extrapolation slopes were tested — numerical differentiation of the Lagrange interpolating polynomial (proposed by Bourgeois and Horne [1993]) and the least squares method (piecewise fitting of a polynomial).

The recommended methodology proposed by Onur and Reynolds [1998] for the pressure derivative calculation using the Laplace transformation is given as follows:

Step 1: The discrete data are approximated by a piecewise linear data function to form a functional representation between the first data point and the last data point. It provides similar accuracy level of the resulted pressure derivative function to a piecewise quadratic method however more simplified. According to the Onur and Reynolds study, the piecewise log-linear interpolation approach gives

highly oscillatory unstable results and is more computational expensive than the others.

Step 2: For the functional representation outside the data interval, log-linear extrapolations on both sides using a least square fitting technique to determine the slopes are recommended. A least squares straight-line fitting of the form $\ln f(t) = \beta \ln t + \ln \alpha$ can be used to determine the constants of the extrapolating functions. The regressed intervals of 0.2 log-cycle after the first data point and 0.7 log-cycle before the last data point are suggested to obtain accurate and representative extrapolations for noisy data. The other extrapolation techniques used in their study show lower accuracy of the derivative functions on the right end.

Step 3: The Laplace transform algorithm using the power-law data functions can be expressed in analytical form as shown in Eq. 2.8.

$$\overline{f}(s) = \frac{\alpha_1}{s^{\upsilon_1}}\gamma(\upsilon_1, st_1) + \frac{1}{s}\left(f_1 e^{-st_1} - f_N e^{-st_N}\right) + \frac{1}{s^2}\sum_{i=2}^{N} m_i (e^{-st_{i-1}} - e^{-st_i}) + \frac{\alpha_{ext}}{s^{\upsilon_{ext}}}[\Gamma(\upsilon_{ext}) - \gamma(\upsilon_{ext}, st_N)] \quad \text{..... (2.8)}$$

Step 4: The pressure derivative can be computed using the property of the Laplace transform of derivative function as shown in Eqs. 2.9 and 2.10. The algorithm in Eq. 2.10 requires more computational time but it is more reliable than Eq. 2.9.

$$\frac{d\Delta p(t)}{d\ln(t)} = t\frac{d\Delta p(t)}{dt} = t\mathcal{L}^{-1}\{\overline{\Delta p}'(s)\} = t\mathcal{L}^{-1}\{s\overline{\Delta p}(s)\} \quad \text{..... (2.9)}$$

$$\frac{d\Delta p(t)}{d\ln(t)} = \mathcal{L}^{-1}\{-\overline{\Delta p}(s) - s\frac{d\overline{\Delta p}(s)}{ds}\} \quad \text{..... (2.10)}$$

It's worth noting that the Laplace transform algorithm presented by Onur and Reynolds was also claimed to work well for generation of integral functions and for convolution/deconvolution purposes (Onur and Reynolds [1998]).

Al-Ajmi [2008] mentioned that there are several techniques suggested by LePage [1961] to numerically transform discrete data into the Laplace domain. Polynomial fits (*e.g.,* spline fittings) and other forms of piecewise functions (*e.g.,* piecewise log-linear, piecewise quadratics) provide a general approach for representing the discrete data such that these data can be transformed through analytical techniques. Al-Ajmi [2008] also noted that insufficient accuracy of extrapolation could lead to errors known as "tail" effects.

Ahmadi [2012] suggest using a piecewise polynomial function called natural cubic spline to represent the discrete data for Laplace transform deconvolution process. In 2017, Ahmadi [2017] proposed a new method using a unit impulse function as the representative function instead. Both representative functions become zero outside the data interval and thus eliminate the requirement for extrapolation of discrete data on both ends.

2.3 Numerical Laplace Inversion

As mentioned earlier, we require a numerical Laplace transform inversion algorithm to obtain smoothed data functions in the real domain, which is the main purpose of our study. In the petroleum literature, several numerical Laplace inversion algorithms have been proposed for convolution/deconvolution and for the computation of the pressure derivative functions. The most popular (and most direct) algorithm is the Stehfest [1970] algorithm.

For reference, Roumboutsos and Stewart [1988] also suggests using the Stehfest numerical Laplace inversion algorithm. However, one limitation of the algorithm is that it requires a strongly continuous base function in the real domain. When dealing with a functions containing discontinuities (*e.g.*, the step rate function), the Durbin and Abate [1984] algorithm was recommended. The Durbin and Abate method is based on Fourier analysis and takes much more computational time than the Stehfest method, and thus, is only used when circumstance require a more robust algorithm (*e.g.*, for data with significant discontinuities).

Similarly, Bourgeois and Horne [1993] also used the Stehfest algorithm to deconvolve pressure data. When their Laplace transform deconvolution algorithm was tested with a field example, values of the Stehfest "*n*" parameter as low as 4 were used (as comment, *n*=4 is a very low value, not associated with highly accurate inversions).

Onur and Reynolds [1998] compared three different numerical inversion algorithms including algorithms by Stehfest, Bellman *et al* [1996], and Crump [1976] to compute smooth pressure derivatives and pressure functions from a noisy pressure data set. The

Gauss-quadrature method for Legendre polynomials is the basis for Bellman method and Fourier series techniques are the basis for the Crump method. According to the Onur and Reynolds' study, among the three algorithms, the Stehfest algorithm provided the smoothest and the most accurate pressure derivative and pressure functions. Thus, two conclusions can be drawn from the Onur and Reynolds' study. First, the Stehfest algorithm should be the preferred method for Laplace transform smoothing efforts. Second, the results of any Laplace transform smoothing methodology will be a function of the numerical inversion process used. While this may seem obvious, we can confirm these observations for our efforts as well.

Al-Ajmi [2008] also commented on the use of the Stehfest algorithm for data smoothing applications and noted that it may cause a loss of accuracy and character if the inverted functions contain step-changes and/or discontinuities. Al-Ajmi noted that Fourier-series based algorithms (*e.g.*, Crump [1976] and Iseger [2006]) provide better accuracy of the inverted functions, especially those with discontinuities. Lastly, Al-Ajmi noted that despite the accuracy of the Iseger algorithm, it yields oscillating results when applied to data set with significant quantities of data noise, and suggested that some form of conditioning or regularization might be required.

3. DEVELOPMENT AND EVALUATION OF THE LAPLACE TRANSFORM METHODOLOGY

The main deliverable of this work is the development of a workflow for using the Laplace transformation of discrete "time-rate" data for the following tasks:

- To generate the smoothed rate, cumulative, and associated derivative functions.
- To utilize these functions in traditional diagnostic analyses (*e.g.*, the *qDb* plot).

This chapter introduces the theoretical foundation of the proposed workflow and summarizes the algorithms required to transform the discrete "time-rate" data into the Laplace domain. The proposed workflow and algorithm then will be examined and evaluated using a synthetic data generated from Arps exponential decline model.

3.1 Laplace Transform Smoothing and Functional Operations

We propose using the *Laplace transformation* to smooth a time-rate data function and to obtain smooth derivatives and cumulative from the "Laplace transform smoothing" methodology. The functions we propose to compute are referenced as follows:

- The Laplace transform smoothed rate function: $\hat{q}(t)$
- The Laplace transform smoothed cumulative function: $\hat{Q}(t)$
- The Laplace transform smoothed rate derivative function: $\hat{q}'(t) = \frac{d}{dt}\hat{q}(t)$

Using the Laplace transform smoothed rate derivative function, we can use the definition of the loss-ratio in Eq. 2.1 to compute the Laplace transform smoothed $D(t)$ function as defined in Eq. 3.1.

$$\widehat{D}(t) \equiv -\frac{1}{\hat{q}(t)}\frac{d}{dt}\hat{q}(t) \quad \text{..... (3.1)}$$

Once the $\widehat{D}(t)$ function is computed, we can compute the Laplace transform smoothed $\hat{b}(t)$ function using the definition of the loss-ratio derivative from Eq. 2.2 as shown in Eq. 3.2 below.

$$\hat{b}(t) \equiv \frac{d}{dt}\left[\frac{1}{\widehat{D}(t)}\right] \quad \text{..... (3.2)}$$

From the available petroleum literature, we find that most of the existing Laplace transform algorithms for discrete data have been applied to the pressure (drop) function, which is an *increasing* data function. Obviously, the rate function [$q(t)$] is continuously decreasing during production and we believe that there may be inherent differences in the application of these Laplace transform discrete data methods for increasing and decreasing functions. Therefore, in addition to applying these methods to the time-rate data function [$q(t)$], we also use the reciprocal of rate data function [$u(t) = 1/q(t)$], which is an *increasing* data function, and may be more suitable for Laplace transform smoothing methodology.

The expressions for the Laplace transform smoothed rate function using the time-rate data function [$q(t)$] and the reciprocal of rate data function [$u(t) = 1/q(t)$] are shown (respectively) as:

$$\hat{q}(t) = \mathcal{L}^{-1}\{\bar{q}(s)\} \quad \text{where } \bar{q}(s) = \mathcal{L}\{q(t)\} \quad \text{.....(3.3)}$$

$$\hat{q}(t) = \frac{1}{\mathcal{L}^{-1}\{\bar{u}(s)\}} \quad \text{where } \bar{u}(s) = \mathcal{L}\{u(t)\} = \mathcal{L}\{1/q(t)\} \quad \text{.....(3.4)}$$

The expressions for the Laplace transform smoothed rate derivative function is derived using the Laplace transform identity of derivative function shown in Eq. 3.5. By using rate [$q(t)$] and its reciprocal [$u(t)$] as the basis-functions, we obtain the expressions for the Laplace transform smoothed rate derivative function as in Eqs. 3.6 and 3.7, respectively.

$$\bar{f}'(s) = s\bar{f}(s) - f(t=0) \quad \text{.....(3.5)}$$

$$\hat{q}'(t) = \frac{d}{dt}\hat{q}(t) = \mathcal{L}^{-1}\{\bar{q}'(s)\} \quad \text{where } \bar{q}'(s) = s\bar{q}(s) - q(t=0) \quad \text{.....(3.6)}$$

$$\hat{q}'(t) = -\left(\frac{1}{\mathcal{L}^{-1}\{\bar{u}(s)\}}\right)^2 \mathcal{L}^{-1}\{\bar{u}'(s)\} \quad \text{where } \bar{u}'(s) = s\bar{u}(s) - u(t=0) \quad \text{.....(3.7)}$$

Alternatively, we can use the Laplace transform identity of the derivative with respect to logarithmic time to obtain the Laplace transform smoothed derivative function. This latter approach was introduced by Onur and Reynolds [1998] and they claimed this approach produces a smoother derivative function — however; this approach requires longer

computational times. In this work, we experimented with this algorithm using a five-year monthly exponentially-declined time-rate data using rate as the basis-function. We found that the resulting rate derivative function is comparable with the result derived using Eq. 3.6 (at least for this experimental case). As the results were quite similar, we chose to limit our study only to Eqs. 3.6 and 3.7. However, we provide the detailed derivations of the alternate differentiation method introduced by Onur and Reynolds, as well as all the derivations of all the expressions in this section of the report (Section 3.1) in **Appendix B** of this thesis report.

As for the Laplace transform smoothed cumulative production, this function can only be computed using the time-rate discrete data as the basis-function. The Laplace transform identity of the integral is given by Eq. 3.8 and is used to derive the smoothed function in Eq. 3.9.

$$\mathcal{L}\left\{\int_0^t f(t)dt\right\} = \frac{\overline{f}(s)}{s} \quad \text{.....(3.8)}$$

$$\widehat{Q}(t) = \mathcal{L}^{-1}\left\{\mathcal{L}\{Q(t)\}\right\} = \mathcal{L}^{-1}\left\{\frac{\overline{q}(s)}{s}\right\} \quad \text{where } Q(t) = \int_0^t q(t)dt \quad \text{.....(3.9)}$$

As for the numerical inversion algorithm, we decided to use the Gaver-Stehfest algorithm throughout this research work as it has a feature to smooth the function. In fact, we expect the smoothing property is a contribution from both the Laplace transformation and the Laplace inversion process.

3.2 Laplace Transform Algorithms for Discrete "Time-Rate" Data

As discussed earlier in the literature review section, there have been several algorithms developed to take the Laplace transform of discrete data. The main differences among those algorithms are the functions used to approximate and/or represent the discrete data prior to being transformed into the Laplace domain. Most data-approximation techniques presented in the literature can be subdivided into three parts that include:

- The extrapolation/interpolation of data from: 0 to t_1.
- The interpolation of data from : t_1 to t_N.
- The extrapolation of data from: t_N to ∞.

Thus, for the sake of simplicity to compare, derive, and explain the Laplace transform algorithms, we subdivided the Laplace transform integral (Eq. 3.10) into three regions as well (as shown in Eqs. 3.11 and 3.12). **Fig. 3.1** shows a schematic for the Laplace transform of discrete data being subdivided into three regions.

$$\mathcal{L}\{f(t)\} = \overline{f}(s) = \int_0^{\infty} f(t)e^{-st}dt \quad \text{.....(3.10)}$$

$$\mathcal{L}\{f(t)\} = \int_{t_0=0}^{t_1} f(t)e^{-st}dt + \int_{t_1}^{t_N} f(t)e^{-st}dt + \int_{t_N}^{\infty} f(t)e^{-st}dt \quad \text{.....(3.11)}$$

$$\mathcal{L}\{f(t)\} = P_1 + P_2 + P_3 \quad \text{.....(3.12)}$$

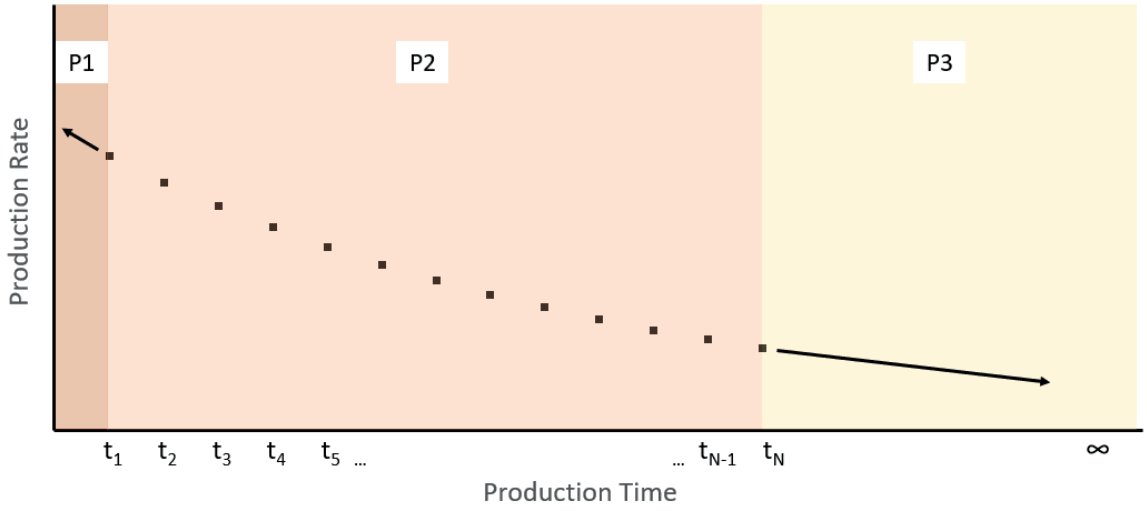

Figure 3.1 — Regions for the Computation of a Laplace Transform Data Expression.

To clarify in words; P_1, P_2, and P_3 can be defined as below.

P_1: The Laplace transform integral of the extrapolating function from $t_0 = 0$ to t_1

P_2: The Laplace transform integral of the interpolating function approximating the discrete data from $t_1 = 0$ to t_N

P_3: The Laplace transform integral of the extrapolating function from t_N to ∞

The previously developed Laplace transform algorithms for discrete data can be summarized in **Table 3.1** below. In **Table 3.1**, we note that the most popular approximating function for P_2 computation appears to be the piecewise linear data function. As noted by Onur and Reynolds [1998], the piecewise linear data function yields a more accurate (or at least on par) derivative function and takes shorter computational time compared to using the piecewise quadratic and log-linear functions. As we also aim to produce derivative functions from the Laplace approach, we decided to use the piecewise linear method for P_2 calculation throughout this research work.

Table 3.1 — Summary of the Approximating and Representative Functions for the Computation of the Laplace Transform of Discrete Data.

Year	Authors	Data Approximation Algorithms for Laplace Transform of Discrete Data		
		P1	**P2**	**P3**
1983	Kucuk& Ayestaran	N/A	Flowrate: exponential, Pressure: 4^{th} degree polynomial	N/A
1986	Guillot& Horne	Linear extrapolation (due to WBS)	1.) Piecewise step data 2.) Cubic spline interpolations	N/A
1988	Roumboutsos & Stewart	Linear extrapolation	Piecewise linear	Linear extrapolation
1993	Bourgeois& Horne	Linear extrapolation (due to WBS)	Piecewise linear	1.) Semi-log extrapolation (in general) 2.) Linear extrapolation for closed outer boundary reservoir system
1998	Onur& Reynolds	1.) Linear extrapolation 2.) Log-linear extrapolation	1.) Piecewise linear 2.) Piecewise quadratic 3.) Piecewise Log-linear	1.) Linear extrapolation 2.) Log-linear extrapolation
2003	Mireles& Blasingame	Linear extrapolation	Piecewise linear	Linear extrapolation
2005	Ilk	Flowrate: Piecewise constant, piecewise linear Unknown pressure derivative: B-spline		
2008	Al-ajmi	1.) Linear extrapolation 2.) Log-linear extrapolation	Piecewise linear	1.) Linear extrapolation 2.) Log-linear extrapolation
2012	Ahmadi	Zero	Cubic spline	Zero
2017	Ahmadi	Zero	Unit impulse function	Zero

The expression for P_2 using a piecewise linear data approximating function is shown in Eq. 3.13. Note that m_i in Eq. 3.13 represents the straight-line slope from t_{i-1} to t_i.

$$P_2 = \frac{1}{s}(f_1 e^{-st_1} - f_N e^{-st_N}) + \frac{1}{s^2}\sum_{i=2}^{N} m_i (e^{-st_{i-1}} - e^{-st_i}) \quad \text{.....(3.13)}$$

where:

$$f_i = f(t_i) \quad \text{and } i=1, 2, 3, \ldots, N \quad \text{.....(3.14)}$$

For the P_1 computation, most authors suggest using a linear and log-linear extrapolation/ interpolation of data. In case that the initial value of data function is known (*e.g.*, the pressure drop function always starts at zero), the interpolation of data to zero could be used. However, in our case, we assume the initial production rate is not known. Thus, an extrapolation on the left-hand side of data is required. Moreover, as we are also using the reciprocal of rate as the basis-function (which is inherently an *increasing* and *positive* data function) in our computation, an extrapolation to negative values at $t = 0$ could happen. Thus, we assume that the initial value for the reciprocal of rate is equal to zero for this case.

Similarly, the computation of P_3 requires an extrapolation on the right-hand side of discrete data. The extrapolation of time-rate data (which is inherently a *decreasing* and *positive* data function) on the right-hand side could extend to negative values at some point in time. In this case, we terminate the extrapolating line at that time point and the functional values beyond this time point is assumed to be zero.

Based on **Table 3.1**, several types of extrapolating functions could be used to represent the data outside the data interval. From literature study, we are convinced that to obtain an accurate Laplace transform of discrete data set, the extrapolation should follow the probable behavior of the data function in real-time space. Thus, we propose a method to observe the behavior of time-rate data by plotting it on four different plotting scales which include Cartesian, Log-Log, Linear-Log and Log-Linear scales. We could select a proper extrapolation technique by observing a straight-line behavior of data on these plots. For example, in case that we observe the data exhibits a straight-line trend on the Log-Log plot, we should extrapolate the data using a straight-line function on a Log-Log scale. Since, we have four types of plots, we propose to use four different extrapolating functions which are essentially the straight-line extrapolations on those four plotting scales. The governing equations for the straight-line extrapolations on the four plotting scales are summarized below (Eqs. 3.15 to 3.18).

- Cartesian plot

$$f(t) = mt + c \quad \text{.....} (3.15)$$

- Log-Log plot

$$\ln(f(t)) = \beta \ln(t) + \ln(\alpha) \quad \text{.....} (3.16)$$

- Linear-Log plot (the abscissa axis (x-axis) is scaled logarithmically)

$$f(t) = m \ln(t) + c \quad \text{.....} (3.17)$$

- Log-Linear plot (the ordinate axis (y-axis) is scaled logarithmically)

$$\ln(f(t)) = \beta t + \ln(\alpha) \quad \text{..... (3.18)}$$

In Eqs. 3.15 and 3.17, the slope and intercept are represented by m and c; whereas, in Eqs. 3.16 and 3.18, they are represented by β and $\ln(\alpha)$. Since, we aim to use this algorithm with production rate data which almost certainly contains data noise, we propose to use the method to obtain these extrapolating constants suggested by Onur and Reynolds [1998]. The method is a least-square regression of a few data points on both ends of the data set. This method is superior to using derivative values because it prevents bias of the slope when dealing with noisy data set. However, the least square method also has its own pitfall. By using the least-square slope and intercept to create the extrapolating functions outside the data interval, there are always discontinuities at the first and the last time points. To solve this issue, we replace the actual data points at both ends with the functional values obtained from the extrapolating functions.

The expressions for P_1 and P_3 can be obtained by substituting those relations in Eqs. 3.15 to 3.18 into the Laplace integral. We have tried to derive P_1 expressions using all four extrapolating functions, however, the expression using a straight-line function on a Linear-Log scale could not be derived explicitly. The P_1 expressions using straight-line extrapolating functions on Cartesian, Log-Log, and Log-Linear scales are shown in Eqs. 3.19, 3.20, and 3.21, respectively.

Straight-line extrapolation on Cartesian scale:

$$P_1 = \frac{1}{s}\left(f_0 - f_1 e^{-st_1}\right) + \frac{1}{s^2} m_1 (1 - e^{-st_1}) \quad \text{where } f_0 = f(t=0) \quad \text{.....(3.19)}$$

Straight-line extrapolation on Log-Log scale:

$$P_1 = \frac{\alpha_1}{s^{\upsilon_1}} \gamma(\upsilon_1, st_1) \quad \text{where } \upsilon_1 = \beta_1 + 1 > 0 \quad \text{.....(3.20)}$$

Straight-line extrapolation on Log-Linear scale:

$$P_1 = \frac{\alpha_1}{\beta_1 - s}[e^{(\beta_1 - s)t_1} - 1] \quad \text{where } s \neq \beta_1 \quad \text{.....(3.21)}$$

It is important to note that Eq. 3.20 is only applicable to the case where the straight-line slope on the Log-Log scale is more than minus one. Thus, we limit the use of this formulation only to *increasing* data functions where the slopes are positive values (certainly exceeds minus one). Lastly, the constants designated by m_1 and β_1 in Eqs. 3.19 to 3.21 refer to the straight-line slope for the interval $t < t_1$.

Similarly, P_3 expressions were derived using all four extrapolation schemes. For each extrapolation scheme, we derived the expressions for *increasing* and *decreasing* functions, separately. The reason is that some further modifications are required for the expressions for decreasing functions as we need to consider possible extrapolations to negative values. All the expressions for P_3 are shown in Eqs. 3.22 to 3.28.

Straight-line extrapolation on Cartesian scale (for increasing data functions):

$$P_3 = \frac{1}{s} f_N e^{-st_N} + \frac{1}{s^2} m_{ext} e^{-st_N} \quad \text{.....(3.22)}$$

Straight-line extrapolation on Cartesian scale (for decreasing data functions):

$$P_3 = \frac{1}{s} f_N e^{-st_N} + \frac{1}{s^2} m_{ext} e^{-st_N} (1 - e^{sf_N / m_{ext}}) \quad \text{.....(3.23)}$$

Straight-line extrapolation on Log-Log scale (for increasing data functions):

$$P_3 = \frac{\alpha_{ext}}{s^{\upsilon_{ext}}} [\Gamma(\upsilon_{ext}) - \gamma(\upsilon_{ext}, st_N)] \quad \text{where } \upsilon_{ext} = \beta_{ext} + 1 > 0 \quad \text{.....(3.24)}$$

Straight-line extrapolation on Linear-Log scale (for increasing data functions):

$$P_3 = \frac{f_N}{s} e^{-st_N} - \frac{m_{ext}}{s} E_i(-st_N) \quad \text{.....(3.25)}$$

Straight-line extrapolation on Linear-Log scale (for decreasing data functions):

$$P_3 = \frac{f_N}{s} e^{-st_N} + \frac{m_{ext}}{s} [E_i(-st_{N+1}) - E_i(-st_N)] \quad \text{.....(3.26)}$$

where

$$t_{N+1} = t_N e^{-f_N / m_{ext}} \quad \text{.....(3.27)}$$

Straight-line extrapolation on Log-Linear scale (for decreasing data functions):

$$P_3 = \frac{f_N}{s-\beta_{ext}} e^{-st_N} \quad \text{where } s > \beta_{ext} \quad \text{.....(3.28)}$$

Note that the P_3 expression using straight-line extrapolation on the Log-Log scale is only valid for *increasing* data function. Similarly, the P_3 expression using straight-line extrapolation on the Log-Linear scale is only valid for *decreasing* data function. The time t_{N+1} represents the time point at which the extrapolated function extends to zero. The constants designated by m_{ext} and β_{ext} in Eqs. 3.22 to 3.28 refer to the straight-line slope for the interval $t > t_N$.

To get a complete Laplace transform expression, we simply sum up P_1, P_2, and P_3. For example, in the case that we decide to use a piecewise linear interpolation and linear extrapolations on both ends. The complete Laplace transform formulation can be expressed in Eqs. 3.29 and 3.30 for *increasing* and *decreasing* data functions, respectively. We call them as the modified Roumboutsos and Stewart algorithms as they use the same data approximation strategy as the original version except that they have different assumptions on the initial-value and the positive nature of the function being transformed.

The modified Roumboutsos and Stewart algorithm with non-zero initial value is defined as (increasing data function):

$$\overline{f}(s) = \frac{f_0}{s} + \frac{1}{s^2}\sum_{i=1}^{N} m_i (e^{-st_{i-1}} - e^{-st_i}) + \frac{1}{s^2} m_{ext} e^{-st_N} \quad \text{.....(3.29)}$$

The modified Roumboutsos and Stewart algorithm with a large-time zero tendency extrapolation feature is given by (decreasing data function):

$$\overline{f}(s) = \frac{f_0}{s} + \frac{1}{s^2}\sum_{i=1}^{N} m_i (e^{-st_{i-1}} - e^{-st_i}) + \frac{1}{s^2} m_{ext} e^{-st_N} (1 - e^{\frac{sf_N}{m_{ext}}}) \quad \text{..... (3.30)}$$

Lastly, the detailed derivations of all the Laplace transform expressions used in this research work are summarized in **Appendix A** of the thesis report.

3.3 Proposed Workflow

The workflow to compute the Laplace transform smoothed rate, rate derivative, and $D(t)$ functions is demonstrated in **Fig. 3.2**. The same workflow can be used to compute the Laplace transform smoothed cumulative production and $b(t)$ functions by changing the basis-functions. **Table 3.2** suggests the basis-function to be used for each Laplace Transform smoothed function.

Table 3.2 — Basis-Functions for the Computation of the Laplace Transform Smoothed Functions

Laplace Transform Smoothed Function	$\hat{q}(t)$, $\hat{q}'(t)$, $\hat{D}(t)$	$\hat{Q}(t)$	$\hat{b}(t)$
Basis-Function	$q(t)$, $u(t) = 1/q(t)$	$q(t)$	$1/\hat{D}(t)$

The workflow can be explained briefly as below:

<u>Step 1</u>: Plot the basis-functions on the four plotting scales.

We start with plotting the basis-functions which are $q(t)$ and $1/q(t)$ on four different types of plots to observe the data behavior near both endpoints. The four types of plots include Cartesian, Log-Log, Linear-Log, and Log-Linear plots.

<u>Step 2</u>: Determine NP1, NP3, lL, and lR to obtain a proper representative function of discrete data.

An example Log-Log plot of the reciprocal of rate function *versus* time from an actual field data case is shown in **Fig. 3.3**. From the Figure, we can see that the Log-Log type extrapolation on the left end and the Cartesian-type extrapolation on the right end are the best options for this data set. In fact, we should consider all four plots, simultaneously. Regression ranges (*lL* and *lR*) of 1.3 and 0.1 were used in this example case. The constant *lR* of 0.1 means that the data points in the last 10 percent of a log cycle were used in the regression to obtain the extrapolating constants on the right end. After obtaining all four parameters (i.e., NP_1, NP_3, *lL*, and *lR*), we can compute the Laplace transform using the expressions presented in Section 3.2.

<u>Step 3</u>: Adjust the Stehfest "n" parameter to obtain accurate and smooth Laplace transform smoothed functions.

From graphical observation of the resulted smoothed function and the original function, we can determine a proper "*n*" parameter to be used. In case of rate derivative and

cumulative production, the Laplace transform smoothed functions can be plotted against the functions computed using the conventional methods (i.e., Bourdet differentiation algorithm for rate derivative and Trapezoidal rule of integration for cumulative production) to determine a proper "n" parameter. The principle is to balance between accuracy and smoothness of the resulted functions. The larger "*n*" leads to more accurate but oscillated functions. The parameter "*n*=8" is recommended by Onur and Reynold [1998] to be used for computing the smoothed derivative function as they result in a derivative function with adequate accuracy and smoothness when applied to noisy data.

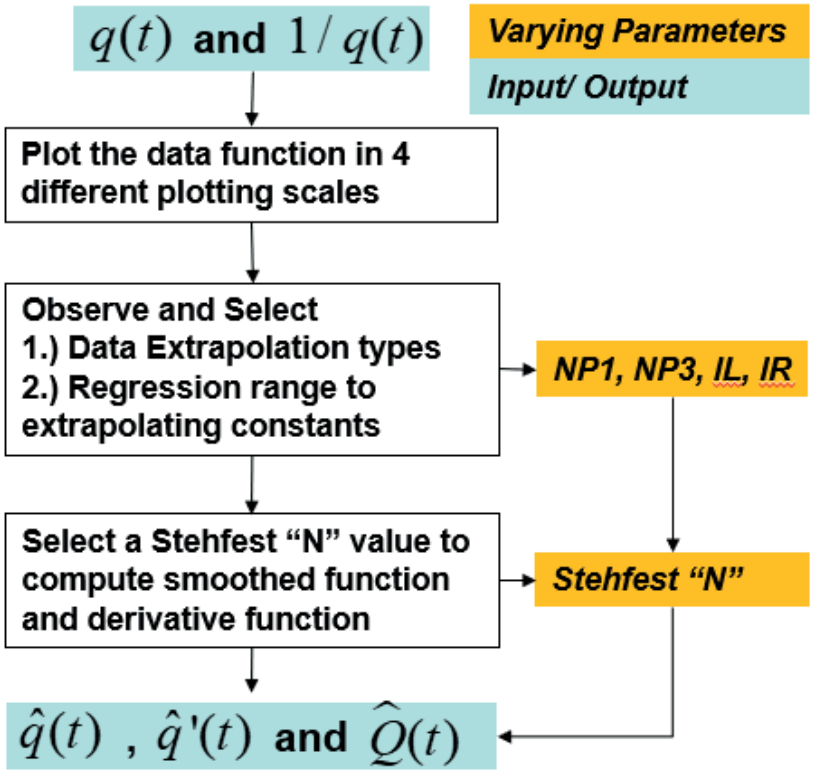

Figure 3.2 — Workflow for the Computation of a Laplace Transform of Discrete Data.

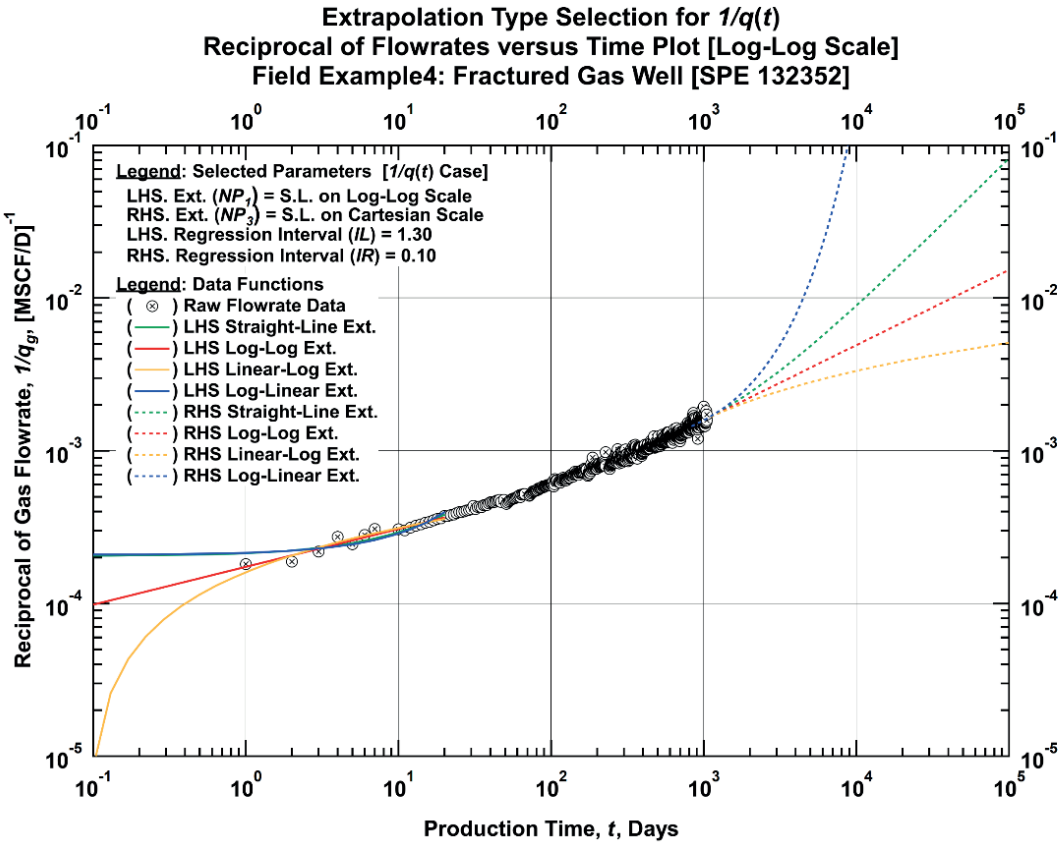

Figure 3.3 — An Example of Reciprocal of Rate versus Time Plot Used to Observed the Data Behavior and Select Extrapolation Types [Log-Log Plot].

The varying parameters in the workflow include:

NP_1: Type of the left-hand side extrapolating function

NP_3: Type of the right-hand side extrapolating function

lL: Regression range for the left-hand side extrapolation

lR: Regression range for the right-hand side extrapolation

n: Stehfest "n" parameter

3.4 Evaluation of the Proposed Workflow

In this section, we are evaluating the previously proposed workflow and algorithms. To do so, we performed a sensitivity study on the following:

- Data type for numerical Laplace transform computation.
- Data frequency and spacing type.
- The duration/history of the data.
- Magnitude of data noise (*i.e.*, Gaussian noise with 1 and 5 percent standard deviation).
- Type of data function (*i.e.*, increasing and decreasing data functions).

As process, we compared and contrasted our functional and statistical experiments using the following plots:

Plot 1: Plot of the Laplace transform of rate [$\overline{q}(s)$] versus the Laplace variable [s] plot:

$$\overline{q}(s) = \mathcal{L}\{q(t)\} \quad \text{..... (3.31)}$$

Plot 2: Plot of the absolute percentage error for the numerically computed Laplace transform of rate [$\overline{q}(s)$] compared to the analytical solution versus the Laplace transform variable [s].

Plot 3: Plot of the Laplace transform rate function [$s\overline{q}(s)$] versus the reciprocal of the Laplace variable [$1/s$]:

$$s\overline{q}(s) = s\mathcal{L}\{q(t)\} \quad \text{..... (3.32)}$$

Plot 4: Plot of the absolute percentage error for the numerically computed Laplace transform rate function [$s\overline{q}(s)$] compared to the analytical solution versus the reciprocal of the Laplace transform variable [$1/s$].

Plot 5: Plot of the flowrate versus time functions for the Laplace transform smoothed rate functions, where the Laplace transform smoothed rate function is defined as:

$$\hat{q}(t) = \mathcal{L}^{-1}\{\overline{q}(s)\} \quad \text{..... (3.3)}$$

Plot 6: Plot of the percentage error of the Laplace transform smoothed rate functions compared to the actual rate versus time.

Plot 7: Plot of the rate derivative versus time functions for the Laplace transform smoothed rate derivative functions, where the Laplace transform smoothed rate derivative function is defined as:

$$\hat{q}'(t) = \mathcal{L}^{-1}\{s\overline{q}(s) - q(t=0)\} \quad \text{..... (3.6)}$$

Plot 8: Plot of the percentage error of the Laplace transform smoothed rate derivative functions compared to the rate derivative from the model versus time.

Plot 9: Plot of the cumulative gas production versus time functions for the Laplace transform smoothed cumulative production functions, where the Laplace transform smoothed rate derivative function is defined as:

$$\hat{Q}(t) = \mathcal{L}^{-1}\{\overline{q}(s)/s\} \quad \text{..... (3.9)}$$

Plot10: Plot of the percentage error of the Laplace transform cumulative production functions compared to the cumulative production from the model versus time.

For the base case of this sensitivity study, we used a five-year monthly synthetic time-rate data set generated from Arps exponential decline model. The inputs used in the model is shown in **Table 3.2**.

Table 3.3 — Input Parameters for Synthetic Time-Rate Data.

Model	q_i **[MSCFD]**	D_i **[day-1]**
Arps Exponential Model	5000	1.65E-3

The reason we used the exponential model because we could obtain the explicit solution of the Laplace transform of the exponential decline time-rate model. The explicit solution is provided in Eq. 3.33. As a result, we could compare the Laplace transform of rate [$\bar{q}(s)$] and the Laplace transform rate [$s\bar{q}(s)$] functions computed form the discrete data (numerical solution) in each case to the analytical solution. Then, the absolute percentage errors against the analytical values can be calculated to be used for the analysis of the accuracy and smoothness of each case.

$$\mathcal{L}\{q_{\exp}(t)\} = \bar{q}_{\exp}(s) = q_i \frac{1}{s + D_i}, s > 0 \quad \text{..... (3.33)}$$

Moreover, we could derive the derivative and cumulative production functions of the exponential decline model in closed forms. Thus, in the same manner, we could compare the numerically computed smoothed functions [$\hat{q}'(t)$, $\widehat{Q}(t)$] using the Laplace transform method in each case to the models.

For the base method to derive those Laplace transform smoothed functions, the modified Roumboutsos and Stewart algorithm (Eq. 3.30) was used for the Laplace transform computation. The Stehfest "n = 18" was used as the base value for the numerical inversion

process except for the case of noisy data sets. Lastly, the extrapolating slopes were obtained from the last two data points on each end of the data set. All the resulted plots are displayed in **Appendix C** of the report. In the main text of the thesis report, we are only discussing the main study's results.

3.4.1 Effects of Data Extrapolation Type

Referring to **Figs. C-1.1 to C-1.10**, we could study the effect from using different extrapolation types in Laplace transformation process. In this sensitivity case, we compared the base method (the modified Roumboutsos and Stewart algorithm) with the method using straight-line extrapolation on Log-Linear scale , which is in fact an exponential extrapolation. Thus, the extrapolation of the base discrete data set (generated from Arps exponential model) using this extrapolation technique essentially provides a replicate of the model. As a result, all the Laplace transform smoothed functions and also the Laplace transform function itself are very accurate compared to the models and the analytical solution, respectively. The reduced accuracies of the smoothed functions in this case are only the contribution of using the piecewise linear data approximation during the data interval. To confirm the above statement, we also computed the smoothed functions using the analytical Laplace transform solution (Eq. 3.33) for comparison. We found that the errors of the smoothed functions computed using the analytical solution are very low (in the magnitude of 10^{-5} to 10^{-4}) and should be the numerical errors from the numerical inversion process.

On the contrary, the smoothed functions (except the cumulative production function) computed using the base method deviate from the model in the late-time interval of the data (after 700-900 days). This phenomenon is described in Onur and Reynolds' work as tail effects. This is a result of improper extrapolations applied at both ends of the data. The absolute percentage errors of the derivative function become as high as ten percent in the last 100 days of the data interval. From observation of the plots in **Figs. C-1.1 to C-1.10**, we can conclude that the derivative function is the most sensitive to the extrapolation functions especially in late-time interval (judging from the highest absolute percentage errors). The smoothed rate function and the Laplace transform of rate have similar error magnitude but less than those of the derivative function. Lastly, the resulted smoothed cumulative production has negligible effect from changing the extrapolated functions.

3.4.2 Effects of Data Frequency and Spacing Type

Referring to **Figs. C-2.1 to C-2.10**, we could study the effect from different data spacing types and frequencies. We consider the monthly sampling rate of our base case as a low frequency data. The high frequency data set contains five data points per month. The other data set is logarithmically spaced with 0.1 to 200 days between each sampling. The smoothed functions computed from the high-frequency data set contain the least errors during the early and middle interval of data compared to those computed form the other two data sets. This benefits from a better data approximation using the piecewise linear interpolation method in high-frequency data set. However, in the late time interval, similar errors are present among all three data sets as a result of improper extrapolation trends (Cartesian straight-line extrapolations on exponentially declined data function). The

logarithmically-spaced data set contains the highest error in late-time interval because the last two data points which contribute to the slope calculation are the furthest apart compared to the other two data sets. Thus, the extrapolating slope is the most deviated from the true exponential decline trend.

3.4.3 Effects of Duration/ History of the Data

Referring to **Figs. C-3.1 to C-3.10**, we could study the effect from different data duration. We compared 3-year, 5-year (base case) and 10-year data sets. Again, the accuracy of the smoothed functions in the early and middle time interval is adequate, however, the late-time interval still contains high absolute percentage errors. The highest errors of all three cases are in the same magnitude, however, come at different time. The longer the data we have, the more delay the error come.

3.4.4 Effects of Magnitude of Data Noise

Referring to **Figs. C-4.1 to C-4.10**, we could study the effect from different magnitude of data noise. We compared the data sets which contain no data noise, 1-percent Gaussian noise, and 5-percent Gaussian noise. It is noted that for noisy data sets, the Stehfest "n=8" was used. In the early and middle time interval, errors of the noised data cases are much higher compared to the case without noise. Especially for the derivative functions, the early-time errors are nearly 100 percent for 5% Gaussian noised case.

3.4.5 Effects of Type of Data Function

Referring to **Figs. C-5.5 to C-5.8**, we compared the effects of using increasing and decreasing data function as the basis-functions. In this case, we cannot compare Plot 1 to

Plot 4, Plot 9, and Plot 10, since the Laplace transform of rate and the cumulative function could not be computed from the reciprocal of rate data. The Laplace transform smoothed rate and rate derivative functions deviates from the true value earlier when using the reciprocal function. However, the maximum error magnitude is still much lower than the case using normal rate function. The reason for lower error magnitude is not known. However, we suspect that it might be the same as for the other sensitivity cases where the Laplace transform smoothed functions contain less errors when the approximating/ extrapolating functions can better represent the model.

4. METHOD VALIDATION

This section summarizes the validation of the proposed methodology using seven different types of synthetic data and four actual field production data.

4.1 Method Validation with Synthetic Data

In order to validate the developed Laplace transform workflow, we applied the workflow to synthetic datasets generated from seven different types of empirical time-rate decline models which are:

- Arps Exponential Model [Arps, 1945]
- Arps Hyperbolic Model [Arps, 1945]
- Arps Harmonic Model [Arps, 1945]
- Modified Hyperbolic Model [Robertson, 1988]
- Power-Law Exponential Model [Ilk, 2008]
- Duong Model [Duong, 2011]
- Logistic Growth Model [Clark, 2011]

Each synthetic data set contains five-year monthly production data. Two synthetic datasets were generated from each model which are the perfect dataset (without data noise) and the noisy dataset (applied Gaussian noise with 5% standard deviation). Thus, totally we are validating the method using 14 time-rate data sets.

For each data set, we compare the Laplace transform smoothed functions (i.e., flowrate, *D*-parameter, *b*-parameter, and cumulative production) to the model to analyze the accuracy and smoothness of the resulted functions. We also compare them with *D*-

parameter, *b*-parameter, and cumulative production functions computed from the conventional approach (Bourdet differentiation and Trapezoidal-rule integration).

As mentioned in the proposed workflow, we used two types of basis-functions which are the rate function and its reciprocal function. Straight-line data interpolation was used for all cases to approximate discrete data set within the data interval. For data extrapolation, we analyzed the characteristics of the basis-functions used in each case through observation of the data displayed on four different types of plots. The most appropriate extrapolation strategies and regression ranges were selected and applied to the basis-functions in each case for the computation of the smoothed functions.

We use both qualitative and quantitative means to validate the method. Quantitatively, we compare the mean absolute percentage errors of each computed functions to the models. As for qualitative consideration, we produced the following plots in each case and observed the characteristics of each plot through time:

Plot 1: Comparison plot of flowrates versus time

1.a Model flowrate,
1.b Synthetic flowrate,
1.c Laplace transform smoothed flowrate using rate as the basis-function, and
1.d Laplace transform smoothed flowrate using the 1/rate as the basis-function

Plot 2: Comparison plot of the absolute percentage errors of flowrates versus time

2.a Synthetic flowrate,
2.b Laplace transform smoothed flowrate using rate as the basis-function,
2.c Laplace transform smoothed flowrate using the 1/rate as the basis-function

Plot 3: Comparison plot of *D*-parameters versus time

3.a Modelled *D*-parameter,

3.b Bourdet derived *D*-parameter (*L*=0.1),

3.c Bourdet derived *D*-parameter (*L*=0.25),

3.d Laplace transform smoothed *D*-parameter using rate as the basis-function,

3.e Laplace transform smoothed *D*-parameter using the reciprocal of rate as the basis-function

Plot 4: Comparison plot of the absolute percentage errors of *D*-parameters versus time

4.a Bourdet derived *D*-parameter (*L*=0.1),

4.b Bourdet derived *D*-parameter (*L*=0.25),

4.c Laplace transform smoothed *D*-parameter using rate as the basis-function,

4.d Laplace transform smoothed *D*-parameter using the reciprocal of rate as the basis-function

Plot 5: Comparison plot of *b*-parameters versus time

5.a Modelled *b*-parameter,

5.b Bourdet derived *b*-parameter (*L*=0.1),

5.c Bourdet derived *b*-parameter (*L*=0.25),

5.d Laplace transform smoothed *b*-parameter using rate as the basis-function,

5.e Laplace transform smoothed *b*-parameter using the reciprocal of rate as the basis-function

Plot 6: Comparison plot of the absolute percentage errors of *b*-parameters versus time

6.a Bourdet derived *b*-parameter (*L*=0.1),

6.b Bourdet derived *b*-parameter (*L*=0.25),

6.c Laplace transform smoothed *b*-parameter using rate as the basis-function,

6.d Laplace transform smoothed *b*-parameter using the reciprocal of rate as the basis-function

Plot 7: Comparison plot of cumulative production versus time

7.a Modelled cumulative production,

7.b Cumulative production computed from trapezoidal-rule integration,

7.c Laplace transform smoothed cumulative production using rate as the basis-function

Plot 8: Comparison plot of the absolute percentage errors of cumulative production versus time

8.a Cumulative production computed from trapezoidal-rule integration,

8.b Laplace transform smoothed cumulative production using rate as the basis-function

All the plots mentioned above are included in **Appendix D** of the thesis report. **Figs. 4.1 to 4.8** show a validation case with a time-rate data set generated from Duong time-rate model and corrupted with Gaussian noise using 5 percent standard deviation.

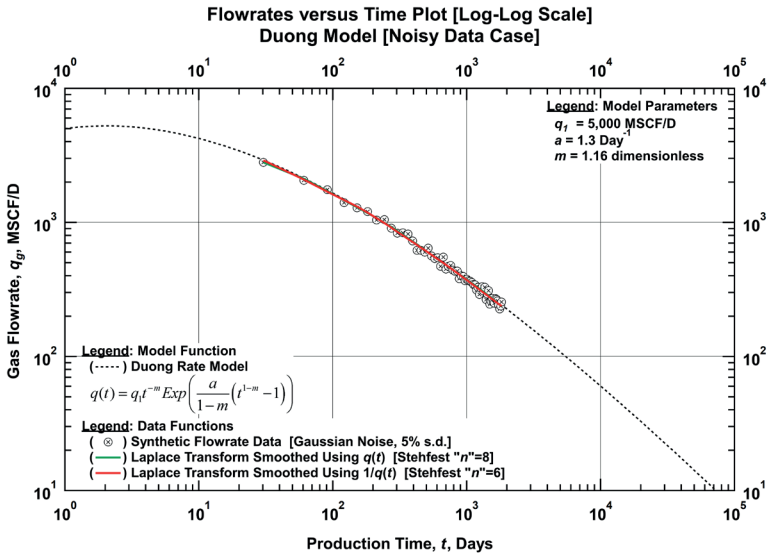

Figure 4.1 — Comparison Plot of the Modelled Flowrate, Synthetic Flowrate, and Laplace Transform Smoothed Flowrates using Rate and Reciprocal of Rate as the Basis Functions Versus Time [Duong Model (Noisy Data Case)].

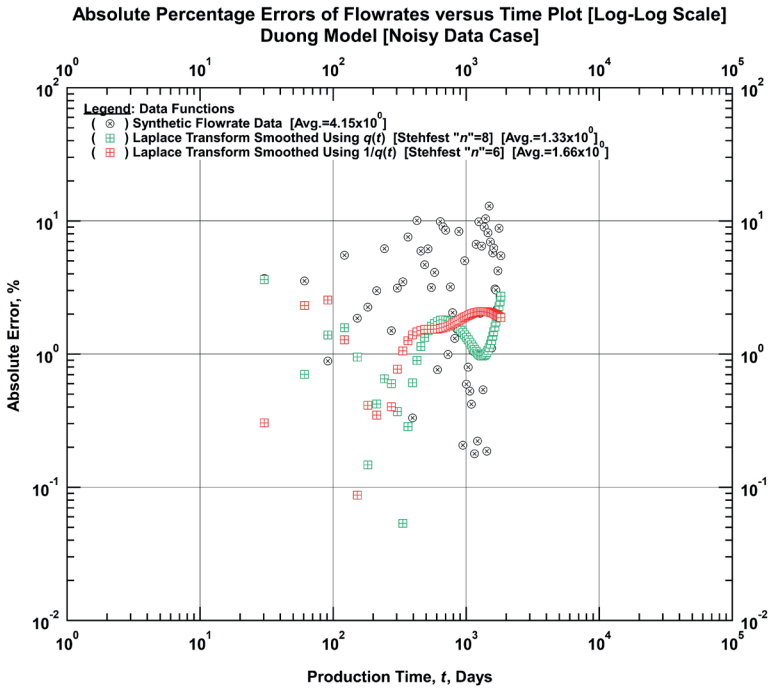

Figure 4.2 — Comparison Plot of the Absolute Percentage Errors of the Synthetic Flowrate and Laplace Transform Smoothed Flowrates using Rate and Reciprocal of Rate as the Basis Functions Versus Time [Duong Model (Noisy Data Case)].

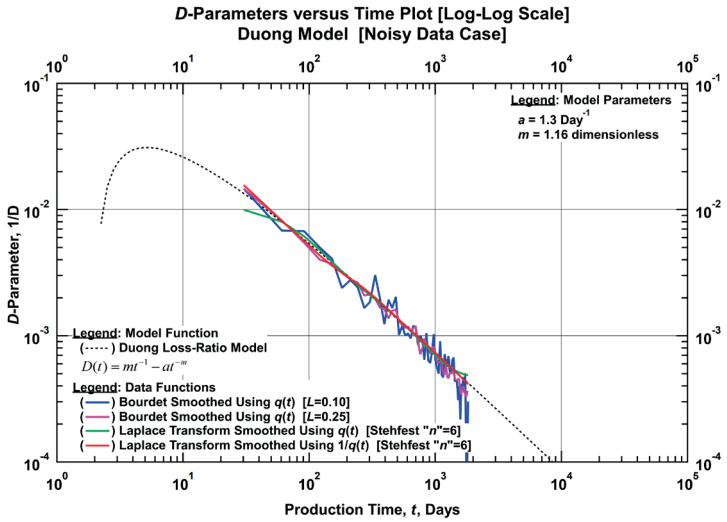

Figure 4.3 — Comparison Plot of the Modelled *D*-Parameters, Bourdet-Derived *D*-Parameters, and Laplace Transform Smoothed *D*-Parameters using Rate and Reciprocal of Rate as the Basis Functions Versus Time [Duong Model (Noisy Data Case)].

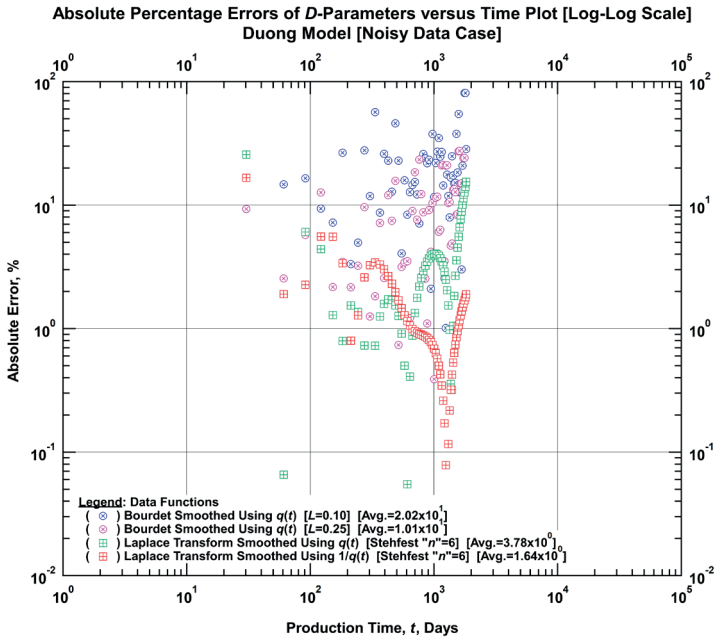

Figure 4.4 — Comparison Plot of the Absolute Percentage Errors of the Bourdet-Derived *D*-Parameters and Laplace Transform Smoothed *D*-Parameters using Rate and Reciprocal of Rate Functions as the Basis Functions Versus Time [Duong Model (Noisy Data Case)].

Figs. 4.1 and 4.2 show that the Laplace transform smoothed algorithm can successfully smooth out the noisy data set with as high as 5 percent data noise. The mean absolute percentage error reduces to less than 2 percent and the smoothed functions still maintain the original characteristic of discrete data very well.

Figs. 4.3 and 4.4 show that the Laplace transform smoothed algorithm could produce very smooth and accurate $D(t)$ functions from the noisy Duong time-rate data set. However, we observe some "tail effects" at both end of the Laplace transform smoothed $D(t)$ function generated using the rate function as the basis-function. This is because the Duong time-rate model behaves more like a straight line on the Log-Log scale. However, the algorithm for the straight-line extrapolation on the Log-Log scale is not applicable for decreasing functions such as the rate function. In fact, it's not applicable for the case with a slope on the Log-Log scale less than minus one, however, as a precaution we avoid using it with decreasing functions. Therefore, we used the closest extrapolation schemes which are the straight-line extrapolation on the Log-Linear scale and Linear-Log scale for the left-hand side and right-hand side extrapolations, respectively. However, this limitation doesn't apply to the case using the reciprocal function (increasing function). As a result, the tail effects are not present in the latter case.

Overall, comparing to the Bourdet differentiation algorithm, the Laplace transform algorithm is still superior both in terms of smoothness and accuracy, especially at the early and late times. From **Figs. 4.3 and 4.4**, we could observe deviations of the Bourdet derived $D(t)$ functions from the true $D(t)$ model. This has been known as the "end-point

effect" which is the result of large smoothing parameter "L" used in the algorithm. For example, if "L=0.25" is used, we could expect the deviation from the true model in the last 25 percent of a log cycle in the computed derivative function.

The mean absolute percentage errors of the $D(t)$ functions computed using Laplace transform approach range from 1.6 to 3.8 percent while those of the Bourdet approach are as high as 10 percent ("L=0.25" case). More importantly, the late-time deviations are less when the Laplace transform approach is used.

Figs. 4.5 and 4.6 show that the Laplace transform smoothed algorithm could produce very smooth and accurate $b(t)$ functions from the noisy Duong time-rate data set. However, we could still observe "tail effect" in the case that uses rate function as the basis-function. This is something that could be expected though, because the previously derived $D(t)$ functions were used as an input for $b(t)$ computations.

Figs. 4.7 and 4.8 show that the Laplace transform smoothed algorithm is superior in computing cumulative production functions compared to the conventional approach which uses the Trapezoidal rule of integration. This is in fact a bit unfair because we use low-frequency data for testing which is kind of the weakness of the Trapezoidal rule integration algorithm. However, this data frequency is what we could expect in real life.

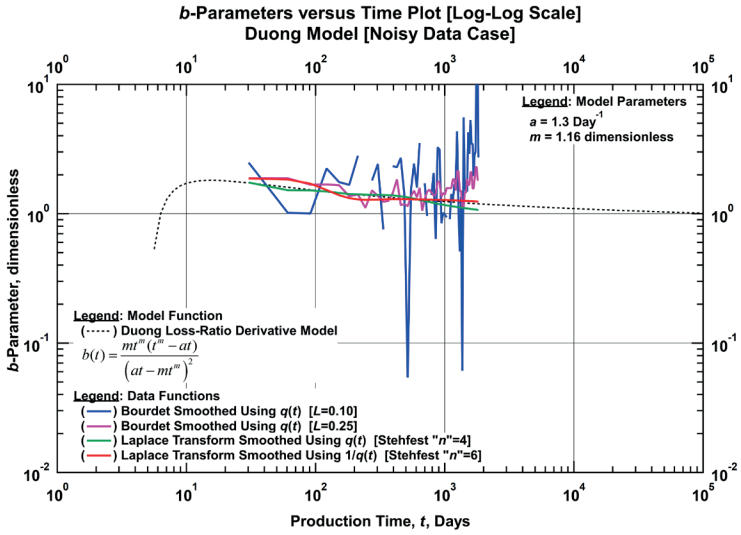

Figure 4.5 — Comparison Plot of the Modelled *b*-Parameters, Bourdet-Derived *b*-Parameters, and Laplace Transform Smoothed *b*-Parameters using Rate and Reciprocal of Rate as the Basis Functions Versus Time [Duong Model (Noisy Data Case)].

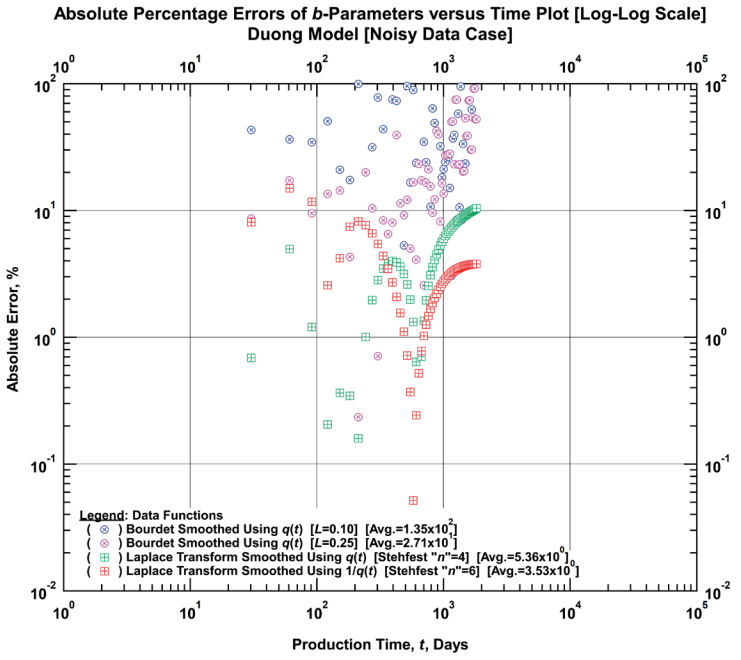

Figure 4.6 — Comparison Plot of the Absolute Percentage Errors of the Bourdet-Derived *b*-Parameters and Laplace Transform Smoothed *b*-Parameters using Rate and Reciprocal of Rate as the Basis Functions versus Time [Duong Model (Noisy Data Case)].

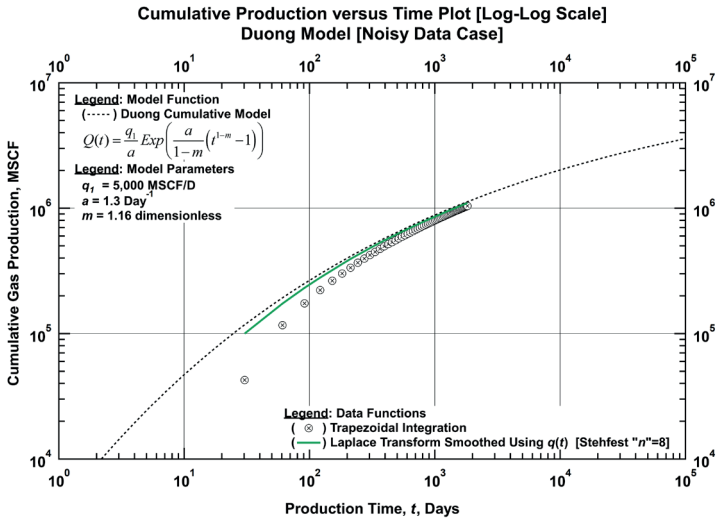

Figure 4.7 — Comparison Plot of the Modelled Cumulative Production, Trapezoidal-Integrated Cumulative Production, and Laplace Transform Smoothed Cumulative Production using Rate as Basis Function versus Time [Duong Model (Noisy Data Case)].

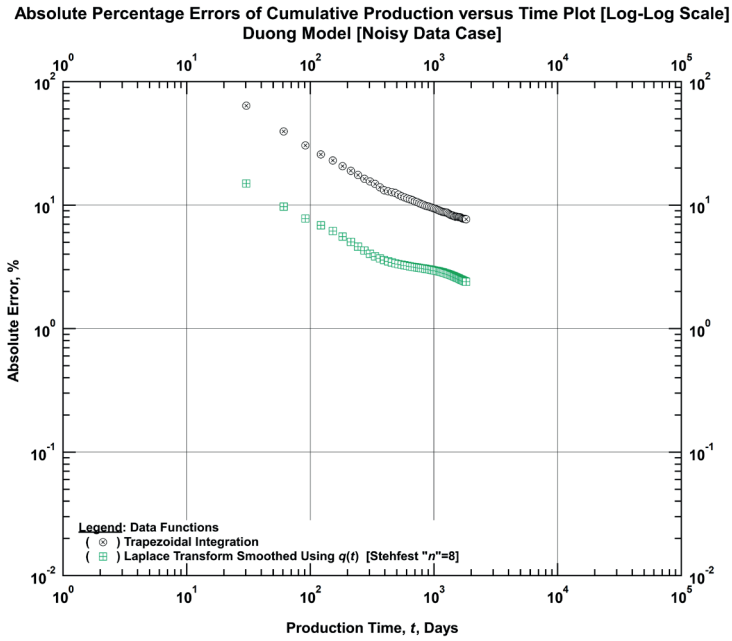

Figure 4.8 — Comparison Plot of the Absolute Percentage Errors of Trapezoidal-Integrated Cumulative Production and Laplace Transform Smoothed Cumulative Production using Rate as Basis Function versus Time [Duong Model (Noisy Data Case)].

Table 4.1 — Input Parameters for Duong Model (Noisy Data Set) Case

Basis Function: Time-Rate Data

Laplace Smoothed Functions	**Rate & Cum. Production**	***D*-Parameter**	***b*-Parameter**
Basis Functions	$q(t)$	$q(t)$	Smoothed $1/D(t)$
Numerical Laplace Transform Parameters			
LHS Extrapolation Type (NP1)	Log-Linear	Log-Linear	Log-Log
RHS Extrapolation Type (NP3)	Linear-Log	Linear-Log	Log-Log
LHS Regression Range (lL)	0.43	0.43	1.30
RHS Regression Range (lR)	0.22	0.22	0.87
Numerical Laplace Inversion Parameter			
Stehfest "n" Parameter	8	6	4

Basis Function: Time-Reciprocal of Rate Data

Laplace Smoothed Functions	**Rate**	***D*-Parameter**	***b*-Parameter**
Basis Functions	$u(t) = 1/q(t)$	$u(t) = 1/q(t)$	Smoothed $1/D(t)$
Numerical Laplace Transform Parameters			
LHS Extrapolation Type (NP1)	Log-Log	Log-Log	Log-Log
RHS Extrapolation Type (NP3)	Log-Log	Log-Log	Log-Log
LHS Regression Range (lL)	0.87	0.87	1.30
RHS Regression Range (lR)	0.22	0.22	0.43
Numerical Laplace Inversion Parameter			
Stehfest "n" Parameter	6	6	6

Table 4.1 shows the inputs we used to compute the Laplace transform smoothed functions in **Figs. 4.1 to 4.8**. We used larger regression ranges for the computation of $b(t)$ function as we observed tail effects in the basis function which are the $D(t)$ functions computed previously.

Table. 4.2 to 4.7 summarize and compare the resulted mean absolute percentage errors of each case. However, it is noted that the mean absolute percentage errors of cumulative production were not calculated as it is more sensible to look at the development of errors through time.

Table 4.2 — Mean Absolute Percentage Errors of Flowrates in Perfect Data Cases.

Models	Mean Absolute Percentage Errors of Flowrates (%)		
	Raw	LP [q]	LP [1/q]
Arps Exponential Model	0	2.10E-02	2.27E-01
Arps Hyperbolic Model	0	2.90E-02	2.75E-02
Arps Harmonic Model	0	2.51E-02	6.33E-06
Modified Hyperbolic Model	0	2.58E-02	3.20E-02
Power-Law Exponential Model	0	6.56E-02	2.49E-02
Duong Model	0	8.32E-02	2.05E-02
Logistic Growth Model	0	1.28E-01	2.86E-02

Table 4.3 — Mean Absolute Percentage Errors of D-Parameters in Perfect Data Cases.

Models	Mean Absolute Percentage Errors of D-Parameters (%)			
	BD [L=0.10]	BD [L=0.25]	LP [q]	LP [1/q]
Arps Exponential Model	3.00E+00	1.02E+01	2.78E-02	1.18E+00
Arps Hyperbolic Model	1.64E+00	5.38E+00	2.69E-01	2.40E-01
Arps Harmonic Model	1.30E+00	3.79E+00	3.57E-01	6.22E-06
Modified Hyperbolic Model	2.15E+00	3.24E+00	5.51E-01	7.15E-01
Power-Law Exponential Model	2.13E-01	8.32E-01	1.09E+00	2.44E-01
Duong Model	3.07E-01	9.13E-01	1.05E+00	1.23E-01
Logistic Growth Model	6.49E-01	1.84E+00	8.37E-01	1.02E-01

Table 4.4 — Mean Absolute Percentage Errors of b-Parameters in Perfect Data Cases.

Models	Mean Absolute Percentage Errors of b-Parameters (%)				Remarks
	BD [L=0.10]	BD [L=0.25]	LP [q]	LP [1/q]	
Arps Exponential Model	1.93E-01	2.70E-01	1.85E-03	3.40E-03	The figures are Mean Absolute Error (not %)
Arps Hyperbolic Model	3.86E+01	5.43E+03	1.58E+00	5.69E-01	
Arps Harmonic Model	1.93E+01	2.69E+01	1.64E+00	1.76E-05	
Modified Hyperbolic Model	1.29E+01	1.11E+01	6.90E+00	7.96E+00	The figures exclude exponential tail
Power-Law Exponential Model	1.36E+00	3.13E+00	1.42E+00	3.83E-01	
Duong Model	1.36E+00	2.79E+00	1.78E+00	4.30E-01	
Logistic Growth Model	2.42E+00	4.63E+00	2.54E+00	6.18E-01	

Table 4.5 — Mean Absolute Percentage Errors of Flowrates in Noisy Data Cases.

Models	Mean Absolute Percentage Errors of Flowrates (%)		
	Raw	LP [q]	LP [1/q]
Arps Exponential Model	4.1	0.9	1.5
Arps Hyperbolic Model	3.9	0.7	0.7
Arps Harmonic Model	5.0	1.0	0.9
Modified Hyperbolic Model	3.7	0.8	0.6
Power-Law Exponential Model	3.7	1.1	0.7
Duong Model	4.2	1.3	1.7
Logistic Growth Model	2.9	1.0	0.9

Table 4.6 — Mean Absolute Percentage Errors of D-Parameters in Noisy Data Cases.

Models	Mean Absolute Percentage Errors of D-Parameters (%)			
	BD [L=0.10]	BD [L=0.25]	LP [q]	LP [1/q]
Arps Exponential Model	16.3	14.9	5.2	8.0
Arps Hyperbolic Model	19.6	12.2	5.3	4.1
Arps Harmonic Model	29.7	14.1	6.8	2.5
Modified Hyperbolic Model	32.1	16.6	6.9	6.7
Power-Law Exponential Model	20.4	8.3	7.8	2.0
Duong Model	20.2	10.1	3.8	1.6
Logistic Growth Model	6.4	3.9	4.1	2.7

Table 4.7 — Mean Absolute Percentage Errors of b-Parameters in Noisy Data Cases.

Models	Mean Absolute Percentage Errors of b-Parameters (%)				Remarks
	BD [L=0.10]	BD [L=0.25]	LP [q]	LP [1/q]	
Arps Exponential Model	8.5	0.5	1.0	1.4	The figures are Mean Absolute Error (not %)
Arps Hyperbolic Model	391.0	59.0	26.6	10.5	
Arps Harmonic Model	1310.0	58.3	42.8	10.3	
Modified Hyperbolic Model	1730.0	48.5	42.7	35.1	The figures exclude exponential tail
Power-Law Exponential Model	89.9	15.5	10.1	3.8	
Duong Model	135.0	27.1	5.4	3.5	
Logistic Growth Model	42.4	9.5	6.7	6.0	

4.1.1 Validation of Laplace Transform Smoothed Rate Function

Table 4.1 and 4.4 suggest satisfactory results when using the developed Laplace transform workflow to produce smoothed rate functions in all the time-rate models both in perfect data and noisy data cases. For the perfect data cases, the mean absolute percentage errors are less than 0.2 percent which is negligible. For the noisy data cases, the mean absolute percentage errors reduce from 3 to 5 percent to less than 1.7 percent. In fact, apart from Arps exponential decline and Duong time-rate models, the errors reduce to less than 1 percent.

4.1.2 Validation of Laplace Transform Smoothed *D*-Parameter Function

By considering the mean absolute percentage errors in **Table 4.2 and 4.5**, the Laplace transform method provides more accurate *D*-parameter functions compared to the Bourdet approach both for perfect data and noisy data cases. For the perfect data cases, the mean absolute percentage errors of the Laplace transform smoothed *D*-parameters are less than 1.2 percent while those of the Bourdet *D*-parameters range from 0.2 to 10 percent. For the noisy data cases, the mean absolute percentage errors of the Laplace transform smoothed *D*-parameters range from 2 to 8 percent while those of the Bourdet *D*-parameters range from 4 to 32 percent.

Another observation is that the Laplace transform method using the reciprocal of rate as the basis-function almost always gives better results except for Arps exponential cases. Especially for Arps harmonic cases, the use of reciprocal of rate provide exceptional results as the reciprocal of the harmonic rate decline function is a straight-line function.

From **Table 4.2**, we observed that the use of Bourdet approach with L=0.25 in perfect data cases give less accurate D-parameter results compared to L=0.1. This is because the end point effects when using high smoothing parameter L. In other words, the errors form the end point effects dominate the errors in the middle interval of the data when we are differentiating perfect data functions.

From graphical observation of D-parameter plots [Plot 3 and 4] in **Appendix D**, the Laplace transform smoothed D-parameter functions contain less deviations at both ends compared to the Bourdet D-parameter functions. Moreover, the Laplace transform approach using the reciprocal of rate as the basis-functions yield more accurate D-parameter functions at both ends compared to using the rate as the basis-function.

4.1.3 Validation of Laplace Transform Smoothed *b*-Parameter Function

Table 4.3 and 4.6 suggest that the Laplace transform method provides more accurate b-parameter functions compared to the Bourdet approach both for perfect data and noisy data cases. For the perfect data cases, the mean absolute percentage errors of the Laplace transform smoothed b-parameters are less than 0.4 to 8 percent (excluding the Arps harmonic case which contains negligible error) while those of the Bourdet b-parameters (L=0.25) range from 2.8 to 26.9 percent (excluding the Arps hyperbolic case which contains very high error). For the noisy data cases, the mean absolute percentage errors of the Laplace transform smoothed b-parameters range from 1 to 43 percent while those of the Bourdet b-parameters (L=0.25) range from 0.5 to 60 percent.

Similar to *D*-parameter function, the method using the reciprocal of rate as the basis-function always gives more accurate *b*-parameter, especially when applied to Arps harmonic model case.

Another advantage of the Laplace transform approach is that it could detect the abrupt change in the derivative value. This is illustrated in the modified hyperbolic model cases, the Laplace transform approach could detect the abrupt change in *b*-value at the switching point that the Bourdet approach could not.

4.1.4 Validation of Laplace Transform Smoothed Cumulative Production Function

Based on the observation of the cumulative plots [Plot 7 and 8] in **Appendix D**, the Laplace transform approach is superior to the Trapezoidal rule approach in all cases. This might be because the trapezoidal rule-integration approach yields inaccurate early-time integration for low-frequency data sets which are used in this validation exercise. However, this shows the strength of the Laplace transform approach to compute the integration of low-frequency discrete data set.

In each synthetic data case, we have selected the most appropriate extrapolating functions based on graphical observation of the discrete data set. From those 14 data sets, we found that the straight-line extrapolation on the Log-Linear scale was the most used for the rate functions while the straight-line extrapolations on the Log-Log scale and Cartesian scale were equally used for the reciprocal of rate functions. When dealing with the noisy data sets, the regression range on the left-hand side of data (*lL*) is from 0.4 to 1.1, while on the

right-hand side, the data regression range (lR) is from 0.1 to 0.4. The regression ranges used for the computation of $b(t)$ function are as large as 1.7 and 0.9 for lL and lR, respectively. The large regression range was used when the basis-function [Laplace transform smoothed $1/D(t)$] is suspected to contain the tail effects.

As mentioned earlier, in the process to obtain the Laplace transform smoothed functions, trial and errors of the Stehfest "n" parameters are required. Using too high "n" value might yield an accurate but oscillating function. However, using too low "n" value results in a very smooth but inaccurate function. In each case, we trialed on the "n" parameter to obtain the function that is both accurate and reasonably smooth. **Table 4.8** summarizes the recommended ranges of Stehfest "n" parameters for the computation of smoothed functions using the proposed Laplace transform approach.

Table 4.8 — Recommended Ranges of the Stehfest "n" Parameters for the Computation of Laplace Transform Smoothed Functions

Laplace Transform Smoothed Functions	***q*(*t*) and *Q*(*t*)**	***D*(*t*)**	***b*(*t*)**
Stehfest Parameter — Perfect Data Cases	16-18	16-18	12-20
Stehfest Parameter — Noisy Data Cases	6-10	6-8	4-6

4.2 Method Validation with Actual Field Data

In order to validate the developed Laplace transform workflow, we applied the method to the following actual field data sets:

- Field Example 1: East Texas Gas Well (SPE 84287)
- Field Example 2: Fractured Gas Well (SPE 132352)
- Field Example 3: Fractured Gas Well (SPE 132352)
- Field Example 4: Fractured Gas Well (SPE 132352)

Each data set contains approximately five to seven years of daily production data. However, due to run-time limitation, we only use the first one thousand data points to compute the Laplace transform smoothed flowrate, $D(t)$, and $b(t)$ functions. Prior to applying the Laplace transform smoothed approach, we edited the raw data by removing shut-in periods and other outliers which may cause high fluctuations in the resulted Laplace transform smoothed functions.

In each case, we compare the resulted Laplace transform smoothed flowrates, D(t) and $b(t)$, and cumulative production functions to the actual flowrate data, Bourdet derived $D(t)$ and $b(t)$ functions, and cumulative production computed using Trapezoidal integration rule, respectively. In fact, we have two versions of the Bourdet derived $D(t)$ and $b(t)$ functions. The first version was computed using only the first thousand data points and the second version was computed using all data points available in each data set (around 1,800 to 2,500 data points). By comparing the Laplace transform derived functions to the first version, we can assess the performance of the Laplace transform approach against the Bourdet approach. As for the second version of $D(t)$ and $b(t)$ functions, which computed

from all data points using L=0.25, they would act like base lines for referencing purpose as we expect that they are more accurate compared to the other two (at least for the interval before 1000 days). This is because the end-point effects would only occur during 1000 to 1800 days for the 1800-point data set and 1400 to 2500 days for 2500-point data set. Thus, the second version would be closest to the true functions.

The accuracy and smoothness of the resulted curves could be observed and accessed through graphical observations of the following plots:

Plot 1: Comparison plot of flowrates and cumulative production versus time

1.a Raw flowrate,
1.b (optional) Edited flowrate,
1.c Laplace transform smoothed flowrate using flowrate as the basis function,
1.d Laplace transform smoothed flowrate using the reciprocal of flowrate as the basis function,
1.e (optional) Cumulative production computed from trapezoidal-rule integration approach,
1.f (optional) Laplace transform smoothed cumulative production using flowrate as the basis function

Plot 2: Comparison plot of flowrates and cumulative production versus time

This plot is similar to Plot 1 except that the Laplace transform smoothed functions were computed using three Stehfest "n" values (6, 12 and 18).

Plot 3: Comparison plot of D-parameters versus time

3.a Bourdet derived D-parameter (L=0.25) (using all data points),

3.b Bourdet derived D-parameter (L=0.10) (using the first thousand data points),

3.c Bourdet derived D-parameter (L=0.25) (using the first thousand data points),

3.d Laplace transform smoothed *D*-parameter using flowrate as the basis function,

3.e Laplace transform smoothed *D*-parameter using the reciprocal of flowrate as the basis function

Plot 4: Comparison plot of *D*-parameters versus time

This plot is similar to Plot 3 except that the Laplace transform smoothed functions were computed using three Stehfest "*n*" values (6, 12 and 18).

Plot 5: Comparison plots of the extrapolations of flowrate data versus time in four different plotting scales (i.e., Cartesian, Log-Log, Linear-Log, Log-Linear scales)

5.a Left and right-hand-side straight-line extrapolations on Cartesian scale,

5.b Left and right-hand-side straight-line extrapolations on Log-Log scale,

5.c Left and right-hand-side straight-line extrapolations on Linear-Log scale,

5.d Left and right-hand-side straight-line extrapolations on Log-Linear scale,

Plot 6: Comparison plots of the extrapolations of the reciprocal of flowrate data versus time in four different plotting scales, i.e. Cartesian, log-log, linear-log, log-linear scales

This plot is similar to plot 5 except that they are for the reciprocal of flowrate data

Plot 7: Comparison plot of *b*-parameters versus time

7.a Bourdet derived *b*-parameter (L=0.25) (using all data points),

7.b Bourdet derived *b*-parameter (L=0.10) (using the first thousand data points),

7.c Bourdet derived *b*-parameter (L=0.25) (using the first thousand data points),

7.d Laplace transform smoothed *b*-parameter using flowrate as the basis function,

7.e Laplace transform smoothed *b*-parameter using the reciprocal of flowrate as the basis function

Plot 8: Comparison plot of *b*-parameters versus time

This plot is similar to plot 7 except that the Laplace transform smoothed functions were computed using two Stehfest "*n*" values (4 and 6).

Plot 9: Comparison plots of the extrapolations of the Laplace transform smoothed Loss-ratio data function $[1/\widehat{D}(t)]$ computed using flowrate as the basis function versus time in four different plotting scales (*i.e.*, Cartesian, log-log, linear-log, log-linear scales).

This plot is similar to Plot 5 except that they are for $1/\widehat{D}(t)$ computed using flowrate data as the basis function.

Plot 10: Comparison plots of the extrapolations of the Laplace transform smoothed Loss-ratio data function $[1/\widehat{D}(t)]$ computed using the reciprocal of the flowrate as the basis function versus time in four different plotting scales (*i.e.*, Cartesian, log-log, linear-log, log-linear scales).

This plot is similar to Plot 5 except that they are for $1/\widehat{D}(t)$ computed using the reciprocal of flowrate data as the basis function.

We note that Plots 1, 3, and 7 use a "best fit" selected Stehfest "*n*" value to compute the Laplace transform smoothed functions.

All the plots for all field data cases are included in **Appendix E** of the thesis report.

Figs. E-1.1 to E-1.10 show the application of the Laplace transform method to Field Example 1. We observe that the Laplace transform approach is reasonably successful in applying to this data set. The smoothed rate function can follow the actual data trend very well. The Laplace transform smoothed *D*-parameter function is also on trend with the Bourdet derived *D*-parameter. However, the Laplace transform approach is superior as it contains less deviation during the late time interval. Similar to what we have seen in synthetic data case, the use of reciprocal of rate as the basis-function yield better results especially the smoothed *D* and *b*-parameters.

Figs. E-2.1 to E-2.10 show the application of the Laplace transform method to Field Example 2. **Fig E-2.3** shows that the Laplace transform approach produces $D(t)$ function with much less tail effect especially the one using the reciprocal of rate as the basis function. **Fig E-2.7** shows that the Laplace transform smoothed $b(t)$ function is not very accurate at late time, however, comparing to the Bourdet approach, the method is still more accurate. From this example case, we could recognize that even small deviation in the $D(t)$ function lead to large deviation in $b(t)$ function.

Figs. E-3.1 to E-3.10 show the application of the Laplace transform method to Field Example 3. **Figs. E-3.3 and E-3.4** show that the Laplace transform smoothed $D(t)$ function could detect the abrupt change in $D(t)$ function very well especially when using high Stehfest "*n*" parameter. **Fig E-3.7** is another example that illustrate the superiority of using the reciprocal of rate function over the rate function itself. The $b(t)$ function generated from using the reciprocal of rate is very accurate even at the late-time interval

while the $b(t)$ functions, which are computed using the Laplace transform approach with rate as the basis function and using the Bourdet approach with both low and high "L" parameters, contain large deviation at the late-time interval. The Stehfest "n" = 18 was selected in this case for the computation of $b(t)$ function because the original $D(t)$ function is quite oscillated and using high "n" value would help capturing those changes.

Figs. E-4.1 to E-4.10 show the application of the Laplace transform method to Field Example 4. The $D(t)$ functions computed in this case are all have similar accuracy (**Figs. E-4.3 and E-4.3**). However, the Laplace transform approach could still produce more accurate $b(t)$ function by using the reciprocal of rate function. The Laplace transform smoothed $b(t)$ function which computed using the rate function is on par with those computed form the Bourdet approach (**Figs. E-4.7 and E-4.8**).

To conclude, we have seen no issue producing the smoothed rate functions from the Laplace transform approach. However, we still observe "tail effects" in the computed $D(t)$ and $b(t)$ functions in all four field examples. In most cases, using the reciprocal of rate functions provides more satisfactory results compared to using the rate functions themselves.

5. SUMMARY, CONCLUSIONS, AND FUTURE WORK

5.1 Summary

We have developed and demonstrated the use of the Laplace transform to smooth, integrate, and differentiate time-rate data of the type used for production forecasting and reserves evaluation (using the *qDb* plot and the cumulative production plot). Specifically, we have adapted, combined, and summarized the Laplace transform algorithms originally proposed for the analysis of well test data by Roumboutsos and Stewart [1988], Bourgeois and Horne [1993], and Onur and Reynolds [1998] for use with discrete "time-rate" (production) data. All derivations for the Laplace transform expressions used in this study are summarized in **Appendix A** and **Appendix B**.

We developed a new workflow to apply the Laplace transform approach for the representation of long-term production data using piecewise data models. This Laplace transform-based workflow is used to provide smoothed rate, rate derivative, $D(t)$, $b(t)$, and cumulative production functions from a set of discrete time-rate data. Our approach includes:

- Selection of the data extrapolation models for early and late-time portions of the discrete data (required for the Laplace transform smoothing methodology),
- Determination of the extrapolating constants, and
- Selection of the "best-fit" Stehfest "n" parameter for numerical inversion.

The proposed workflow is specifically designed to be used with production rate and reciprocal rate data (the reciprocal rate function is used because it is an increasing function

and often has better Laplace transform characteristics than using the continuously decreasing rate function).

As an evaluation of our procedures, we used 5 years of synthetic time-rate data presented on a monthly basis as the *base case* for our sensitivity study, where these data were generated using the Arps [1945] exponential time-rate decline model. In our sensitivity study, we evaluate the effects of various factors — specifically: the data extrapolation model used for a given case, the data frequency/data spacing, duration of data, the magnitude of data noise, and type of data model used for a given scenario. In this work we found that the data extrapolation model had the most influence on the accuracy of the results. We also found (logically), that the less extrapolation we require (*i.e.*, the larger range of data we have), the more accurate the smoothed results will be.

From our scenario tests made using both synthetic and field data, the Laplace transform method has shown that it can produce more accurate (and smoother) rate derivative and cumulative production functions compared to the conventional approach proposed by Bourdet [1983]. We also compared the use of rate and reciprocal of rate as the basis-functions to generate the Laplace transform smoothed data functions and found the reciprocal of rate to be superior in the majority of cases. In summary, the data extrapolation model and Stehfest "*n*" parameter utilized in Laplace transform inversion process are the controlling factors for the proposed Laplace transform data smoothing methodology for "time-rate" data.

5.2 Conclusions

In this work we establish the following conclusions regarding the Laplace Transform method for processing time-rate data:

- The methodology does require some editing of the original time-rate data (selection and elimination of outliers, reduction to a manageable data set (*e.g.*, <1000 points), and possible "re-zeroing" of data which have operational features (*e.g.*, production shut-ins/restarts)).
- For synthetic cases with added random noise, the proposed Laplace Transform-based methodology performed exceptionally well — including those cases where derivatives are required (*e.g.*, the Arps *D*- and *b*- parameters as functions of time).
- The methodology does require care in the extrapolation formulations. Inappropriate extrapolations yield deviations in the resulting smoothed data functions (particularly during early and late-time periods, and we note that these are called "tail" or "endpoint" effects. As would be expected, the smoothed rate derivative functions are the most sensitive to the given extrapolation scheme.
- The straight-line extrapolation log-linear model appears to be the best overall extrapolation model for time-rate data. As for the reciprocal of rate data, the Cartesian and log-log straight-line extrapolation models appear to work equally well.

5.3 Recommendation for Future Work

- The proposed methodology does require significant computational effort (the nature of the Laplace transform process for discrete data), and while this work is essentially just "integration," the size of a given dataset does present challenges for our present implementation of this methodology. We believe it prudent to suggest that future work consider methods to manage very large to extremely large datasets (*e.g.*, hundreds of thousands to tens of millions of data points). While this is not "practical" in the sense

that most flowrates are reported hourly or daily, we envision a future where rates can and will be reported on at a sampling rate of a few seconds.

- Although not used in this implementation, we can envision the use of "pre-smoothing" methods as well as "regularization" techniques for ensuring the robustness of the Laplace transformed data functions. Such functions would be "smoother" and "stiffer," and potentially yield less detail in the computed data functions, but we recommend testing of such methods.
- Lastly, we recommend consideration of other inversion techniques beyond the "Gaver-Stehfest" and other such "sampling" algorithms for the numerical inversion of the Laplace transform function. We believe that there may be additional benefit from using more rigorous numerical inversion schemes, and recommend pursuing such tasks.

NOMENCLATURE

t = Time, days

$f(t)$ = Time function

$\mathcal{L}$ = Laplace transform operator

$\mathcal{L}^{-1}$ = Inverse of Laplace transform operator

$\overline{f}(s)$ = Laplace transform of $f(t)$

s = Laplace variable, 1/day

$q(t)$ = Rate function, MSCF/D for gas (STB/D for oil)

$\overline{q}(s)$ = Laplace Transform of rate function

$u(t)$ = Reciprocal of rate function, $[\text{MSCF/D}]^{-1}$ for gas ($[\text{STB/D}]^{-1}$ for oil)

$\overline{u}(s)$ = Laplace Transform of reciprocal of rate function

$p(t)$ = Pressure function, psi

$\overline{p}(s)$ = Laplace Transform of pressure function

$Q(t)$ = Cumulative production function, MSCF for gas (STB for oil)

D = Reciprocal of loss ratio, 1/day

b = Loss ratio derivative, dimensionless

n = Parameter in the Stehfest inversion algorithm, dimensionless

f_i = Functional value at time t_i

L = Smoothing parameter in Bourdet differentiation algorithm

m_i = Straight-line cord slope from interval t_{i-1} to t_i

m_{ext} = Slope of the right-hand side extrapolated lines

β = Slope of straight-line on Log-Log and Log-Linear scales

α = Intercept of straight-line on Log-Log and Log-Linear scales

γ = First Incomplete Gamma function

Γ = Gamma function, second Incomplete Gamma function

N = Total number of discrete data points

$\hat{q}(t)$ = Laplace transform smoothed rate function

$\hat{Q}(t)$ = Laplace transform smoothed cumulative function

$\hat{q}'(t)$ = Laplace transform smoothed rate derivative function

$\hat{D}(t)$ = Laplace transform smoothed *D*-parameter function

$\hat{b}(t)$ = Laplace transform smoothed *b*-parameter function

REFERENCES

Al-Ajmi, N. M., Ahmadi, M., Ozkan, E. et al. 2008. Numerical Inversion of Laplace Transforms in the Solution of Transient Flow Problems With Discontinuities. Presented at the SPE Annual Technical Conference and Exhibition, Denver, Colorado, USA. doi:10.2118/116255-MS

Blasingame, T.A. 1994. Math Lecture 5 - The Laplace Transform, Class Notes PETE 620, College Station, TX, Texas A&M University. http://www.pe.tamu.edu/blasingame/data/z_zCourse_Archive/P620_16C/P620_16C_Lectures_(base)/P620_Lec_05_Mod1_ML_05_LaplaceTrans.pdf

Ahmadi, M., Gonzalez, O. G., Ozkan, E. et al. 2012. Improving Well-Performance-Data Analysis in Laplace Space by Using Cubic Splines and Boundary Mirroring. Presented at the SPE Annual Technical Conference and Exhibition, San Antonio, Texas, USA. doi:10.2118/159734-MS

Ahmadi, M., Sartipizadeh, H., and Ozkan, E. 2017. A new pressure-rate deconvolution algorithm based on Laplace transformation and its application to measured well responses. Journal of Petroleum Science and Engineering 157: 68-80. https://doi.org/10.1016/j.petrol.2017.06.060

Al-Ajmi, N. M., Ahmadi, M., Ozkan, E. et al. 2008. Numerical Inversion of Laplace Transforms in the Solution of Transient Flow Problems With Discontinuities. Presented at the SPE Annual Technical Conference and Exhibition, Denver, Colorado, USA. doi:10.2118/116255-MS

Arps, J. J. 1945. Analysis of Decline Curves. doi:10.2118/945228-G

Bourdet, D., Ayoub, J. A., and Pirard, Y. M. 1989. Use of Pressure Derivative in Well Test Interpretation. doi:10.2118/12777-PA

Bourgeois, M. and Horne, R. N. 1993. Well Test Model Recognition Using Laplace Space Type Curves. doi:10.2118/22682-PA

Clark, A. J., Lake, L. W., and Patzek, T. W. 2011. Production Forecasting with Logistic Growth Models. Presented at the SPE Annual Technical Conference and Exhibition, Denver, Colorado, USA. doi:10.2118/144790-MS

Duong, A. N. 2011. Rate-Decline Analysis for Fracture-Dominated Shale Reservoirs. SPE Reservoir Evaluation and Engineering 14 (03): 377-387. doi:10.2118/137748-PA

Collins, P., Ilk, D., and Blasingame, T. A. 2014. Practical Considerations for Forecasting Production Data in Unconventional Reservoirs — Variable Pressure Drop Case. Presented at the SPE Annual Technical Conference and Exhibition, Amsterdam, The Netherlands. doi:10.2118/170945-MS

Fetkovich, M. J., Bradley, M. D., Works, A. M. et al. 1990. Depletion Performance of Layered Reservoirs Without Crossflow. SPE Formation Evaluation 5 (03): 310-318. doi:10.2118/18266-PA.

Fetkovich, M. J., Fetkovich, E. J., and Fetkovich, M. D. 1996. Useful Concepts for Decline Curve Forecasting, Reserve Estimation, and Analysis. SPE Reservoir Engineering 11 (01): 13-22. doi:10.2118/28628-PA

Guillot, A. Y. and Horne, R. N. 1986. Using Simultaneous Downhole Flow-Rate and Pressure Measurements To Improve Analysis of Well Tests. SPE Formation Evaluation 1 (03): 217-226. doi:10.2118/12958-PA

Ilk, D., Rushing, J. A., Perego, A. D. et al. 2008. Exponential vs. Hyperbolic Decline in Tight Gas Sands: Understanding the Origin and Implications for Reserve Estimates Using Arps' Decline Curves. Presented at the SPE Annual Technical Conference and Exhibition, Denver, Colorado, USA. doi:10.2118/116731-MS

Johnson, R. H. and Bollens, A. L. 1927. The Loss Ratio Method of Extrapolating Oil Well Decline Curves. doi:10.2118/927771-

Kucuk, F. and Ayestaran, L. 1985. Analysis of Simultaneously Measured Pressure and Sandface Flow Rate in Transient Well Testing (includes associated papers 13937 and 14693). doi:10.2118/12177-PA

Lee, W. J. and Sidle, R. E. 2010. Gas Reserves Estimation in Resource Plays. Presented at the SPE Unconventional Gas Conference, Pittsburgh, Pennsylvania, USA. doi:10.2118/130102-MS

Mattar, L. 2008. Production Analysis and Forecasting of Shale Gas Reservoirs: Case History-Based Approach. Presented at the SPE Shale Gas Production Conference, Fort Worth, Texas, USA. doi:10.2118/119897-MS

Mireles, T. J. and Blasingame, T. A. 2003. Application of Convolution Theory for Solving Non-Linear Flow Problems: Gas Flow Systems. Presented at the SPE Annual Technical Conference and Exhibition, Denver, Colorado. doi:10.2118/84073-MS

Okouma Mangha, V., Ilk, D., Blasingame, T. A. et al. 2012. Practical Considerations for Decline Curve Analysis in Unconventional Reservoirs - Application of Recently Developed Rate-Time Relations. Presented at the SPE Hydrocarbon

Economics and Evaluation Symposium, Calgary, Alberta, Canada. doi:10.2118/162910-MS

Onur, M. and Reynolds, A. C. 1998. Well Testing Applications of Numerical Laplace Transformation of Sampled-Data. doi:10.2118/36554-PA

Roumboutsos, A. and Stewart, G. 1988. A Direct Deconvolution or Convolution Algorithm for Well Test Analysis. Society of Petroleum Engineers. doi:10.2118/18157-MS

Rushing, J. A., Perego, A. D., Sullivan, R. et al. 2007. Estimating Reserves in Tight Gas Sands at HP/HT Reservoir Conditions: Use and Misuse of an Arps Decline Curve Methodology. Presented at the SPE Annual Technical Conference and Exhibition, Anaheim, California, U.S.A. doi:10.2118/109625-MS.

Stehfest, H. 1970. Numerical Inversion of Laplace Transforms. Communications, ACM 13 (1): 47-49

Yu, S. 2013. Best Practice of Using Empirical Methods for Production Forecast and EUR Estimation in Tight/Shale Gas Reservoirs. Presented at the SPE Unconventional Resources Conference — Canada, Calgary, AB, Canada. doi:10.2118/167118-MS

APPENDIX A

DERIVATION OF THE EXPRESSIONS FOR NUMERICAL LAPLACE TRANSFORM OF DISCRETE DATA

A.1 Introduction

We are to derive and summarize the expressions for numerical Laplace transform of discrete data using several types of data approximation techniques. Some data approximation techniques have been proposed elsewhere, however, for the sake of completeness; we re-derived and presented them here. We start with the Laplace transform definition which is

$$\mathcal{L}\{f(t)\} = \overline{f}(s) = \int_0^\infty f(t)e^{-st}dt \quad \text{..... (A-1)}$$

According to Eq. A-1, the knowledge of the function being transformed over the semi-infinite time interval, $0 \le t \le \infty$, is required in the computation of the Laplace transform. However, generally for the case of discrete data, a finite interval of data is known from t_1. to t_N. As a result, extrapolations of data are required from t_1. to t_0 and from t_N. to ∞ in order to represent the functional values outside the discrete data interval. Thus, a simple and straightforward way to derive the Laplace transform expressions would be to separate the integral in Eq. A-1 into three integral terms as shown in Eq. A-2.

$$\overline{f}(s) = \int_{t_0=0}^{t_1} f(t)e^{-st}dt + \int_{t_1}^{t_N} f(t)e^{-st}dt + \int_{t_N}^{\infty} f(t)e^{-st}dt \quad \text{..... (A-2)}$$

We named the three integral parts in Eq. A-2 as P1, P2, and P3 respectively from the left to the right.

$$\overline{f}(s) = P_1 + P_2 + P_3 \quad \text{..... (A-3)}$$

To clarify, P_1, P_2, and P_3 can be defined as below.

P_1: The Laplace transform integral of the extrapolated function from $t_0 = 0$ to t_1

P_2: The Laplace transform integral of the interpolated function approximating the discrete data from t_1 to t_N

P_3: The Laplace transform integral of the extrapolated function from t_N to ∞

For P_2 computation, we used two types of data functions to approximate the discrete data from t_1 to t_N. Those are a piecewise linear data function and a piecewise log-linear data function. For P_1 and P_3 computation, several strategies have been discussed in the literature such as those in Roumboutsos and Stewart [1988], Bourgeois and Horne [1993], and Onur and Reynolds [1998]. We studied those strategies and came up with a generalized technique using straight-line extrapolations on four different plotting scales, i.e. Cartesian, log-log, linear-log, and log-linear scales. Tables A-1, A-2, and A-3 summarize the Laplace transform expressions using these data approximation and extrapolation techniques as a discrete data representation. As we will be using these equations with time-rate discrete data function, all equations summarized in the tables are for positive functions. If not specifically mentioned, they could be used for both increasing and decreasing positive functions.

Table A-1 — The expressions for P_1 using various types of extrapolating functions

Extrapolating Functions	**Expressions**	**Equations**
Straight Line on Cartesian Scale	$P_1 = \frac{1}{s}\left(f_0 - f_1 e^{-st_1}\right) + \frac{1}{s^2} m_1 (1 - e^{-st_1})$	(A-16)
Straight Line on Log-Log Scale	Increasing Data Function $P_1 = \frac{\alpha_1}{s^{\upsilon_1}} \gamma(\upsilon_1, st_1)$ Only valid for $\upsilon_1 > 0$ which corresponds to $\beta_1 > -1$	(A-46)
Straight Line on Log-Linear Scale	$P_1 = \frac{\alpha_1}{\beta_1 - s}[e^{(\beta_1 - s)t_1} - 1]$ For $s \neq \beta_1$	(A-84)

Table A-2 — The expressions for P_2 using various types of approximating functions

Approximating Functions	**Expressions**	**Equations**
Piecewise Linear Data Function	$P_2 = \frac{1}{s}\left(f_1 e^{-st_1} - f_N e^{-st_N}\right) + \frac{1}{s^2}\sum_{i=2}^{N} m_i (e^{-st_{i-1}} - e^{-st_i})$	(A-14)
Piecewise Log-Linear Data Function	Increasing Data Function $P_2 = \sum_{i=2}^{N} \frac{\alpha_i}{s^{\upsilon_i}}[\gamma(\upsilon_i, st_i) - \gamma(\upsilon_i, st_{i-1})]$ Only valid for $\upsilon_i > 0$ which corresponds to $\beta_i > -1$	(A-42)

Table A-3 — The expressions for P_3 using various types of extrapolating functions

Extrapolating Functions	**Expressions**	**Equations**
Straight Line on Cartesian Scale	Decreasing Data Function $P_3 = \frac{1}{s} f_N e^{-st_N} + \frac{1}{s^2} m_{ext} e^{-st_N} (1 - e^{sf_N / m_{ext}})$ Increasing Data Function $P_3 = \frac{1}{s} f_N e^{-st_N} + \frac{1}{s^2} m_{ext} e^{-st_N}$	(A-22) (A-17)
Straight Line on Log-Log Scale	Increasing Data Function $P_3 = \frac{\alpha_{ext}}{s^{\upsilon_{ext}}} [\Gamma(\upsilon_{ext}) - \gamma(\upsilon_{ext}, st_N)]$ Only valid for $\upsilon_{ext} > 0$ which corresponds to $\beta_{ext} > -1$	(A-51)
Straight Line on Linear-Log Scale	Decreasing Data Function $t_{N+1} = t_N e^{-f_N / m_{ext}}$ $P_3 = \frac{f_N}{s} e^{-st_N} + \frac{m_{ext}}{s} [E_i(-st_{N+1}) - E_i(-st_N)]$ Increasing Data Function $P_3 = \frac{f_N}{s} e^{-st_N} - \frac{m_{ext}}{s} E_i(-st_N)$	(A-69) (A-80) (A-67)
Straight Line on Log-Linear Scale	Decreasing Data Function $P_3 = \frac{f_N}{s - \beta_{ext}} e^{-st_N}$ For $s > \beta_{ext}$	(A-88)

A.2 Derivation of the Laplace Transform Expression Using a Piecewise Linear Data Approximation

We are to derive an expression for the numerical Laplace transform of discrete data using a piecewise linear data approximation. This strategy was proposed by Roumboutsos and Stewart [1988] where the entire function in the semi-infinite domain will be approximated and represented by several connected straight-line cords, consequently, they could be transformed into the Laplace domain analytically.

First, we are recalling the Laplace transform definition for discrete data from Eq. A-2.

$$\overline{f}(s) = \int_{t_0=0}^{t_1} f(t)e^{-st}dt + \int_{t_1}^{t_N} f(t)e^{-st}dt + \int_{t_N}^{\infty} f(t)e^{-st}dt \quad \text{..... (A-2)}$$

From Eq. A-2, we can see that we need the knowledge of $f(t)$ from three data intervals. The first and the third terms requires the knowledge of the function from $t_0 = 0$ to t_1 and from t_N to infinity, respectively. We are using straight-line extrapolations to represent the function in those intervals. For the second term, the functional value of discrete data from t_1 to t_N will be approximated by a piecewise linear data function. To elaborate, the data function will be represented by several cords between the specified knot points ($t_1, t_2, t_3, ..., t_N$). Each cord is a straight line with a slope of m_i where each m_i represents the slope of the function from t_{i-1} to t_i. The backward difference approach will be used to compute each m_i as shown in Eq. A-4.

$$m_i = \frac{f_i - f_{i-1}}{t_i - t_{i-1}} \quad ; i = 2,...,N \quad \text{..... (A-4)}$$

where

$$f_i = f(t_i) \quad ; i = 1,2,...,N$$

By rearranging Eq. A-4, we can determine the straight-line function between two knot-points from time t_{i-1} to t_i ,which is represented by $f_i(t)$, as in Eq. A-5. in

$$f_i(t) = f_{i-1} + m_i(t - t_{i-1}) \quad ; i = 2,...,N \text{ and } t_{i-1} \le t \le t_i \quad \text{..... (A-5)}$$

Eq. A-5 serves as an approximating function of discrete data from t_1 to t_N

Similarly, the functional value from $t_0 = 0$ to t_1 can also be represented by Eq. A-5 using $i = 1$ as shown in Eq. A-6.

$$f_1(t) = f_0 + m_1(t - t_0) \quad ; t_0 \le t \le t_1 \qquad \text{(A-6)}$$

For the time interval t_N to infinity, we name the straight-line slope and function as m_{ext} and $f_{N+1}(t)$, respectively. The function can be expressed as

$$f_{N+1}(t) = f_N + m_{ext}(t - t_N) \quad ; t_N \le t \le t_{N+1} \qquad \text{(A-7)}$$

The constant m_1 and m_{ext} in Eq. A-6 and A-7 can be obtained from the least-square fittings of the last few data points from both ends of discrete data. It is noted that in Eq. A-7 the infinite time is represented by t_{N+1} to make the equation generic. In general, t_{N+1} only represents the infinite time, however, we are also deriving a case for decreasing rate data function where negative value is not allowed which makes t_{N+1} less than infinity. The detail will be discussed later.

By combining all three approximating functions from Eqs. A-5, A-6, and A-7, we obtain a piecewise linear approximating function used to represent our discrete data set which is

$$f(t) = \sum_{i=1}^{N+1} f_i(t) = f_1(t) + \sum_{i=2}^{N} f_i(t) + f_{N+1}(t) \qquad \text{(A-8)}$$

Taking the Laplace transform on both sides of Eq. A-8 and using linearity property of the Laplace transform, we have

$$\mathcal{L}\{f(t)\} = \mathcal{L}\left\{\sum_{i=1}^{N+1} f_i(t)\right\} = \mathcal{L}\{f_1(t)\} + \mathcal{L}\left\{\sum_{i=2}^{N} f_i(t)\right\} + \mathcal{L}\{f_{N+1}(t)\} \qquad \text{(A-9)}$$

which can be rewritten as

$$\overline{f}(s) = \sum_{i=1}^{N+1} \overline{f_i}(s) = \overline{f_1}(s) + \sum_{i=2}^{N} \overline{f_i}(s) + \overline{f_{N+1}}(s) \qquad \text{(A-10)}$$

where

$$\overline{f}(s) = \mathcal{L}\{f(t)\} \quad \text{And} \quad \overline{f_i}(s) = \mathcal{L}\{f_i(t)\}$$

Next, we are determining $\overline{f_i}(s)$ which is the Laplace transform of each straight-line cord.

First, we take the Laplace transform of Eq. A-5 which also serves as the general form of Eq. A-6 and Eq. A-7, we get

$$\overline{f_i}(s) = \int_{t_{i-1}}^{t_i} [f_{i-1} + m_i(t_i - t_{i-1})]e^{-st}dt \quad \text{(A-11)}$$

Integrating the right-hand side of Eq. A-11, we get

$$\overline{f_i}(s) = \frac{1}{s}\left(f_{i-1}e^{-st_{i-1}} - f_i e^{-st_i}\right) + \frac{1}{s^2}m_i(e^{-st_{i-1}} - e^{-st_i}) \quad \text{(A-12)}$$

Recalling another form of $\overline{f}(s)$ from Eq. A-3 which is

$$\overline{f}(s) = P_1 + P_2 + P_3 \quad \text{(A-3)}$$

We know that P_1, P_2, and P_3 are equivalent to $\overline{f_1}(s)$, $\sum_{i=2}^{N}\overline{f_i}(s)$, $\overline{f_{N+1}}(s)$ in Eq. A-10, respectively. Therefore, using the relation in Eq. A-12, we can derive P_1, P_2, and P_3 as in Eqs. A-13, A-14, and A-15, respectively.

$$P_1 = \overline{f_1}(s) = \frac{1}{s}\left(f_0 e^{-st_0} - f_1 e^{-st_1}\right) + \frac{1}{s^2}m_1(e^{-st_0} - e^{-st_1}) \quad \text{(A-13)}$$

$$P_2 = \sum_{i=2}^{N}\overline{f_i}(s) = \frac{1}{s}\left(f_1 e^{-st_1} - f_N e^{-st_N}\right) + \frac{1}{s^2}\sum_{i=2}^{N}m_i(e^{-st_{i-1}} - e^{-st_i}) \quad \text{(A-14)}$$

$$P_3 = \overline{f_{N+1}}(s) = \frac{1}{s}\left(f_N e^{-st_N} - f_{N+1}e^{-st_{N+1}}\right) + \frac{1}{s^2}m_{ext}(e^{-st_N} - e^{-st_{N+1}}) \quad \text{(A-15)}$$

The first term on the right-hand side of Eq. A-14 is the result of cancelling out the repetitive terms when the summation term is expanded.

Since $t_0 = 0$, Eq. A-13 becomes

$$P_1 = \overline{f_1}(s) = \frac{1}{s}\left(f_0 - f_1 e^{-st_1}\right) + \frac{1}{s^2} m_1 (1 - e^{-st_1}) \quad \text{..... (A-16)}$$

And since $t_{N+1} = \infty$, the exponential terms with t_{N+1} in Eq. A-15 becomes zero, thus Eqs. A-15 becomes

$$P_3 = \overline{f_{N+1}}(s) = \frac{1}{s} f_N e^{-st_N} + \frac{1}{s^2} m_{ext} e^{-st_N} \quad \text{..... (A-17)}$$

Combining Eqs. A-14, A-16, and A-17 and rearranging, we have derived the expression for the numerical Laplace transform of discrete data using a piecewise linear data function, similar to what presented in Roumboutsos and Stewart [1988]. The expression is shown in Eq. A-18.

$$\overline{f}(s) = \frac{f_0}{s} + \frac{1}{s^2} \sum_{i=1}^{N} m_i (e^{-st_{i-1}} - e^{-st_i}) + \frac{1}{s^2} m_{ext} e^{-st_N} \quad \text{..... (A-18)}$$

The main difference from R&S's equation is that they assumed $f_0 = 0$ and thus the first term in Eq. A-18 is eliminated. The zero initial-value assumption makes sense if we take the Laplace transform of pressure drop function which always starts at zero. However, we would like to leave Eq. A-18 in generic form thus it could be applied to broader range of data type, e.g. decreasing discrete time-rate data function. In our case, f_0 is an unknown value. It will be obtained from the equation of the left-hand side extrapolation.

Moreover, we also have further modification to the R&S's equation to be used specifically for time-rate discrete data. When a time-rate data is being transformed, the right-hand side extrapolation should stop at $f(t_{N+1}) = 0$ to reflect the true nature of rate functions which could not be negative values. The functional value after this point is assigned to be zero. To determine t_{N+1} at which $f(t_{N+1}) = 0$, we firstly recall the relation of the straight-line slope in Eq. A-4, we have

$$m_i = \frac{f_i - f_{i-1}}{t_i - t_{i-1}} \quad ; i = 2,...,N \quad \text{..... (A-4)}$$

Applying Eq. A-4 using $i = N+1$ for the right-hand side extrapolation interval, we can derive the equation for the extrapolating slope on the R.H.S of data as

$$m_{ext} = \frac{f_{N+1} - f_N}{t_{N+1} - t_N} \quad \text{..... (A-19)}$$

Rearranging Eq. A-19 and substituting $f_{N+1} = 0$, we can determine the time at which the rate function reduces to zero which is

$$t_{N+1} = t_N - \frac{f_N}{m_{ext}} \quad \text{..... (A-20)}$$

Substituting t_{N+1} from Eq. A-20 and $f_{N+1} = 0$ into Eq. A-15, we have

$$P_3 = \frac{1}{s}\left(f_N e^{-st_N}\right) + \frac{1}{s^2} m_{ext}\left(e^{-st_N} - e^{-st_N + s\frac{f_N}{m_{ext}}}\right) \quad \text{..... (A-21)}$$

Rearranging, we have

$$P_3 = \frac{1}{s} f_N e^{-st_N} + \frac{1}{s^2} m_{ext} e^{-st_N}\left(1 - e^{sf_N/m_{ext}}\right) \quad \text{..... (A-22)}$$

Hence, by assuming that the extrapolation tail stops at zero, the Laplace transform expression for decreasing discrete data becomes

$$\overline{f}(s) = \frac{f_0}{s} + \frac{1}{s^2}\sum_{i=1}^{N} m_i\left(e^{-st_{i-1}} - e^{-st_i}\right) + \frac{1}{s^2} m_{ext} e^{-st_N}\left(1 - e^{\frac{sf_N}{m_{ext}}}\right) \quad \text{..... (A-23)}$$

A.3 Derivation of the Laplace Transform Expression Using a Piecewise Log-Linear Data Approximation

We are to develop the Laplace transform expression of discrete data using a piecewise log-linear data approximation. In this approach, the discrete data function will be represented by cords between the specified knot points. Each cord is a straight line in the log-log scale with a slope of β_i computed from an expression in Eq. A-24 where β_i represents the slope from time t_{i-1} to t_i.

$$\beta_i = \frac{\ln(f_i / f_{i-1})}{\ln(t_i / t_{i-1})} \quad \text{(A-24)}$$

where

$$f_i = f(t_i)$$

Rearranging Eq. A-24, we have

$$\ln(f_{i-1}) = \ln(f_i) - \ln(t_i^{\beta_i}) + \ln(t_{i-1}^{\beta_i}) \quad \text{(A-25)}$$

By letting $t_{i-1} = 1$ and replacing f_{i-1} with a constant α_i, we get

$$\ln(\alpha_i) = \ln(f_i) - \ln(t_i^{\beta_i}) \quad \text{(A-26)}$$

Exponentiating both sides, we get

$$\alpha_i = \frac{f_i}{t_i^{\beta_i}} \quad \text{(A-27)}$$

We can now compute an α_i from Eq. A-27.

Next, we are considering Eq. A-26 which can be rearranged as

$$\ln(f_i) = \beta_i \ln(t_i) + \ln(\alpha_i) \quad \text{(A-28)}$$

Eq. A-28 is in a form of straight-line equation having β_i and $\ln(\alpha_i)$ as the slope and the intercept, respectively. Since, these two constants computed from f_i and f_{i-1}, they could be used for the constants for the function between time t_{i-1} to t_i. The function could be written as

$$\ln(f_i(t)) = \beta_i \ln(t) + \ln(\alpha_i) \quad ; t_{i-1} \le t \le t_i \quad \text{..... (A-28)}$$

Exponentiating both sides, we can obtain $f_i(t)$ which is the function between two knot-points from time t_{i-1} to t_i as shown in Eq. A-29.

$$f_i(t) = \alpha_i t^{\beta_i} = \alpha_i t^{\upsilon_i - 1} \quad ; t_{i-1} \le t \le t_i \quad \text{..... (A-29)}$$

Taking the Laplace transform of Eq. A-29, we can have the Laplace transform of each cord, $\overline{f}_i(s)$, as

$$\overline{f}_i(s) = \alpha_i \int_{t_{i-1}}^{t_i} [t^{\upsilon_i - 1}] e^{-st} dt \quad \text{..... (A-30)}$$

Considering the limits in Eq. A-30 as well as arbitrary integrand, $I(t) = t^{\upsilon_i - 1} e^{-st}$, we can rewrite the integral in Eq. A-30 as

$$\int_{t_{i-1}}^{t_i} I(t)dt = \int_0^{\infty} I(t)dt - \int_{t_i}^{\infty} I(t)dt - \int_0^{t_{i-1}} I(t)dt \quad \text{..... (A-31)}$$

From Gradshteyn& Ryzhik, using the integral definition of the Gamma function, we have

$$\int_0^{\infty} t^{\upsilon_i - 1} e^{-st} dt = s^{-\upsilon_i} \Gamma(\upsilon_i) \quad \text{..... (A-32)}$$

$$\int_{t_i}^{\infty} t^{\upsilon_i - 1} e^{-st} dt = s^{-\upsilon_i} \Gamma(\upsilon_i, st_i) \quad \text{..... (A-33)}$$

$$\int_0^{t_{i-1}} t^{\upsilon_i - 1} e^{-st} dt = s^{-\upsilon_i} \gamma(\upsilon_i, st_{i-1}) \quad \text{..... (A-34)}$$

It is important to note that, since we use the integral definition of the Gamma function to derive above three relations, they are only valid for $\upsilon_i > 0$ which corresponds to $\beta_i > -1$.

Substituting Eqs. A-32, A-33, and A-34 into Eq. A-31, we get

$$\int_{t_{i-1}}^{t_i} I(t)dt = s^{-\upsilon_i}[\Gamma(\upsilon_i) - \Gamma(\upsilon_i, st_i) - \gamma(\upsilon_i, st_{i-1})] \quad \text{(A-35)}$$

Substituting Eq. A-35 into Eq. A-30, we obtain

$$\overline{f_i}(s) = \frac{\alpha_i}{s^{\upsilon_i}}[\Gamma(\upsilon_i) - \Gamma(\upsilon_i, st_i) - \gamma(\upsilon_i, st_{i-1})] \quad \text{(A-36)}$$

The functions given in Eq. A-36 are

$$\Gamma(v) = \int_0^\infty e^{-t}t^{v-1}dt \quad \text{is the Gamma function} \quad \text{(A-37)}$$

$$\gamma(v,z) = \sum_{n=0}^{\infty}(-1)^n \frac{z^{v+n}}{n!(v+n)} \quad \text{is the first Incomplete Gamma function} \quad \text{(A-38)}$$

$$\Gamma(v,z) = \Gamma(v) - \gamma(v,z) = \int_z^\infty e^{-t}t^{v-1}dt \quad \text{is the second Incomplete Gamma function} \quad \text{(A-39)}$$

Using the relation in Eq. A-39, Eq. A-36 becomes

$$\overline{f_i}(s) = \frac{\alpha_i}{s^{\upsilon_i}}[\gamma(\upsilon_i, st_i) - \gamma(\upsilon_i, st_{i-1})] \quad \text{(A-40)}$$

Next, we are recalling Eqs. A-3 and A-10 which are the expressions for the numerical Laplace transform of discrete data using a piecewise function.

$$\overline{f}(s) = P_1 + P_2 + P_3 \quad \text{(A-3)}$$

$$\overline{f}(s)=\sum_{i=1}^{N+1}\overline{f_i}(s)=\overline{f_1}(s)+\sum_{i=2}^{N}\overline{f_i}(s)+\overline{f_{N+1}}(s) \quad \text{(A-10)}$$

where

$$\overline{f}(s)=\mathcal{L}\{f(t)\} \quad \text{And} \quad \overline{f_i}(s)=\mathcal{L}\{f_i(t)\}$$

From Eqs. A-3, A-10, and A-40, we can obtain P_1, P_2, and P_3 as shown in Eqs. A-41, A-42, and A-43, respectively.

$$P_1=\overline{f_1}(s)=\frac{\alpha_1}{s^{\upsilon_1}}[\gamma(\upsilon_1,st_1)-\gamma(\upsilon_1,st_0)] \quad \text{(A-41)}$$

$$P_2=\sum_{i=2}^{N}\overline{f_i}(s)=\sum_{i=2}^{N}\frac{\alpha_i}{s^{\upsilon_i}}[\gamma(\upsilon_i,st_i)-\gamma(\upsilon_i,st_{i-1})] \quad \text{(A-42)}$$

$$P_3=\overline{f_{N+1}}(s)=\frac{\alpha_{ext}}{s^{\upsilon_{ext}}}[\gamma(\upsilon_{ext},st_{N+1})-\gamma(\upsilon_{ext},st_N)] \quad \text{(A-43)}$$

Since $t_0=0$, Eq. A-41 becomes

$$P_1=\frac{\alpha_1}{s^{\upsilon_1}}[\gamma(\upsilon_1,st_1)-\gamma(\upsilon_1,0)] \quad \text{(A-44)}$$

Using the definition of the first incomplete Gamma function in Eq. A-38, we have

$$\gamma(\upsilon_1,0)=0 \quad \text{(A-45)}$$

Substituting into Eq. A-44, we have

$$P_1=\frac{\alpha_1}{s^{\upsilon_1}}\gamma(\upsilon_1,st_1) \quad \text{(A-46)}$$

Since $t_{N+1}=\infty$, Eq. A-43 becomes

$$P_3=\frac{\alpha_{ext}}{s^{\upsilon_{ext}}}[\gamma(\upsilon_{ext},\infty)-\gamma(\upsilon_{ext},st_N)] \quad \text{(A-47)}$$

From the relation in Eq. A-39, we can change the first incomplete Gamma function to the second incomplete Gamma function. Eq. A-47 becomes

$$\begin{aligned} P_3 &= \frac{\alpha_{ext}}{s^{\upsilon_{ext}}}[\Gamma(\upsilon_{ext}) - \Gamma(\upsilon_{ext},\infty) - \Gamma(\upsilon_{ext}) + \Gamma(\upsilon_{ext},st_N)] \\ &= \frac{\alpha_{ext}}{s^{\upsilon_{ext}}}[\Gamma(\upsilon_{ext},st_N) - \Gamma(\upsilon_{ext},\infty)] \end{aligned} \quad \text{..... (A-48)}$$

From the definition of the second incomplete Gamma function in Eq. A-39, we have

$$\Gamma(\upsilon_{ext},\infty) = 0 \quad \text{..... (A-49)}$$

Substituting into Eq. A-48, we have

$$P_3 = \frac{\alpha_{ext}}{s^{\upsilon_{ext}}}\Gamma(\upsilon_{ext},st_N) \quad \text{..... (A-50)}$$

Which is equivalent to

$$P_3 = \frac{\alpha_{ext}}{s^{\upsilon_{ext}}}[\Gamma(\upsilon_{ext}) - \gamma(\upsilon_{ext},st_N)] \quad \text{..... (A-51)}$$

In conclusion, we can derive P_1, P_2, and P_3 as shown in Eqs. A-46, A-42, and A-51, respectively.

By combining three parts, we get the expression for the numerical Laplace transform of discrete data using a piecewise log-linear data function.

$$\overline{f}(s) = \frac{\alpha_1}{s^{\upsilon_1}}\gamma(\upsilon_1,st_1) + \sum_{i=2}^{N}\frac{\alpha_i}{s^{\upsilon_i}}[\gamma(\upsilon_i,st_i) - \gamma(\upsilon_i,st_{i-1})] + \frac{\alpha_{ext}}{s^{\upsilon_{ext}}}[\Gamma(\upsilon_{ext}) - \gamma(\upsilon_{ext},st_N)] \quad \text{..... (A-52)}$$

As mentioned earlier, the expression in Eq. A-52 is only valid for the case where υ_1, υ_i, and $\upsilon_{ext} > 0$. In other words, the log-linear slope, β_1, β_i, and β_{ext}, must be more than -1. To avoid violating this limitation, we limit the use of Eq. A-52 only for increasing data function where only positive log-linear slopes are expected, e.g. the reciprocal of discrete time-rate data. However, even with the reciprocal of rate function where the overall data trend increases with time and that

β_1 and β_{ext} are certainly positive values, there is still a possibility that some β_i can be negative and less than -1. Thus, we propose to obtain P_2 only from the piecewise linear approach.

We can obtain the expression which uses a piecewise linear data function to approximate the discrete data from t_1 to t_N .and a piecewise log-linear data function for the extrapolated intervals by combining three parts from Eqs. A-46, A-14, and A-51 for P_1, P_2 and P_3 respectively. The expression is shown below.

$$\overline{f}(s) = \frac{\alpha_1}{s^{\upsilon_1}}\gamma(\upsilon_1, st_1) + \frac{1}{s}\left(f_1 e^{-st_1} - f_N e^{-st_N}\right) + \frac{1}{s^2}\sum_{i=2}^{N} m_i (e^{-st_{i-1}} - e^{-st_i}) + \frac{\alpha_{ext}}{s^{\upsilon_{ext}}}[\Gamma(\upsilon_{ext}) - \gamma(\upsilon_{ext}, st_N)] \quad \text{..... (A-53)}$$

A.4 Derivation of the Laplace Transform Expressions of the Extrapolation Functions

In this research work, we use four different types of extrapolation functions. In the previous sections, we have already derived the Laplace transform expressions for two types which are straight-line extrapolations on Cartesian and log-log scales. In this section, we are restating P_1 and P_3 from those derivations and deriving the expressions for the remaining types which are straight-line extrapolations on linear-log and log-linear scales. The governing equations for the straight-line extrapolations on four plotting scales are summarized below.

- Cartesian plot

$$f(t) = mt + c \quad \text{..... (A-54)}$$

- Log-log plot

$$\ln(f(t)) = \beta \ln(t) + \ln(\alpha) \quad \text{..... (A-55)}$$

- Linear-log plot (the abscissa axis (x-axis) is scaled logarithmically)

$$f(t) = m \ln(t) + c \quad \text{..... (A-56)}$$

- Log-linear plot (the ordinate axis (y-axis) is scaled logarithmically)

$$\ln(f(t)) = \beta t + \ln(\alpha) \quad \text{..... (A-57)}$$

It is noted that the constants in each model can be determined by least-square straight-line fittings using first few data points on both ends of the discrete dataset.

A.4.1 Straight-Line Extrapolation on a Cartesian Scale

For the Cartesian straight-line extrapolation, the P_1 and P_3 expressions were provided earlier as shown in Eqs. A-13 and A-15.

$$P_1 = \frac{1}{s}\left(f_0 e^{-st_0} - f_1 e^{-st_1}\right) + \frac{1}{s^2} m_1 (e^{-st_0} - e^{-st_1}) \quad \text{..... (A-13)}$$

$$P_3 = \frac{1}{s}\left(f_N e^{-st_N} - f_{N+1} e^{-st_{N+1}}\right) + \frac{1}{s^2} m_{ext} (e^{-st_N} - e^{-st_{N+1}}) \quad \text{..... (A-15)}$$

Generally, we have $t_0 = 0$, as a result, Eq. A-13 can be simplified to

$$P_1 = \frac{1}{s}\left(f_0 - f_1 e^{-st_1}\right) + \frac{1}{s^2} m_1 (1 - e^{-st_1}) \quad \text{..... (A-16)}$$

By assuming that the extrapolation goes to the infinite time, the expression for P_3 in Eq. A-15 can be modified to

$$P_3 = \frac{1}{s} f_N e^{-st_N} + \frac{1}{s^2} m_{ext} e^{-st_N} \quad \text{..... (A-17)}$$

When we are dealing with decreasing function, i.e. time-rate data, it makes sense to assume the extrapolated line on the right end stops at zero. As a result, the expression for P_3 in Eq. A-15 becomes

$$P_3 = \frac{1}{s} f_N e^{-st_N} + \frac{1}{s^2} m_{ext} e^{-st_N} (1 - e^{sf_N / m_{ext}}) \quad \text{..... (A-22)}$$

It is noted that m_1 and m_{ext} can be obtained from the least-square regressions of the few data points on left and right ends of the dataset, respectively.

A.4.2 Straight-Line Extrapolation on a Log-Log Scale

The function for log-linear relation is recalled from Eq. A-55

$$\ln(f(t)) = \beta \ln(t) + \ln(\alpha) \quad \text{(A-55)}$$

For the log-log straight-line extrapolation, the P_1 and P_3 expressions were provided earlier as shown in Eqs. A-46 and A-51.

$$P_1 = \frac{\alpha_1}{s^{\upsilon_1}} \gamma(\upsilon_1, st_1) \quad \text{(A-46)}$$

$$P_3 = \frac{\alpha_{ext}}{s^{\upsilon_{ext}}} [\Gamma(\upsilon_{ext}) - \gamma(\upsilon_{ext}, st_N)] \quad \text{(A-51)}$$

It is noted that α_1, υ_1 and $\alpha_{ext}, \upsilon_{ext}$ can be obtained from the least-square regressions of the few data points on left and right ends of the dataset, respectively.

A.4.3 Straight-Line Extrapolation on a Linear-Log Scale

We are to develop the Laplace transform expression of the extrapolated function of the form

$$f(t) = m \ln(t) + c \quad \text{(A-56)}$$

Recalling the Laplace transform expressions, we have

$$\overline{f}(s) = \int_{t_0=0}^{t_1} f(t)e^{-st}dt + \int_{t_1}^{t_N} f(t)e^{-st}dt + \int_{t_N}^{\infty} f(t)e^{-st}dt \quad \text{(A-2)}$$

$$\overline{f}(s) = P_1 + P_2 + P_3 \quad \text{(A-3)}$$

We cannot determine the closed form of P_1 and none could be found in the literature either. Thus, we will consider only P_3 in this study. From Eq. A-2 and A-3, we know that

$$P_3 = \int_{t_N}^{\infty} f(t)e^{-st}dt \quad \text{..... (A-58)}$$

From Eq. A-56, we can determine the extrapolation on the right-hand side of data as

$$f(t) = f_N + m_{ext}\ln(t/t_N) \quad \text{For } t \geq t_N \quad \text{..... (A-59)}$$

Substituting Eq. A-59 into Eq. A-58, we get

$$P_3 = \int_{t_N}^{\infty} e^{-st}[f_N + m_{ext}\ln(t/t_N)]dt$$

$$= f_N \int_{t_N}^{\infty} e^{-st}dt + m_{ext}\int_{t_N}^{\infty} e^{-st}\ln(t/t_N)dt$$

$$P_3 = \frac{f_N}{s}e^{-st_N} + m_{ext}\int_{t_N}^{\infty} e^{-st}\ln(t/t_N)dt \quad \text{..... (A-60)}$$

Considering the second term on the right-hand side of Eq. A-60, we have

$$m_{ext}\int_{t_N}^{\infty} e^{-st}\ln(t/t_N)dt = -\frac{m_{ext}}{s}\int_{t_N}^{\infty}[-se^{-st}\ln(t/t_N)]dt \quad \text{..... (A-61)}$$

Integrating by parts by using the relation in Eq. A-62

$$\int_a^b udv = [uv]_a^b - \int_a^b vdu \quad \text{..... (A-62)}$$

By letting u and v terms in Eq. A-62 to be as below

$$u = \ln(t/t_N)$$
$$du = (1/t)dt$$
$$v = e^{-st}$$
$$dv = -se^{-st}dt$$

We have

$$m_{ext}\int_{t_N}^{\infty} e^{-st}\ln(t/t_N)dt = -\frac{m_{ext}}{s}([\ln(t/t_N)e^{-st}]_{t_N}^{\infty} - \int_{t_N}^{\infty} e^{-st}(1/t)dt)$$
$$= \frac{m_{ext}}{s}\int_{t_N}^{\infty} e^{-st}(1/t)dt \quad \text{..... (A-63)}$$

Transforming the integrating variable by letting

$z = st$
$dz = sdt$
$@\, t = t_N, z = st_N$
$@\, t = \infty, z = \infty$

Eq. A-63 becomes

$$m_{ext}\int_{t_N}^{\infty} e^{-st}\ln(t/t_N)dt = \frac{m_{ext}}{s}\int_{z=st_N}^{z=\infty} e^{-z}\frac{s}{z}\frac{dz}{s}$$
$$= \frac{m_{ext}}{s}\int_{z=st_N}^{z=\infty} (e^{-z}/z)dz \quad \text{..... (A-64)}$$

From the definition of Exponential Integral function, we have

$$-E_i(-x) = \int_{x}^{\infty}(e^{-z}/z)dz \quad \text{..... (A-65)}$$

Using the definition in Eq. A-65, Eq. A-64 becomes

$$m_{ext}\int_{t_N}^{\infty} e^{-st}\ln(t/t_N)dt = -\frac{m_{ext}}{s}E_i(-st_N) \quad \text{..... (A-66)}$$

Substituting Eq. A-66 into Eq. A-60, we have

$$P_3 = \frac{f_N}{s}e^{-st_N} - \frac{m_{ext}}{s}E_i(-st_N) \quad \text{..... (A-67)}$$

In the case of decreasing rate function, the extrapolation should stop at zero to reflect the real characteristic of a rate function. The time at which rate reaches zero can be determined using Eq. A-59. By letting $f(t_{N+1}) = 0$ for $t = t_{N+1}$, we have

$$0 = f_N + m_{ext} \ln(t_{N+1} / t_N) \quad \text{for } t_{N+1} \geq t_N \quad \text{..... (A-68)}$$

Rearranging, we have

$$t_{N+1} = t_N e^{-\frac{f_N}{m_{ext}}} \quad \text{for } t_{N+1} \geq t_N \quad \text{..... (A-69)}$$

We are assuming that functional value after t_{N+1} is zero. Thus, we can modify Eq. A-58 to be

$$P_3 = \int_{t_N}^{t_{N+1}} f(t) e^{-st} dt \quad \text{..... (A-70)}$$

Recalling Eq. A-59, we have

$$f(t) = f_N + m_{ext} \ln(t / t_N) \quad \text{for } t_{N+1} \geq t \geq t_N \quad \text{..... (A-59)}$$

Substituting Eq. A-59 into Eq. A-70 we get

$$\begin{aligned} P_3 &= \int_{t_N}^{t_{N+1}} e^{-st} [f_N + m_{ext} \ln(t / t_N)] dt \\ &= f_N \int_{t_N}^{t_{N+1}} e^{-st} dt + m_{ext} \int_{t_N}^{t_{N+1}} e^{-st} \ln(t / t_N) dt \\ &= \frac{f_N}{s} [-e^{-st}]_{t_N}^{t_{N+1}} + m_{ext} \int_{t_N}^{t_{N+1}} e^{-st} \ln(t / t_N) dt \end{aligned}$$

$$P_3 = \frac{f_N}{s} [e^{-st_N} - e^{-st_{N+1}}] + m_{ext} \int_{t_N}^{t_{N+1}} e^{-st} \ln(t / t_N) dt \quad \text{..... (A-71)}$$

Considering the second term on the right-hand side of Eq. A-71, we can rewrite the term as

$$m_{ext}\int_{t_N}^{t_{N+1}} e^{-st}\ln(t/t_N)dt = m_{ext}\int_{t_N}^{\infty} e^{-st}\ln(t/t_N)dt - m_{ext}\int_{t_{N+1}}^{\infty} e^{-st}\ln(t/t_N)dt \quad \text{..... (A-72)}$$

The first term on the right-hand side of Eq. A-72, we have already derived in Eq. A-66. Thus, we are considering the second term on the right-hand side of Eq. A-72. We can rewrite the term as

$$-m_{ext}\int_{t_{N+1}}^{\infty} e^{-st}\ln(t/t_N)dt = \frac{m_{ext}}{s}\int_{t_{N+1}}^{\infty} -se^{-st}\ln(t/t_N)dt \quad \text{..... (A-73)}$$

Integrating by parts by using the relation in Eq. A-62

$$\int_a^b udv = [uv]_a^b - \int_a^b vdu \quad \text{..... (A-62)}$$

By letting u and v terms in Eq. A-62 to be as below

$$u = \ln(t/t_N)$$
$$du = (1/t)dt$$
$$v = e^{-st}$$
$$dv = -se^{-st}dt$$

Eq. A-73 becomes

$$-m_{ext}\int_{t_{N+1}}^{\infty} e^{-st}\ln(t/t_N)dt = \frac{m_{ext}}{s}([\ln(t/t_N)e^{-st}]_{t_{N+1}}^{\infty} + \int_{t_{N+1}}^{\infty} e^{-st}(1/t)dt)$$
$$= \frac{m_{ext}}{s}((0 - \ln(t_{N+1}/t_N)e^{-st_{N+1}}) + \int_{t_{N+1}}^{\infty} e^{-st}(1/t)dt)$$

$$-m_{ext}\int_{t_{N+1}}^{\infty} e^{-st}\ln(t/t_N)dt = -\frac{m_{ext}}{s}\ln(\frac{t_{N+1}}{t_N})e^{-st_{N+1}} - \frac{m_{ext}}{s}\int_{t_{N+1}}^{\infty} e^{-st}(1/t)dt \quad \text{..... (A-74)}$$

Transforming the integrating variable in the second term on the right-hand side of Eq. A-74 by letting

$$z = st$$
$$dz = sdt$$
$$@t = t_{N+1}, z = st_{N+1}$$
$$@t = \infty, z = \infty$$

Eq. A-74 becomes

$$-m_{ext}\int_{t_{N+1}}^{\infty} e^{-st}\ln(t/t_N)dt = -\frac{m_{ext}}{s}\ln(\frac{t_{N+1}}{t_N})e^{-st_{N+1}} - \frac{m_{ext}}{s}\int_{z=st_{N+1}}^{z=\infty}(\frac{e^{-z}}{z})dz \quad \text{..... (A-75)}$$

Recalling the definition of Exponential Integral function, we have

$$-E_i(-x) = \int_x^{\infty}(e^{-z}/z)dz \quad \text{..... (A-65)}$$

Using the definition in Eq. A-65, Eq. A-75 becomes

$$-m_{ext}\int_{t_{N+1}}^{\infty} e^{-st}\ln(t/t_N)dt = -\frac{m_{ext}}{s}\ln(\frac{t_{N+1}}{t_N})e^{-st_{N+1}} + \frac{m_{ext}}{s}E_i(-st_{N+1}) \quad \text{..... (A-76)}$$

Substituting Eq. A-76 into Eq. A-72, we have

$$m_{ext}\int_{t_N}^{t_{N+1}} e^{-st}\ln(t/t_N)dt = m_{ext}\int_{t_N}^{\infty} e^{-st}\ln(t/t_N)dt - \frac{m_{ext}}{s}\ln(\frac{t_{N+1}}{t_N})e^{-st_{N+1}} + \frac{m_{ext}}{s}E_i(-st_{N+1}) \quad \text{..... (A-77)}$$

Recalling the relation in Eq. A-66 which is

$$m_{ext}\int_{t_N}^{\infty} e^{-st}\ln(t/t_N)dt = -\frac{m_{ext}}{s}E_i(-st_N) \quad \text{..... (A-66)}$$

Substituting into Eq. A-77, we have

$$m_{ext}\int_{t_N}^{t_{N+1}} e^{-st}\ln(t/t_N)dt = \frac{m_{ext}}{s}[-\ln(\frac{t_{N+1}}{t_N})e^{-st_{N+1}} - E_i(-st_N) + E_i(-st_{N+1})] \quad \text{..... (A-78)}$$

Substituting Eq. A-78 into Eq. A-71, we have the expression for P_3

$$P_3 = \frac{f_N}{s}[e^{-st_N} - e^{-st_{N+1}}] + \frac{m_{ext}}{s}[-\ln(\frac{t_{N+1}}{t_N})e^{-st_{N+1}} - E_i(-st_N) + E_i(-st_{N+1})] \quad \text{..... (A-79)}$$

We can further simplify the relation by using the relation in Eq. A-69 which is

$$t_{N+1} = t_N e^{-\frac{f_N}{m_{ext}}} \quad \text{for } t_{N+1} \geq t_N \quad \text{..... (A-69)}$$

Substituting into the third term on the right-hand side of Eq. A-79, we have

$$P_3 = \frac{f_N}{s}e^{-st_N} + \frac{m_{ext}}{s}[E_i(-st_{N+1}) - E_i(-st_N)] \quad \text{..... (A-80)}$$

A.4.4 Straight-Line Extrapolation on a Log-Linear Scale

We are to develop the Laplace transform expression of the extrapolated function of the form

$$\ln(f(t)) = \beta t + \ln(\alpha) \quad \text{..... (A-57)}$$

Exponentiating both sides, we get

$$f(t) = \alpha e^{\beta t} \quad \text{..... (A-81)}$$

Recalling the Laplace transform expressions we have

$$\overline{f}(s) = \int_{t_0=0}^{t_1} f(t)e^{-st}dt + \int_{t_1}^{t_N} f(t)e^{-st}dt + \int_{t_N}^{\infty} f(t)e^{-st}dt \quad \text{..... (A-2)}$$

$$\overline{f}(s) = P_1 + P_2 + P_3 \quad \text{..... (A-3)}$$

Firstly, we are considering P_1. From Eqs. A-2 and A-3, we know that

$$P_1 = \int_0^{t_1} f(t)e^{-st}dt \quad \text{..... (A-82)}$$

From Eq. A-81, we can determine the extrapolated function on the left-hand side of data as

$$f(t) = \alpha_1 e^{\beta_1 t} \quad \text{for } t \le t_1 \quad \text{..... (A-83)}$$

Substituting Eq. A-83 into Eq. A-82, we have

$$P_1 = \alpha_1 \int_0^{t_1} e^{(\beta_1 - s)t} dt$$

$$= \frac{\alpha_1}{\beta_1 - s} [e^{(\beta_1 - s)t}]_0^{t_1}$$

$$P_1 = \frac{\alpha_1}{\beta_1 - s} [e^{(\beta_1 - s)t_1} - 1] \quad \text{for } s \ne \beta_1 \quad \text{..... (A-84)}$$

Next, we are considering P_3. Recalling Eq. A-58, we have

$$P_3 = \int_{t_N}^{\infty} f(t) e^{-st} dt \quad \text{..... (A-58)}$$

From Eq. A-81, we can determine the extrapolated function on the right-hand side of data as

$$f(t) = \alpha_{ext} e^{\beta_{ext} t} \quad \text{for } t \ge t_N \quad \text{..... (A-85)}$$

Substituting Eq. A-85 into Eq. A-58, we get

$$P_3 = \alpha_{ext} \int_{t_N}^{\infty} e^{(\beta_{ext} - s)t} dt$$

$$= \frac{\alpha_{ext}}{\beta_{ext} - s} [e^{(\beta_{ext} - s)t}]_{t_N}^{\infty}$$

$$P_3 = \frac{\alpha_{ext}}{s - \beta_{ext}} [e^{(\beta_{ext} - s)t_N}] \quad \text{for } s > \beta_{ext} \quad \text{..... (A-86)}$$

From Eq. A-85, we know that

$$f_N = \alpha_{ext} e^{\beta_{ext} t_N} \quad \text{..... (A-87)}$$

Substituting Eq. A-87 into Eq. A-86, we have

$$P_3 = \frac{f_N}{s - \beta_{ext}} e^{-st_N} \quad \text{for } s > \beta_{ext} \quad \text{..... (A-88)}$$

References

A.1 Bourgeois, M. and Horne, R. N. 1993. Well Test Model Recognition Using LaPlace Space Type Curves. doi:10.2118/22682-PA.

A.2 Onur, M. and Reynolds, A. C. 1998. Well Testing Applications of Numerical Laplace Transformation of Sampled-Data. doi:10.2118/36554-PA.

A.3 Roumboutsos, A. and Stewart, G. 1988. A Direct Deconvolution or Convolution Algorithm for Well Test Analysis. Presented at the SPE Annual Technical Conference and Exhibition, Houston, Texas. 1988/1/1/. doi: 10.2118/18157-MS.

Nomenclature

t	=	Time, day
$f(t)$	=	Time function
$\mathcal{L}$	=	Laplace transform operator
$\overline{f}(s)$	=	Laplace transform of f(t)
s	=	Laplace variable, 1/day
m	=	Straight-line cord slope
i	=	Number index of discrete data points
N	=	Total number of discrete data points
c	=	Straight-line cord constant
β	=	Slope of log-log straight line
υ	=	Constant related to slope of log-log straight line
α	=	Intercept of log-log straight line
γ	=	First Incomplete Gamma function
Γ	=	Gamma function, second Incomplete Gamma function
E_i	=	Exponential Integral function
I	=	Arbitrary integrand

APPENDIX B

DERIVATION OF THE LAPLACE TRANSFORM EXPRESSIONS FOR A SMOOTHED FUNCTION AND FUNCTIONAL OPERATIONS

B.1 Introduction

We derived the expressions for smoothing a time function and computing the derivative and the integral of a time function using the Laplace transform properties. Although, in this research work, we focus on the time-rate discrete data function, we derived all the expressions in generic terms so that they would be applicable for any time functions. In order to apply these expressions to a discrete time-rate data, the knowledge of numerical Laplace transform of discrete data described in **Appendix A** can be used. We also derived the expressions for computing the reciprocal of the Loss-ratio (*D*-parameter) and the derivative of the Loss-ratio (*b*-parameter) from a time-rate data using the Laplace transform method.

In our derivation, we used two types of basis-functions to be taken into the Laplace domain which are the time function itself and the reciprocal of the time function. Table B-1 and B-2 summarize the derived expressions for the Laplace transform smoothed function, the Laplace transform derivative function, and the Laplace transform integral function using time function and its reciprocal as the basis functions, respectively. The smoothed function can be obtained simply by taking the Laplace transform of the time function and invert it back into time space. For the derivative and the integral computation, we use the identities of the Laplace transform of derivative and integral function, then we invert them back into time domain. Detailed derivation will be provided later.

Table B-1 — Summary of the Expressions for the Laplace Transform Smoothed Function, the Laplace Transform Derivative Function, and the Laplace Transform Integral Function using Time Function as the Basis Function.

	Expressions	**Eqs.**
Basis Functions	$f(t)$	
Laplace Transform Smoothed Functions	$\widehat{f}(t) = \mathcal{L}^{-1}\{\overline{f}(s)\}$ Where $\overline{f}(s) = \mathcal{L}\{f(t)\}$	(B-1)
Laplace Transform Derivative Functions (Method 1)	$\widehat{f}'(t) = \mathcal{L}^{-1}\{\overline{f}'(s)\}$ Where $\overline{f}'(s) = s\overline{f}(s) - f(t=0)$	(B-8)
Laplace Transform Derivative Functions (Method 2)	$\widehat{f}'(t) = \frac{1}{t}\mathcal{L}^{-1}\left\{-\overline{f}(s) - s\frac{d\overline{f}(s)}{ds}\right\}$	(B-16)
Laplace Transform Integral Functions	$\widehat{F}(t) = \mathcal{L}^{-1}\left\{\frac{\overline{f}(s)}{s}\right\}$	(B-45)

Table B-2 — Summary of the Expressions for the Laplace Transform Smoothed Function, the Laplace Transform Derivative Function, and the Laplace Transform Integral Function using the Reciprocal of Time Function as the Basis Function.

	Expressions	**Eqs.**
Basis Functions	$r(t) = 1 / f(t)$	
Laplace Transform Smoothed Functions	$\widehat{f}(t) = \dfrac{1}{\mathcal{L}^{-1}\{\bar{r}(s)\}}$ Where $\bar{r}(s) = \mathcal{L}\{r(t)\}$	(B-3)
Laplace Transform Derivative Functions (Method 1)	$\widehat{f}'(t) = -\left(\dfrac{1}{\mathcal{L}^{-1}\{\bar{r}(s)\}}\right)^2 \mathcal{L}^{-1}\{\bar{r}'(s)\}$ Where $\bar{r}'(s) = s\bar{r}(s) - r(t=0)$	(B-20)
Laplace Transform Derivative Functions (Method 2)	$\widehat{f}'(t) = -\dfrac{1}{t}\left(\dfrac{1}{\mathcal{L}^{-1}\{\bar{r}(s)\}}\right)^2 \mathcal{L}^{-1}\left\{-\bar{r}(s) - s\dfrac{d\bar{r}(s)}{ds}\right\}$	(B-28)
Laplace Transform Integral Functions	N/A	

B.2 Derivation of the Expressions for the Laplace Transform Smoothed Function

We can simply utilize the smoothing capability of the Laplace transform and the Laplace transform inversion to smooth the noisy data. The expression can be found below.

$$\hat{f}(t) = \mathcal{L}^{-1}\{\mathcal{L}\{f(t)\}\} = \mathcal{L}^{-1}\{\bar{f}(s)\} \quad \text{.....(B-1)}$$

As a side note, in this work, our targeted time function is in a form of discrete time-rate data, e.g. daily production rate and monthly production rate. The smoothness and accuracy of the smoothed function are dependent on the representativeness of the approximating function used in the numerical Laplace transformation process and the Stehfest "n" parameter used in the numerical Laplace inversion process. The smaller "n" parameter yields less accurate but smoother function.

Alternatively, we can use the reciprocal of time function instead of the time function itself.

Let $r(t) = 1/f(t)$, we have

$$\mathcal{L}\left\{\frac{1}{f(t)}\right\} = \mathcal{L}\{r(t)\} = \bar{r}(s) \quad \text{.....(B-2)}$$

The expression for the Laplace transform smoothed function would be as below.

$$\hat{f}(t) = \frac{1}{\mathcal{L}^{-1}\{\mathcal{L}\{1/f(t)\}\}} = \frac{1}{\mathcal{L}^{-1}\{\bar{r}(s)\}} \quad \text{.....(B-3)}$$

B.3 Derivation of the Expressions for the Laplace Transform Derivative Function

First, we will use time function as the basis function for the derivation. The Laplace transform derivative function can be defined as

$$\hat{f}'(t) = \mathcal{L}^{-1}\left\{\mathcal{L}\left\{f'(t)\right\}\right\} \quad \text{.....(B-4)}$$

Alternatively, we can also use the relationship between derivative with respect to logarithmic time and time derivative as shown in Eq. B-5.

$$f'(t) = \frac{df(t)}{dt} = \frac{1}{t}\left[t\frac{df(t)}{dt}\right] = \frac{1}{t}\left[\frac{df(t)}{d\ln(t)}\right] = \frac{1}{t}f'_{\ln(t)}(t) \quad \text{.....(B-5)}$$

Then, we can define the Laplace transform derivative as

$$\widehat{f}'(t) = \frac{1}{t}\widehat{f}'_{\ln(t)}(t) \quad \text{.....(B-6)}$$

We call the expressions in Eq. B-4 and B-6, which will be used to compute Laplace transform derivative function, as method 1 and method 2, respectively.

To derive the method 1 Laplace transform derivative expression, we use the property of the Laplace transform of derivative functions shown in Eq. B-7.

$$\mathcal{L}\{f'(t)\} = \mathcal{L}\left\{\frac{df(t)}{dt}\right\} = \overline{f}'(s) = s\overline{f}(s) - f(t=0) \quad \text{.....(B-7)}$$

Substituting in Eq. B-4, we have

$$\hat{f}'(t) = \mathcal{L}^{-1}\left\{\overline{f}'(s)\right\} = \mathcal{L}^{-1}\left\{s\overline{f}(s) - f(t=0)\right\} \quad \text{.....(B-8)}$$

Next, we are deriving the method 2. Firstly, we recall the relation in Eq. B-6

$$\widehat{f}'(t) = \frac{1}{t}\widehat{f}'_{\ln(t)}(t) \quad \text{.....(B-6)}$$

It can be rewritten as

$$\begin{aligned}\hat{f}'(t) &= \frac{1}{t}\mathcal{L}^{-1}\{\mathcal{L}\{f'_{\ln(t)}(t)\}\} \\ &= \frac{1}{t}\mathcal{L}^{-1}\{\mathcal{L}\{tf'(t)\}\}\end{aligned} \quad \text{.....(B-9)}$$

We are to determine the Laplace transform of the logarithmic time derivative function on the right-hand side of Eq. B-9. First, we need to prove the identity in Eq. B-10

$$\mathcal{L}\{tf(t)\} = -\frac{d\overline{f}(s)}{ds} \quad \text{.....(B-10)}$$

From the definition of the Laplace transform, we know that

$$\mathcal{L}\{f(t)\} = \overline{f}(s) = \int_0^\infty e^{-st} f(t)dt \quad \text{.....(B-11)}$$

Taking the derivative with respect to the Laplace variable, s, on both sides, we get

$$\begin{aligned}\frac{d\overline{f}(s)}{ds} &= \frac{d}{ds}\int_0^\infty e^{-st} f(t)dt \\ &= \int_0^\infty \frac{\partial}{\partial s}(e^{-st} f(t))dt\end{aligned}$$

$$\frac{d\overline{f}(s)}{ds} = -\int_0^\infty te^{-st} f(t)dt \quad \text{.....(B-12)}$$

Using the Laplace transform definition in Eq. B-11, the expression in Eq. B-12 is equivalent to the expression in Eq. B-10. This proves that the identity in Eq. B-10 is true. Then, we can determine $\mathcal{L}\{tf'(t)\}$ by letting $g(t) = f'(t)$ and using the relationship in Eq. B-10, we have

$$\mathcal{L}\{tf'(t)\} = \mathcal{L}\{tg(t)\} = -\frac{d\overline{g}(s)}{ds} \quad \text{.....(B-13)}$$

Since, $\overline{g}(s) = \overline{f}'(s)$, we have

$$\mathcal{L}\{tf'(t)\} = -\frac{d\overline{f}'(s)}{ds} \quad \text{.....(B-14)}$$

Substituting Eq. B-7 into Eq. B-14, we have

$$\begin{aligned}\mathcal{L}\{tf'(t)\} &= -\frac{d\overline{f}'(s)}{ds} \\ &= -\frac{d}{ds}\{s\overline{f}(s) - f(t=0)\} \\ &= -\frac{d}{ds}\{s\overline{f}(s)\}\end{aligned}$$

$$\mathcal{L}\{tf'(t)\} = -\overline{f}(s) - s\frac{d\overline{f}(s)}{ds} \quad \text{.....(B-15)}$$

Substituting Eq. B-15 into Eq. B-9, we obtain

$$\hat{f}'(t) = \frac{1}{t}\mathcal{L}^{-1}\left\{-\bar{f}(s) - s\frac{d\bar{f}(s)}{ds}\right\} \quad \text{.....(B-16)}$$

We now have two derivative algorithms to compute using the property of the Laplace transform. Onur and Reynolds [1998] suggested that the algorithm in Eq. B-13 requires more computation time than the algorithm in Eq. B-8, however, it yields more reliable results.

Next, we are considering the reciprocal of time function as the basis function for derivative computation. To derive the expression for the derivative function using method 2, we firstly differentiate the reciprocal of time function.

$$\frac{d}{dt}\left(r(t)\right) = \frac{d}{dt}\left(\frac{1}{f(t)}\right) = -\frac{1}{(f(t))^2}\frac{df(t)}{dt} \quad \text{.....(B-17)}$$

Rearranging, we get

$$\frac{df(t)}{dt} = -(f(t))^2\frac{d}{dt}\left(\frac{1}{f(t)}\right) \quad \text{.....(B-18)}$$

From Eq. B-18, we can define the Laplace transform derivative function as

$$\hat{f}'(t) = -(\hat{f}(t))^2\mathcal{L}^{-1}\left\{\mathcal{L}\left\{\frac{d}{dt}\left(\frac{1}{f(t)}\right)\right\}\right\} \quad \text{.....(B-19)}$$

Redefining in terms of the reciprocal of time function, we have

$$\hat{f}'(t) = -\left(\frac{1}{\mathcal{L}^{-1}\{\bar{r}(s)\}}\right)^2\mathcal{L}^{-1}\left\{\bar{r}'(s)\right\} \quad \text{.....(B-20)}$$

Using the relation in Eq. B-7 to determine the Laplace transform of the reciprocal function, we have

$$\bar{r}'(s) = s\bar{r}(s) - r(0) \quad \text{.....(B-21)}$$

Substituting into Eq. B-20, we have

$$\hat{f}'(t) = -\left(\frac{1}{\mathcal{L}^{-1}\{\bar{r}(s)\}}\right)^2 \mathcal{L}^{-1}\{s\bar{r}(s) - r(t=0)\} \quad \text{.....(B-22)}$$

Apart from the expression in Eq. B-22, we will prove it using the same concept which we used to derive Eq. B-16. We are starting with the derivative of the basis function with respect to logarithmic time, in this case, we are using the reciprocal of time function as the basis function.

Differentiating the reciprocal of time function with respect to logarithmic time, we have

$$\frac{d\left(r(t)\right)}{d\ln t} = \frac{d}{d\ln t}\left(\frac{1}{f(t)}\right) = t\frac{d}{dt}\left(\frac{1}{f(t)}\right) = -\frac{t}{(f(t))^2}\frac{df(t)}{dt} \quad \text{.....(B-23)}$$

Rearranging, we get

$$\frac{df(t)}{dt} = -\frac{(f(t))^2}{t}\left\{t\frac{d}{dt}\left(\frac{1}{f(t)}\right)\right\} \quad \text{.....(B-24)}$$

From Eq. B-24, we can define the Laplace transform derivative function as

$$\hat{f}'(t) = -\frac{(\hat{f}(t))^2}{t}\mathcal{L}^{-1}\left\{\mathcal{L}\left\{t\frac{d}{dt}\left(\frac{1}{f(t)}\right)\right\}\right\} \quad \text{.....(B-25)}$$

Redefining in terms of the reciprocal of time function, we have

$$\hat{f}'(t) = -\frac{1}{t}\left(\frac{1}{\mathcal{L}^{-1}\{\bar{r}(s)\}}\right)^2 \mathcal{L}^{-1}\left\{\mathcal{L}\left\{tr'(t)\right\}\right\} \quad \text{.....(B-26)}$$

Recalling Eq. B-15, we know that

$$\mathcal{L}\{tf'(t)\} = -\bar{f}(s) - s\frac{d\bar{f}(s)}{ds} \quad \text{.....(B-15)}$$

Thus, we have

$$\mathcal{L}\{tr'(t)\} = -\bar{r}(s) - s\frac{d\bar{r}(s)}{ds} \quad \text{.....(B-27)}$$

Substituting into Eq. B-26, we obtain

$$\hat{f}'(t) = -\frac{1}{t}\left(\frac{1}{\mathcal{L}^{-1}\{\bar{r}(s)\}}\right)^2 \mathcal{L}^{-1}\left\{-\bar{r}(s) - s\frac{d\bar{r}(s)}{ds}\right\} \quad \text{.....(B-28)}$$

In Eqs. B-16 and B-28, we require the derivative of $\bar{f}(s)$ and $\bar{r}(s)$ with respect to the Laplace variable. To derive that, we need to have an explicit form of $\bar{f}(s)$ and $\bar{r}(s)$ which is shown exhaustively in Appendix A. We showed several forms of the Laplace transform of discrete data using several types of approximating functions. Here, we will provide an example of the derivative of $\bar{f}(s)$ using the piecewise linear approximation form of $\bar{f}(s)$ (Eq. B-29).

Recalling the expression for the Laplace transform of a time function using the piecewise linear data approximating approach from Eq. A-19, we have

$$\bar{f}(s) = \frac{f_0}{s} + \frac{1}{s^2}\sum_{i=1}^{N} m_i(e^{-st_{i-1}} - e^{-st_i}) + \frac{1}{s^2} m_{ext} e^{-st_N}\left(1 - e^{\frac{sf_N}{m_{ext}}}\right) \quad \text{..... (A-19)}$$

Differentiating both sides with the Laplace variable, we have

$$\begin{aligned}\frac{d}{ds}\bar{f}(s) &= \frac{d}{ds}\left(\frac{f_0}{s}\right) + \frac{d}{ds}\left(\frac{1}{s^2}\sum_{i=1}^{N} m_i(e^{-st_{i-1}} - e^{-st_i})\right) + \frac{d}{ds}\left(\frac{1}{s^2} m_{ext} e^{-st_N}\left(1 - e^{\frac{sf_N}{m_{ext}}}\right)\right) \\ &= -\frac{f_0}{s^2} + \frac{1}{s^2}\sum_{i=1}^{N} m_i(t_i e^{-st_i} - t_{i-1}e^{-st_{i-1}}) + \frac{2}{s^3}\sum_{i=1}^{N} m_i(e^{-st_i} - e^{-st_{i-1}}) \\ &\quad + m_{ext}\left(\left(\frac{1}{s^2}\left(t_N - \frac{f_N}{m_{ext}}\right) + \frac{2}{s^3}\right)e^{-st_N + \frac{sf_N}{m_{ext}}} - \left(\frac{1}{s^2}t_N + \frac{2}{s^3}\right)e^{-st_N}\right)\end{aligned}$$

$$\begin{aligned}\frac{d}{ds}\bar{f}(s) &= -\frac{f_0}{s^2} + \frac{1}{s^2}\sum_{i=1}^{N} m_i(t_i e^{-st_i} - t_{i-1}e^{-st_{i-1}}) + \frac{2}{s^3}\sum_{i=1}^{N} m_i(e^{-st_i} - e^{-st_{i-1}}) \\ &\quad + m_{ext} e^{-st_N + \frac{sf_N}{m_{ext}}}\left(\frac{1}{s^2}\left(t_N - \frac{f_N}{m_{ext}}\right) + \frac{2}{s^3}\right) - m_{ext} e^{-st_N}\left(\frac{1}{s^2}t_N + \frac{2}{s^3}\right)\end{aligned} \quad \text{.....(B-29)}$$

where

$$f_i = f(t_i), t_i = 0,1,2,...,N;$$

$$m_i = \frac{f_i - f_{i-1}}{t_i - t_{i-1}}$$

B.4 Derivation of the Expressions for the Laplace Transform Derived *D* and *b*-Parameters

Utilizing the Laplace transform derivative expressions derived earlier in Eq. B-8, B-16, B-22, and B-28, we can derive the expressions for computing *D* and *b*-parameters from a time-rate discrete data. *D* and *b*-parameters could be computed using their definitions proposed by Johnson and Bollens [1928] in Eqs. B-30 and B-31, respectively.

$$\frac{1}{D(t)} \equiv -\frac{q(t)}{dq(t)/dt}$$ Definition of the Loss-Ratio .....(B-30)

$$b(t) \equiv \frac{d}{dt}\left[\frac{1}{D(t)}\right] \equiv -\frac{d}{dt}\left[\frac{q(t)}{dq(t)/dt}\right]$$ Definition of the Loss-Ratio Derivative.....(B-31)

For *D*-parameter computation, we can rearrange the relation in Eq. B-30

$$D(t) \equiv -\frac{1}{q(t)}\frac{dq(t)}{dt}$$ .....(B-32)

Rewriting with the Laplace transform accent to indicate that the function is computed using the Laplace transform method, we have

$$\hat{D}(t) \equiv -\frac{1}{\hat{q}(t)}\hat{q}'(t)$$ .....(B-33)

Substituting the Laplace transform derivative expressions from Eqs. B-8, B-16, B-22, and B-28 into Eq. B-33, we get four different expressions for *D*-parameter. The first two expressions use time-rate data function as the basis function and the other two use the reciprocal of rate data as the basis function.

$$\hat{D}(t) \equiv -\frac{1}{\mathcal{L}^{-1}\left\{\bar{q}(s)\right\}} \mathcal{L}^{-1}\{s\bar{q}(s) - q(t=0)\} \quad \text{.....(B-34)}$$

$$\hat{D}(t) \equiv -\frac{1}{\hat{q}(t)} \frac{1}{t} \mathcal{L}^{-1}\left\{-\bar{q}(s) - s\frac{d\bar{q}(s)}{ds}\right\} \quad \text{.....(B-35)}$$

$$\hat{D}(t) \equiv \frac{1}{\mathcal{L}^{-1}\{\bar{u}(s)\}} \mathcal{L}^{-1}\{s\bar{u}(s) - u(t=0)\} \quad \text{.....(B-36)}$$

$$\widehat{D}(t) \equiv \frac{1}{\mathcal{L}^{-1}\{\bar{u}(s)\}} \frac{1}{t} \mathcal{L}^{-1}\left\{-\bar{u}(s) - s\frac{d\bar{u}(s)}{ds}\right\} \quad \text{.....(B-37)}$$

where $q(t)$ is the rate function and $\bar{q}(s) = \mathcal{L}\{q(t)\}$;

And $u(t) = 1/q(t)$ and $\bar{u}(s) = \mathcal{L}\{u(t)\} = \mathcal{L}\{1/q(t)\}$

For *b*-parameter computation, we can use the definition in Eq. B-31

$$b(t) \equiv \frac{d}{dt}\left[\frac{1}{D(t)}\right] \quad \text{.....(B-31)}$$

Considering the *D*-parameter derived from the Laplace method earlier, we have

$$b(t) \equiv \frac{d}{dt}\left[\frac{1}{\widehat{D}(t)}\right] \quad \text{.....(B-38)}$$

Taking the Laplace transform on both sides, we have

$$\bar{b}(s) = \mathcal{L}\left\{\frac{d}{dt}\left(\frac{1}{\widehat{D}(t)}\right)\right\} \quad \text{.....(B-39)}$$

Where $\bar{b}(s) = \mathcal{L}\{b(t)\}$,

Recalling the relation in Eq. B-7, we have

$$\mathcal{L}\{f'(t)\} = \mathcal{L}\left\{\frac{df(t)}{dt}\right\} = \overline{f}'(s) = s\overline{f}(s) - f(t=0) \quad \text{.....(B-7)}$$

Using the relation in Eq. B-7, Eq. B-39 becomes

$$\overline{b}(s) = s\mathcal{L}\left\{\frac{1}{\widehat{D}(t)}\right\} - \frac{1}{\widehat{D}(t=0)} \quad \text{.....(B-40)}$$

Taking the Laplace inversion, we obtain the expression for the Laplace transform derived *b*-parameter as below.

$$\hat{b}(t) = \mathcal{L}^{-1}\{\overline{b}(s)\} = \mathcal{L}^{-1}\left\{s\mathcal{L}\left\{\frac{1}{\widehat{D}(t)}\right\} - \frac{1}{\widehat{D}(t=0)}\right\} \quad \text{.....(B-41)}$$

B.5 Derivation of the Expression for the Laplace Transform Integral Function

We are deriving the expression for integrating a time function using the property of the Laplace transform. The basis function for this case is only limited to the time-function itself. The reciprocal function does not work out in this case. First, we are defining the integral function as

$$F(t) = \int_0^t f(t)dt \quad \text{.....(B-42)}$$

Taking the Laplace transform on both sides of Eq. B-42, we have

$$\mathcal{L}\{F(t)\} = \mathcal{L}\{\int_0^t f(t)dt\} \quad \text{.....(B-43)}$$

Using the property of the Laplace transform of integral functions,

$$\mathcal{L}\{F(t)\} = \frac{\overline{f}(s)}{s} \quad \text{.....(B-44)}$$

Where $\overline{f}(s) = \mathcal{L}\{f(t)\}$

Applying the inverse Laplace transform, we obtain the expression for the Laplace transform integral function as

$$\widehat{F}(t) = \mathcal{L}^{-1}\left\{\mathcal{L}\{F(t)\}\right\} = \mathcal{L}^{-1}\left\{\frac{\overline{f}(s)}{s}\right\} \quad \text{.....(B-45)}$$

References

B.1 Onur, M. and Reynolds, A. C. 1998. Well Testing Applications of Numerical Laplace Transformation of Sampled-Data. doi:10.2118/36554-PA.

Nomenclature

t	=	Time, day
f, g	=	Time function
f'	=	Derivative of a time function
F	=	Integral of a time function
r	=	Reciprocal of a time function
$\mathcal{L}$	=	Laplace transform operator
$\mathcal{L}^{-1}$	=	Inverse of Laplace transform operator
$\overline{f}(s)$	=	Laplace transform of f(t)
s	=	Laplace variable, 1/day
q	=	Rate function, Mscf/day for gas(bbl/day for oil)
u	=	Reciprocal of rate function, $[\text{Mscf/day}]^{-1}$ for gas($[\text{bbl/day}]^{-1}$ for oil)
D	=	Reciprocal of loss ratio, 1/day
b	=	Loss ratio derivative, dimensionless
n	=	Parameter in the Stehfest inversion algorithm, dimensionless
m	=	Cord slope
m_{ext}	=	Slope of the right-hand side extrapolate line
N	=	Total number of discrete data points
$\widehat{f}$	=	The Laplace transform smoothed function
$\widehat{f}'$	=	The Laplace transform derivative function
$\widehat{F}$	=	The Laplace transform integral function
$\widehat{D}$	=	The Laplace transform derived *D*-parameter
$\hat{b}$	=	The Laplace transform derived *b*-parameter

APPENDIX C

SENSITIVITY CASES

The goal of this work is to study the effects of various data characteristics to the resulted Laplace transform smoothed functions, i.e. Laplace transform smoothed rate function, Laplace transform smoothed derivative function, and Laplace transform smoothed integral function. We used a five-year monthly synthetic time-rate data generated from Arps exponential decline model as the base case. For the base case, the so-called modified Roumboutsos and Stewart Laplace transform algorithm is used. We aim to study the effects of the following:

- Data extrapolation type for numerical Laplace transform computation
- Data frequency and spacing type
- Data extent
- Data noise
- Data function type [increasing data function versus decreasing data function]

C.1 Effects of Data Extrapolation Types

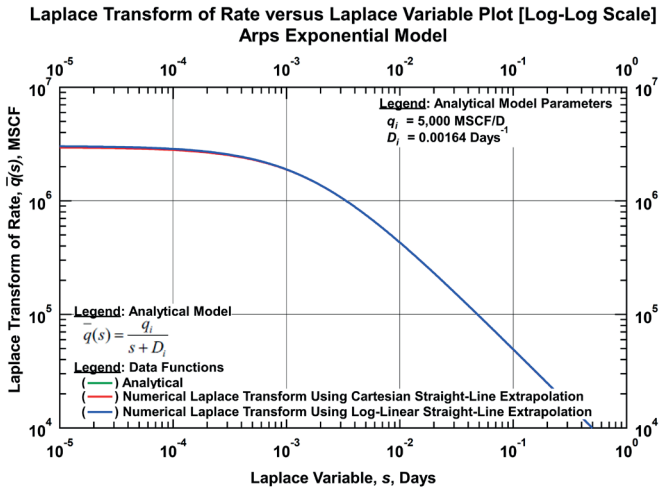

Figure C-1.1 — Comparison Plot of the Laplace Transform of the Synthetic Flowrate Using Analytical Solution, Numerical Solution with Cartesian Straight-Line Extrapolation, and Numerical Solution with Log-Linear Straight-Line Extrapolation Versus Laplace Transform Variable.

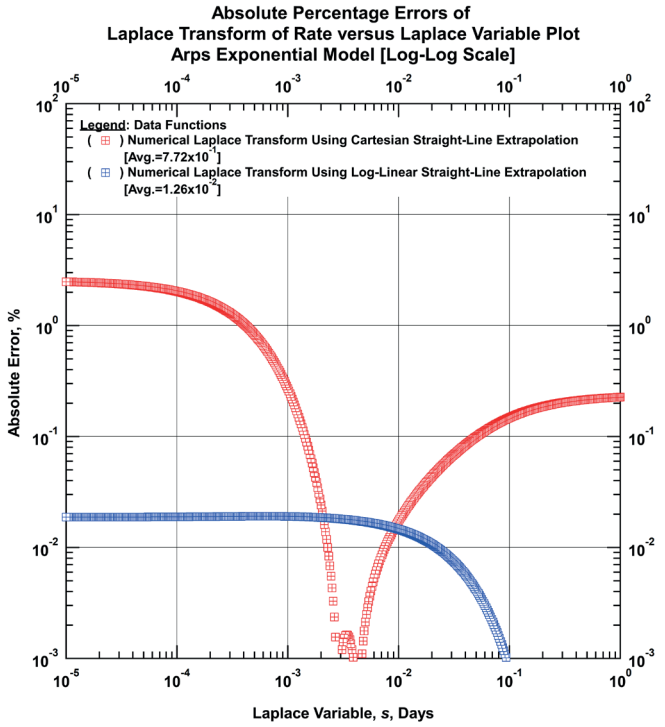

Figure C-1.2 — Comparison Plot of the Absolute Percentage Errors of the Laplace Transform of the Synthetic Flowrate Using Numerical Solution with Cartesian Straight-Line Extrapolation and Numerical Solution with Log-Linear Straight-Line Extrapolation Versus Laplace Transform Variable

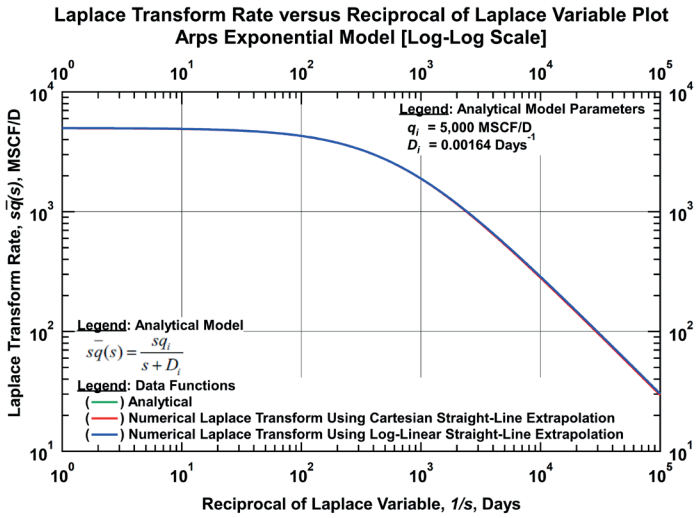

Figure C-1.3 — Comparison Plot of the Laplace Transform Rates Using Analytical Solution, Numerical Solution with Cartesian Straight-Line Extrapolation, and Numerical Solution with Log-Linear Straight-Line Extrapolation Versus Reciprocal of Laplace Transform Variable

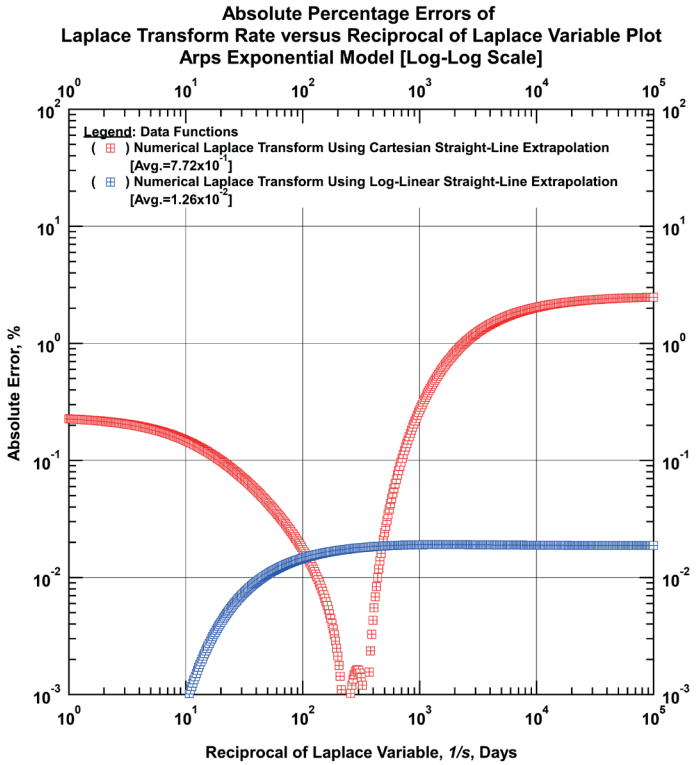

Figure C-1.4 — Comparison Plot of the Absolute Percentage Errors of the Laplace Transform Rates Using Numerical Solution with Cartesian Straight-Line Extrapolation and Numerical Solution with Log-Linear Straight-Line Extrapolation Versus Reciprocal of Laplace Transform Variable

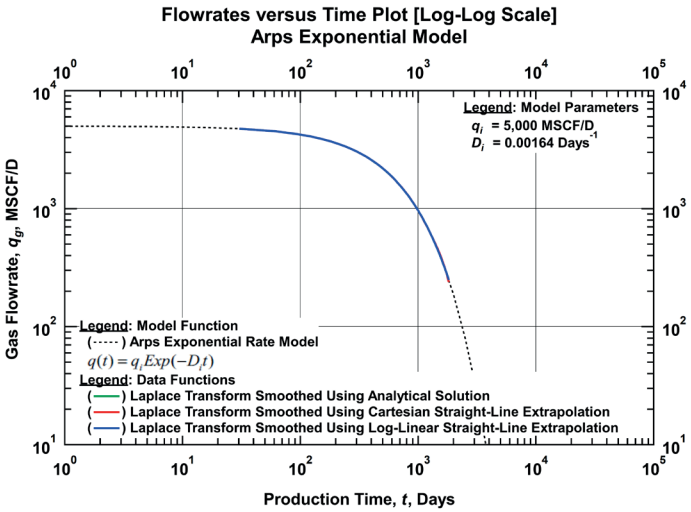

Figure C-1.5 — Comparison Plot of the Laplace Transform Smoothed Flowrates Using Analytical Solution, Numerical Solution with Cartesian Straight-Line Extrapolation, and Numerical Solution with Log-Linear Straight-Line Extrapolation Versus Time

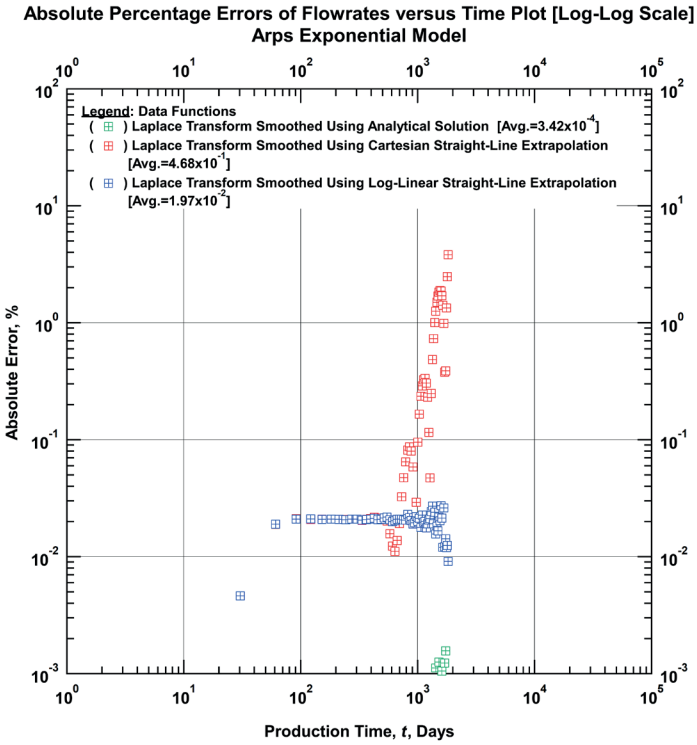

Figure C-1.6 — Comparison Plot of the Absolute Percentage Errors of the Laplace Transform Smoothed Flowrates Using Analytical Solution, Numerical Solution with Cartesian Straight-Line Extrapolation, and Numerical Solution with Log-Linear Straight-Line Extrapolation Versus Time

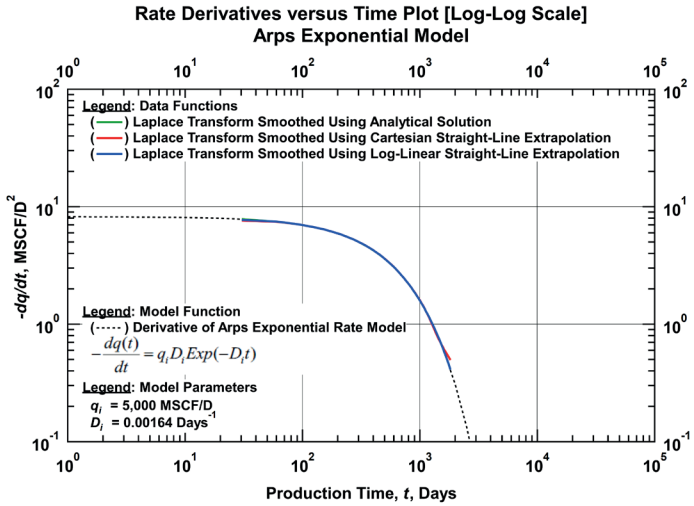

Figure C-1.7 — Comparison Plot of the Laplace Transform Smoothed Rate Derivatives Using Analytical Solution, Numerical Solution with Cartesian Straight-Line Extrapolation, and Numerical Solution with Log-Linear Straight-Line Extrapolation Versus Time

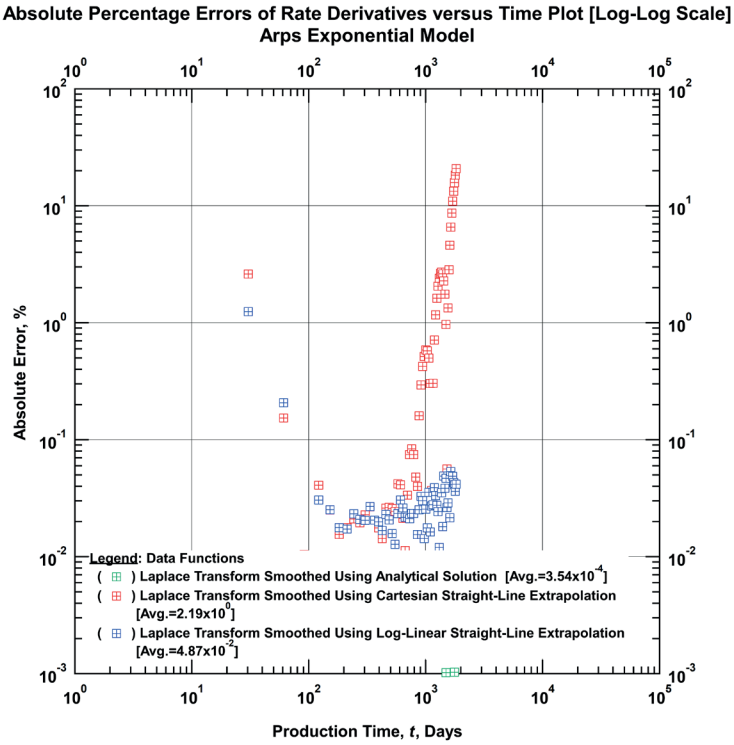

Figure C-1.8 — Comparison Plot of the Absolute Percentage Errors of the Laplace Transform Smoothed Rate Derivatives Using Analytical Solution, Numerical Solution with Cartesian Straight-Line Extrapolation, and Numerical Solution with Log-Linear Straight-Line Extrapolation Versus Time

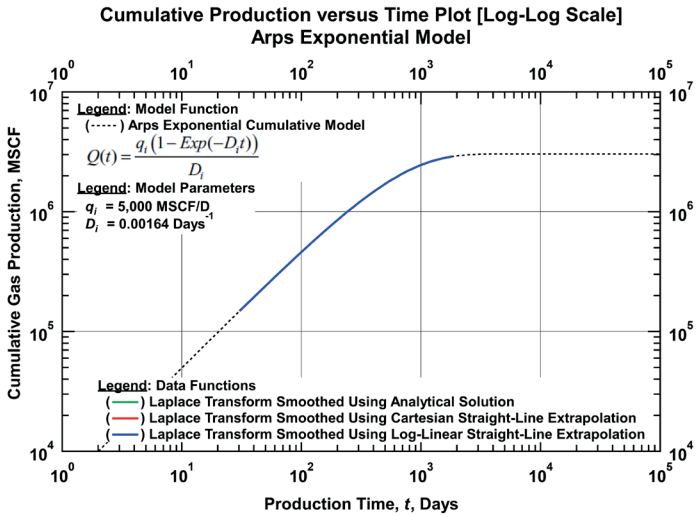

Figure C-1.9 — Comparison Plot of the Laplace Transform Smoothed Cumulative Production Using Analytical Solution, Numerical Solution with Cartesian Straight-Line Extrapolation, and Numerical Solution with Log-Linear Straight-Line Extrapolation Versus Time

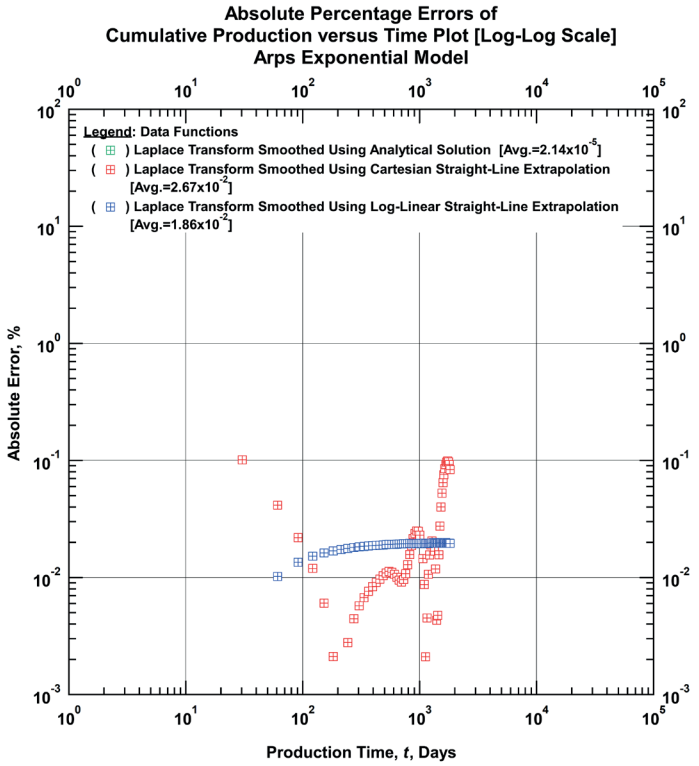

Figure C-1.10 — Comparison Plot of the Absolute Percentage Errors of the Laplace Transform Smoothed Cumulative Production Using Analytical Solution, Numerical Solution with Cartesian Straight-Line Extrapolation, and Numerical Solution with Log-Linear Straight-Line Extrapolation Versus Time

C.2 Effects of Data Frequency and Spacing Type

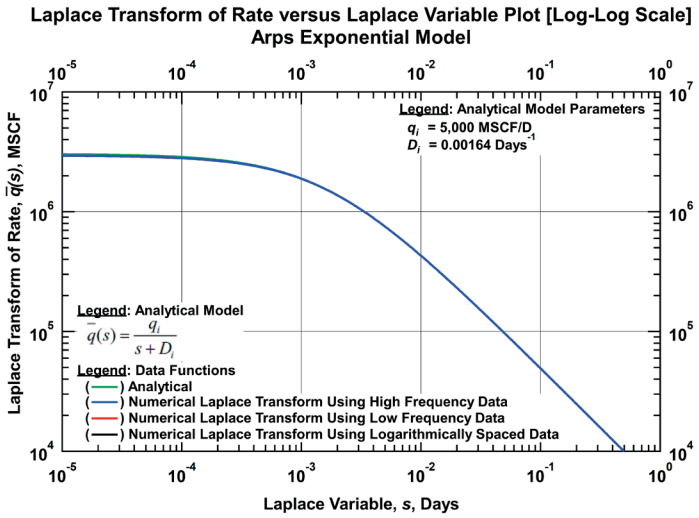

Figure C-2.1 — Comparison Plot of the Analytical Laplace Transform, the Numerical Laplace Transform of High-Frequency Data, Low-Frequency Data, and Logarithmically-Spaced Data Versus Laplace Transform Variable.

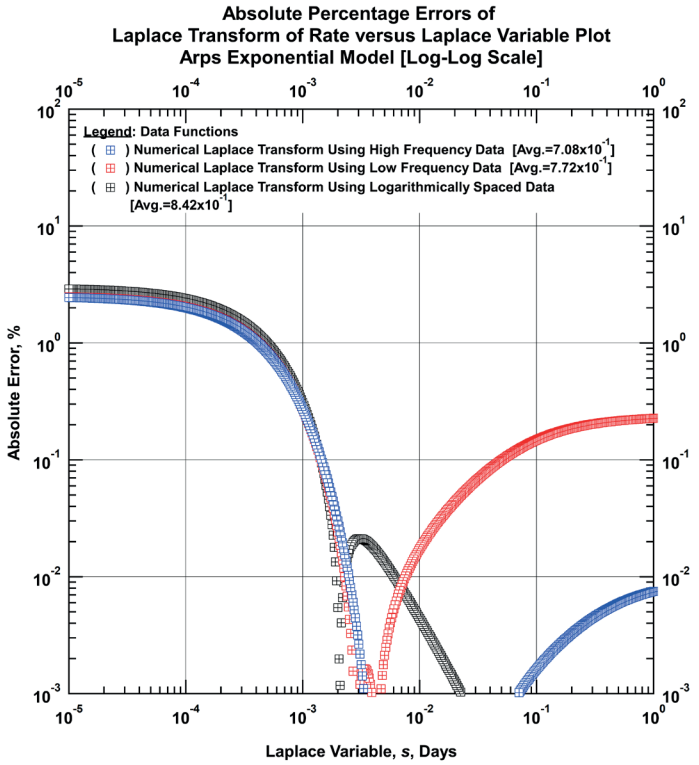

Figure C-2.2 — Comparison Plot of the Absolute Percentage Errors of the Numerical Laplace Transform of High-Frequency Data, Low-Frequency Data, and Logarithmically-Spaced Data Versus Laplace Transform Variable

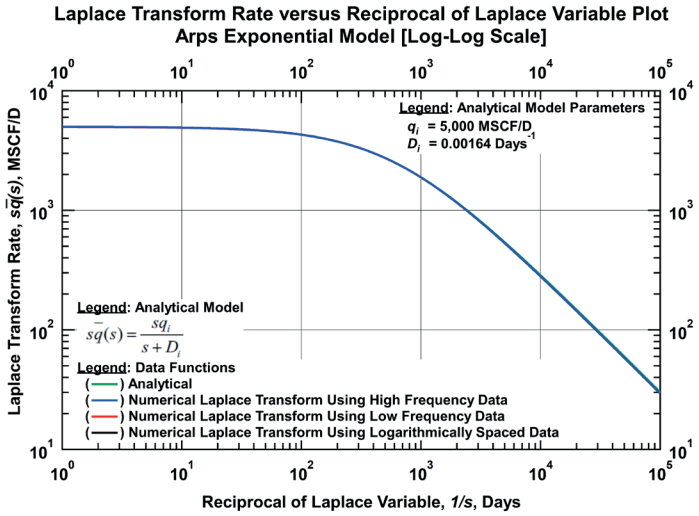

Figure C-2.3 — Comparison Plot of the Analytical Laplace Transform Rate, the Numerical Laplace Transform Rates of High-Frequency Data, Low-Frequency Data, and Logarithmically-Spaced Data Versus Reciprocal of Laplace Transform Variable

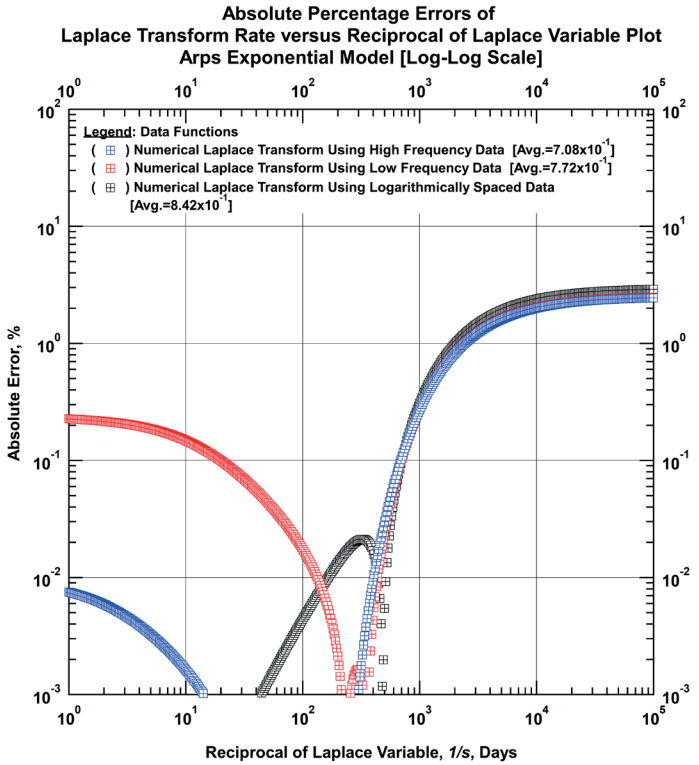

Figure C-2.4 — Comparison Plot of the Absolute Percentage Errors of the Numerical Laplace Transform Rates of High-Frequency Data, Low-Frequency Data, and Logarithmically-Spaced Data Versus Reciprocal of Laplace Transform Variable

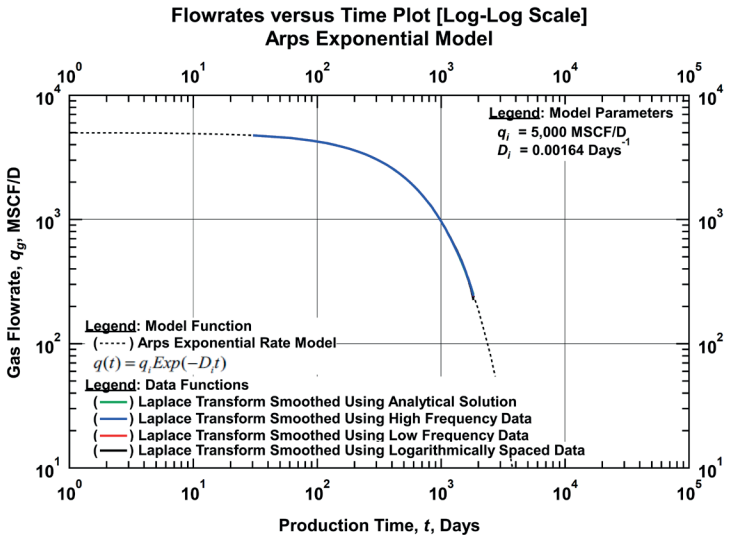

Figure C-2.5 — Comparison Plot of the Laplace Transform Smoothed Flowrates Using Analytical Solution, Numerical Solution of High-Frequency Data, Low-Frequency Data, and Logarithmically-Spaced Data Versus Time

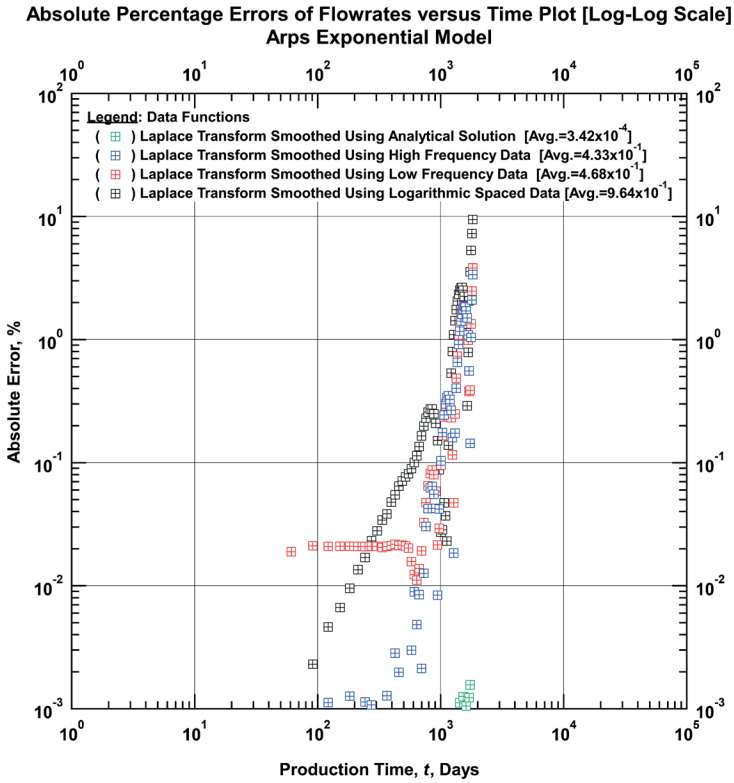

Figure C-2.6 — Comparison Plot of the Absolute Percentage Errors of the Laplace Transform Smoothed Flowrates Using Analytical Solution, Numerical Solution of High-Frequency Data, Low-Frequency Data, and Logarithmically-Spaced Data Versus Time

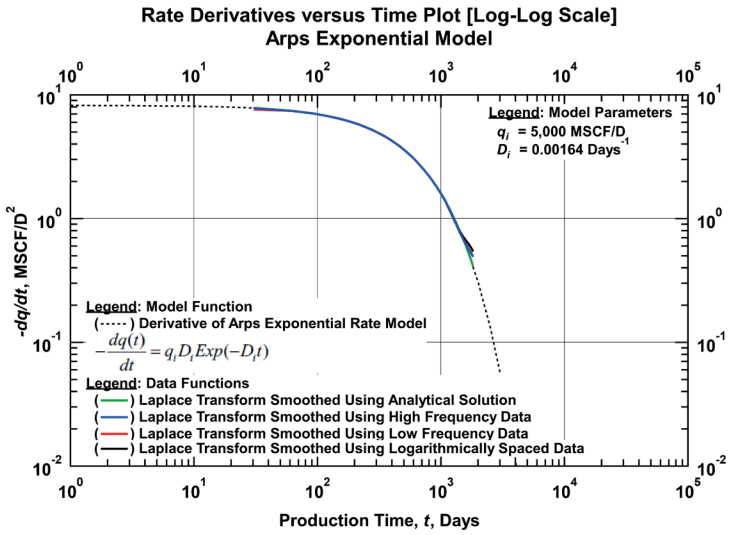

Figure C-2.7 — Comparison Plot of the Laplace Transform Smoothed Rate Derivatives Using Analytical Solution, Numerical Solution of High-Frequency Data, Low-Frequency Data, and Logarithmically-Spaced Data Versus Time

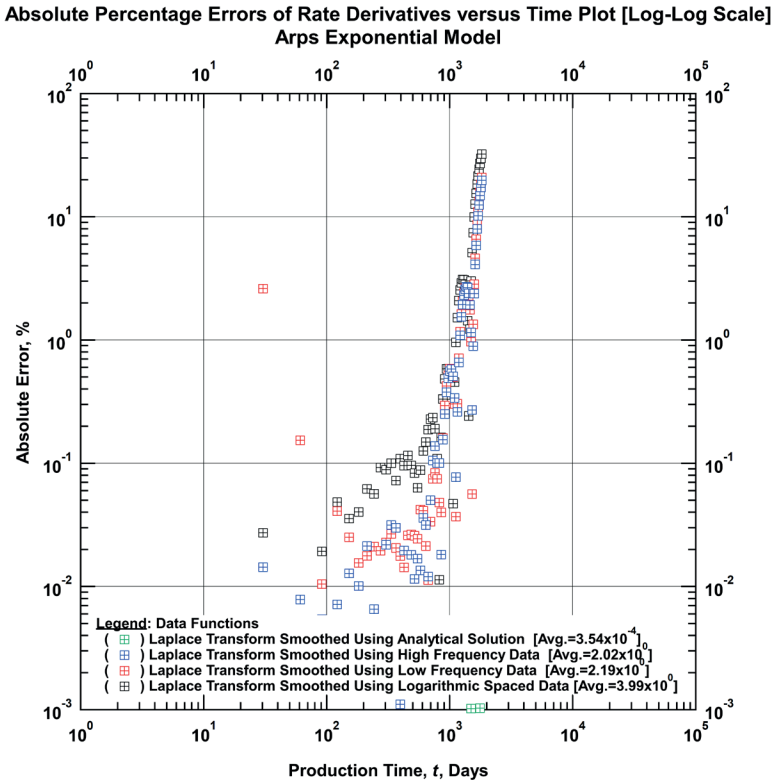

Figure C-2.8 — Comparison Plot of the Absolute Percentage Errors of the Laplace Transform Smoothed Rate Derivatives Using Analytical Solution, Numerical Solution of High-Frequency Data, Low-Frequency Data, and Logarithmically-Spaced Data Versus Time

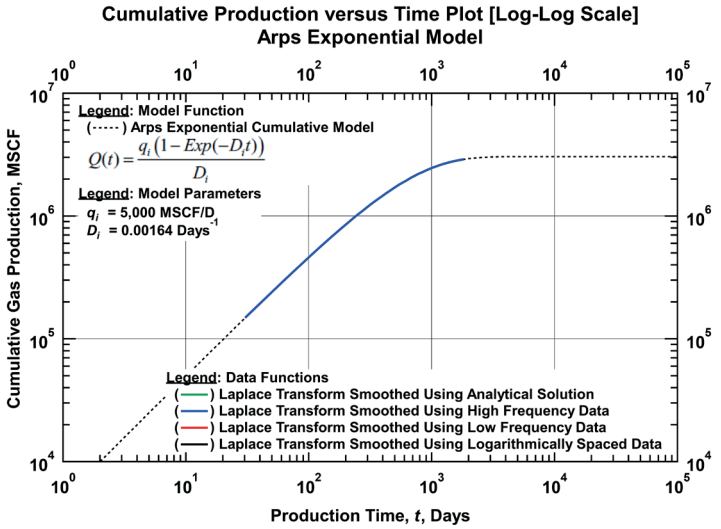

Figure C-2.9 — Comparison Plot of the Laplace Transform Smoothed Cumulative Production Using Analytical Solution, Numerical Solution of High-Frequency Data, Low-Frequency Data, and Logarithmically-Spaced Data Versus Time

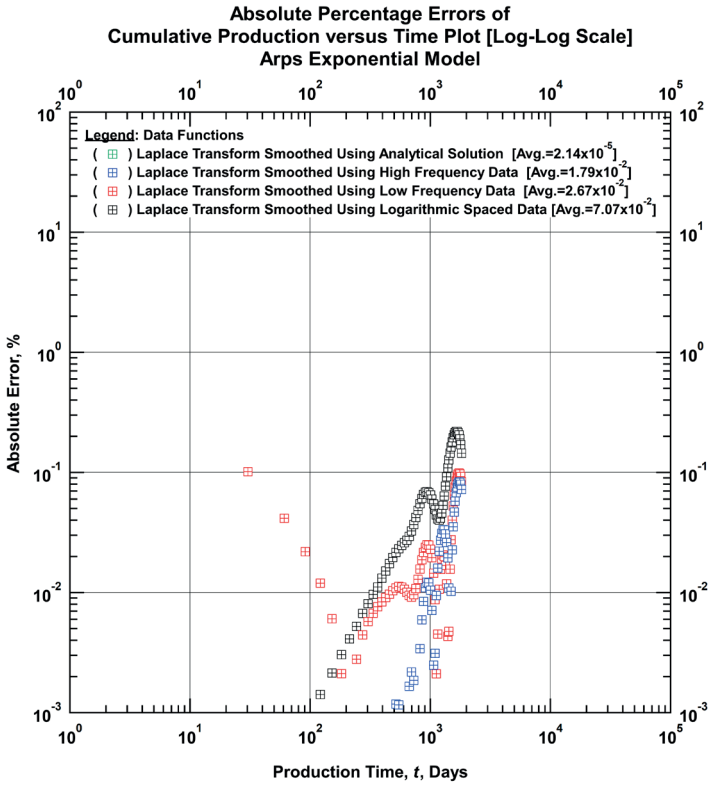

Figure C-2.10 — Comparison Plot of the Absolute Percentage Errors of the Laplace Transform Smoothed Cumulative Production Using Analytical Solution, Numerical Solution of High-Frequency Data, Low-Frequency Data, and Logarithmically-Spaced Data Versus Time

C.3 Effects of Data Extent

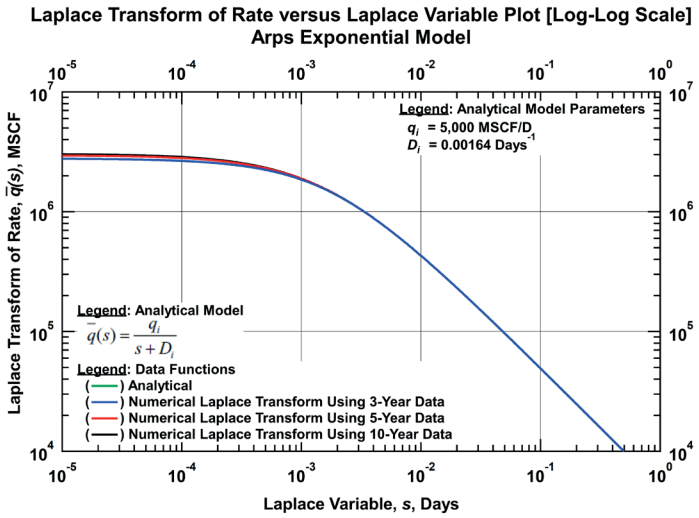

Figure C-3.1 — Comparison Plot of the Analytical Laplace Transform, the Numerical Laplace Transform of 3-Year Data, 5-Year Data, and 10-Year Data Versus Laplace Transform Variable.

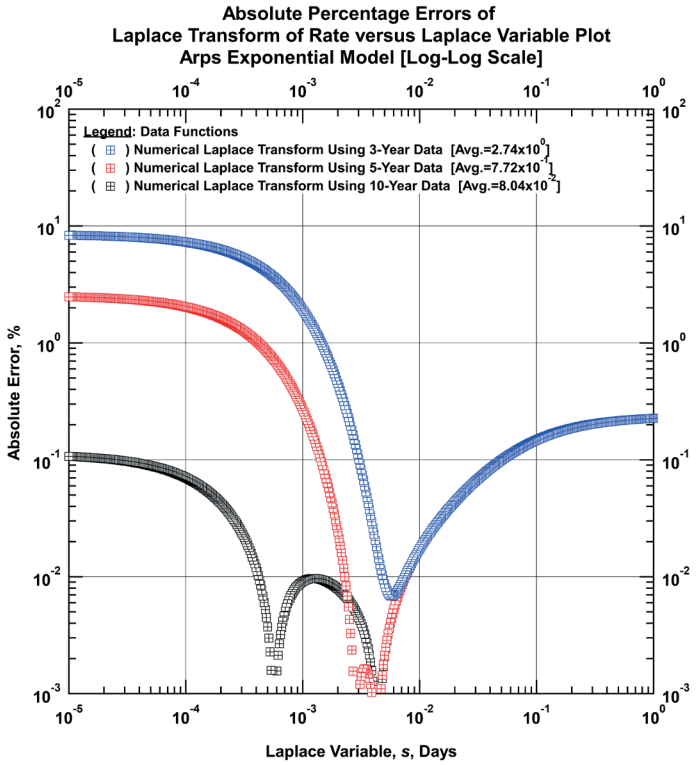

Figure C-3.2 — Comparison Plot of the Absolute Percentage Errors of the Numerical Laplace Transform of 3-Year Data, 5-Year Data, and 10-Year Data Versus Laplace Transform Variable

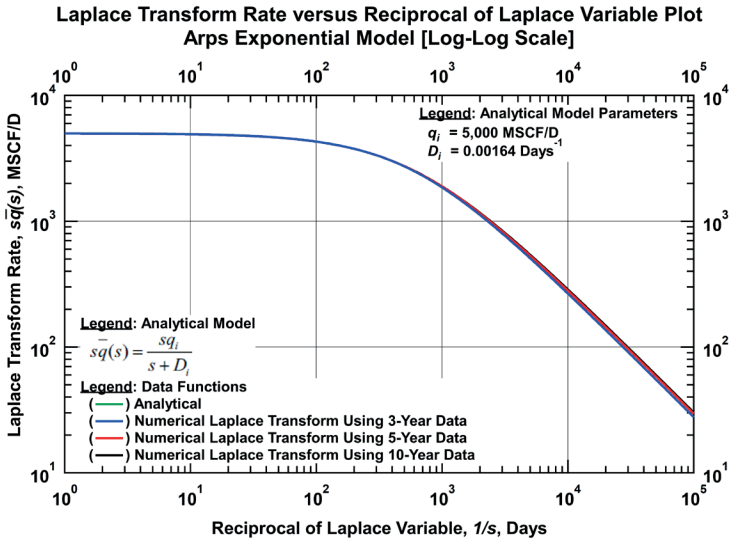

Figure C-3.3 — Comparison Plot of the Analytical Laplace Transform Rate, the Numerical Laplace Transform Rates of 3-Year Data, 5-Year Data, and 10-Year Data Versus Reciprocal of Laplace Transform Variable

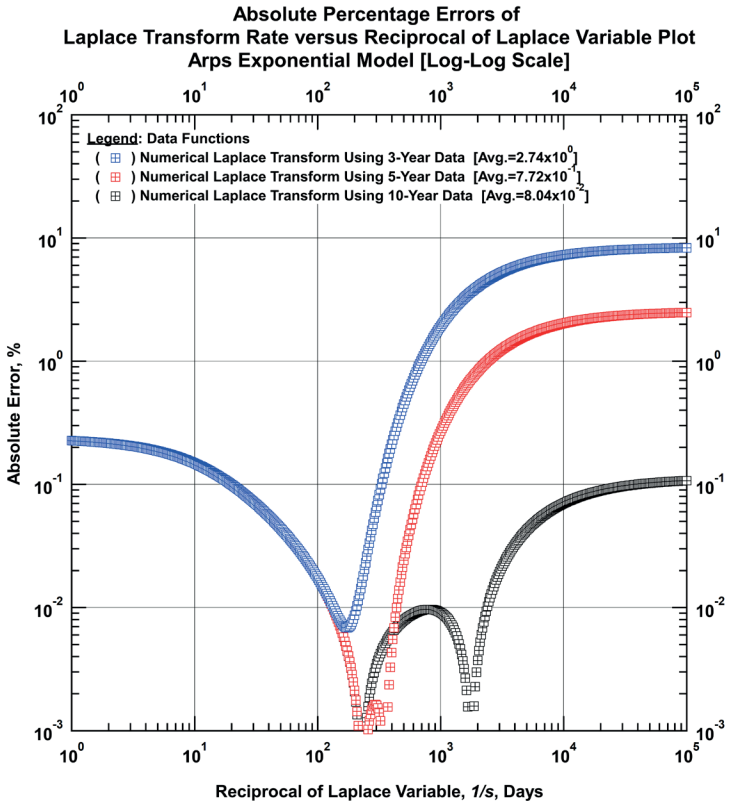

Figure C-3.4 — Comparison Plot of the Absolute Percentage Errors of the Numerical Laplace Transform Rates of 3-Year Data, 5-Year Data, and 10-Year Data Versus Reciprocal of Laplace Transform Variable

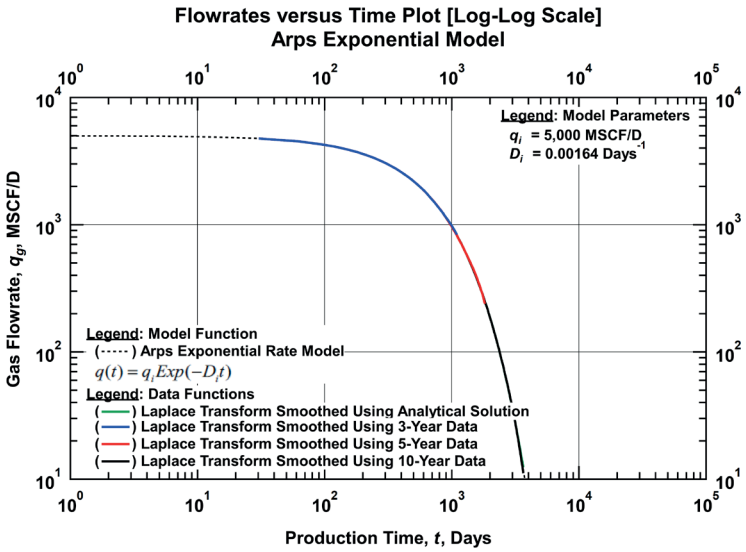

Figure C-3.5 — Comparison Plot of the Laplace Transform Smoothed Flowrates Using Analytical Solution, Numerical Solution of 3-Year Data, 5-Year Data, and 10-Year Data Versus Time

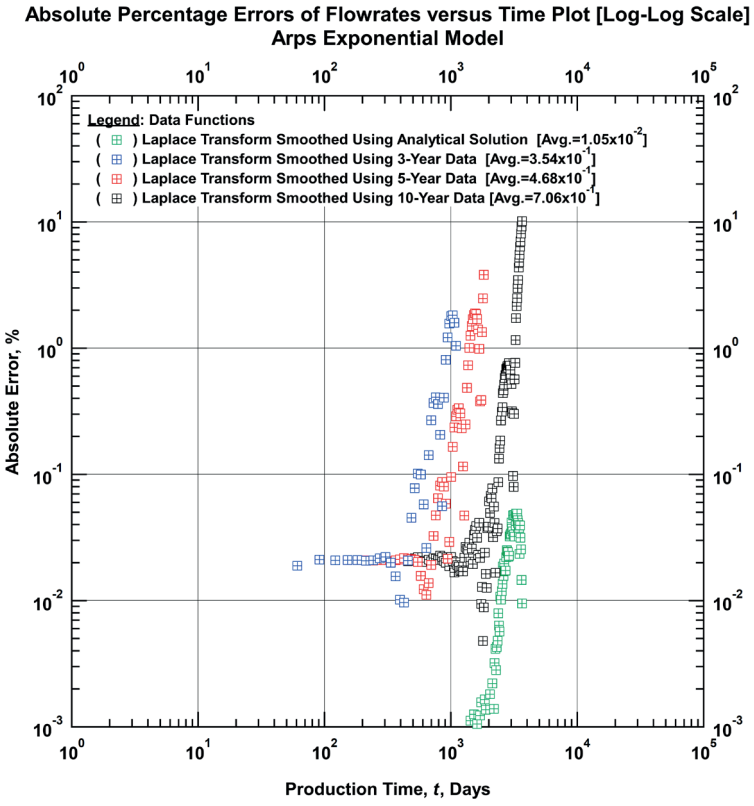

Figure C-3.6 — Comparison Plot of the Absolute Percentage Errors of the Laplace Transform Smoothed Flowrates Using Analytical Solution, Numerical Solution of 3-Year Data, 5-Year Data, and 10-Year Data Versus Time

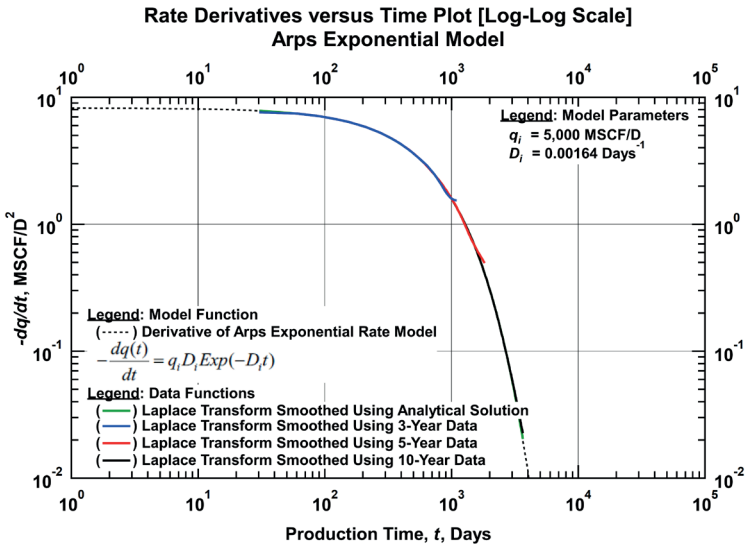

Figure C-3.7 — Comparison Plot of the Laplace Transform Smoothed Rate Derivatives Using Analytical Solution, Numerical Solution of 3-Year Data, 5-Year Data, and 10-Year Data Versus Time

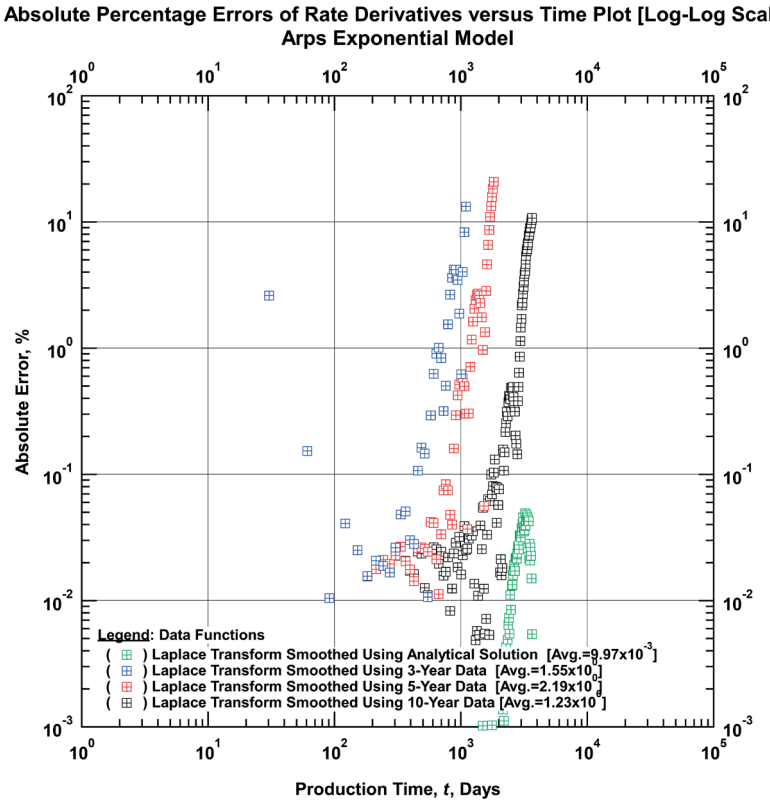

Figure C-3.8 — Comparison Plot of the Absolute Percentage Errors of the Laplace Transform Smoothed Rate Derivatives Using Analytical Solution, Numerical Solution of 3-Year Data, 5-Year Data, and 10-Year Data Versus Time

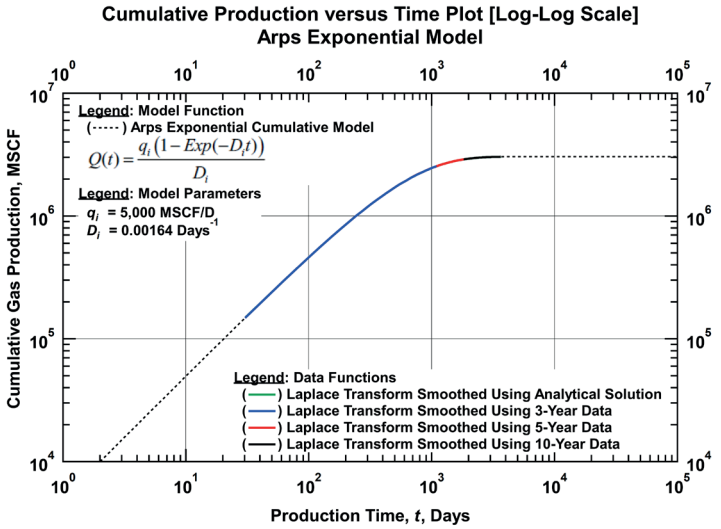

Figure C-3.9 — Comparison Plot of the Laplace Transform Smoothed Cumulative Production Using Analytical Solution, Numerical Solution of 3-Year Data, 5-Year Data, and 10-Year Data Versus Time

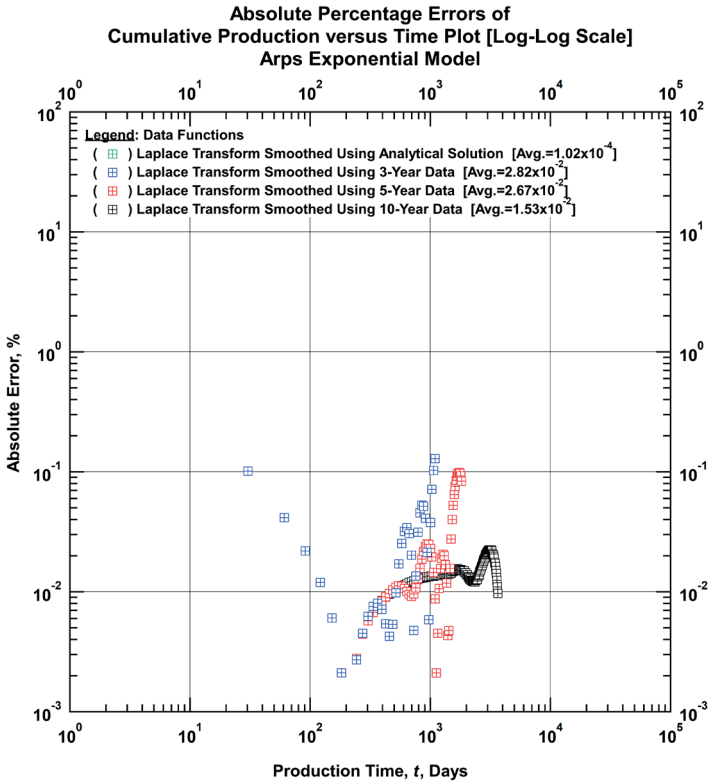

Figure C-3.10 — Comparison Plot of the Absolute Percentage Errors of the Laplace Transform Smoothed Cumulative Production Using Analytical Solution, Numerical Solution of 3-Year Data, 5-Year Data, and 10-Year Data Versus Time

C.4 Effects of Data Noise

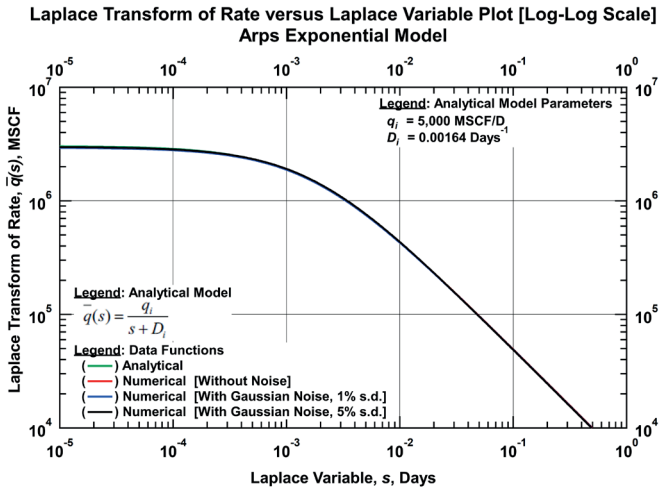

Figure C-4.1 — Comparison Plot of the Analytical Laplace Transform, the Numerical Laplace Transform of Data Without Noise, Data with 1-Percent Gaussian Noise, and Data with 5-Percent Gaussian Noise Versus Laplace Transform Variable.

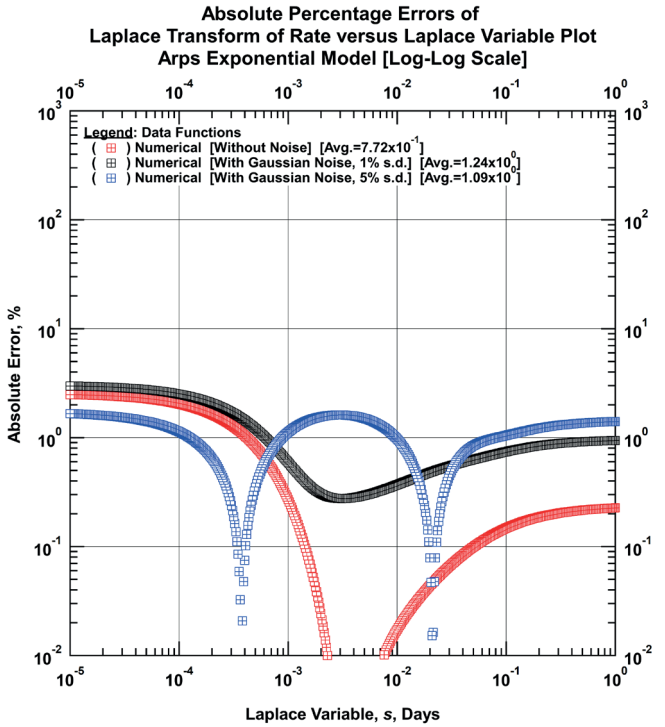

Figure C-4.2 — Comparison Plot of the Absolute Percentage Errors of the Numerical Laplace Transform of Data Without Noise, Data with 1-Percent Gaussian Noise, and Data with 5-Percent Gaussian Noise Versus Laplace Transform Variable

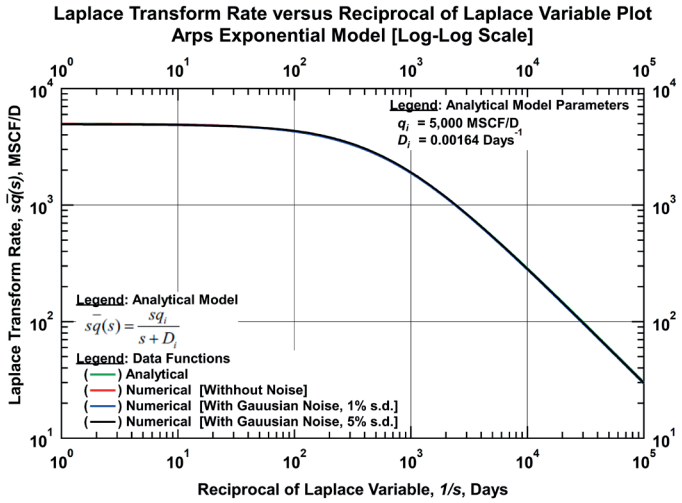

Figure C-4.3 — Comparison Plot of the Analytical Laplace Transform Rate, the Numerical Laplace Transform Rates of Data Without Noise, Data with 1-Percent Gaussian Noise, and Data with 5-Percent Gaussian Noise Versus Reciprocal of Laplace Transform Variable

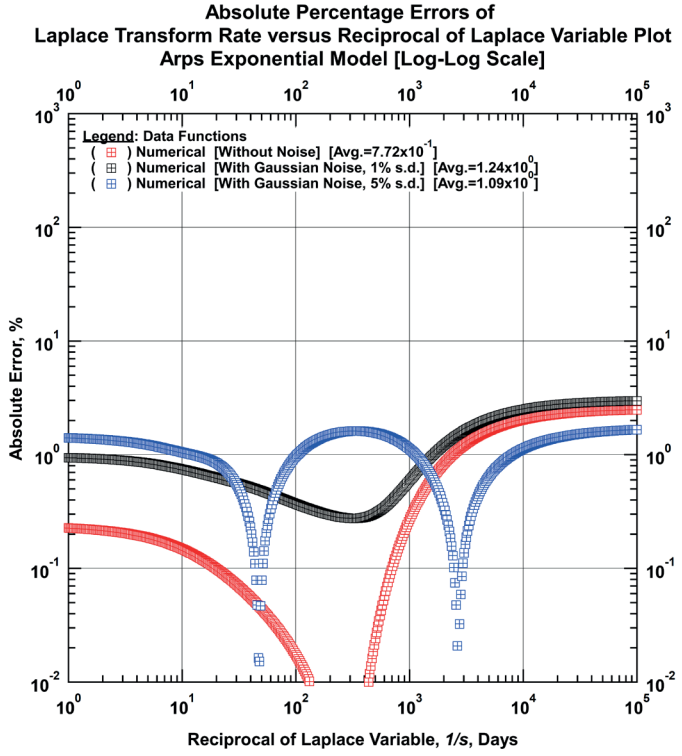

Figure C-4.4 — Comparison Plot of the Absolute Percentage Errors of the Numerical Laplace Transform Rates of Data Without Noise, Data with 1-Percent Gaussian Noise, and Data with 5-Percent Gaussian Noise Versus Reciprocal of Laplace Transform Variable

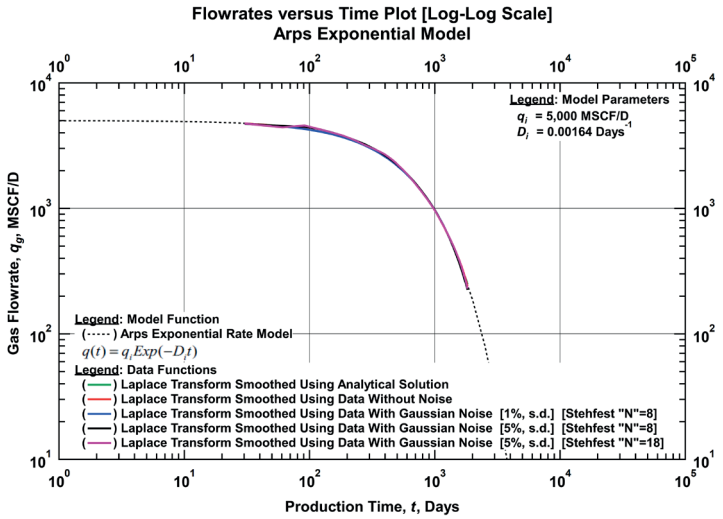

Figure C-4.5 — Comparison Plot of the Laplace Transform Smoothed Flowrates Using Analytical Solution, Numerical Solution of Data Without Noise, Data with 1-Percent Gaussian Noise, and Data with 5-Percent Gaussian Noise Versus Time

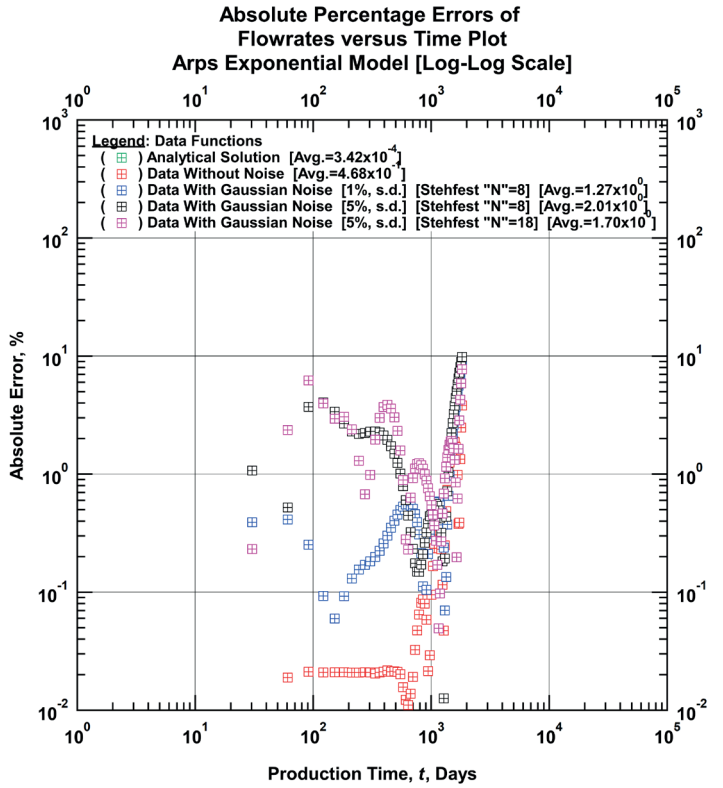

Figure C-4.6 — Comparison Plot of the Absolute Percentage Errors of the Laplace Transform Smoothed Flowrates Using Analytical Solution, Numerical Solution of Data Without Noise, Data with 1-Percent Gaussian Noise, and Data with 5-Percent Gaussian Noise Versus Time

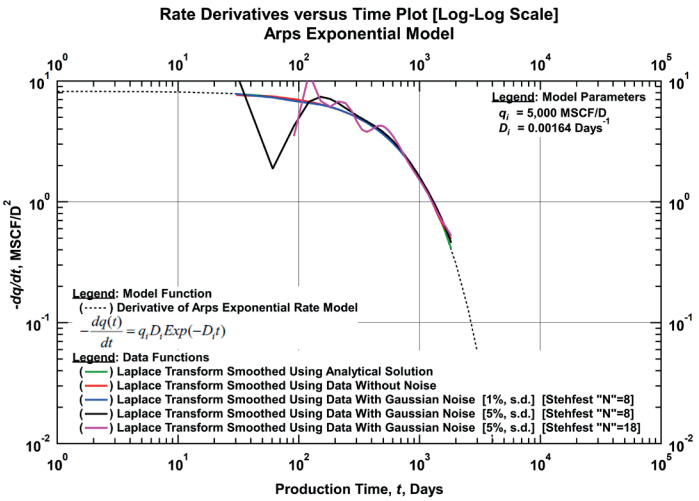

Figure C-4.7 — Comparison Plot of the Laplace Transform Smoothed Rate Derivatives Using Analytical Solution, Numerical Solution of Data Without Noise, Data with 1-Percent Gaussian Noise, and Data with 5-Percent Gaussian Noise Versus Time

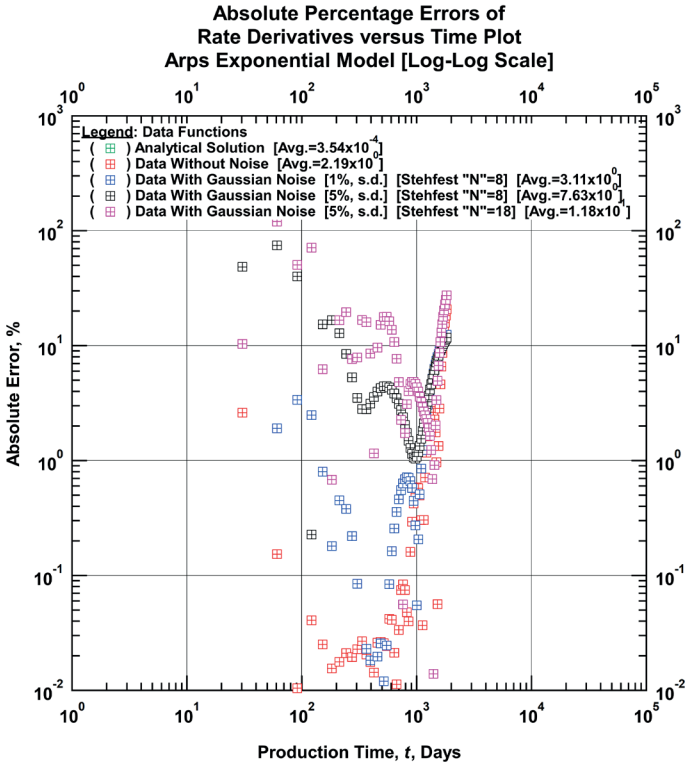

Figure C-4.8 — Comparison Plot of the Absolute Percentage Errors of the Laplace Transform Smoothed Rate Derivatives Using Analytical Solution, Numerical Solution of Data Without Noise, Data with 1-Percent Gaussian Noise, and Data with 5-Percent Gaussian Noise Versus Time

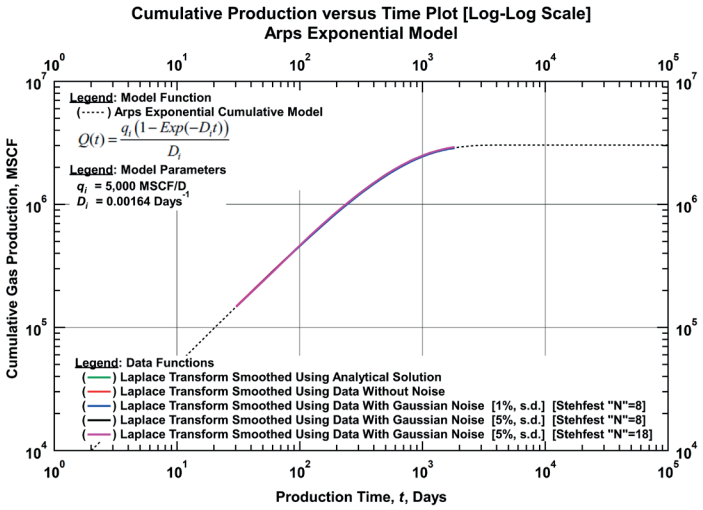

Figure C-4.9 — Comparison Plot of the Laplace Transform Smoothed Cumulative Production Using Analytical Solution, Numerical Solution of Data Without Noise, Data with 1-Percent Gaussian Noise, and Data with 5-Percent Gaussian Noise Versus Time

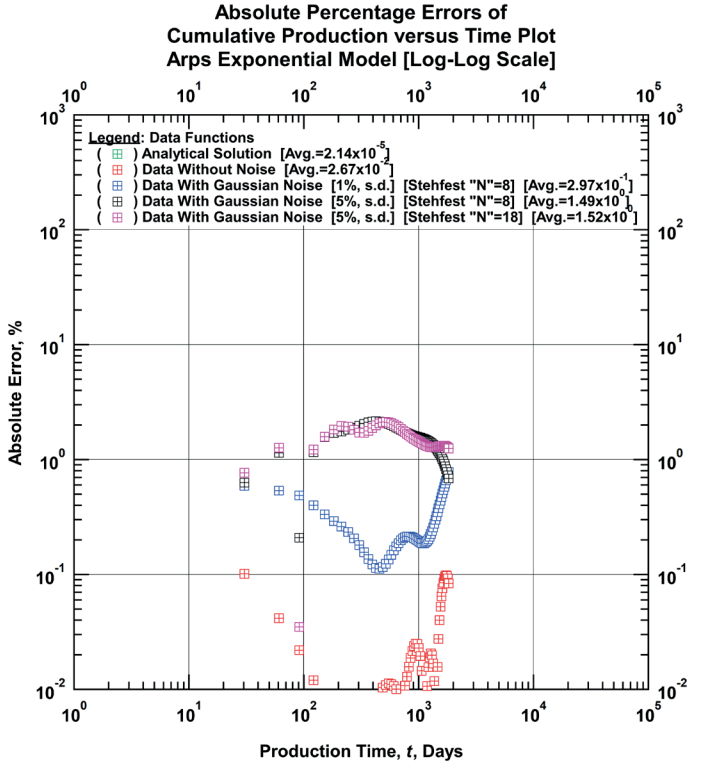

Figure C-4.10 — Comparison Plot of the Absolute Percentage Errors of the Laplace Transform Smoothed Cumulative Production Using Analytical Solution, Numerical Solution of Data Without Noise, Data with 1-Percent Gaussian Noise, and Data with 5-Percent Gaussian Noise Versus Time

C.5 Effects of Data Function Type (Increasing Data Function vs Decreasing Data Function)

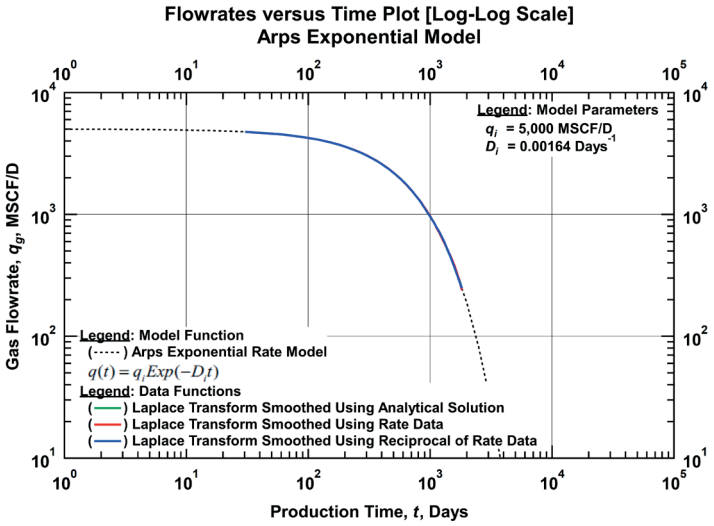

Figure C-5.1 — Comparison Plot of the Laplace Transform Smoothed Flowrates Using Analytical Solution, Numerical Solution of Rate Data, and Reciprocal of Rate Data Versus Time

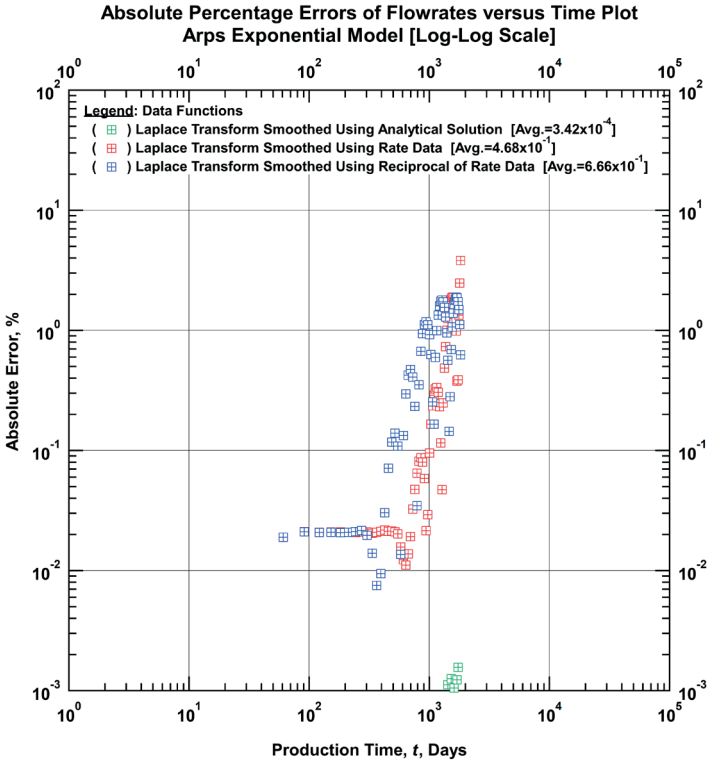

Figure C-5.2 — Comparison Plot of the Absolute Percentage Errors of the Laplace Transform Smoothed Flowrates Using Analytical Solution, Numerical Solution of Rate Data, and Reciprocal of Rate Data Versus Time

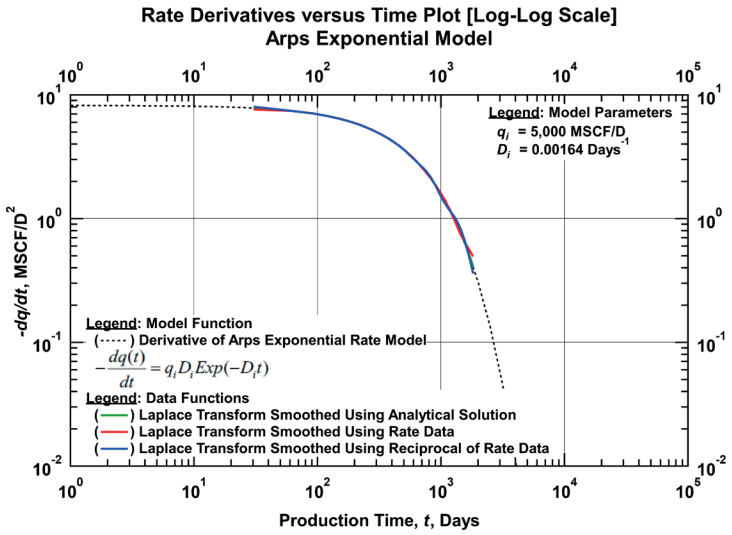

Figure C-5.3 — Comparison Plot of the Laplace Transform Smoothed Rate Derivatives Using Analytical Solution, Numerical Solution of Rate Data, and Reciprocal of Rate Data Versus Time

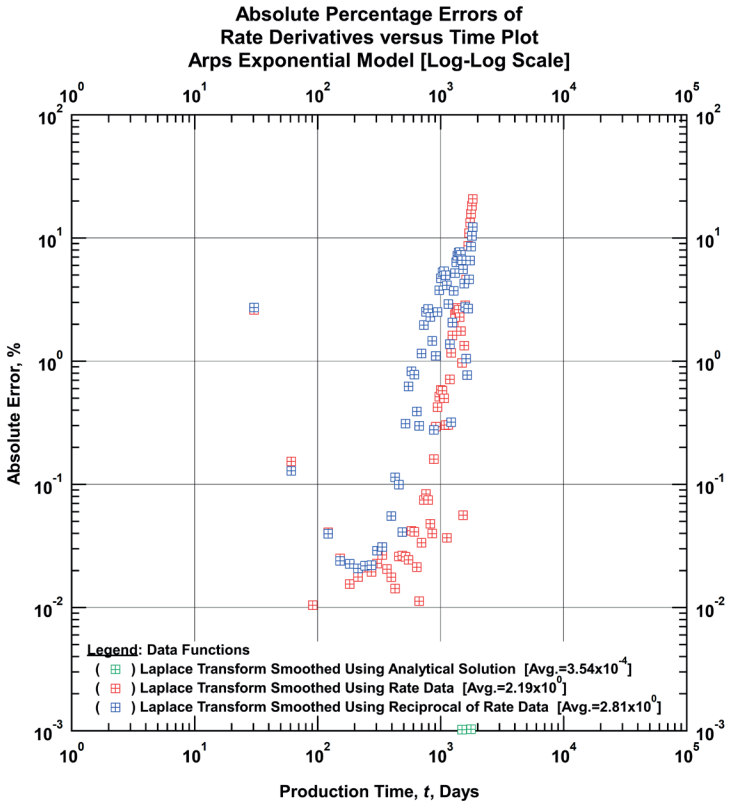

Figure C-5.4 — Comparison Plot of the Absolute Percentage Errors of the Laplace Transform Smoothed Rate Derivatives Using Analytical Solution, Numerical Solution of Rate Data, and Reciprocal of Rate Data Versus Time

References

A.1 Roumboutsos, A. and Stewart, G. 1988. A Direct Deconvolution or Convolution Algorithm for Well Test Analysis. Presented at the SPE Annual Technical Conference and Exhibition, Houston, Texas. 1988/1/1/. doi: 10.2118/18157-MS.

APPENDIX D

METHOD VALIDATION WITH SYNTHETIC TIME-RATE DATA

Thirteen method validation cases are presented in this appendix including:

- Arps exponential model (perfect data case)
- Arps exponential model (noisy data case)
- Arps hyperbolic model (perfect data case)
- Arps hyperbolic model (noisy data case)
- Arps harmonic model (perfect data case)
- Arps harmonic model (noisy data case)
- Modified hyperbolic model (perfect data case)
- Modified hyperbolic model (noisy data case
- Power-law exponential model (perfect data case)
- Power-law exponential model (noisy data case)
- Duong model (perfect data case)
- Logistic growth model (perfect data case)
- Logistic growth model (noisy data case)

D.1 Arps Exponential Model (Perfect Data Case)

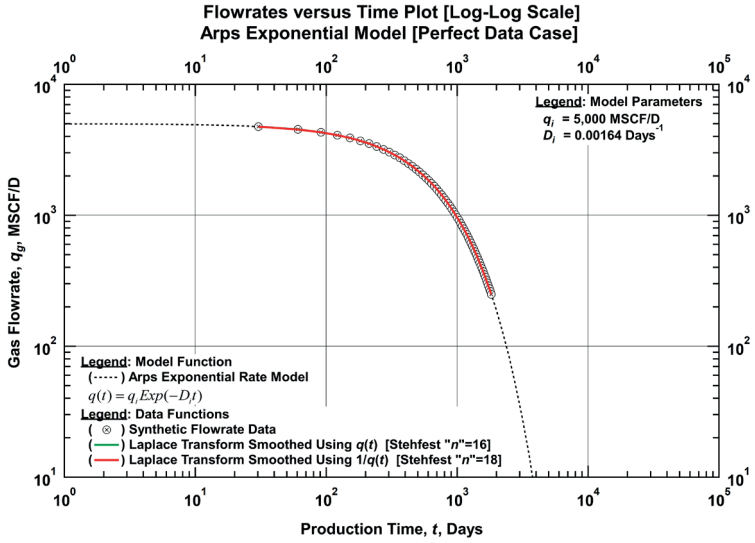

Figure D-1.1 — Comparison Plot of the Modelled Flowrate, Synthetic Flowrate, and Laplace Transform Smoothed Flowrates using Rate and Reciprocal of Rate as the Basis Functions Versus Time [Arps Exponential Model (Perfect Data Case)].

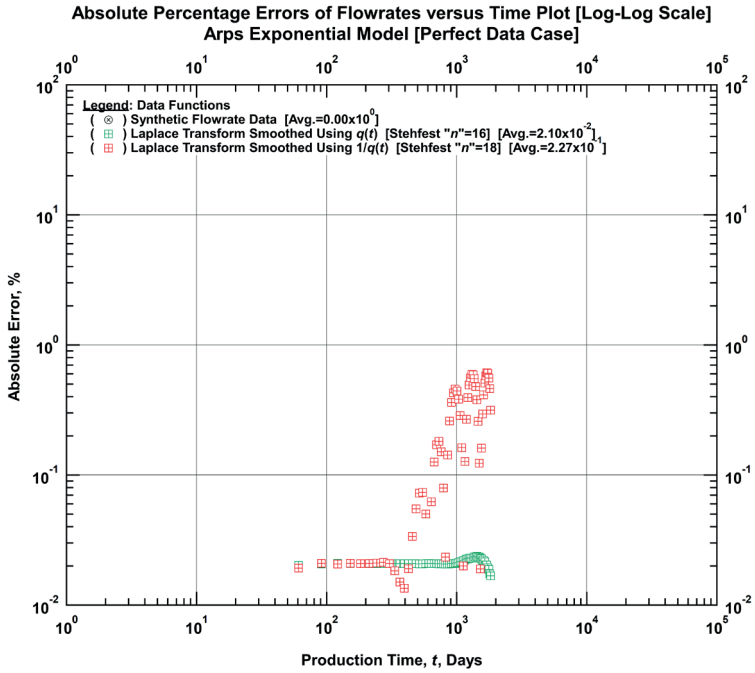

Figure D-1.2 — Comparison Plot of the Absolute Percentage Errors of the Synthetic Flowrate and Laplace Transform Smoothed Flowrates using Rate and Reciprocal of Rate as the Basis Functions Versus Time [Arps Exponential Model (Perfect Data Case)].

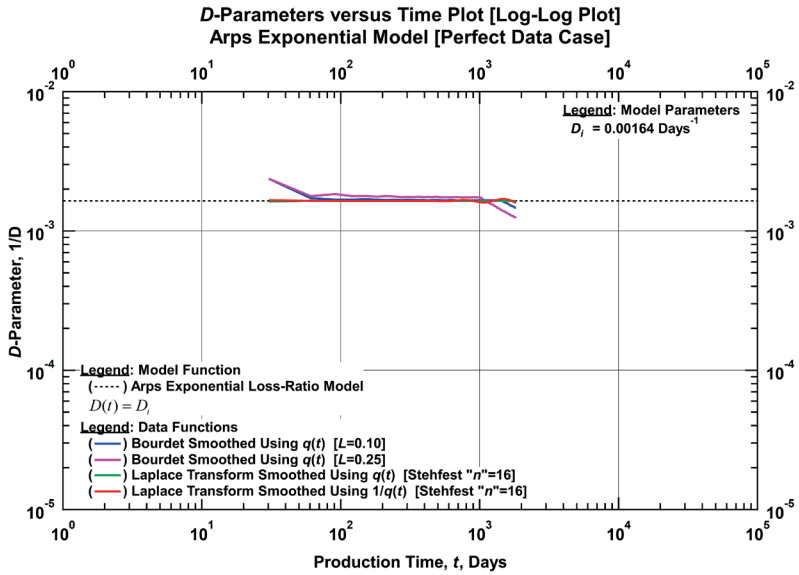

Figure D-1.3 — Comparison Plot of the Modelled *D*-Parameters, Bourdet-Derived *D*-Parameters, and Laplace Transform Smoothed *D*-Parameters using Rate and Reciprocal of Rate as the Basis Functions Versus Time [Arps Exponential Model (Perfect Data Case)].

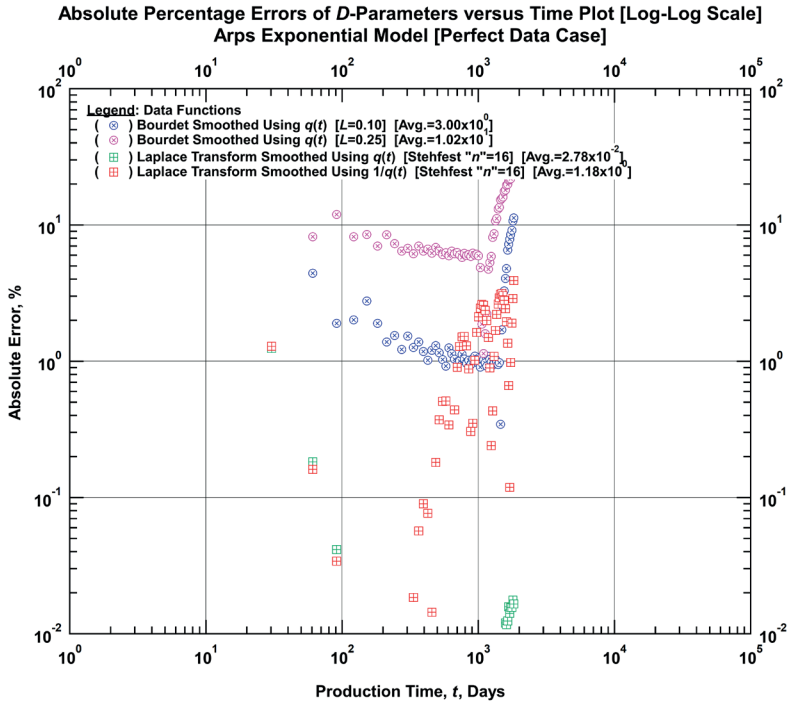

Figure D-1.4 — Comparison Plot of the Absolute Percentage Errors of the Bourdet-Derived *D*-Parameters and Laplace Transform Smoothed *D*-Parameters using Rate and Reciprocal of Rate Functions as the Basis Functions Versus Time [Arps Exponential Model (Perfect Data Case)].

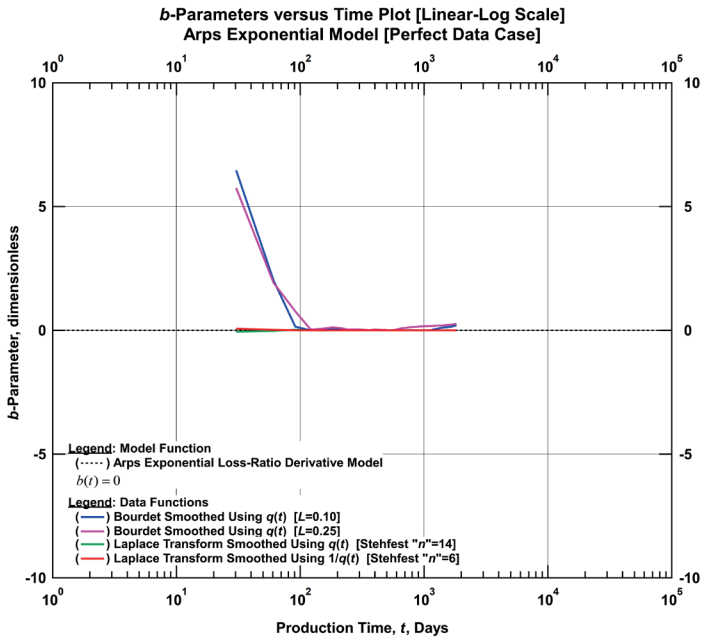

Figure D-1.5 — Comparison Plot of the Modelled *b*-Parameters, Bourdet-Derived *b*-Parameters, and Laplace Transform Smoothed *b*-Parameters using Rate and Reciprocal of Rate as the Basis Functions Versus Time [Arps Exponential Model (Perfect Data Case)].

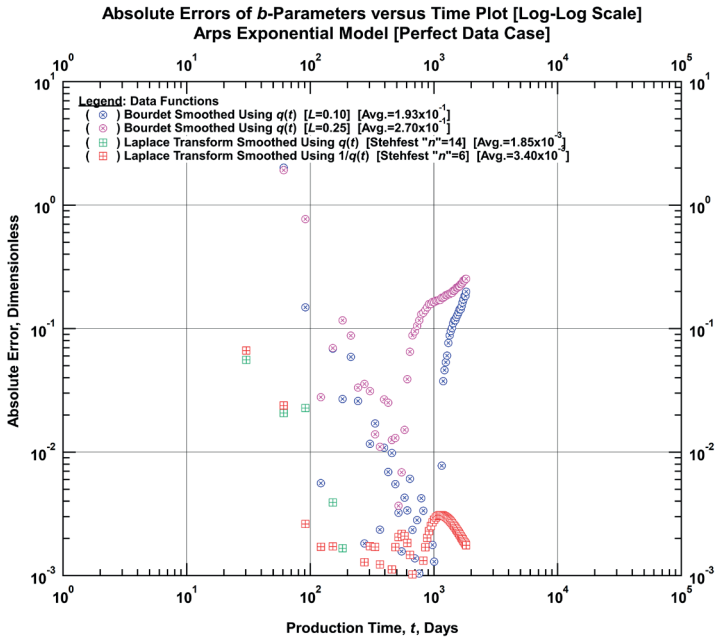

Figure D-1.6 — Comparison Plot of the Absolute Percentage Errors of the Bourdet-Derived *b*-Parameters and Laplace Transform Smoothed *b*-Parameters using Rate and Reciprocal of Rate as the Basis Functions versus Time [Arps Exponential Model (Perfect Data Case)].

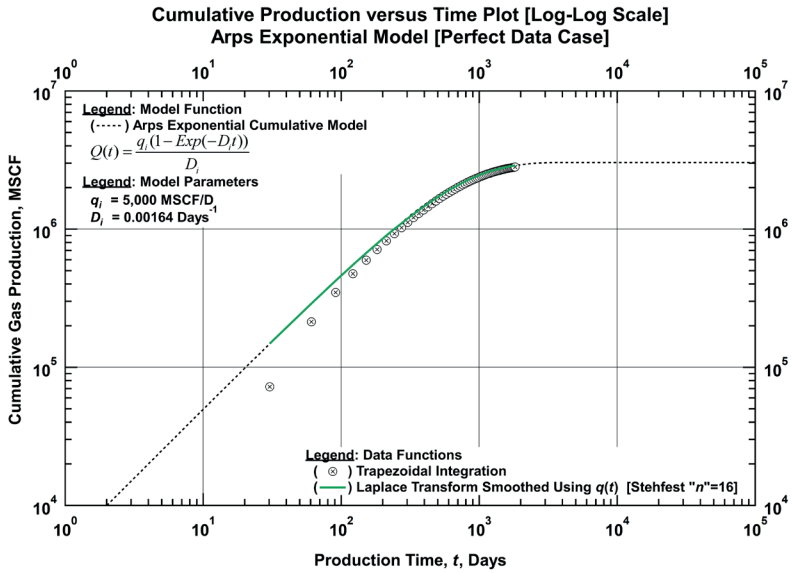

Figure D-1.7 — Comparison Plot of the Modelled Cumulative Production, Trapezoidal-Integrated Cumulative Production, and Laplace Transform Smoothed Cumulative Production using Rate as Basis Function versus Time [Arps Exponential Model (Perfect Data Case)].

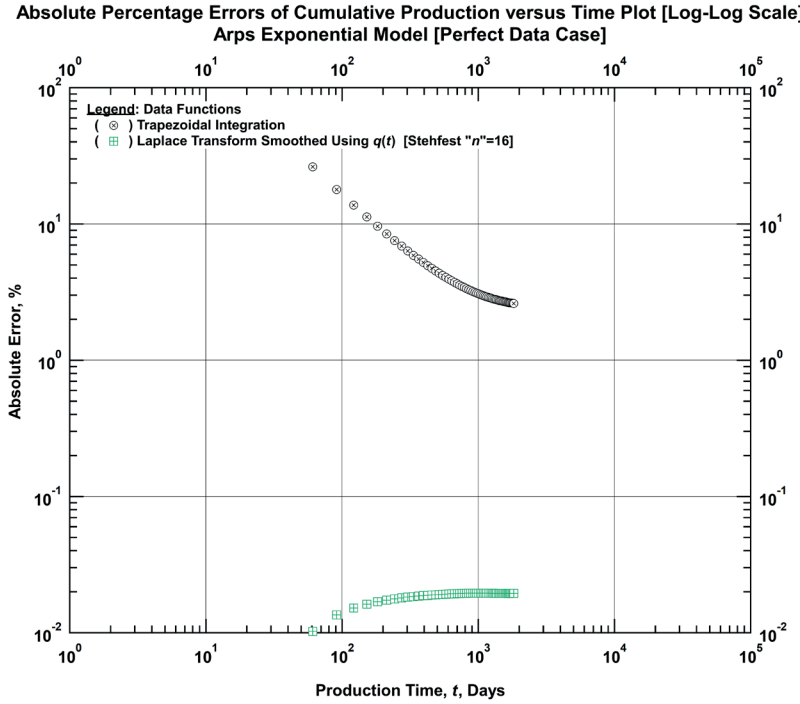

Figure D-1.8 — Comparison Plot of the Absolute Percentage Errors of Trapezoidal-Integrated Cumulative Production and Laplace Transform Smoothed Cumulative Production using Rate as Basis Function versus Time [Arps Exponential Model (Perfect Data Case)].

Table D-1 — Input Parameters for Arps Exponential Model (Perfect Data Set) Case.

Basis Function: Time-Rate Data

Laplace Smoothed Functions	**Rate & Cum. Production**	**D-Parameter**	**b-Parameter**
Basis Functions	$q(t)$	$q(t)$	$1/D(t)$
Numerical Laplace Transform Parameters			
LHS Extrapolation Type (NP1)	Log-Linear	Log-Linear	Straight Line
RHS Extrapolation Type (NP3)	Log-Linear	Log-Linear	Straight Line
LHS Regression Range (lL)	0.35	0.35	1.09
RHS Regression Range (lR)	0.01	0.01	0.43
Numerical Laplace Inversion Parameter			
Stehfest "n" Parameter	16	16	14

Basis Function: Time-Reciprocal of Rate Data

Laplace Smoothed Functions	**Rate**	**D-Parameter**	**b-Parameter**
Basis Functions	$1/q(t)$	$1/q(t)$	$1/D(t)$
Numerical Laplace Transform Parameters			
LHS Extrapolation Type (NP1)	Log-Linear	Log-Linear	Straight Line
RHS Extrapolation Type (NP3)	Log-Log	Log-Log	Straight Line
LHS Regression Range (lL)	0.35	0.35	1.09
RHS Regression Range (lR)	0.01	0.01	0.43
Numerical Laplace Inversion Parameter			
Stehfest "n" Parameter	18	16	6

D.2 Arps Exponential Model (Noisy Data Case)

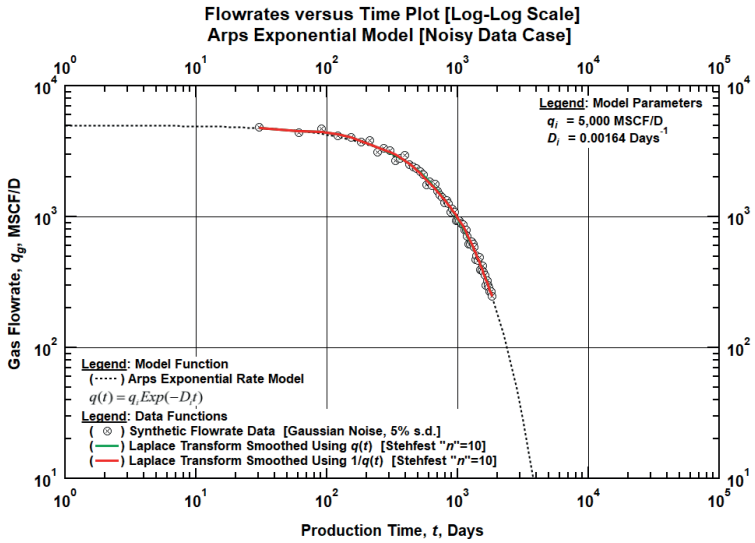

Figure D-2.1 — Comparison Plot of the Modelled Flowrate, Synthetic Flowrate, and Laplace Transform Smoothed Flowrates using Rate and Reciprocal of Rate as the Basis Functions Versus Time [Arps Exponential Model (Noisy Data Case)].

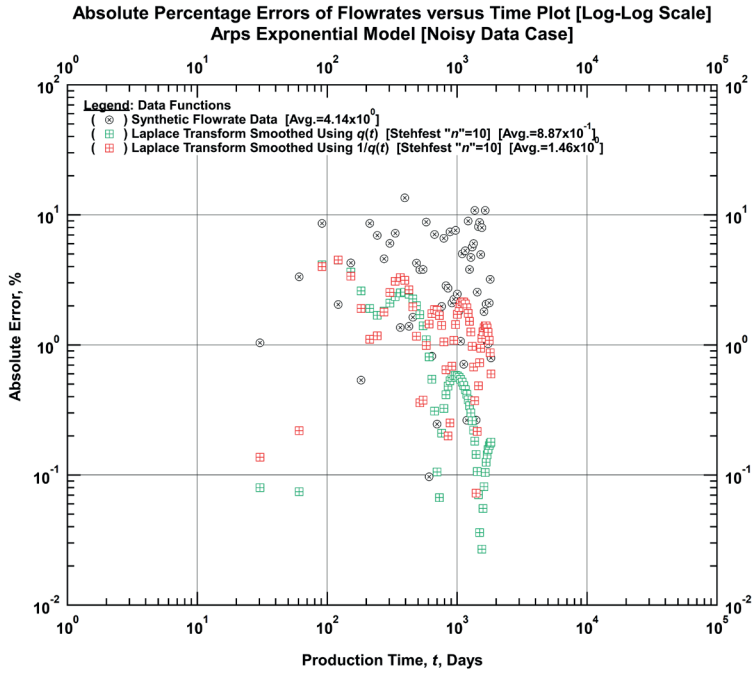

Figure D-2.2 — Comparison Plot of the Absolute Percentage Errors of the Synthetic Flowrate and Laplace Transform Smoothed Flowrates using Rate and Reciprocal of Rate as the Basis Functions Versus Time [Arps Exponential Model (Noisy Data Case)].

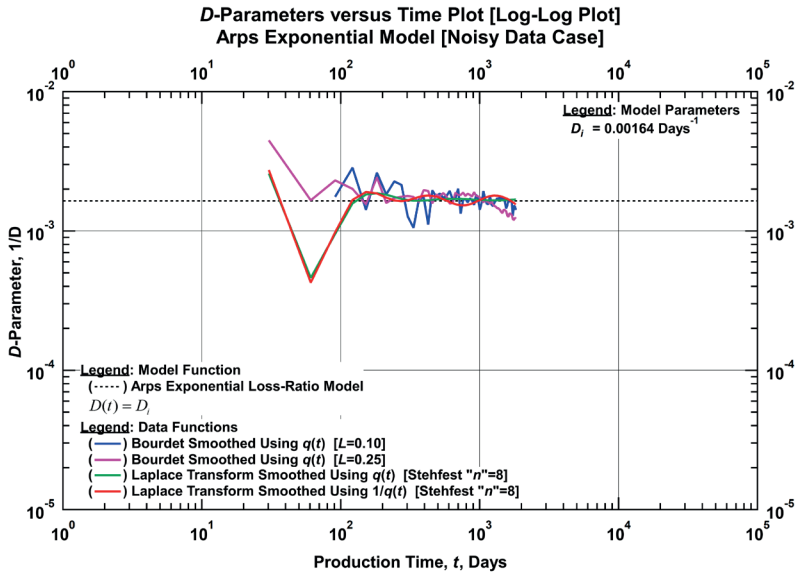

Figure D-2.3 — Comparison Plot of the Modelled *D*-Parameters, Bourdet-Derived *D*-Parameters, and Laplace Transform Smoothed *D*-Parameters using Rate and Reciprocal of Rate as the Basis Functions Versus Time [Arps Exponential Model (Noisy Data Case)].

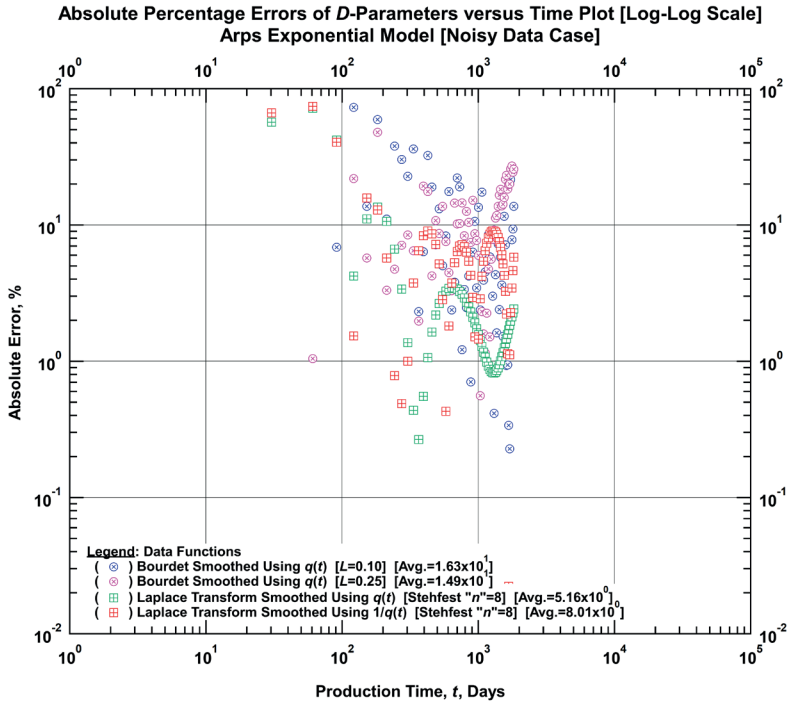

Figure D-2.4 — Comparison Plot of the Absolute Percentage Errors of the Bourdet-Derived *D*-Parameters and Laplace Transform Smoothed *D*-Parameters using Rate and Reciprocal of Rate Functions as the Basis Functions Versus Time [Arps Exponential Model (Noisy Data Case)].

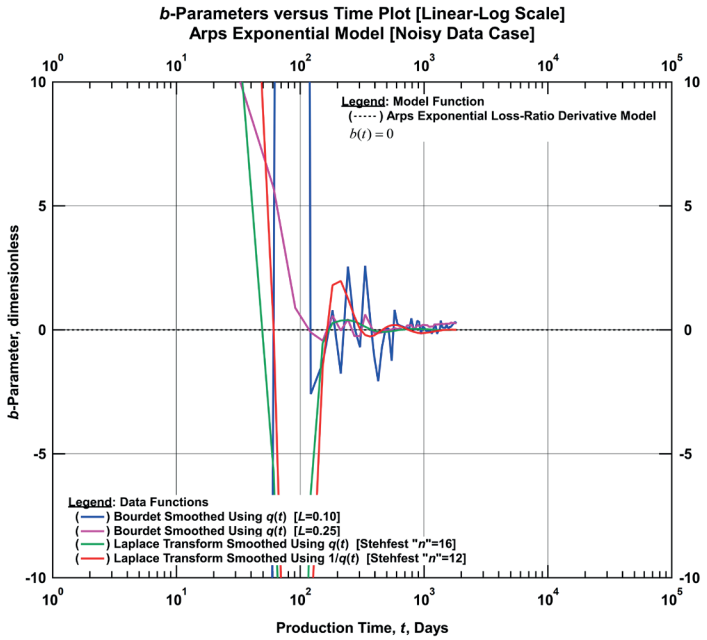

Figure D-2.5 — Comparison Plot of the Modelled *b*-Parameters, Bourdet-Derived *b*-Parameters, and Laplace Transform Smoothed *b*-Parameters using Rate and Reciprocal of Rate as the Basis Functions Versus Time [Arps Exponential Model (Noisy Data Case)].

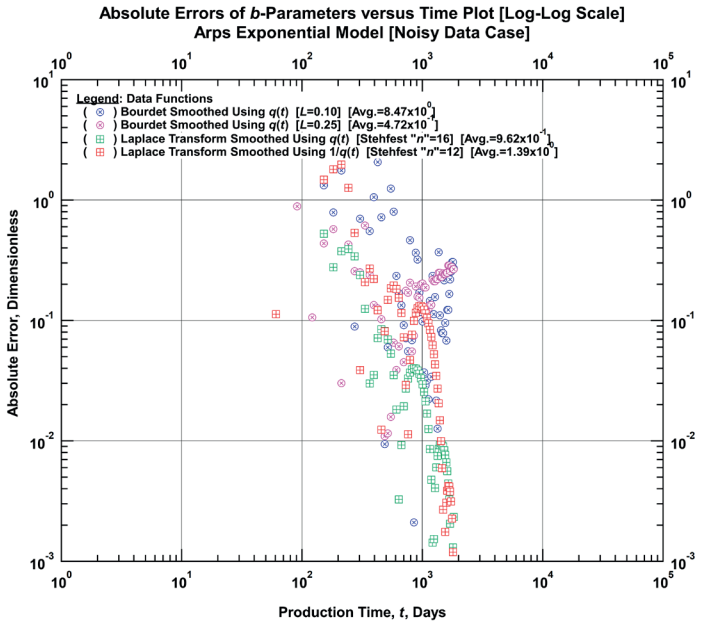

Figure D-2.6 — Comparison Plot of the Absolute Percentage Errors of the Bourdet-Derived *b*-Parameters and Laplace Transform Smoothed *b*-Parameters using Rate and Reciprocal of Rate as the Basis Functions versus Time [Arps Exponential Model (Noisy Data Case)].

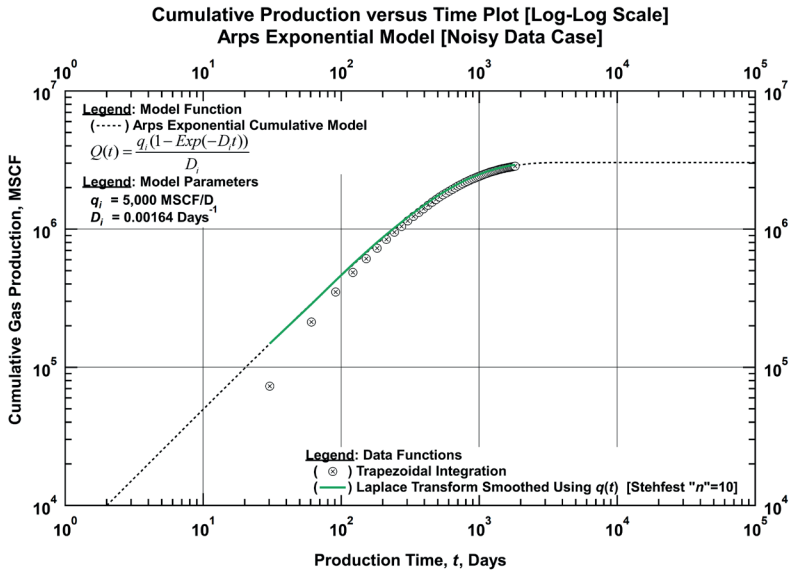

Figure D-2.7 — Comparison Plot of the Modelled Cumulative Production, Trapezoidal-Integrated Cumulative Production, and Laplace Transform Smoothed Cumulative Production using Rate as Basis Function versus Time [Arps Exponential Model (Noisy Data Case)].

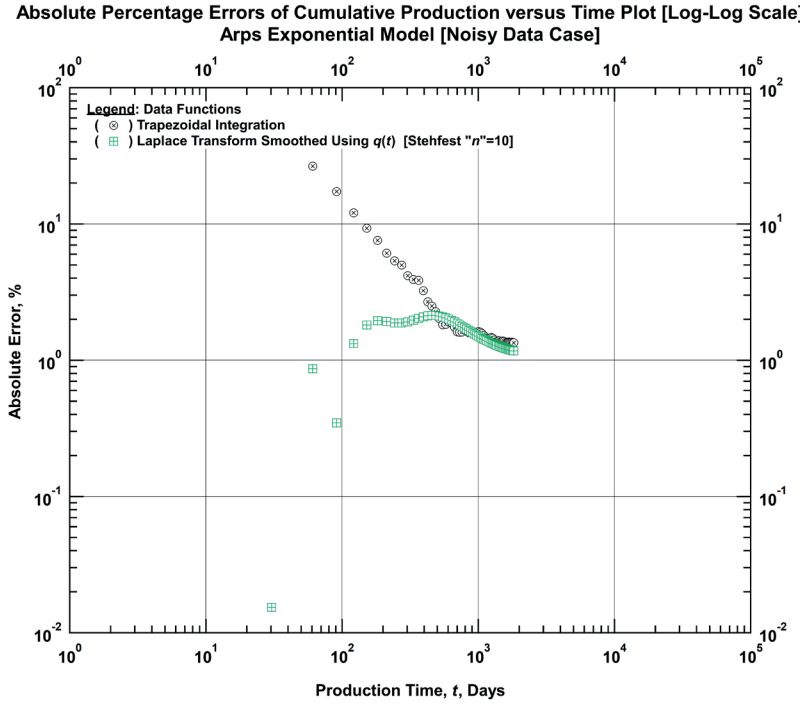

Figure D-2.8 — Comparison Plot of the Absolute Percentage Errors of Trapezoidal-Integrated Cumulative Production and Laplace Transform Smoothed Cumulative Production using Rate as Basis Function versus Time [Arps Exponential Model (Noisy Data Case)].

Table D-2 — Input Parameters for Arps Exponential Model (Noisy Data Set) Case.

Basis Function: Time-Rate Data

Laplace Smoothed Functions	**Rate & Cum. Production**	**D-Parameter**	**b-Parameter**
Basis Functions	$q(t)$	$q(t)$	$1/D(t)$
Numerical Laplace Transform Parameters			
LHS Extrapolation Type (NP1)	Log-Linear	Log-Linear	Straight Line
RHS Extrapolation Type (NP3)	Log-Linear	Log-Linear	Straight Line
LHS Regression Range (lL)	0.87	0.87	0.87
RHS Regression Range (lR)	0.17	0.17	0.43
Numerical Laplace Inversion Parameter			
Stehfest "n" Parameter	10	8	16

Basis Function: Time-Reciprocal of Rate Data

Laplace Smoothed Functions	**Rate**	**D-Parameter**	**b-Parameter**
Basis Functions	$1/q(t)$	$1/q(t)$	$1/D(t)$
Numerical Laplace Transform Parameters			
LHS Extrapolation Type (NP1)	Log-Linear	Log-Linear	Straight Line
RHS Extrapolation Type (NP3)	Log-Log	Log-Log	Straight Line
LHS Regression Range (lL)	0.87	0.87	1.74
RHS Regression Range (lR)	0.04	0.04	0.43
Numerical Laplace Inversion Parameter			
Stehfest "n" Parameter	10	8	12

D.3 Arps Hyperbolic Model (Perfect Data Case)

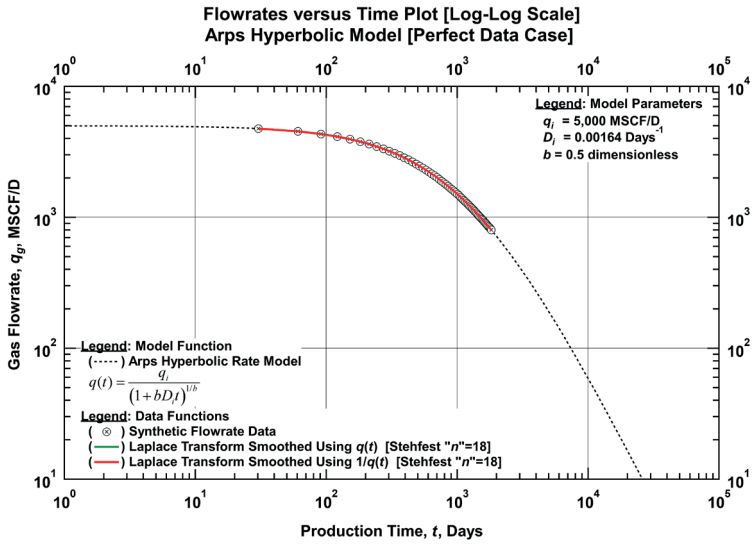

Figure D-3.1 — Comparison Plot of the Modelled Flowrate, Synthetic Flowrate, and Laplace Transform Smoothed Flowrates using Rate and Reciprocal of Rate as the Basis Functions Versus Time [Arps Hyperbolic Model (Perfect Data Case)].

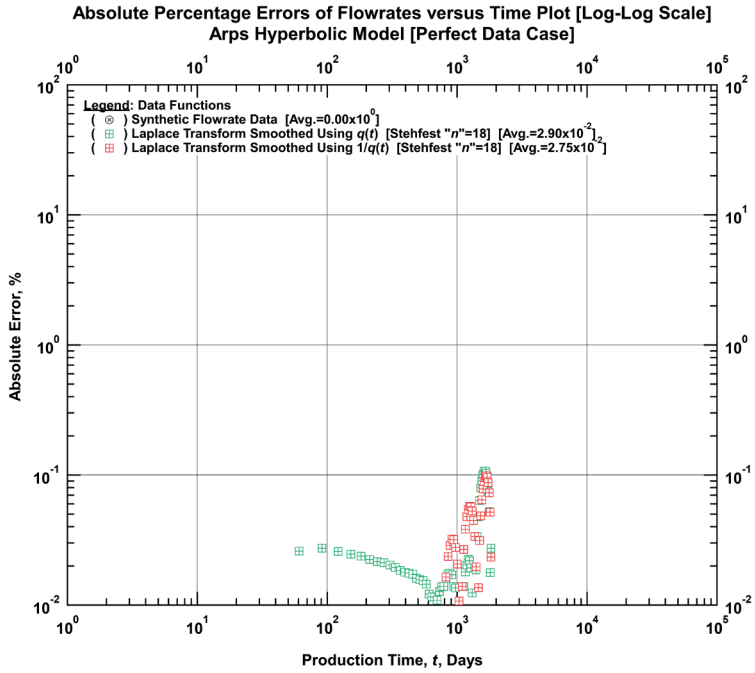

Figure D-3.2 — Comparison Plot of the Absolute Percentage Errors of the Synthetic Flowrate and Laplace Transform Smoothed Flowrates using Rate and Reciprocal of Rate as the Basis Functions Versus Time [Arps Hyperbolic Model (Perfect Data Case)].

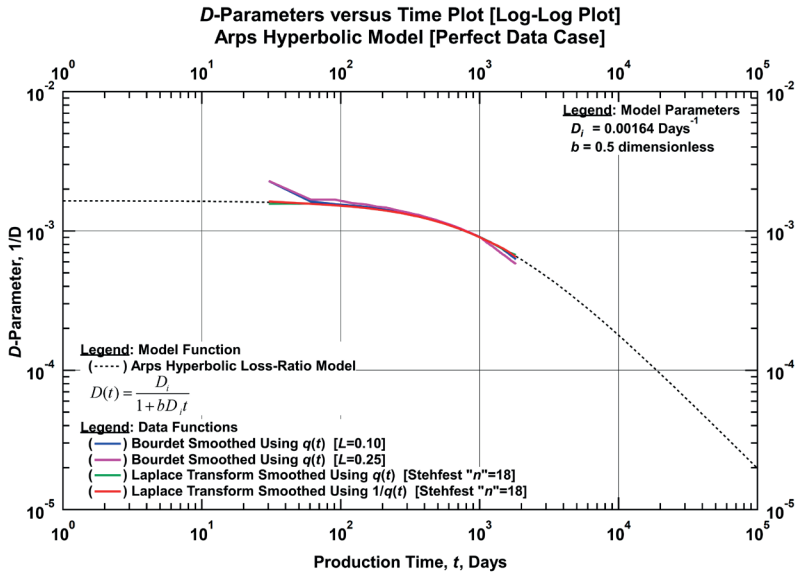

Figure D-3.3 — Comparison Plot of the Modelled *D*-Parameters, Bourdet-Derived *D*-Parameters, and Laplace Transform Smoothed *D*-Parameters using Rate and Reciprocal of Rate as the Basis Functions Versus Time [Arps Hyperbolic Model (Perfect Data Case)].

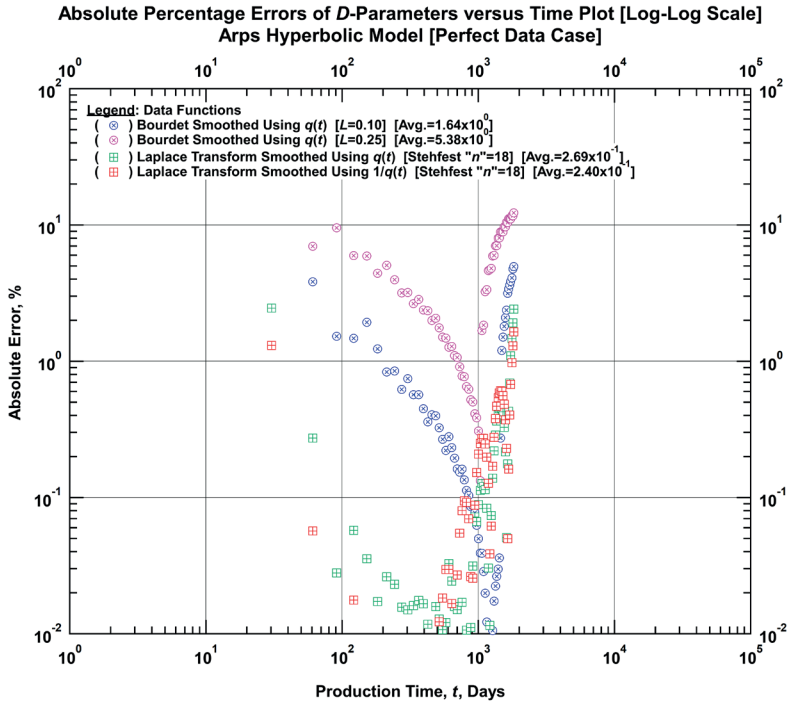

Figure D-3.4 — Comparison Plot of the Absolute Percentage Errors of the Bourdet-Derived *D*-Parameters and Laplace Transform Smoothed *D*-Parameters using Rate and Reciprocal of Rate Functions as the Basis Functions Versus Time [Arps Hyperbolic Model (Perfect Data Case)].

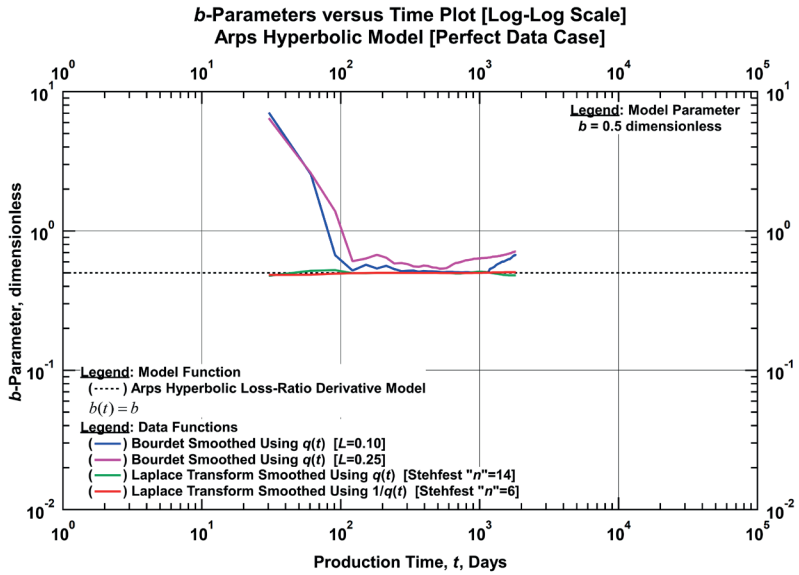

Figure D-3.5 — Comparison Plot of the Modelled *b*-Parameters, Bourdet-Derived *b*-Parameters, and Laplace Transform Smoothed *b*-Parameters using Rate and Reciprocal of Rate as the Basis Functions Versus Time [Arps Hyperbolic Model (Perfect Data Case)].

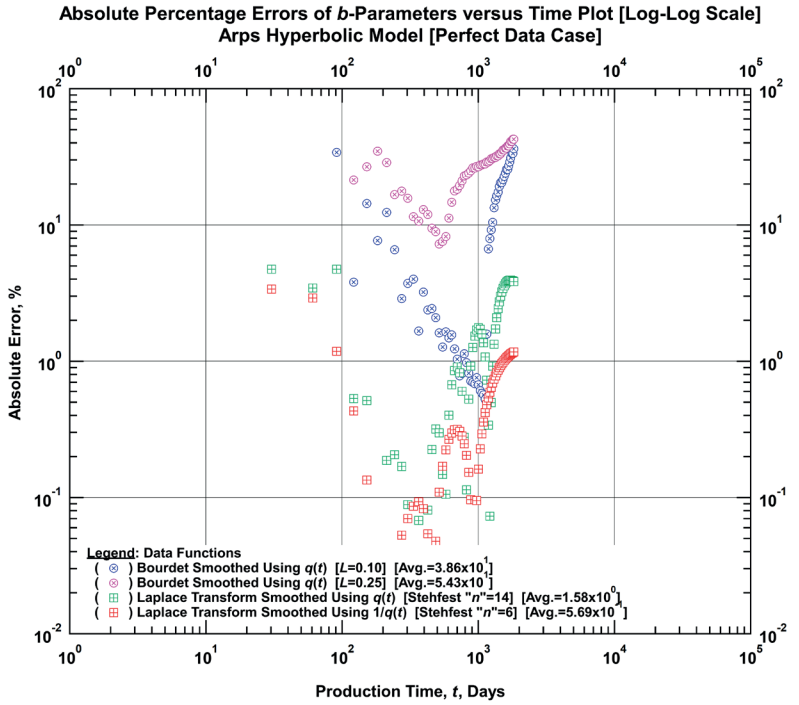

Figure D-3.6 — Comparison Plot of the Absolute Percentage Errors of the Bourdet-Derived *b*-Parameters and Laplace Transform Smoothed *b*-Parameters using Rate and Reciprocal of Rate as the Basis Functions versus Time [Arps Hyperbolic Model (Perfect Data Case)].

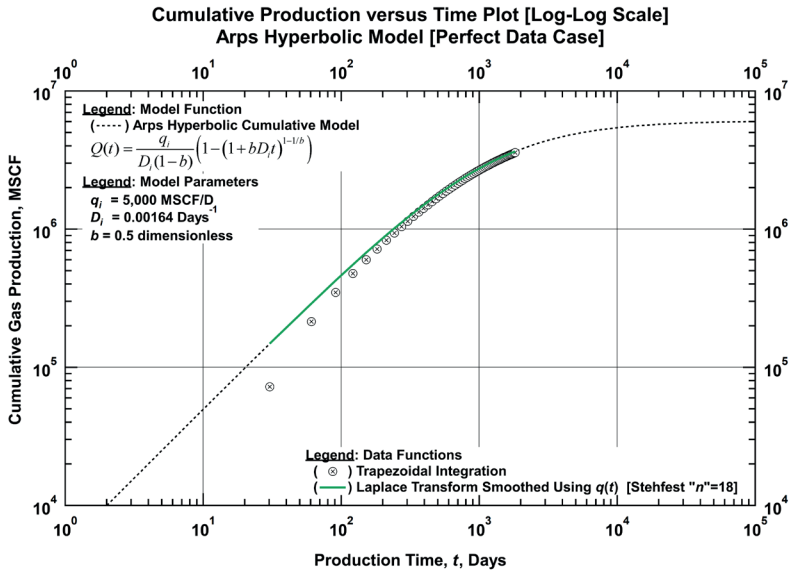

Figure D-3.7 — Comparison Plot of the Modelled Cumulative Production, Trapezoidal-Integrated Cumulative Production, and Laplace Transform Smoothed Cumulative Production using Rate as Basis Function versus Time [Arps Hyperbolic Model (Perfect Data Case)].

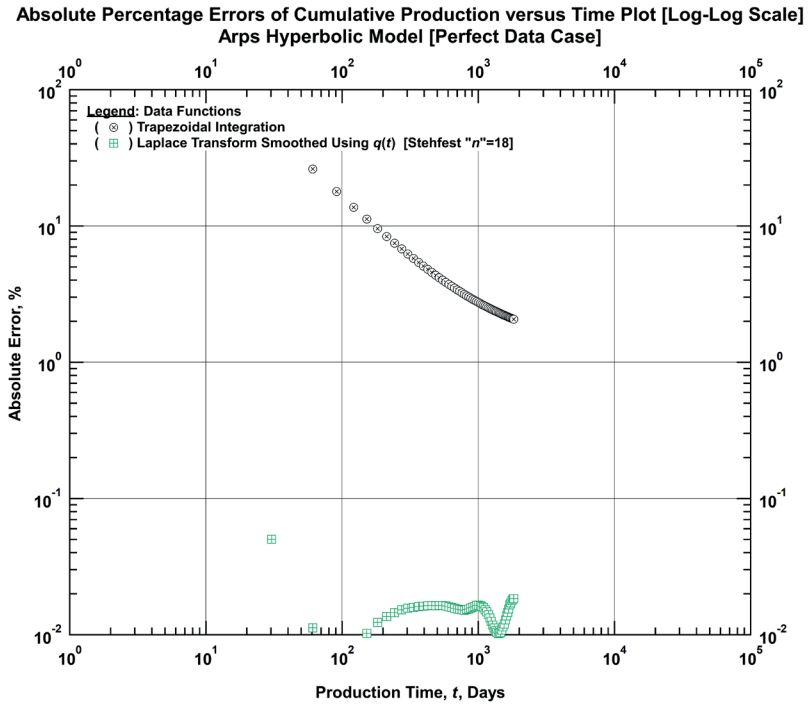

Figure D-3.8 — Comparison Plot of the Absolute Percentage Errors of Trapezoidal-Integrated Cumulative Production and Laplace Transform Smoothed Cumulative Production using Rate as Basis Function versus Time [Arps Hyperbolic Model (Perfect Data Case)].

Table D-3 — Input Parameters for Arps Hyperbolic Model (Perfect Data Set) Case.

Basis Function: Time-Rate Data

Laplace Smoothed Functions	**Rate & Cum. Production**	**D-Parameter**	**b-Parameter**
Basis Functions	$q(t)$	$q(t)$	$1/D(t)$
Numerical Laplace Transform Parameters			
LHS Extrapolation Type (NP1)	Log-Linear	Log-Linear	Straight Line
RHS Extrapolation Type (NP3)	Log-Linear	Log-Linear	Straight Line
LHS Regression Range (lL)	0.35	0.35	1.74
RHS Regression Range (lR)	0.01	0.01	0.43
Numerical Laplace Inversion Parameter			
Stehfest "n" Parameter	18	18	14

Basis Function: Time-Reciprocal of Rate Data

Laplace Smoothed Functions	**Rate**	**D-Parameter**	**b-Parameter**
Basis Functions	$1/q(t)$	$1/q(t)$	$1/D(t)$
Numerical Laplace Transform Parameters			
LHS Extrapolation Type (NP1)	Striaght Line	Striaght Line	Straight Line
RHS Extrapolation Type (NP3)	Log-Log	Log-Log	Straight Line
LHS Regression Range (lL)	0.35	0.35	1.74
RHS Regression Range (lR)	0.01	0.01	0.43
Numerical Laplace Inversion Parameter			
Stehfest "n" Parameter	18	18	6

D.4 Arps Hyperbolic Model (Noisy Data Case)

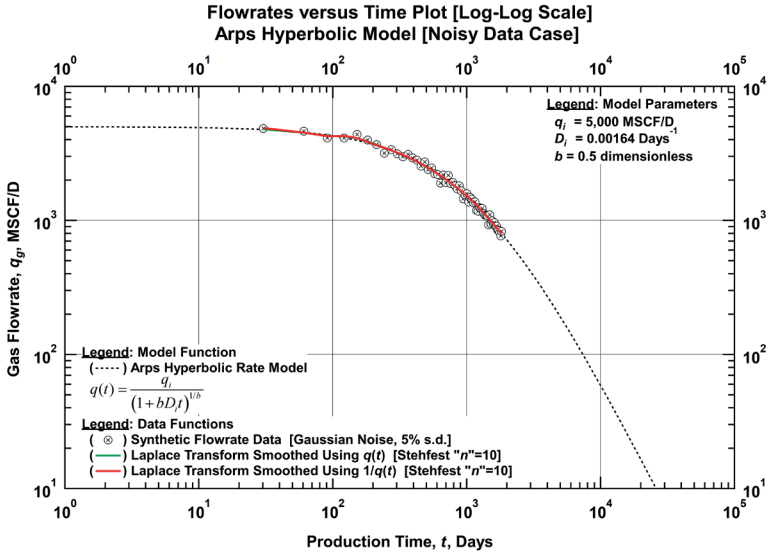

Figure D-4.1 — Comparison Plot of the Modelled Flowrate, Synthetic Flowrate, and Laplace Transform Smoothed Flowrates using Rate and Reciprocal of Rate as the Basis Functions Versus Time [Arps Hyperbolic Model (Noisy Data Case)].

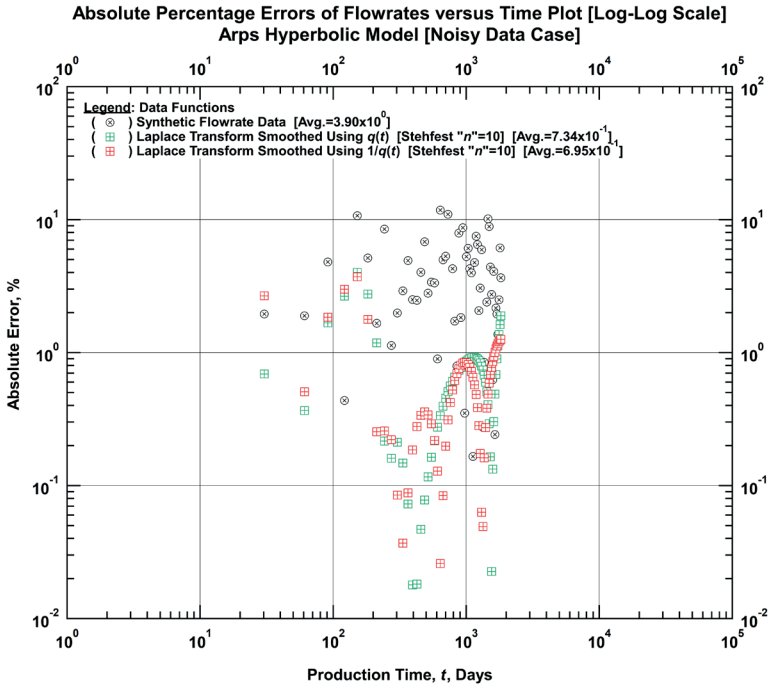

Figure D-4.2 — Comparison Plot of the Absolute Percentage Errors of the Synthetic Flowrate and Laplace Transform Smoothed Flowrates using Rate and Reciprocal of Rate as the Basis Functions Versus Time [Arps Hyperbolic Model (Noisy Data Case)].

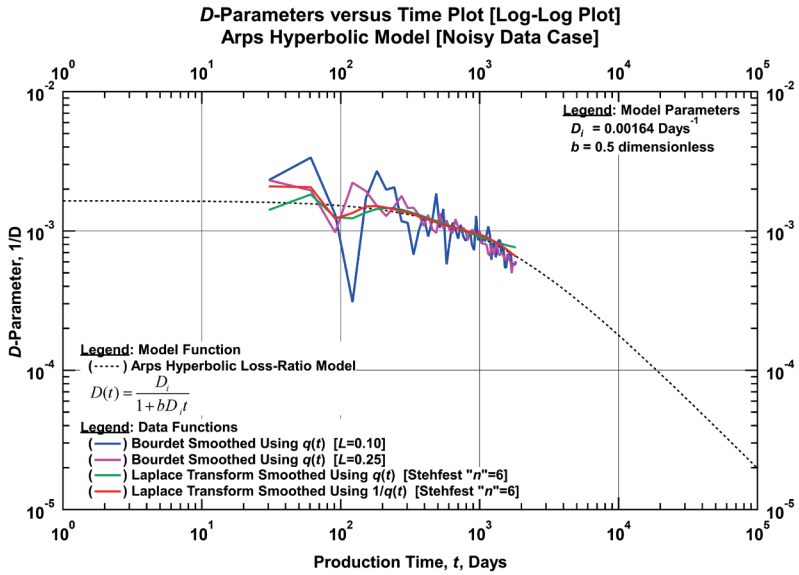

Figure D-4.3 — Comparison Plot of the Modelled *D*-Parameters, Bourdet-Derived *D*-Parameters, and Laplace Transform Smoothed *D*-Parameters using Rate and Reciprocal of Rate as the Basis Functions Versus Time [Arps Hyperbolic Model (Noisy Data Case)].

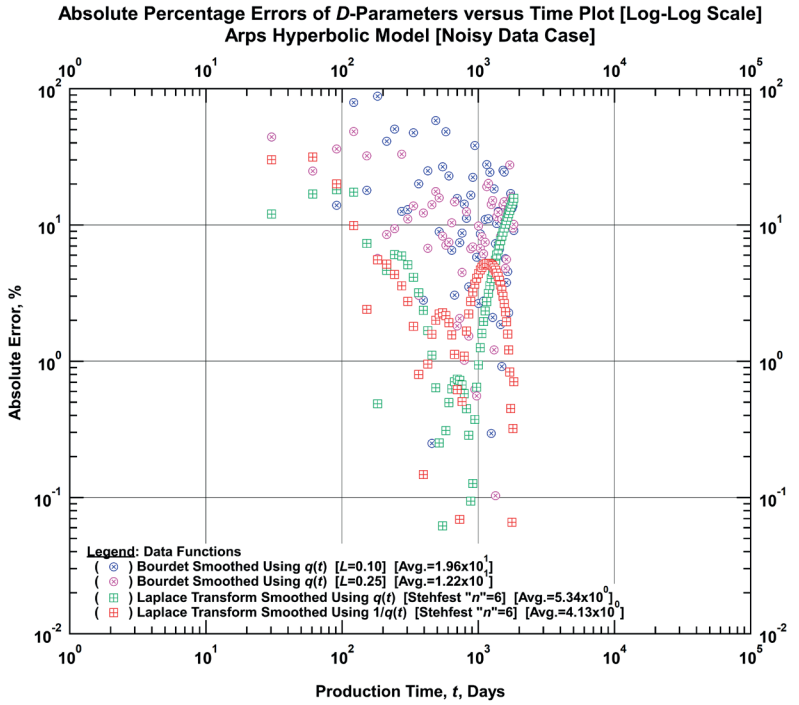

Figure D-4.4 — Comparison Plot of the Absolute Percentage Errors of the Bourdet-Derived *D*-Parameters and Laplace Transform Smoothed *D*-Parameters using Rate and Reciprocal of Rate Functions as the Basis Functions Versus Time [Arps Hyperbolic Model (Noisy Data Case)].

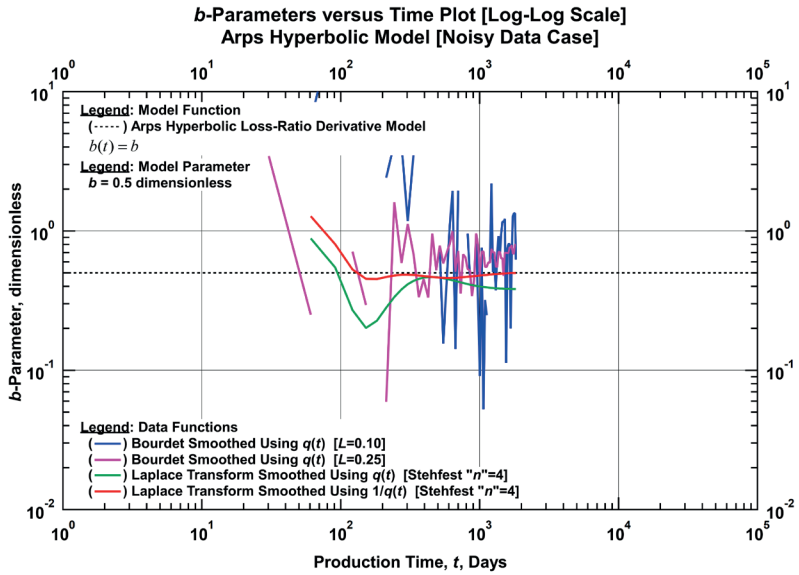

Figure D-4.5 — Comparison Plot of the Modelled *b*-Parameters, Bourdet-Derived *b*-Parameters, and Laplace Transform Smoothed *b*-Parameters using Rate and Reciprocal of Rate as the Basis Functions Versus Time [Arps Hyperbolic Model (Noisy Data Case)].

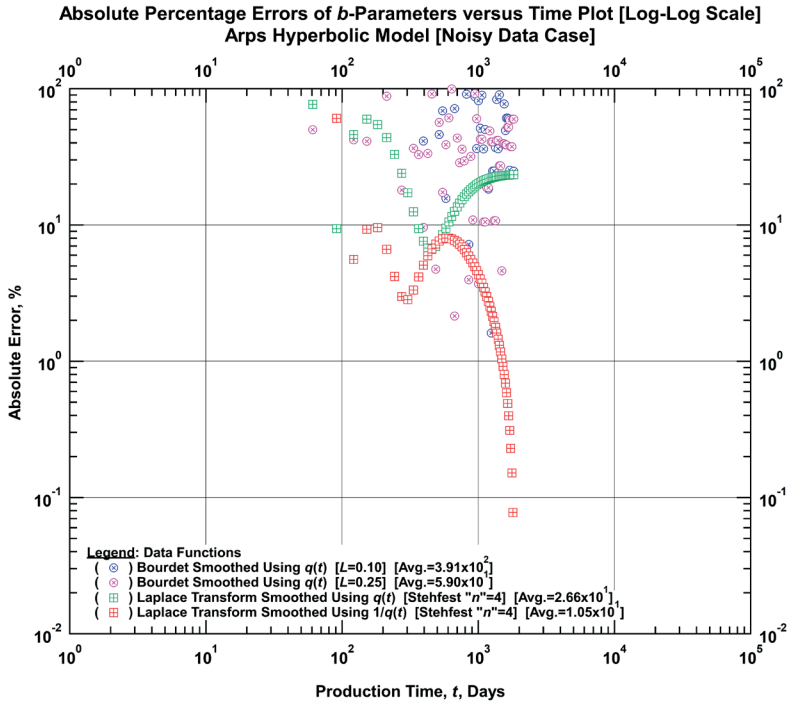

Figure D-4.6 — Comparison Plot of the Absolute Percentage Errors of the Bourdet-Derived *b*-Parameters and Laplace Transform Smoothed *b*-Parameters using Rate and Reciprocal of Rate as the Basis Functions versus Time [Arps Hyperbolic Model (Noisy Data Case)].

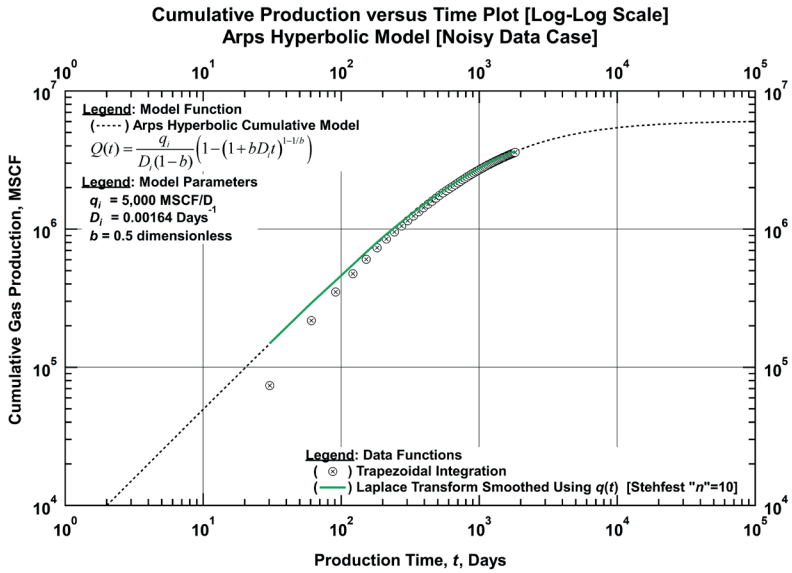

Figure D-4.7 — Comparison Plot of the Modelled Cumulative Production, Trapezoidal-Integrated Cumulative Production, and Laplace Transform Smoothed Cumulative Production using Rate as Basis Function versus Time [Arps Hyperbolic Model (Noisy Data Case)].

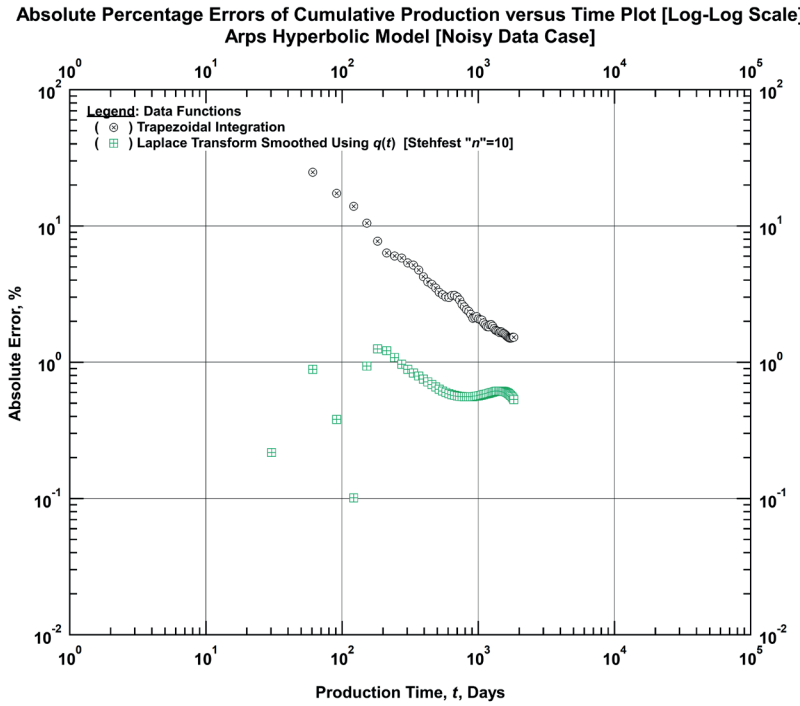

Figure D-4.8 — Comparison Plot of the Absolute Percentage Errors of Trapezoidal-Integrated Cumulative Production and Laplace Transform Smoothed Cumulative Production using Rate as Basis Function versus Time [Arps Hyperbolic Model (Noisy Data Case)].

Table D-4 — Input Parameters for Arps Hyperbolic Model (Noisy Data Set) Case.

Basis Function: Time-Rate Data

Laplace Smoothed Functions	**Rate & Cum. Production**	**D-Parameter**	**b-Parameter**
Basis Functions	$q(t)$	$q(t)$	$1/D(t)$
Numerical Laplace Transform Parameters			
LHS Extrapolation Type (NP1)	Log-Linear	Log-Linear	Straight Line
RHS Extrapolation Type (NP3)	Log-Linear	Log-Linear	Straight Line
LHS Regression Range (lL)	1.09	1.09	0.87
RHS Regression Range (lR)	0.09	0.09	0.43
Numerical Laplace Inversion Parameter			
Stehfest "n" Parameter	10	6	4

Basis Function: Time-Reciprocal of Rate Data

Laplace Smoothed Functions	**Rate**	**D-Parameter**	**b-Parameter**
Basis Functions	$1/q(t)$	$1/q(t)$	$1/D(t)$
Numerical Laplace Transform Parameters			
LHS Extrapolation Type (NP1)	Striaght Line	Striaght Line	Straight Line
RHS Extrapolation Type (NP3)	Log-Log	Log-Log	Straight Line
LHS Regression Range (lL)	1.09	1.09	1.74
RHS Regression Range (lR)	0.09	0.09	0.43
Numerical Laplace Inversion Parameter			
Stehfest "n" Parameter	10	6	4

D.5 Arps Harmonic Model (Perfect Data Case)

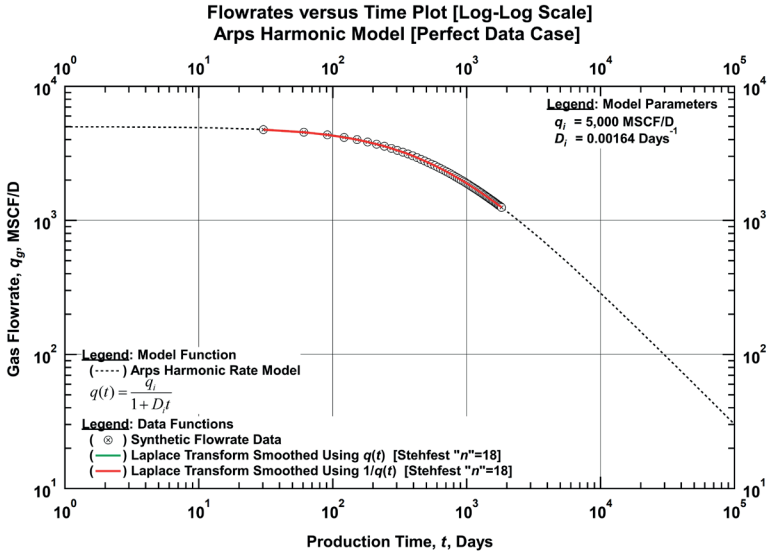

Figure D-5.1 — Comparison Plot of the Modelled Flowrate, Synthetic Flowrate, and Laplace Transform Smoothed Flowrates using Rate and Reciprocal of Rate as the Basis Functions Versus Time [Arps Harmonic Model (Perfect Data Case)].

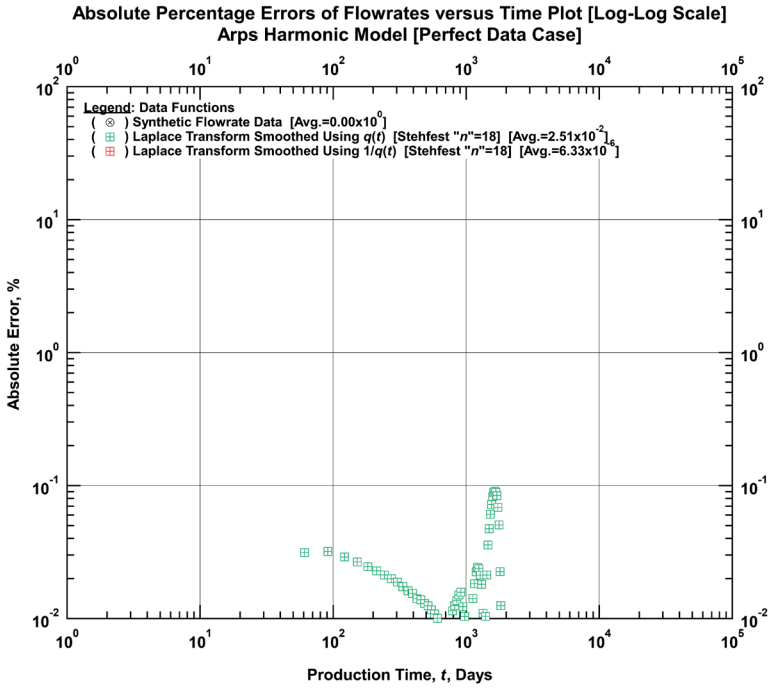

Figure D-5.2 — Comparison Plot of the Absolute Percentage Errors of the Synthetic Flowrate and Laplace Transform Smoothed Flowrates using Rate and Reciprocal of Rate as the Basis Functions Versus Time [Arps Harmonic Model (Perfect Data Case)].

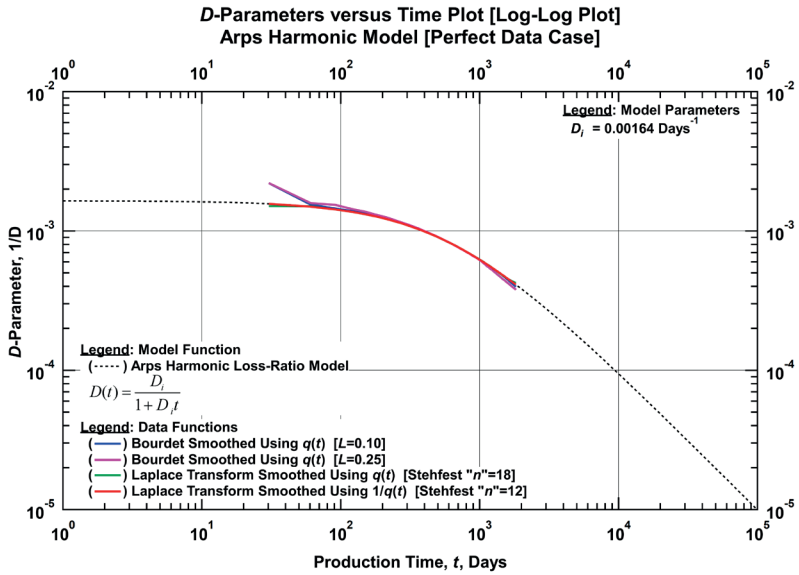

Figure D-5.3 — Comparison Plot of the Modelled *D*-Parameters, Bourdet-Derived *D*-Parameters, and Laplace Transform Smoothed *D*-Parameters using Rate and Reciprocal of Rate as the Basis Functions Versus Time [Arps Harmonic Model (Perfect Data Case)].

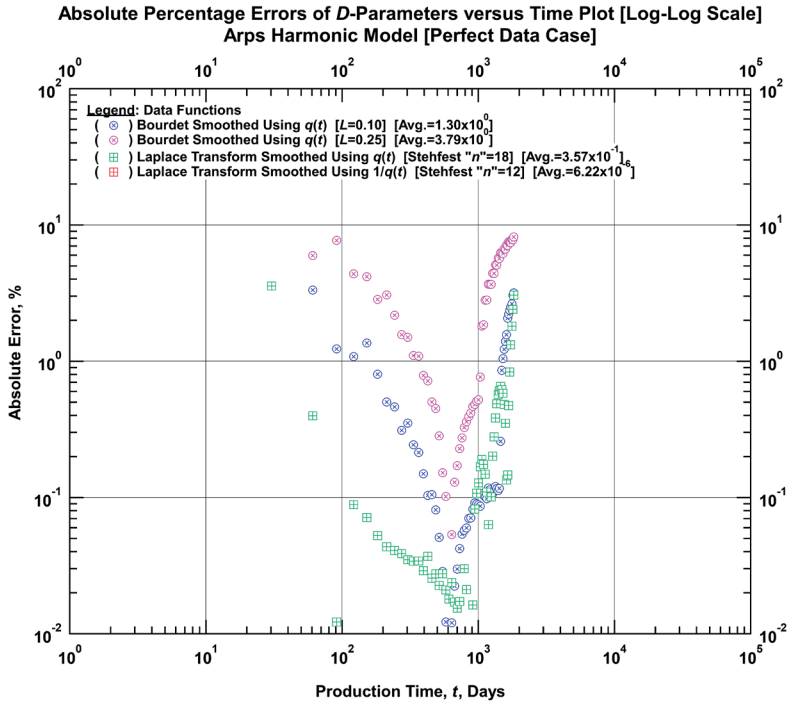

Figure D-5.4 — Comparison Plot of the Absolute Percentage Errors of the Bourdet-Derived *D*-Parameters and Laplace Transform Smoothed *D*-Parameters using Rate and Reciprocal of Rate Functions as the Basis Functions Versus Time [Arps Harmonic Model (Perfect Data Case)].

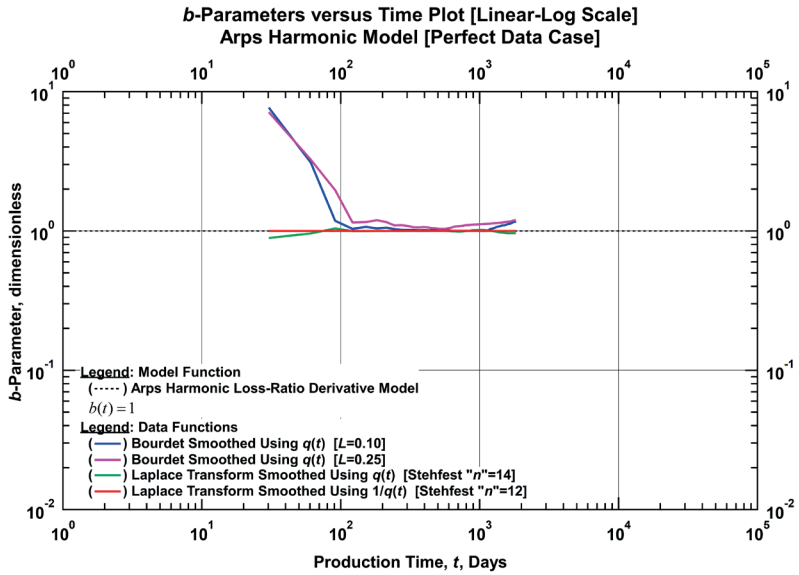

Figure D-5.5 — Comparison Plot of the Modelled *b*-Parameters, Bourdet-Derived *b*-Parameters, and Laplace Transform Smoothed *b*-Parameters using Rate and Reciprocal of Rate as the Basis Functions Versus Time [Arps Harmonic Model (Perfect Data Case)].

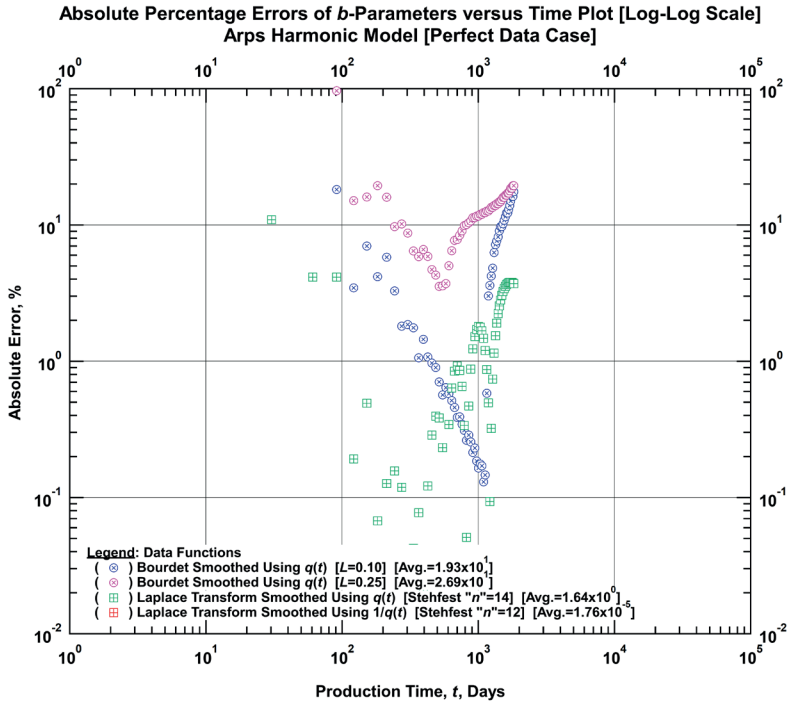

Figure D-5.6 — Comparison Plot of the Absolute Percentage Errors of the Bourdet-Derived *b*-Parameters and Laplace Transform Smoothed *b*-Parameters using Rate and Reciprocal of Rate as the Basis Functions versus Time [Arps Harmonic Model (Perfect Data Case)].

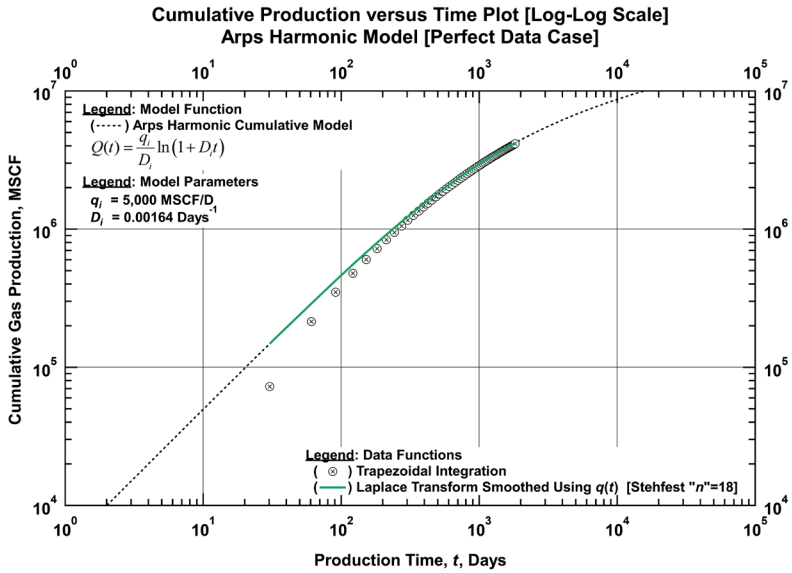

Figure D-5.7 — Comparison Plot of the Modelled Cumulative Production, Trapezoidal-Integrated Cumulative Production, and Laplace Transform Smoothed Cumulative Production using Rate as Basis Function versus Time [Arps Harmonic Model (Perfect Data Case)].

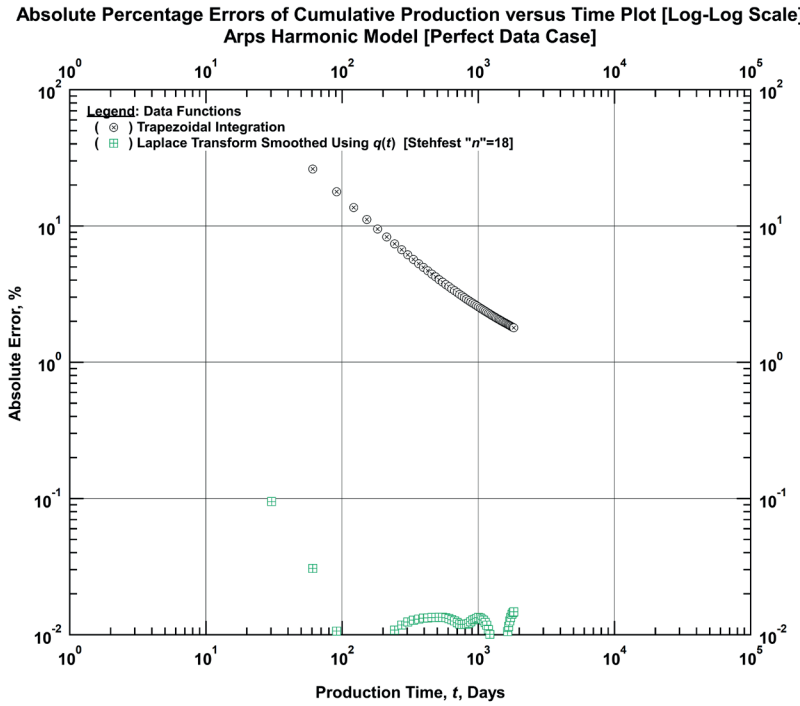

Figure D-5.8 — Comparison Plot of the Absolute Percentage Errors of Trapezoidal-Integrated Cumulative Production and Laplace Transform Smoothed Cumulative Production using Rate as Basis Function versus Time [Arps Harmonic Model (Perfect Data Case)].

Table D-5 — Input Parameters for Arps Harmonic Model (Perfect Data Set) Case.

Basis Function: Time-Rate Data

Laplace Smoothed Functions	**Rate & Cum. Production**	**D-Parameter**	**b-Parameter**
Basis Functions	$q(t)$	$q(t)$	$1/D(t)$
Numerical Laplace Transform Parameters			
LHS Extrapolation Type (NP1)	Log-Linear	Log-Linear	Straight Line
RHS Extrapolation Type (NP3)	Log-Linear	Log-Linear	Straight Line
LHS Regression Range (lL)	0.35	0.35	1.30
RHS Regression Range (lR)	0.01	0.01	0.43
Numerical Laplace Inversion Parameter			
Stehfest "n" Parameter	18	18	14

Basis Function: Time-Reciprocal of Rate Data

Laplace Smoothed Functions	**Rate**	**D-Parameter**	**b-Parameter**
Basis Functions	$1/q(t)$	$1/q(t)$	$1/D(t)$
Numerical Laplace Transform Parameters			
LHS Extrapolation Type (NP1)	Straight Line	Straight Line	Straight Line
RHS Extrapolation Type (NP3)	Straight Line	Straight Line	Straight Line
LHS Regression Range (lL)	0.35	0.35	1.30
RHS Regression Range (lR)	0.01	0.01	0.43
Numerical Laplace Inversion Parameter			
Stehfest "n" Parameter	18	12	12

D.6 Arps Harmonic Model (Noisy Data Case)

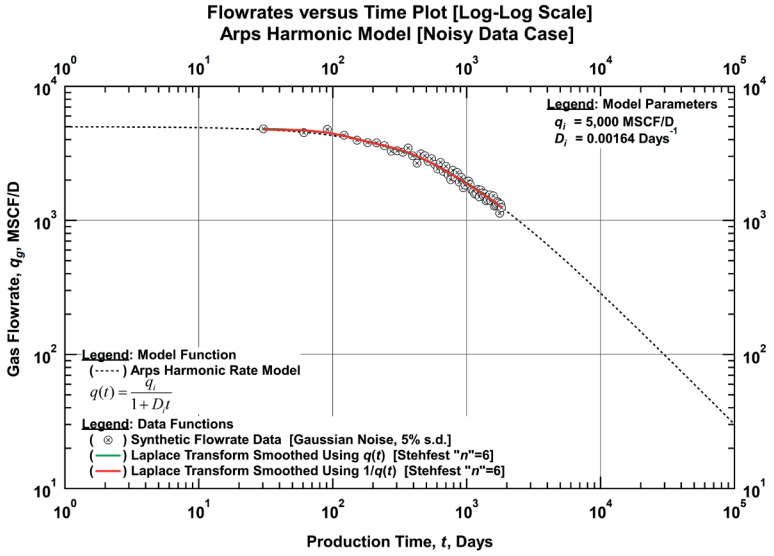

Figure D-6.1 — Comparison Plot of the Modelled Flowrate, Synthetic Flowrate, and Laplace Transform Smoothed Flowrates using Rate and Reciprocal of Rate as the Basis Functions Versus Time [Arps Harmonic Model (Noisy Data Case)].

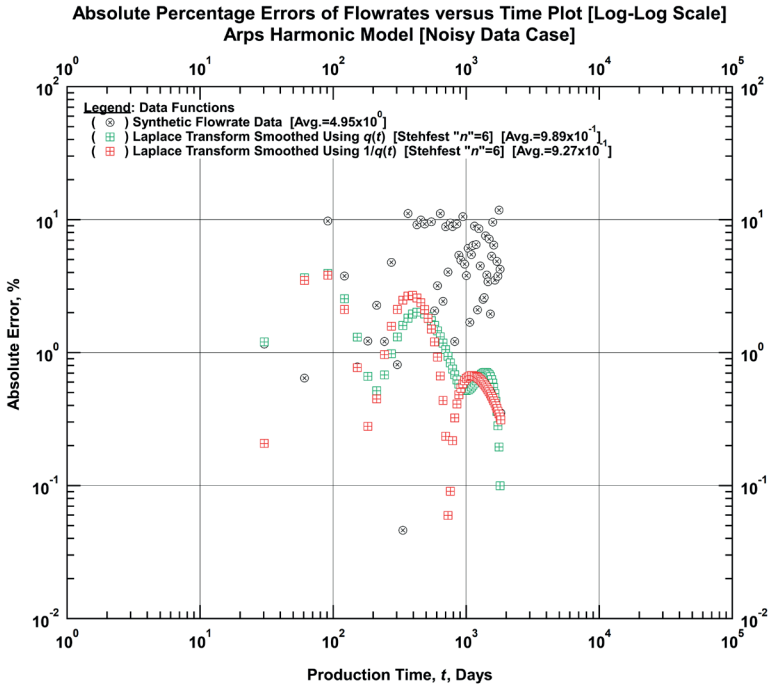

Figure D-6.2 — Comparison Plot of the Absolute Percentage Errors of the Synthetic Flowrate and Laplace Transform Smoothed Flowrates using Rate and Reciprocal of Rate as the Basis Functions Versus Time [Arps Harmonic Model (Noisy Data Case)].

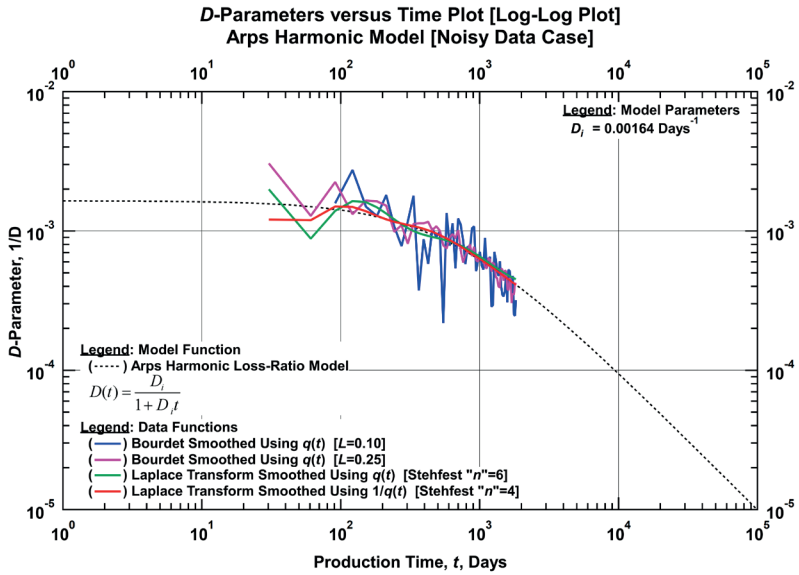

Figure D-6.3 — Comparison Plot of the Modelled *D*-Parameters, Bourdet-Derived *D*-Parameters, and Laplace Transform Smoothed *D*-Parameters using Rate and Reciprocal of Rate as the Basis Functions Versus Time [Arps Harmonic Model (Noisy Data Case)].

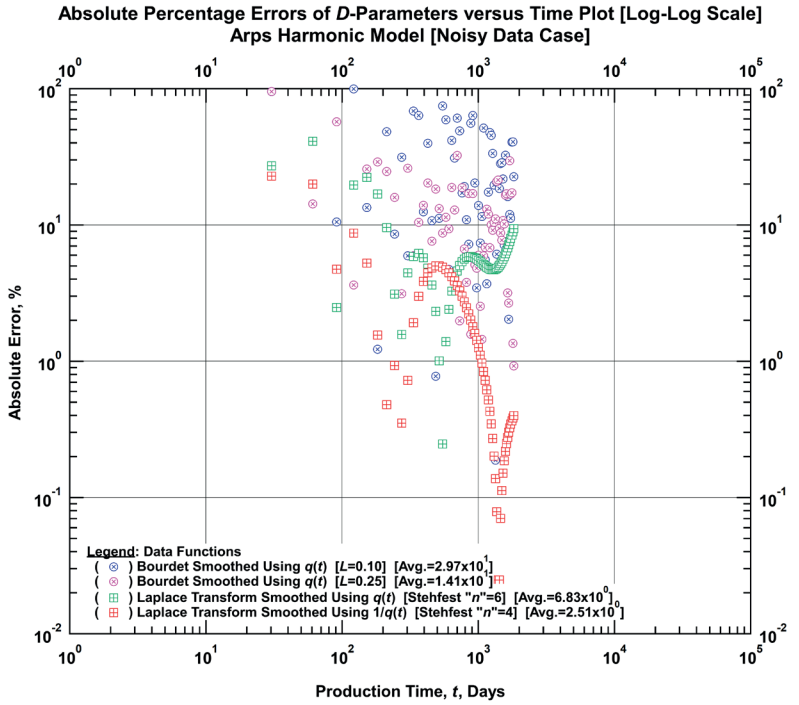

Figure D-6.4 — Comparison Plot of the Absolute Percentage Errors of the Bourdet-Derived *D*-Parameters and Laplace Transform Smoothed *D*-Parameters using Rate and Reciprocal of Rate Functions as the Basis Functions Versus Time [Arps Harmonic Model (Noisy Data Case)].

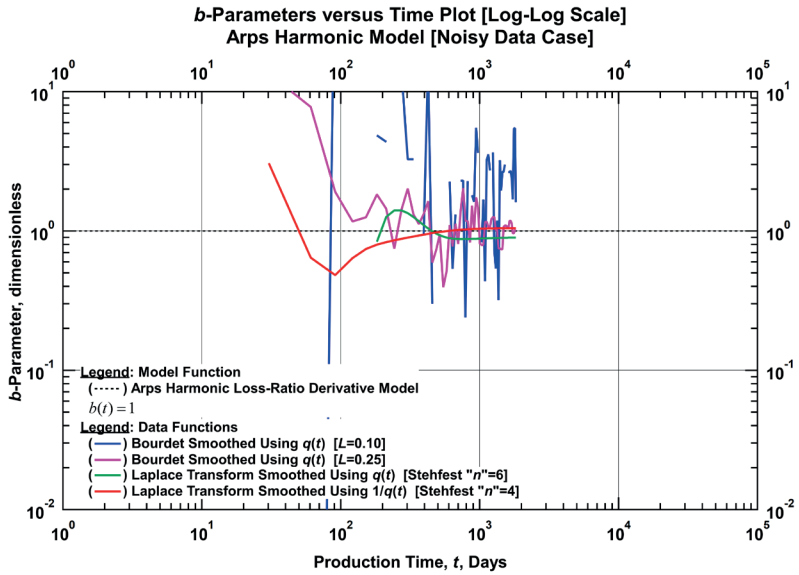

Figure D-6.5 — Comparison Plot of the Modelled *b*-Parameters, Bourdet-Derived *b*-Parameters, and Laplace Transform Smoothed *b*-Parameters using Rate and Reciprocal of Rate as the Basis Functions Versus Time [Arps Harmonic Model (Noisy Data Case)].

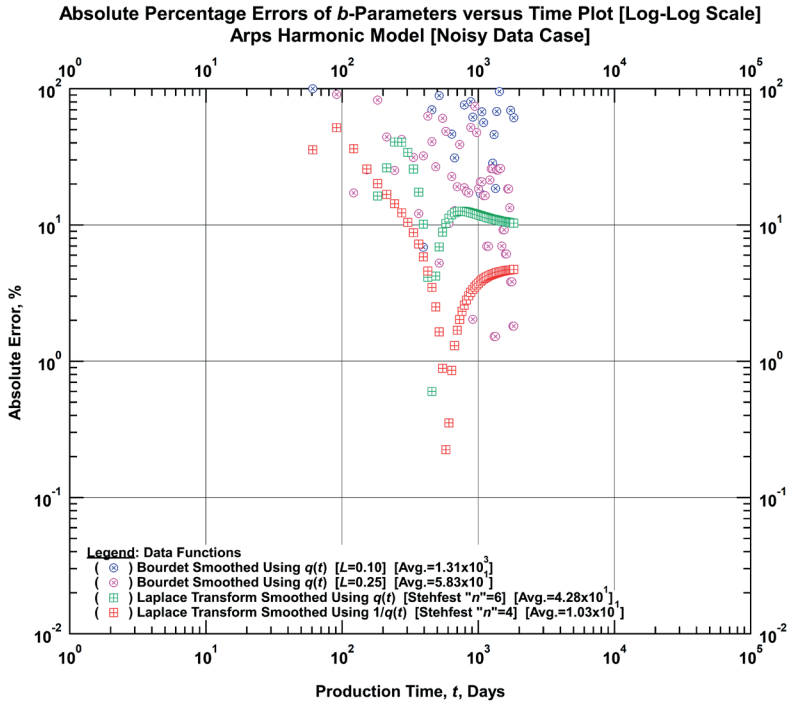

Figure D-6.6 — Comparison Plot of the Absolute Percentage Errors of the Bourdet-Derived *b*-Parameters and Laplace Transform Smoothed *b*-Parameters using Rate and Reciprocal of Rate as the Basis Functions versus Time [Arps Harmonic Model (Noisy Data Case)].

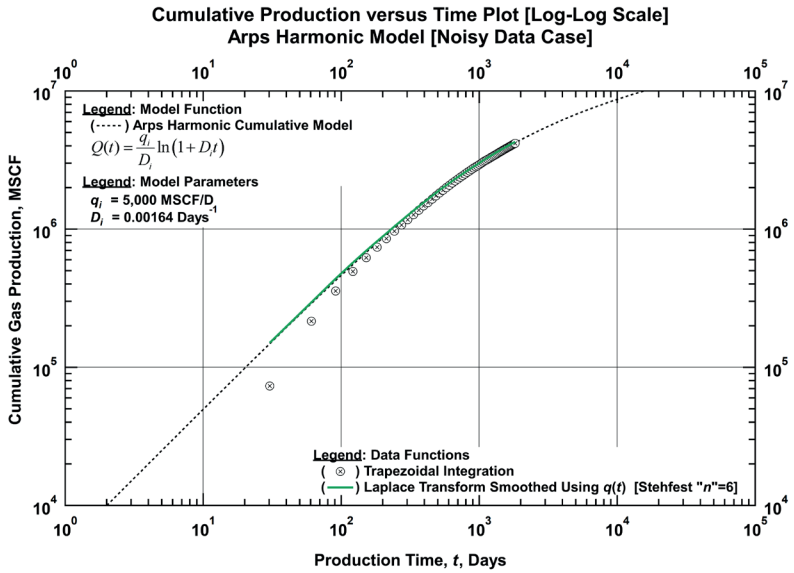

Figure D-6.7 — Comparison Plot of the Modelled Cumulative Production, Trapezoidal-Integrated Cumulative Production, and Laplace Transform Smoothed Cumulative Production using Rate as Basis Function versus Time [Arps Harmonic Model (Noisy Data Case)].

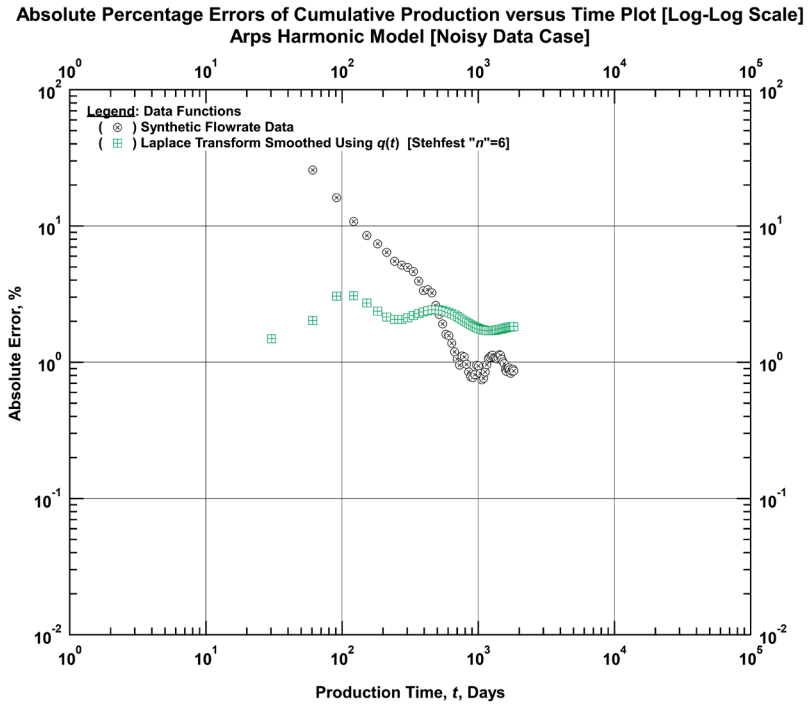

Figure D-6.8 — Comparison Plot of the Absolute Percentage Errors of Trapezoidal-Integrated Cumulative Production and Laplace Transform Smoothed Cumulative Production using Rate as Basis Function versus Time [Arps Harmonic Model (Noisy Data Case)].

Table D-6 — Input Parameters for Arps Harmonic Model (Noisy Data Set) Case.

Basis Function: Time-Rate Data

Laplace Smoothed Functions	**Rate & Cum. Production**	**D-Parameter**	**b-Parameter**
Basis Functions	$q(t)$	$q(t)$	$1/D(t)$
Numerical Laplace Transform Parameters			
LHS Extrapolation Type (NP1)	Log-Linear	Log-Linear	Straight Line
RHS Extrapolation Type (NP3)	Log-Linear	Log-Linear	Straight Line
LHS Regression Range (lL)	0.87	0.87	0.87
RHS Regression Range (lR)	0.22	0.22	0.43
Numerical Laplace Inversion Parameter			
Stehfest "n" Parameter	6	6	6

Basis Function: Time-Reciprocal of Rate Data

Laplace Smoothed Functions	**Rate**	**D-Parameter**	**b-Parameter**
Basis Functions	$1/q(t)$	$1/q(t)$	$1/D(t)$
Numerical Laplace Transform Parameters			
LHS Extrapolation Type (NP1)	Striaght Line	Striaght Line	Straight Line
RHS Extrapolation Type (NP3)	Striaght Line	Striaght Line	Straight Line
LHS Regression Range (lL)	1.30	1.30	1.74
RHS Regression Range (lR)	0.43	0.43	0.43
Numerical Laplace Inversion Parameter			
Stehfest "n" Parameter	6	4	4

D.7 Modified Hyperbolic Model (Perfect Data Case)

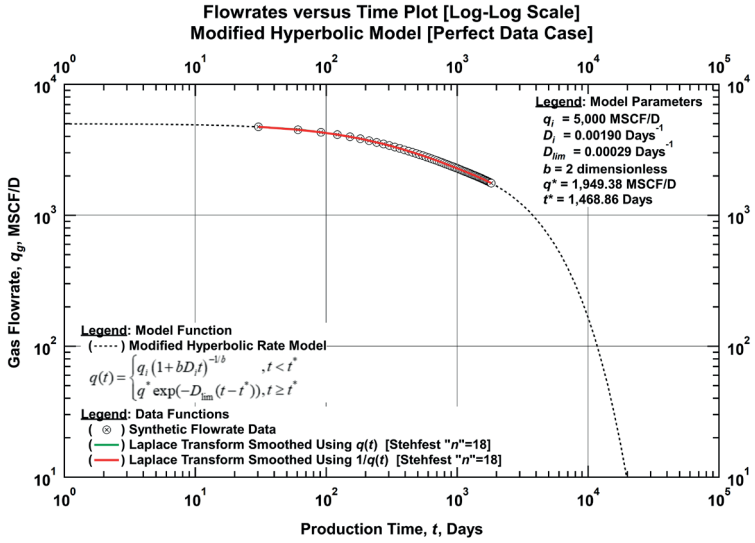

Figure D-7.1 — Comparison Plot of the Modelled Flowrate, Synthetic Flowrate, and Laplace Transform Smoothed Flowrates using Rate and Reciprocal of Rate as the Basis Functions Versus Time [Modified Hyperbolic Model (Perfect Data Case)].

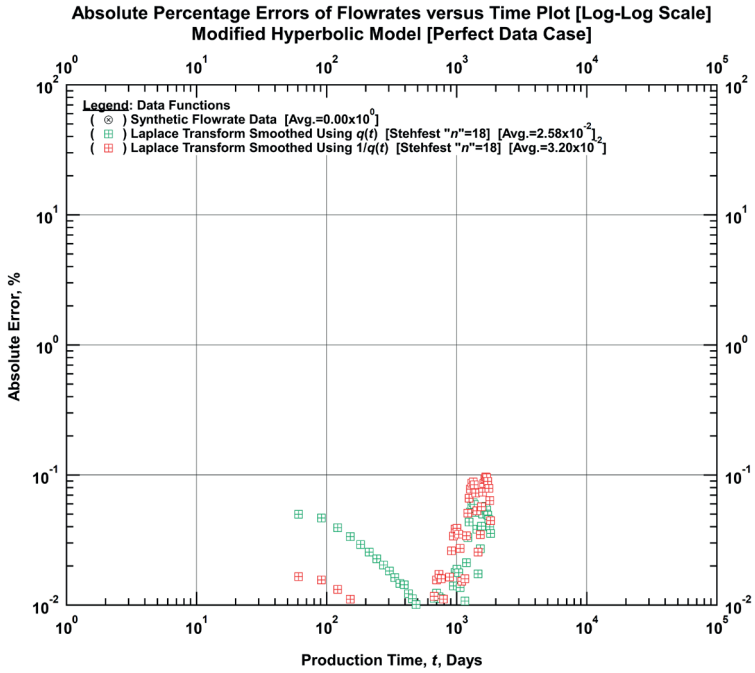

Figure D-7.2 — Comparison Plot of the Absolute Percentage Errors of the Synthetic Flowrate and Laplace Transform Smoothed Flowrates using Rate and Reciprocal of Rate as the Basis Functions Versus Time [Modified Hyperbolic Model (Perfect Data Case)].

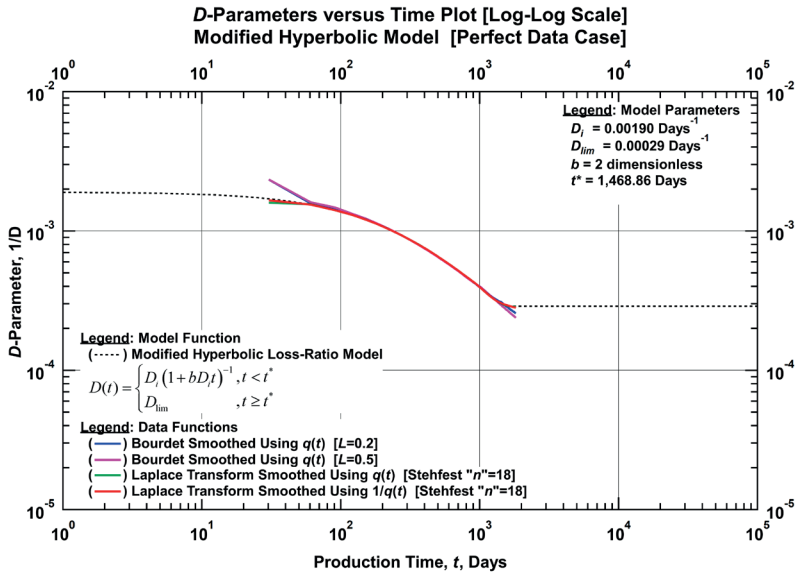

Figure D-7.3 — Comparison Plot of the Modelled *D*-Parameters, Bourdet-Derived *D*-Parameters, and Laplace Transform Smoothed *D*-Parameters using Rate and Reciprocal of Rate as the Basis Functions Versus Time [Modified Hyperbolic Model (Perfect Data Case)].

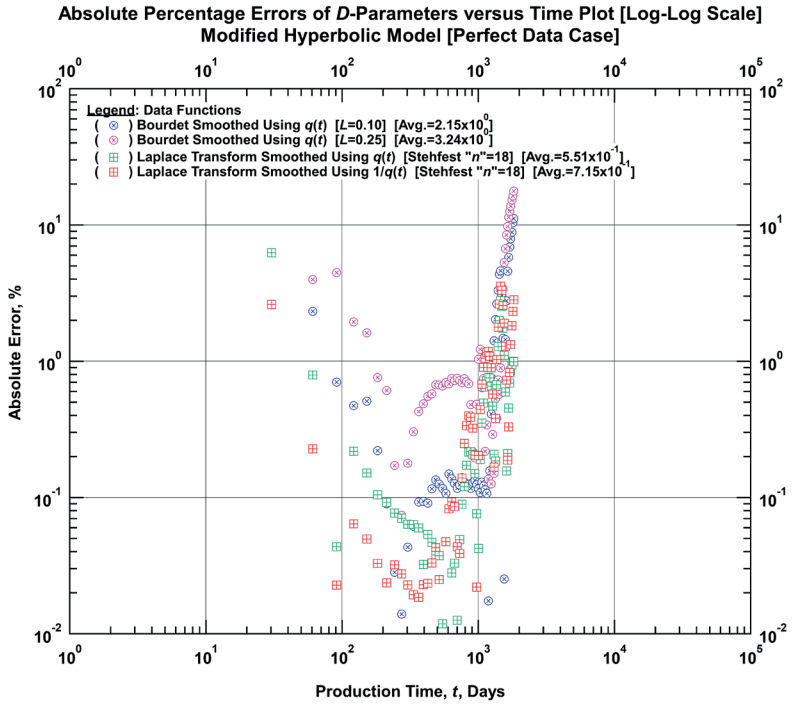

Figure D-7.4 — Comparison Plot of the Absolute Percentage Errors of the Bourdet-Derived *D*-Parameters and Laplace Transform Smoothed *D*-Parameters using Rate and Reciprocal of Rate Functions as the Basis Functions Versus Time [Modified Hyperbolic Model (Perfect Data Case)].

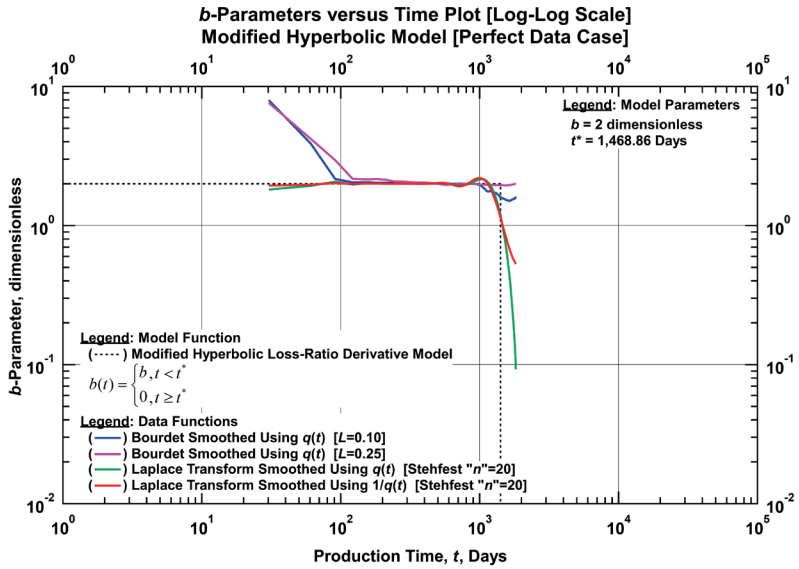

Figure D-7.5 — Comparison Plot of the Modelled *b*-Parameters, Bourdet-Derived *b*-Parameters, and Laplace Transform Smoothed *b*-Parameters using Rate and Reciprocal of Rate as the Basis Functions Versus Time [Modified Hyperbolic Model (Perfect Data Case)].

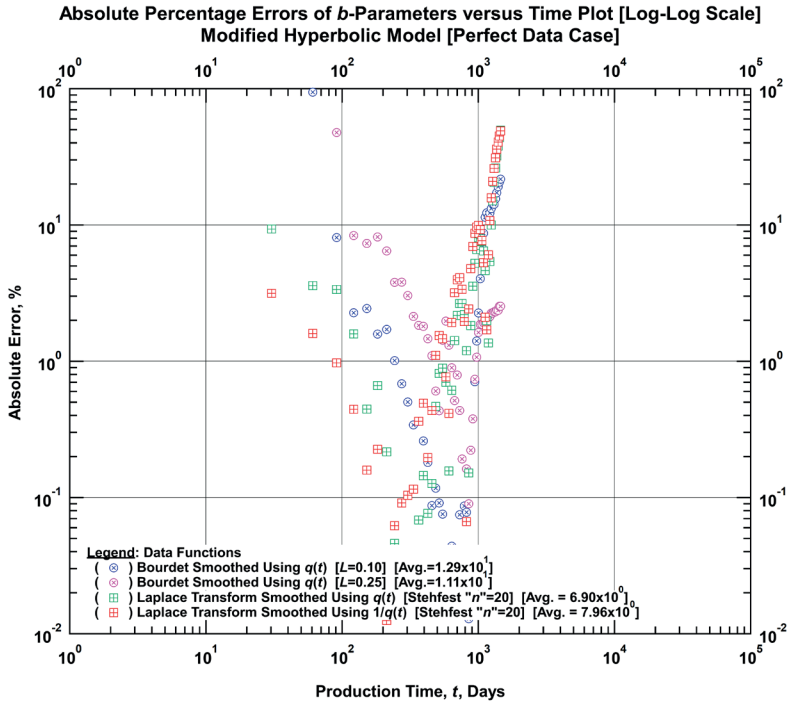

Figure D-7.6 — Comparison Plot of the Absolute Percentage Errors of the Bourdet-Derived *b*-Parameters and Laplace Transform Smoothed *b*-Parameters using Rate and Reciprocal of Rate as the Basis Functions versus Time [Modified Hyperbolic Model (Perfect Data Case)].

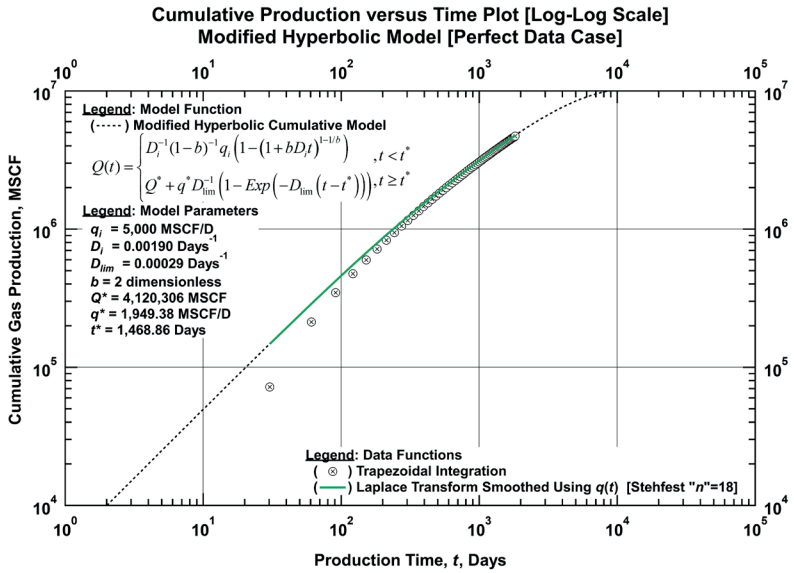

Figure D-7.7 — Comparison Plot of the Modelled Cumulative Production, Trapezoidal-Integrated Cumulative Production, and Laplace Transform Smoothed Cumulative Production using Rate as Basis Function versus Time [Modified Hyperbolic Model (Perfect Data Case)].

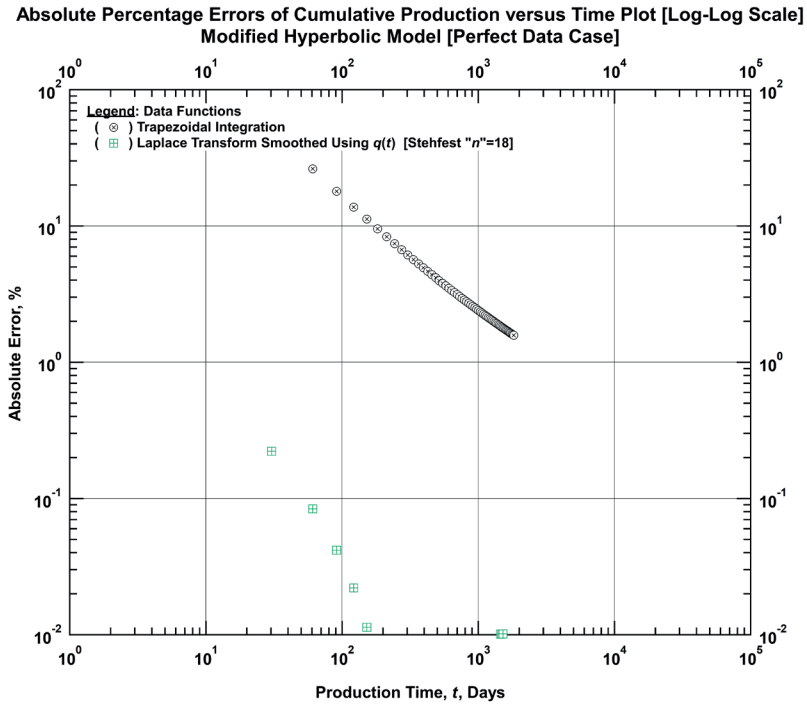

Figure D-7.8 — Comparison Plot of the Absolute Percentage Errors of Trapezoidal-Integrated Cumulative Production and Laplace Transform Smoothed Cumulative Production using Rate as Basis Function versus Time [Modified Hyperbolic Model (Perfect Data Case)].

Table D-7 — Input Parameters for Modified Hyperbolic Model (Perfect Data Set) Case.

Basis Function: Time-Rate Data

Laplace Smoothed Functions	**Rate & Cum. Production**	**D-Parameter**	**b-Parameter**
Basis Functions	$q(t)$	$q(t)$	$1/D(t)$
Numerical Laplace Transform Parameters			
LHS Extrapolation Type (NP1)	Log-Linear	Log-Linear	Straight Line
RHS Extrapolation Type (NP3)	Log-Linear	Log-Linear	Linear-Log
LHS Regression Range (lL)	0.35	0.35	1.30
RHS Regression Range (lR)	0.01	0.01	0.01
Numerical Laplace Inversion Parameter			
Stehfest "n" Parameter	18	18	20

Basis Function: Time-Reciprocal of Rate Data

Laplace Smoothed Functions	**Rate**	**D-Parameter**	**b-Parameter**
Basis Functions	$1/q(t)$	$1/q(t)$	$1/D(t)$
Numerical Laplace Transform Parameters			
LHS Extrapolation Type (NP1)	Straight Line	Straight Line	Straight Line
RHS Extrapolation Type (NP3)	Straight Line	Straight Line	Linear-Log
LHS Regression Range (lL)	0.35	0.35	1.30
RHS Regression Range (lR)	0.01	0.01	0.01
Numerical Laplace Inversion Parameter			
Stehfest "n" Parameter	18	18	20

D.8 Modified Hyperbolic Model (Noisy Data Case)

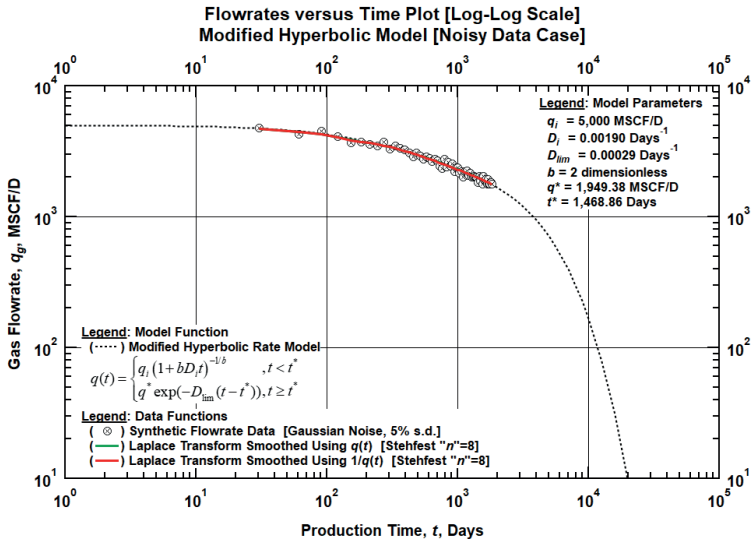

Figure D-8.1 — Comparison Plot of the Modelled Flowrate, Synthetic Flowrate, and Laplace Transform Smoothed Flowrates using Rate and Reciprocal of Rate as the Basis Functions Versus Time [Modified Hyperbolic Model (Noisy Data Case)].

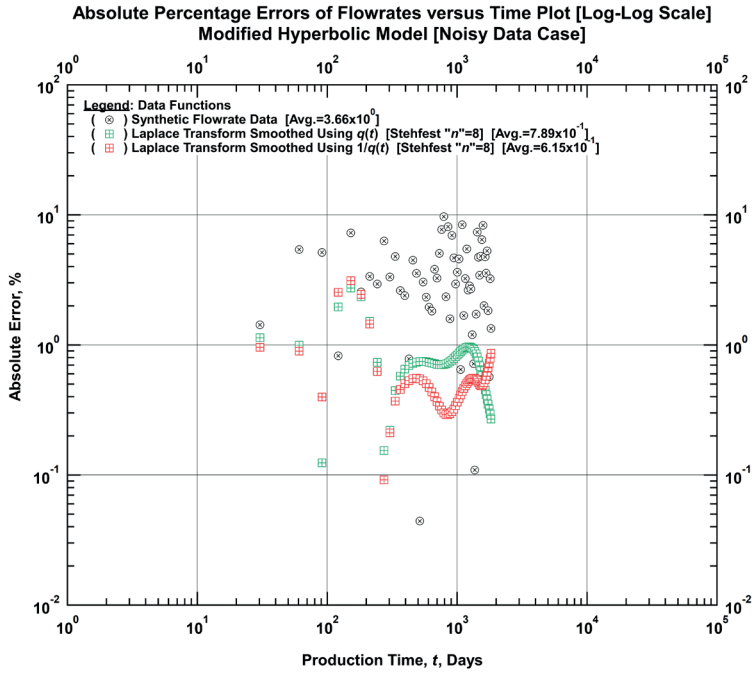

Figure D-8.2 — Comparison Plot of the Absolute Percentage Errors of the Synthetic Flowrate and Laplace Transform Smoothed Flowrates using Rate and Reciprocal of Rate as the Basis Functions Versus Time [Modified Hyperbolic Model (Noisy Data Case)].

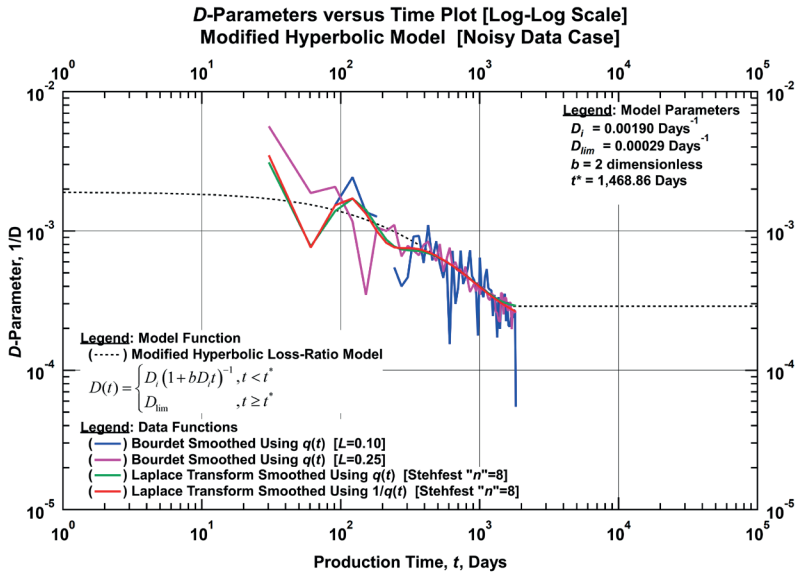

Figure D-8.3 — Comparison Plot of the Modelled *D*-Parameters, Bourdet-Derived *D*-Parameters, and Laplace Transform Smoothed *D*-Parameters using Rate and Reciprocal of Rate as the Basis Functions Versus Time [Modified Hyperbolic Model (Noisy Data Case)].

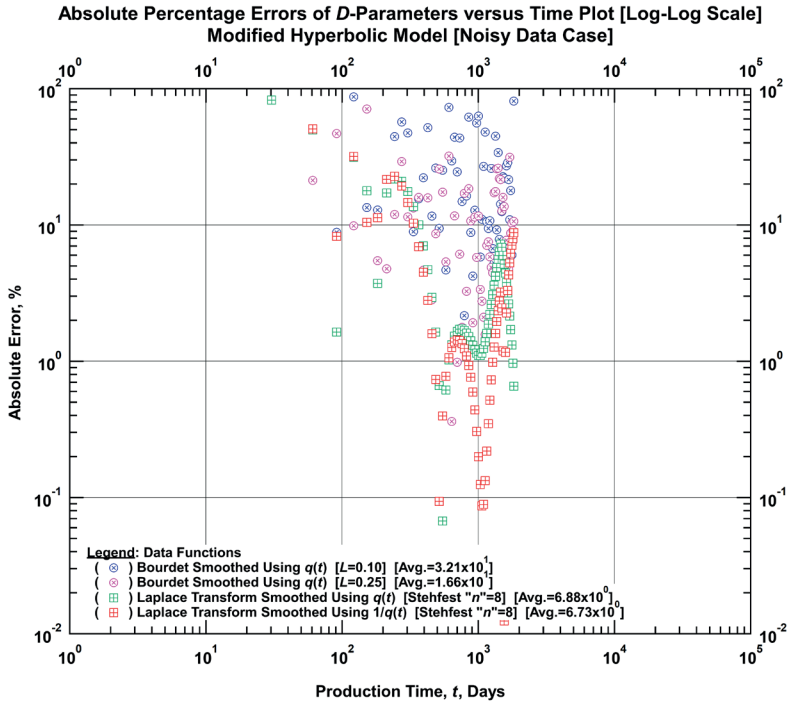

Figure D-8.4 — Comparison Plot of the Absolute Percentage Errors of the Bourdet-Derived *D*-Parameters and Laplace Transform Smoothed *D*-Parameters using Rate and Reciprocal of Rate Functions as the Basis Functions Versus Time [Modified Hyperbolic Model (Noisy Data Case)].

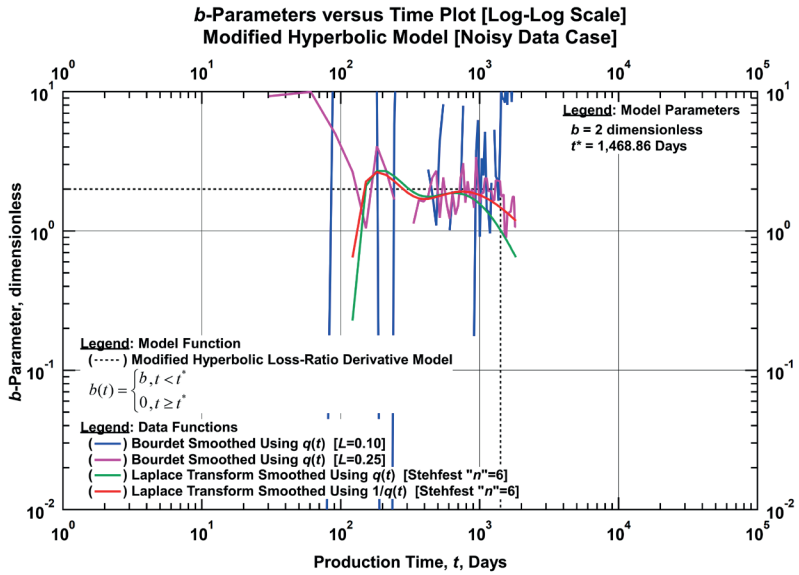

Figure D-8.5 — Comparison Plot of the Modelled *b*-Parameters, Bourdet-Derived *b*-Parameters, and Laplace Transform Smoothed *b*-Parameters using Rate and Reciprocal of Rate as the Basis Functions Versus Time [Modified Hyperbolic Model (Noisy Data Case)].

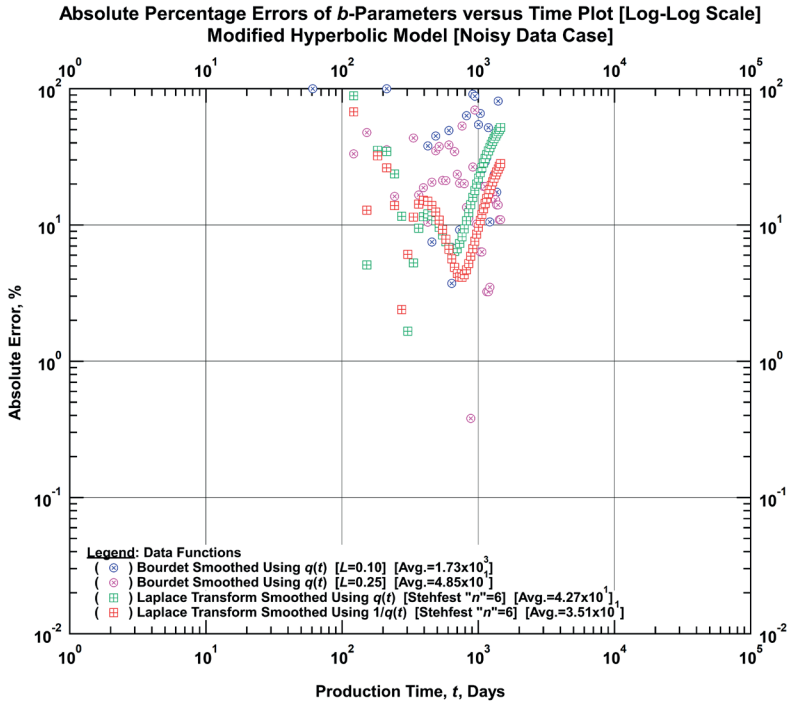

Figure D-8.6 — Comparison Plot of the Absolute Percentage Errors of the Bourdet-Derived *b*-Parameters and Laplace Transform Smoothed *b*-Parameters using Rate and Reciprocal of Rate as the Basis Functions versus Time [Modified Hyperbolic Model (Noisy Data Case)].

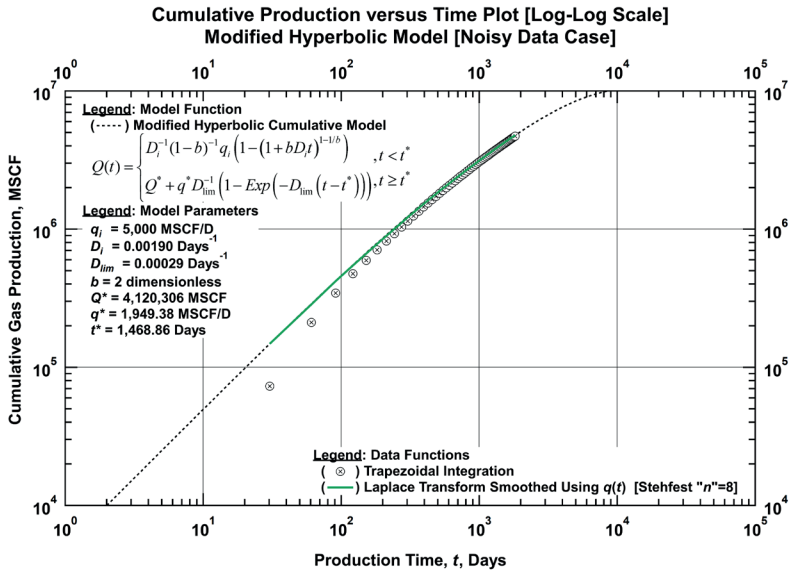

Figure D-8.7 — Comparison Plot of the Modelled Cumulative Production, Trapezoidal-Integrated Cumulative Production, and Laplace Transform Smoothed Cumulative Production using Rate as Basis Function versus Time [Modified Hyperbolic Model (Noisy Data Case)].

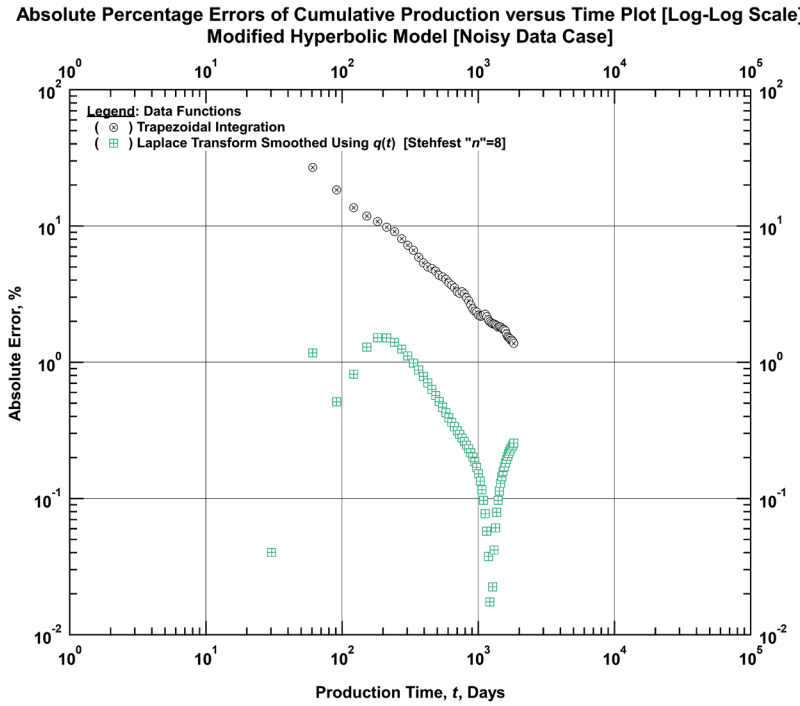

Figure D-8.8 — Comparison Plot of the Absolute Percentage Errors of Trapezoidal-Integrated Cumulative Production and Laplace Transform Smoothed Cumulative Production using Rate as Basis Function versus Time [Modified Hyperbolic Model (Noisy Data Case)].

Table D-8 — Input Parameters for Modified Hyperbolic Model (Noisy Data Set) Case.

Basis Function: Time-Rate Data

Laplace Smoothed Functions	**Rate & Cum. Production**	**D-Parameter**	**b-Parameter**
Basis Functions	$q(t)$	$q(t)$	$1/D(t)$
Numerical Laplace Transform Parameters			
LHS Extrapolation Type (NP1)	Log-Linear	Log-Linear	Straight Line
RHS Extrapolation Type (NP3)	Log-Linear	Log-Linear	Linear-Log
LHS Regression Range (lL)	0.78	0.78	1.30
RHS Regression Range (lR)	0.22	0.22	0.01
Numerical Laplace Inversion Parameter			
Stehfest "n" Parameter	8	8	6

Basis Function: Time-Reciprocal of Rate Data

Laplace Smoothed Functions	**Rate**	**D-Parameter**	**b-Parameter**
Basis Functions	$1/q(t)$	$1/q(t)$	$1/D(t)$
Numerical Laplace Transform Parameters			
LHS Extrapolation Type (NP1)	Striaght Line	Striaght Line	Straight Line
RHS Extrapolation Type (NP3)	Striaght Line	Striaght Line	Linear-Log
LHS Regression Range (lL)	0.78	0.78	1.30
RHS Regression Range (lR)	0.22	0.22	0.01
Numerical Laplace Inversion Parameter			
Stehfest "n" Parameter	8	8	6

D.9 Power-Law Exponential Model (Perfect Data Case)

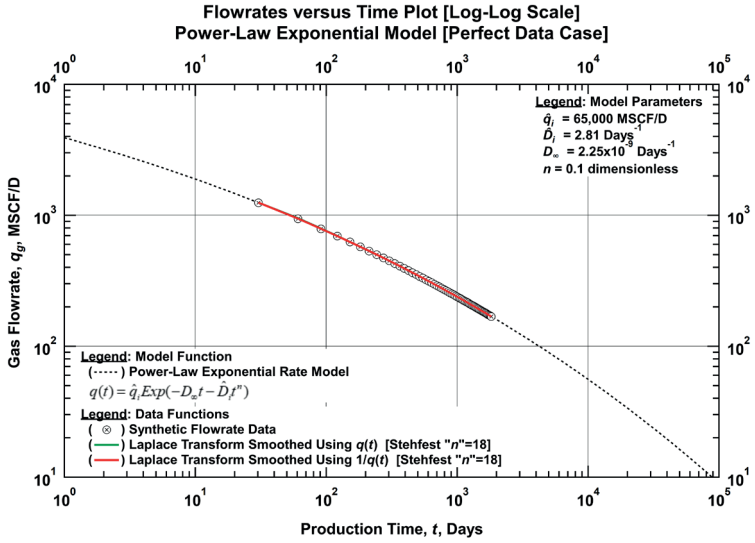

Figure D-9.1 — Comparison Plot of the Modelled Flowrate, Synthetic Flowrate, and Laplace Transform Smoothed Flowrates using Rate and Reciprocal of Rate as the Basis Functions Versus Time [Power-Law Exponential Model (Perfect Data Case)].

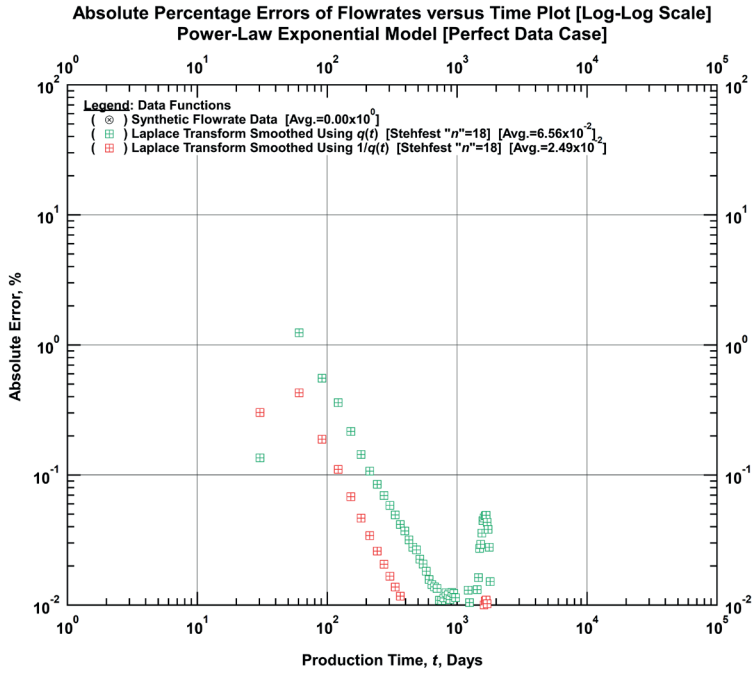

Figure D-9.2 — Comparison Plot of the Absolute Percentage Errors of the Synthetic Flowrate and Laplace Transform Smoothed Flowrates using Rate and Reciprocal of Rate as the Basis Functions Versus Time [Power-Law Exponential Model (Perfect Data Case)].

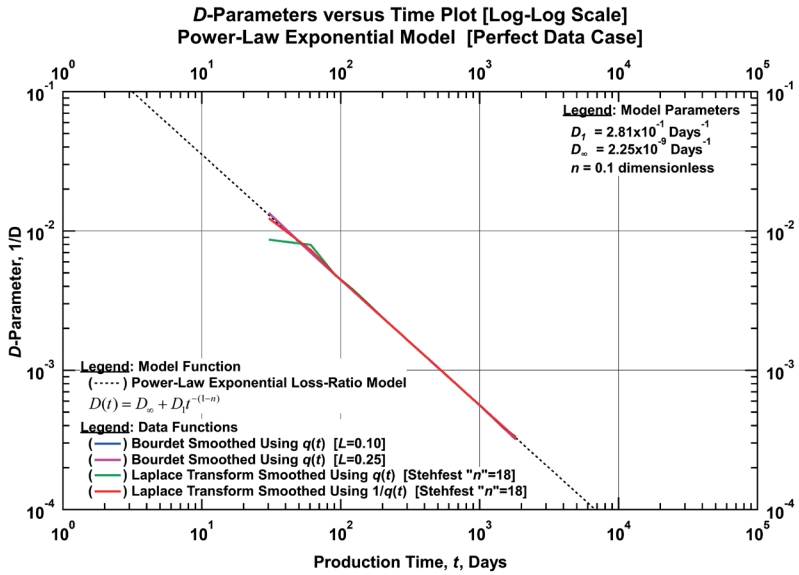

Figure D-9.3 — Comparison Plot of the Modelled *D*-Parameters, Bourdet-Derived *D*-Parameters, and Laplace Transform Smoothed *D*-Parameters using Rate and Reciprocal of Rate as the Basis Functions Versus Time [Power-Law Exponential Model (Perfect Data Case)].

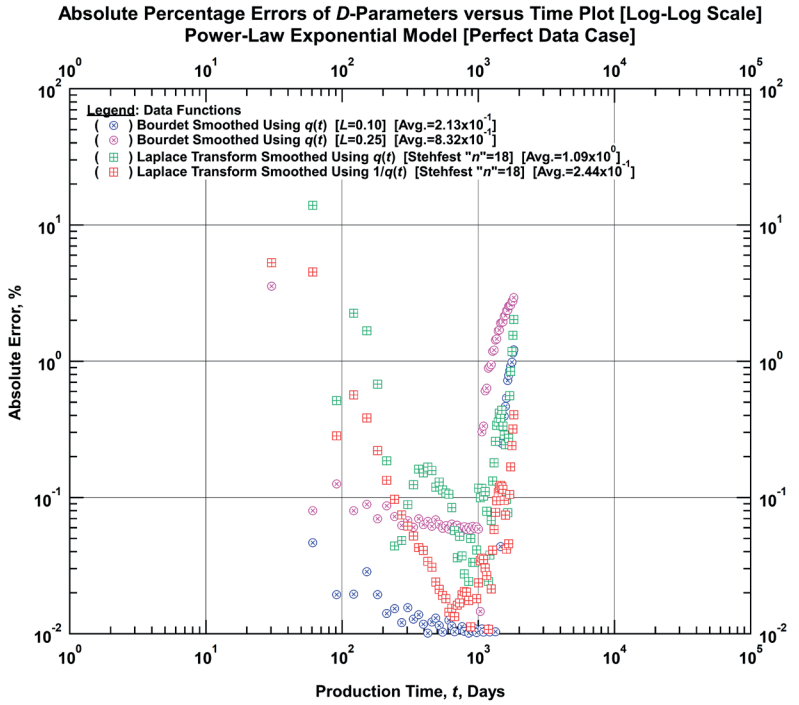

Figure D-9.4 — Comparison Plot of the Absolute Percentage Errors of the Bourdet-Derived *D*-Parameters and Laplace Transform Smoothed *D*-Parameters using Rate and Reciprocal of Rate Functions as the Basis Functions Versus Time [Power-Law Exponential Model (Perfect Data Case)].

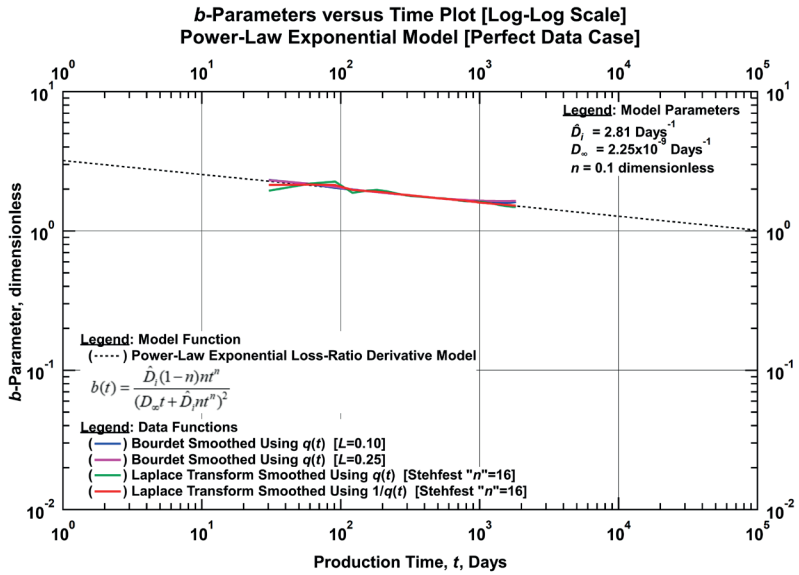

Figure D-9.5 — Comparison Plot of the Modelled *b*-Parameters, Bourdet-Derived *b*-Parameters, and Laplace Transform Smoothed *b*-Parameters using Rate and Reciprocal of Rate as the Basis Functions Versus Time [Power-Law Exponential Model (Perfect Data Case)].

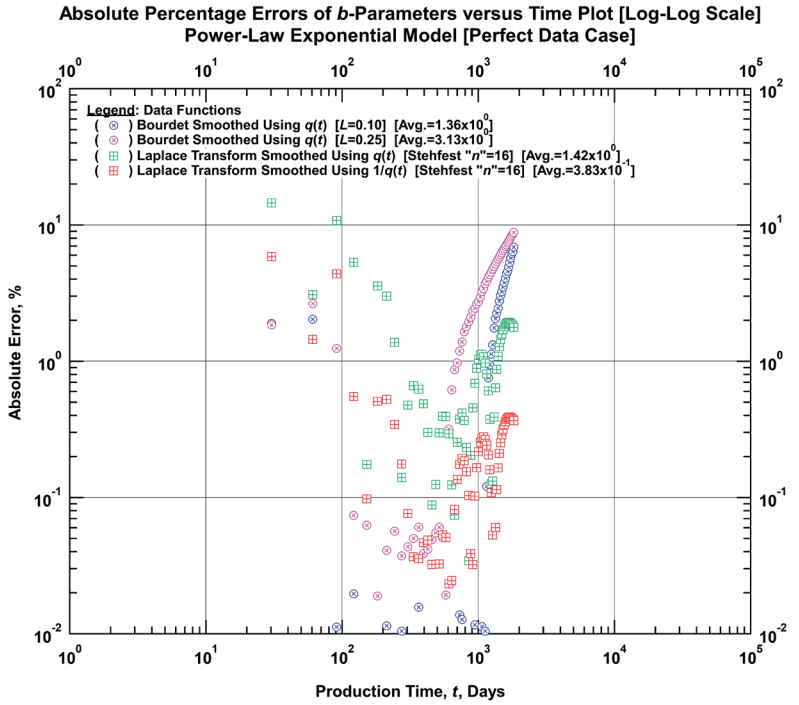

Figure D-9.6 — Comparison Plot of the Absolute Percentage Errors of the Bourdet-Derived *b*-Parameters and Laplace Transform Smoothed *b*-Parameters using Rate and Reciprocal of Rate as the Basis Functions versus Time [Power-Law Exponential Model (Perfect Data Case)].

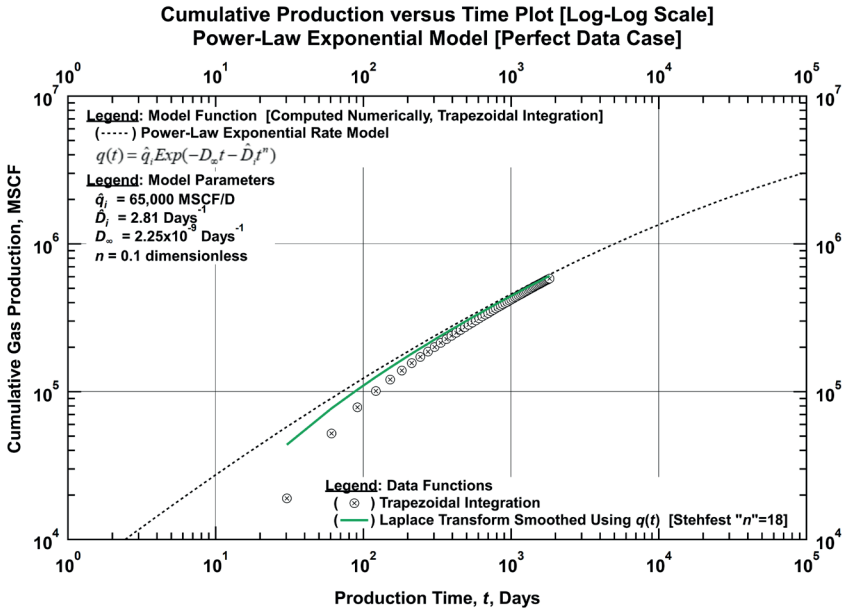

Figure D-9.7 — Comparison Plot of the Modelled Cumulative Production, Trapezoidal-Integrated Cumulative Production, and Laplace Transform Smoothed Cumulative Production using Rate as Basis Function versus Time [Power-Law Exponential Model (Perfect Data Case)].

It is noted that a closed form for cumulative production of Power-law exponential model does not exist. We estimated cumulative production in Figure D-9.7 by using trapezoidal rule integration with very fine logarithmically-spaced time-grid rate data. As a result, we cannot compute the errors of cumulative production using the trapezoidal integration approach and Laplace transform smoothed approach.

Table D-9 — Input Parameters for Power-Law Exponential Model (Perfect Data Set) Case.

Basis Function: Time-Rate Data

Laplace Smoothed Functions	**Rate & Cum. Production**	**D-Parameter**	**b-Parameter**
Basis Functions	$q(t)$	$q(t)$	$1/D(t)$
Numerical Laplace Transform Parameters			
LHS Extrapolation Type (NP1)	Log-Linear	Log-Linear	Log-Log
RHS Extrapolation Type (NP3)	Linear-Log	Linear-Log	Log-Log
LHS Regression Range (lL)	0.35	0.35	1.74
RHS Regression Range (lR)	0.01	0.01	0.43
Numerical Laplace Inversion Parameter			
Stehfest "n" Parameter	18	18	16

Basis Function: Time-Reciprocal of Rate Data

Laplace Smoothed Functions	**Rate**	**D-Parameter**	**b-Parameter**
Basis Functions	$1/q(t)$	$1/q(t)$	$1/D(t)$
Numerical Laplace Transform Parameters			
LHS Extrapolation Type (NP1)	Log-Log	Log-Log	Log-Log
RHS Extrapolation Type (NP3)	Log-Log	Log-Log	Log-Log
LHS Regression Range (lL)	0.35	0.35	1.74
RHS Regression Range (lR)	0.01	0.01	0.43
Numerical Laplace Inversion Parameter			
Stehfest "n" Parameter	18	18	16

D.10 Power-Law Exponential Model (Noisy Data Case)

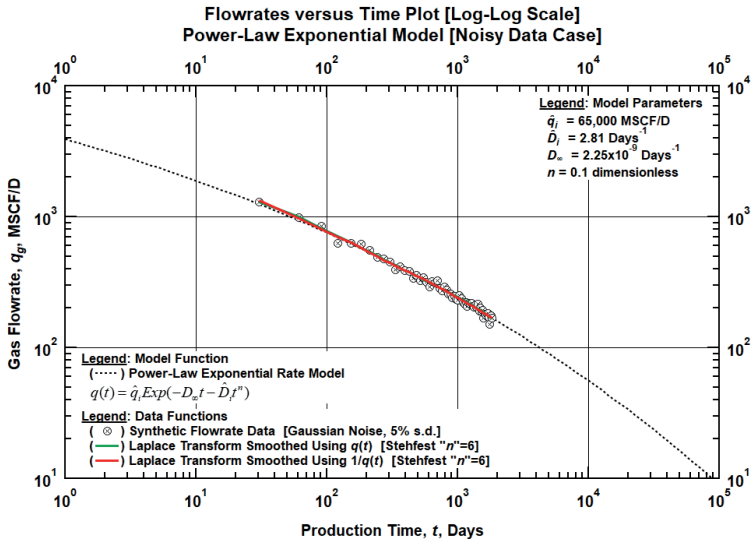

Figure D-10.1 — Comparison Plot of the Modelled Flowrate, Synthetic Flowrate, and Laplace Transform Smoothed Flowrates using Rate and Reciprocal of Rate as the Basis Functions Versus Time [Power-Law Exponential Model (Noisy Data Case)].

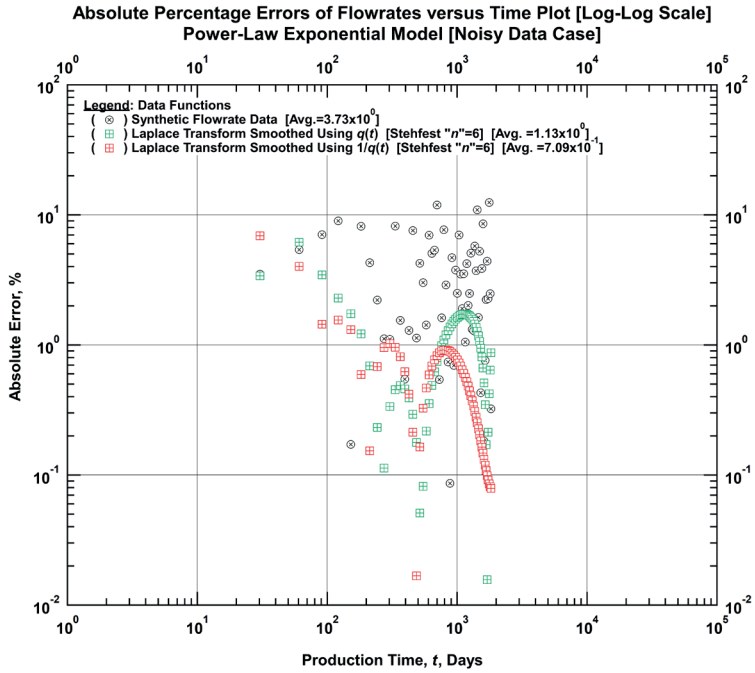

Figure D-10.2 — Comparison Plot of the Absolute Percentage Errors of the Synthetic Flowrate and Laplace Transform Smoothed Flowrates using Rate and Reciprocal of Rate as the Basis Functions Versus Time [Power-Law Exponential Model (Noisy Data Case)].

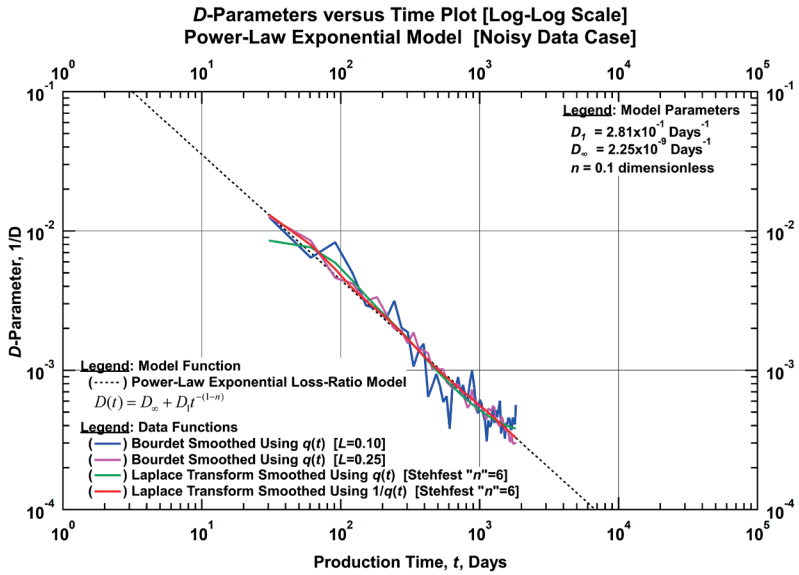

Figure D-10.3 — Comparison Plot of the Modelled *D*-Parameters, Bourdet-Derived *D*-Parameters, and Laplace Transform Smoothed *D*-Parameters using Rate and Reciprocal of Rate as the Basis Functions Versus Time [Power-Law Exponential Model Noisy Data Case)].

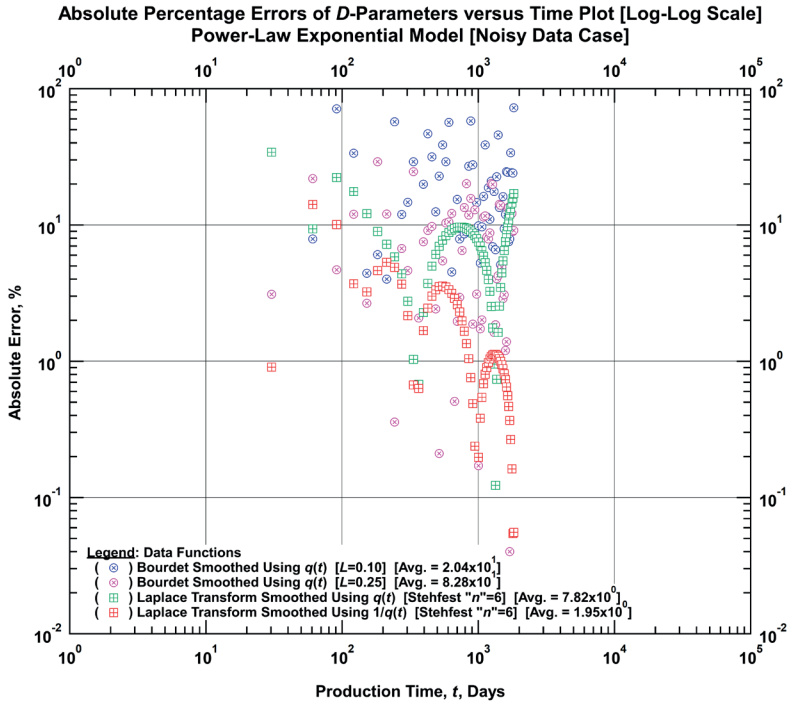

Figure D-10.4 — Comparison Plot of the Absolute Percentage Errors of the Bourdet-Derived *D*-Parameters and Laplace Transform Smoothed *D*-Parameters using Rate and Reciprocal of Rate Functions as the Basis Functions Versus Time [Power-Law Exponential Model (Noisy Data Case)].

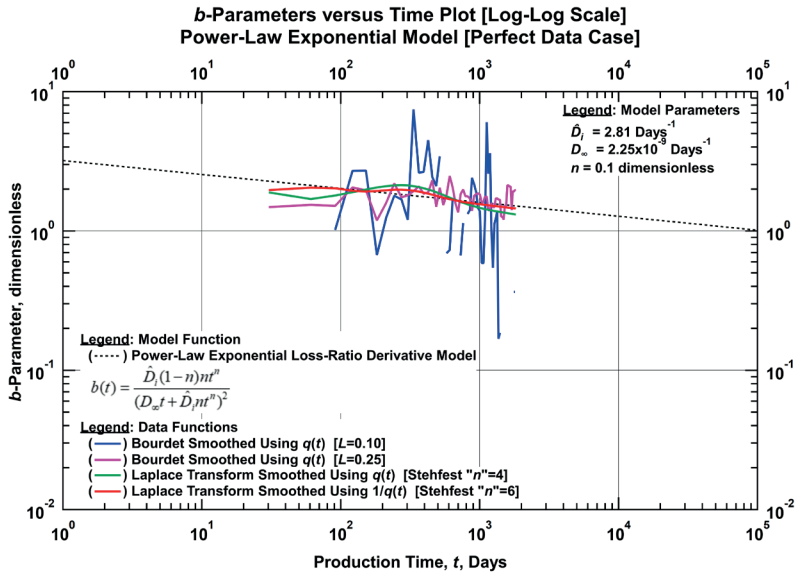

Figure D-10.5 — Comparison Plot of the Modelled *b*-Parameters, Bourdet-Derived *b*-Parameters, and Laplace Transform Smoothed *b*-Parameters using Rate and Reciprocal of Rate as the Basis Functions Versus Time [Power-Law Exponential Model (Noisy Data Case)].

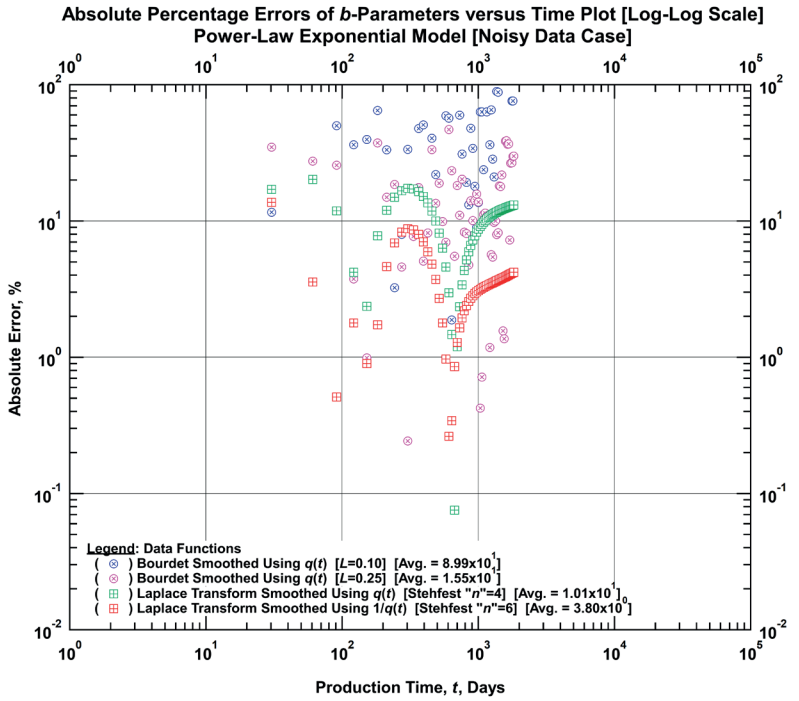

Figure D-10.6 — Comparison Plot of the Absolute Percentage Errors of the Bourdet-Derived *b*-Parameters and Laplace Transform Smoothed *b*-Parameters using Rate and Reciprocal of Rate as the Basis Functions versus Time [Power-Law Exponential Model (Noisy Data Case)].

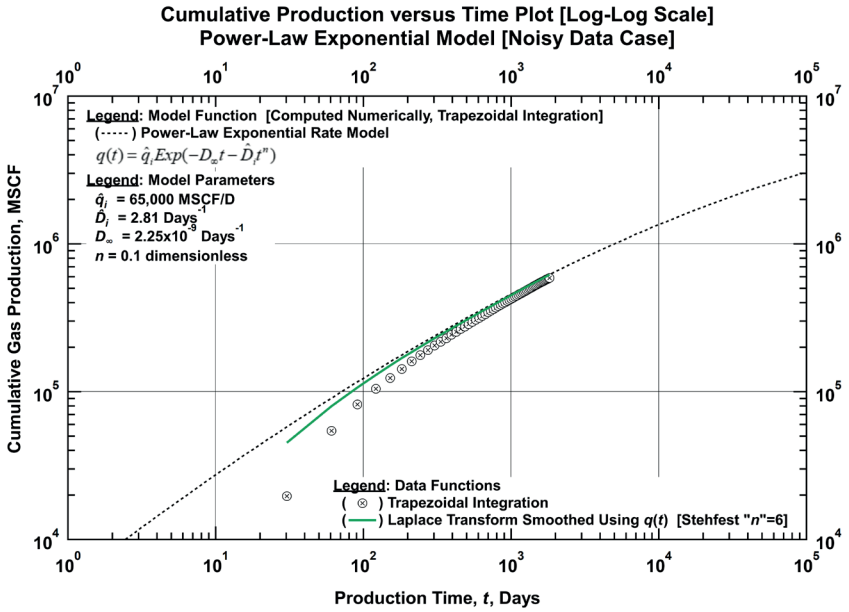

Figure D-10.7 — Comparison Plot of the Modelled Cumulative Production, Trapezoidal-Integrated Cumulative Production, and Laplace Transform Smoothed Cumulative Production using Rate as Basis Function versus Time [Power-Law Exponential Model (Noisy Data Case)].

As described in the previous section for the perfect data case of power-law exponential model, the errors plot cannot be computed.

Table D-10 — Input Parameters for Power-Law Exponential Model (Noisy Data Set) Case.

Basis Function: Time-Rate Data

Laplace Smoothed Functions	**Rate & Cum. Production**	**D-Parameter**	**b-Parameter**
Basis Functions	$q(t)$	$q(t)$	$1/D(t)$
Numerical Laplace Transform Parameters			
LHS Extrapolation Type (NP1)	Log-Linear	Log-Linear	Log-Log
RHS Extrapolation Type (NP3)	Linear-Log	Linear-Log	Log-Log
LHS Regression Range (lL)	0.43	0.43	1.74
RHS Regression Range (lR)	0.22	0.22	0.87
Numerical Laplace Inversion Parameter			
Stehfest "n" Parameter	6	6	4

Basis Function: Time-Reciprocal of Rate Data

Laplace Smoothed Functions	**Rate**	**D-Parameter**	**b-Parameter**
Basis Functions	$1/q(t)$	$1/q(t)$	$1/D(t)$
Numerical Laplace Transform Parameters			
LHS Extrapolation Type (NP1)	Log-Log	Log-Log	Log-Log
RHS Extrapolation Type (NP3)	Log-Log	Log-Log	Log-Log
LHS Regression Range (lL)	0.87	0.87	1.74
RHS Regression Range (lR)	0.43	0.43	0.43
Numerical Laplace Inversion Parameter			
Stehfest "n" Parameter	6	6	6

D.11 Duong Model (Perfect Data Case)

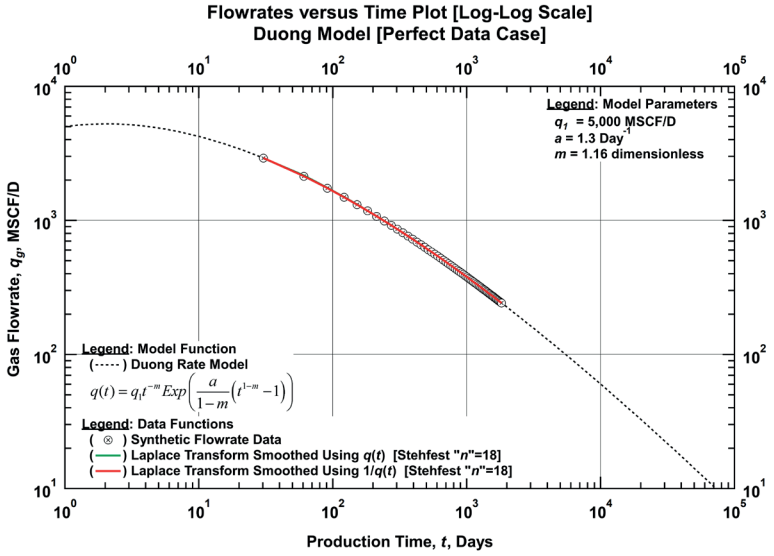

Figure D-11.1 — Comparison Plot of the Modelled Flowrate, Synthetic Flowrate, and Laplace Transform Smoothed Flowrates using Rate and Reciprocal of Rate as the Basis Functions Versus Time [Duong Model (Perfect Data Case)].

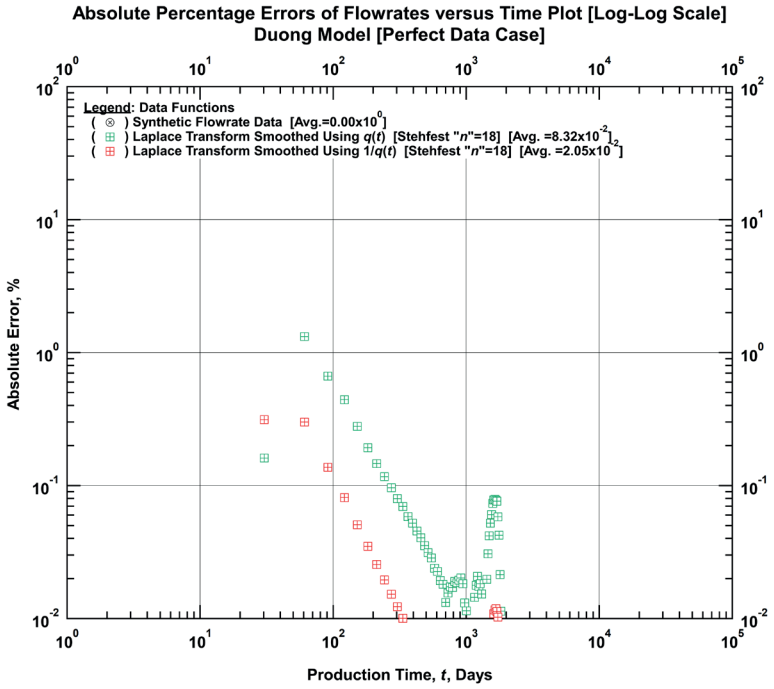

Figure D-11.2 — Comparison Plot of the Absolute Percentage Errors of the Synthetic Flowrate and Laplace Transform Smoothed Flowrates using Rate and Reciprocal of Rate as the Basis Functions Versus Time [Duong Model (Perfect Data Case)].

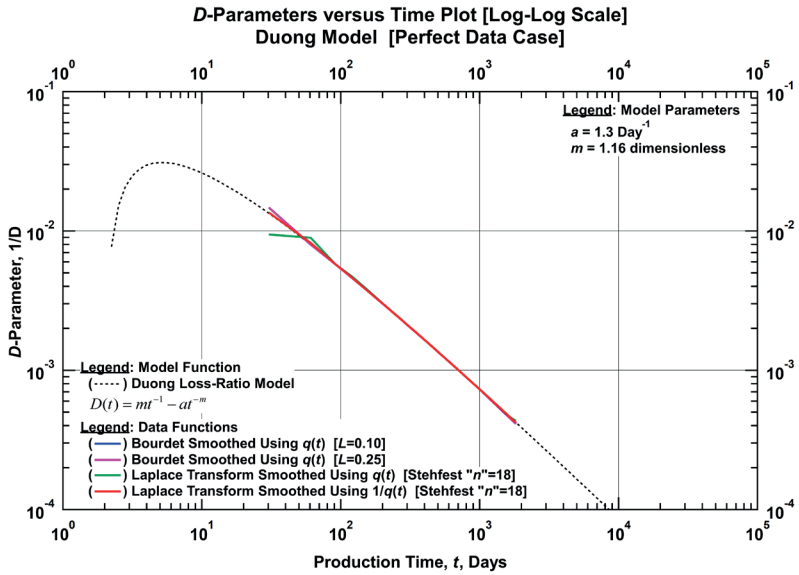

Figure D-11.3 — Comparison Plot of the Modelled *D*-Parameters, Bourdet-Derived *D*-Parameters, and Laplace Transform Smoothed *D*-Parameters using Rate and Reciprocal of Rate as the Basis Functions Versus Time [Duong Model (Perfect Data Case)].

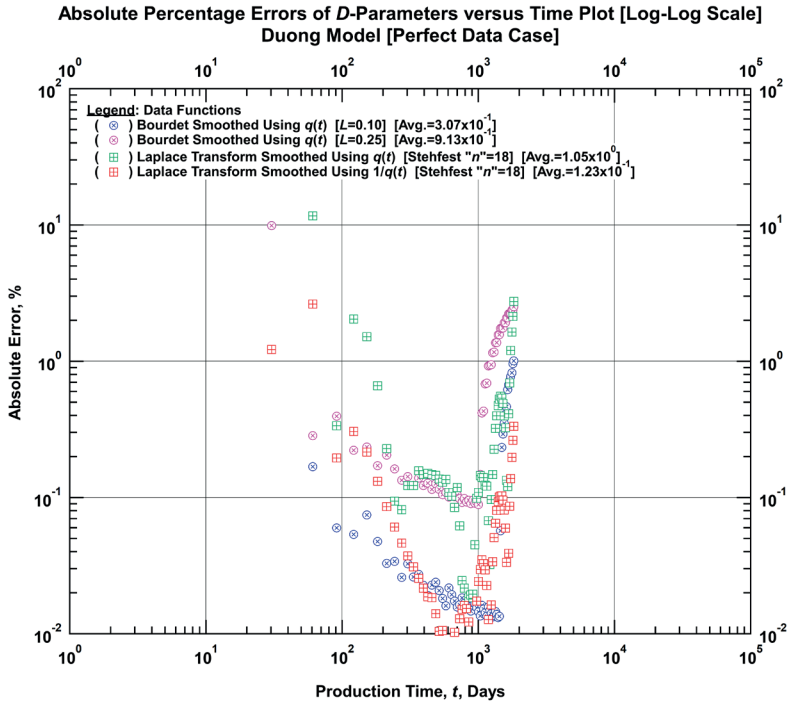

Figure D-11.4 — Comparison Plot of the Absolute Percentage Errors of the Bourdet-Derived *D*-Parameters and Laplace Transform Smoothed *D*-Parameters using Rate and Reciprocal of Rate Functions as the Basis Functions Versus Time [Duong Model (Perfect Data Case)].

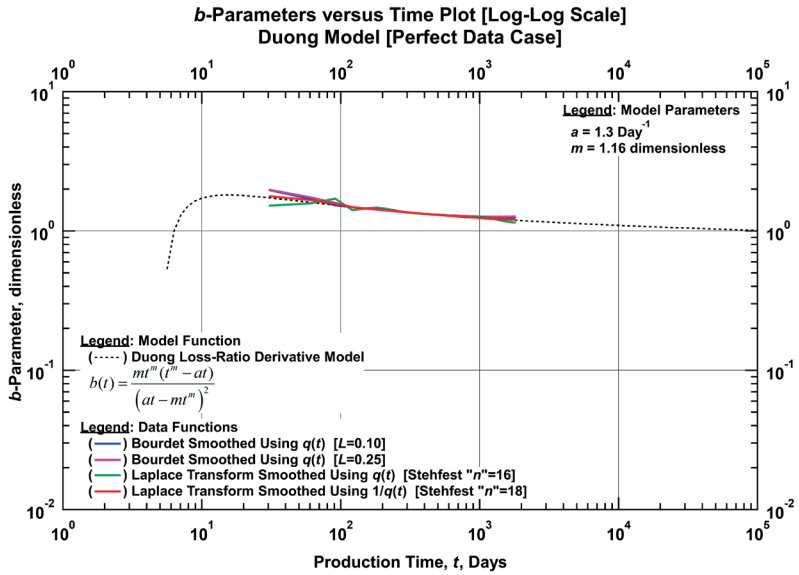

Figure D-11.5 — Comparison Plot of the Modelled *b*-Parameters, Bourdet-Derived *b*-Parameters, and Laplace Transform Smoothed *b*-Parameters using Rate and Reciprocal of Rate as the Basis Functions Versus Time [Duong Model (Perfect Data Case)].

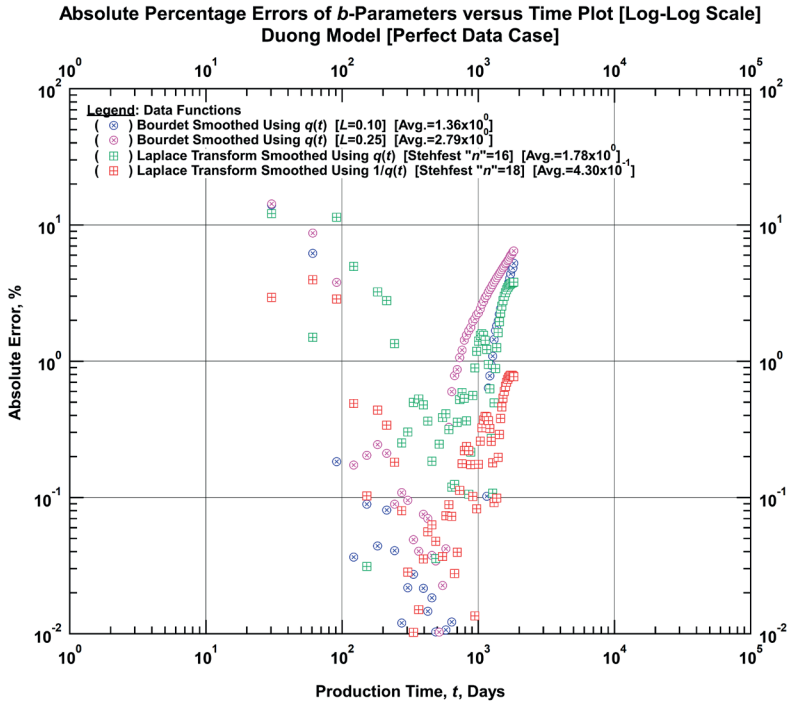

Figure D-11.6 — Comparison Plot of the Absolute Percentage Errors of the Bourdet-Derived *b*-Parameters and Laplace Transform Smoothed *b*-Parameters using Rate and Reciprocal of Rate as the Basis Functions versus Time [Duong Model (Perfect Data Case)].

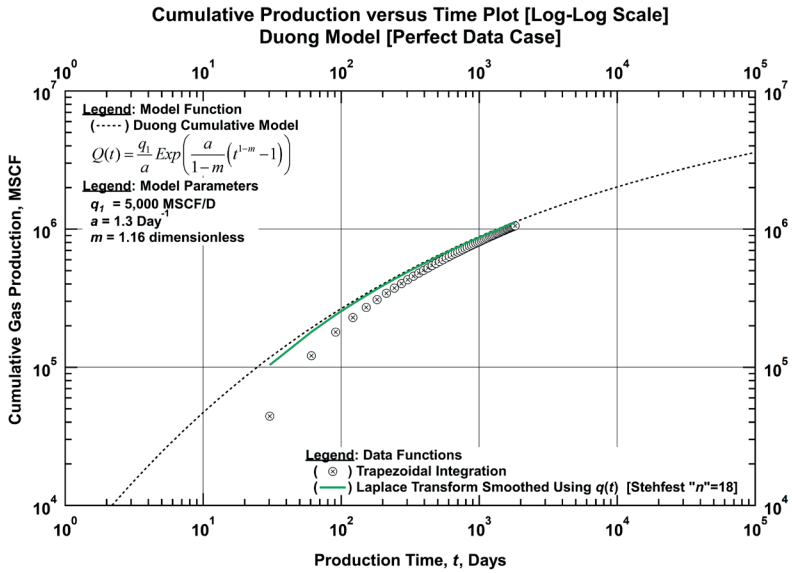

Figure D-11.7 — Comparison Plot of the Modelled Cumulative Production, Trapezoidal-Integrated Cumulative Production, and Laplace Transform Smoothed Cumulative Production using Rate as Basis Function versus Time [Duong Model (Perfect Data Case)].

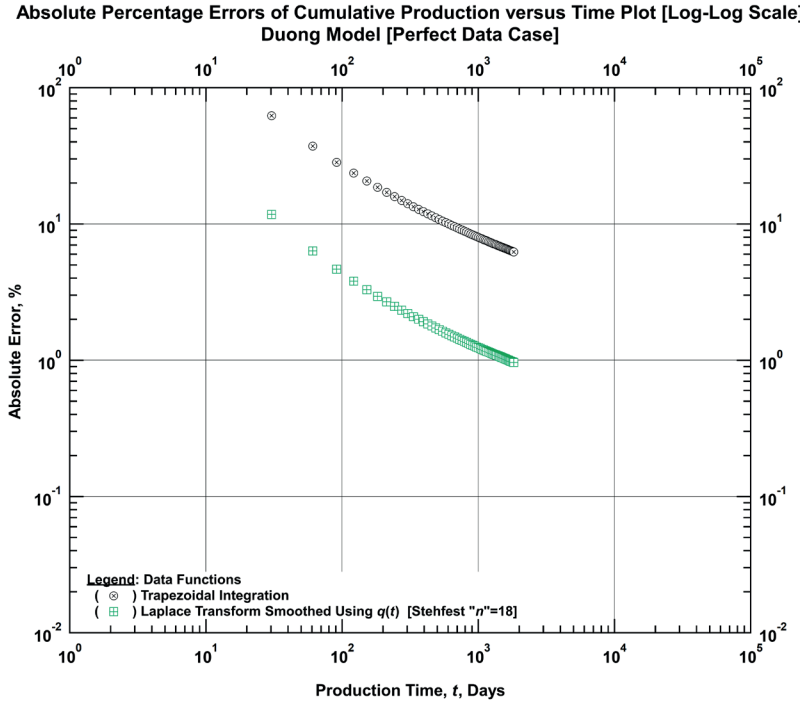

Figure D-11.8 — Comparison Plot of the Absolute Percentage Errors of Trapezoidal-Integrated Cumulative Production and Laplace Transform Smoothed Cumulative Production using Rate as Basis Function versus Time [Duong Model (Perfect Data Case)].

Table D-11 — Input Parameters for Duong Model (Perfect Data Set) Case.

Basis Function: Time-Rate Data

Laplace Smoothed Functions	**Rate & Cum. Production**	**D-Parameter**	**b-Parameter**
Basis Functions	$q(t)$	$q(t)$	$1/D(t)$
Numerical Laplace Transform Parameters			
LHS Extrapolation Type (NP1)	Log-Linear	Log-Linear	Log-Log
RHS Extrapolation Type (NP3)	Linear-Log	Linear-Log	Log-Log
LHS Regression Range (lL)	0.35	0.35	1.09
RHS Regression Range (lR)	0.01	0.01	0.35
Numerical Laplace Inversion Parameter			
Stehfest "n" Parameter	18	18	16

Basis Function: Time-Reciprocal of Rate Data

Laplace Smoothed Functions	**Rate**	**D-Parameter**	**b-Parameter**
Basis Functions	$1/q(t)$	$1/q(t)$	$1/D(t)$
Numerical Laplace Transform Parameters			
LHS Extrapolation Type (NP1)	Log-Log	Log-Log	Log-Log
RHS Extrapolation Type (NP3)	Log-Log	Log-Log	Log-Log
LHS Regression Range (lL)	0.35	0.35	0.87
RHS Regression Range (lR)	0.01	0.01	0.17
Numerical Laplace Inversion Parameter			
Stehfest "n" Parameter	18	18	18

D.12 Logistic Growth Model (Perfect Data Case)

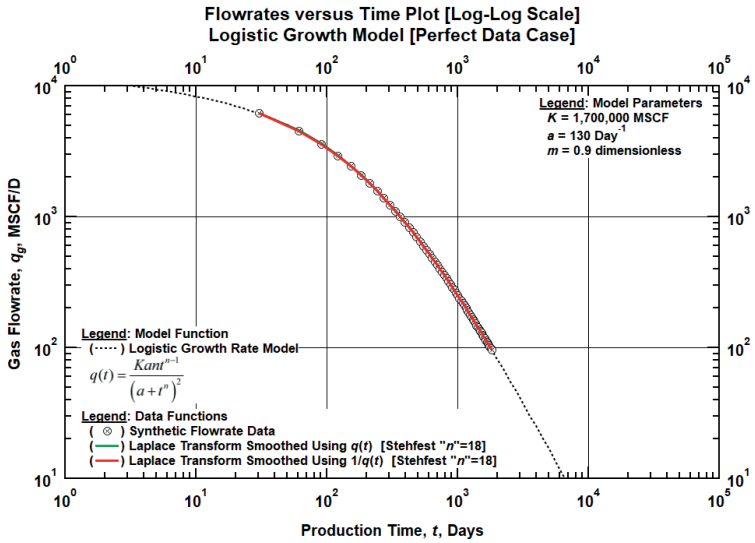

Figure D-12.1 — Comparison Plot of the Modelled Flowrate, Synthetic Flowrate, and Laplace Transform Smoothed Flowrates using Rate and Reciprocal of Rate as the Basis Functions Versus Time [Logistic Growth Model (Perfect Data Case)].

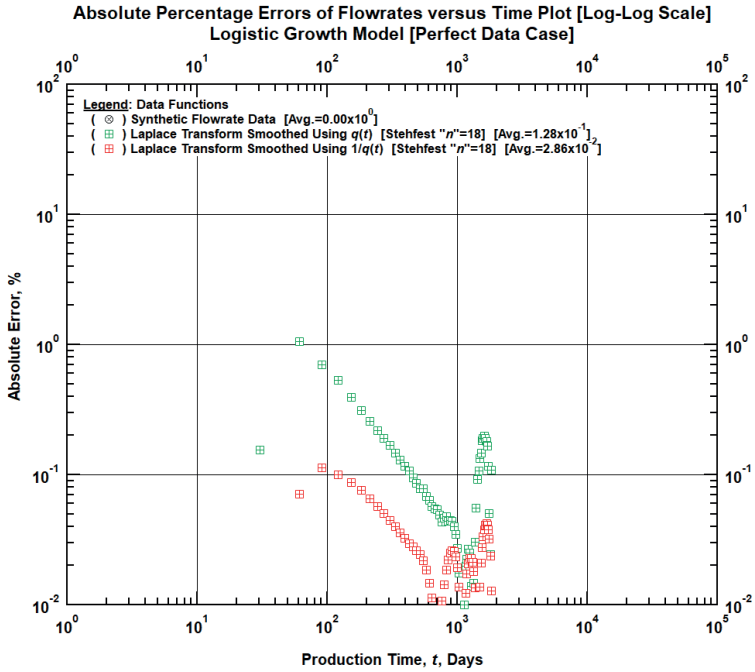

Figure D-12.2 — Comparison Plot of the Absolute Percentage Errors of the Synthetic Flowrate and Laplace Transform Smoothed Flowrates using Rate and Reciprocal of Rate as the Basis Functions Versus Time [Logistic Growth Model (Perfect Data Case)].

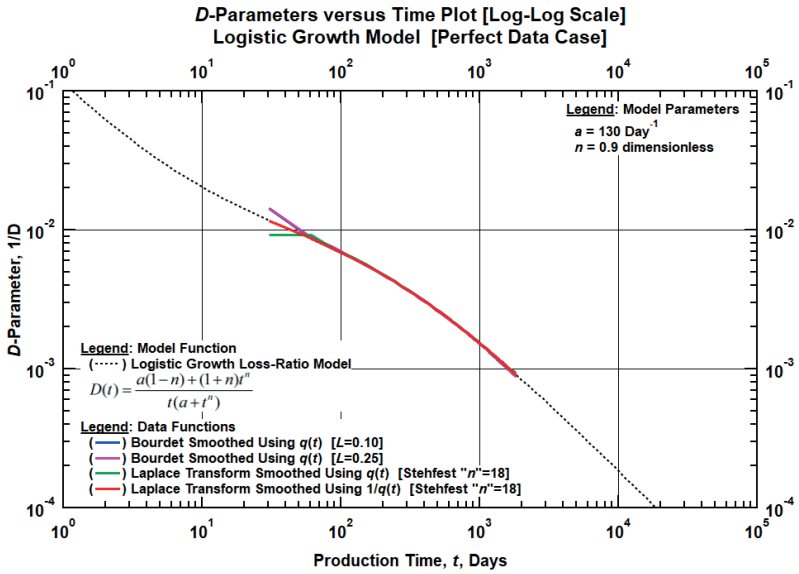

Figure D-12.3 — Comparison Plot of the Modelled *D*-Parameters, Bourdet-Derived *D*-Parameters, and Laplace Transform Smoothed *D*-Parameters using Rate and Reciprocal of Rate as the Basis Functions Versus Time [Logistic Growth Model (Perfect Data Case)].

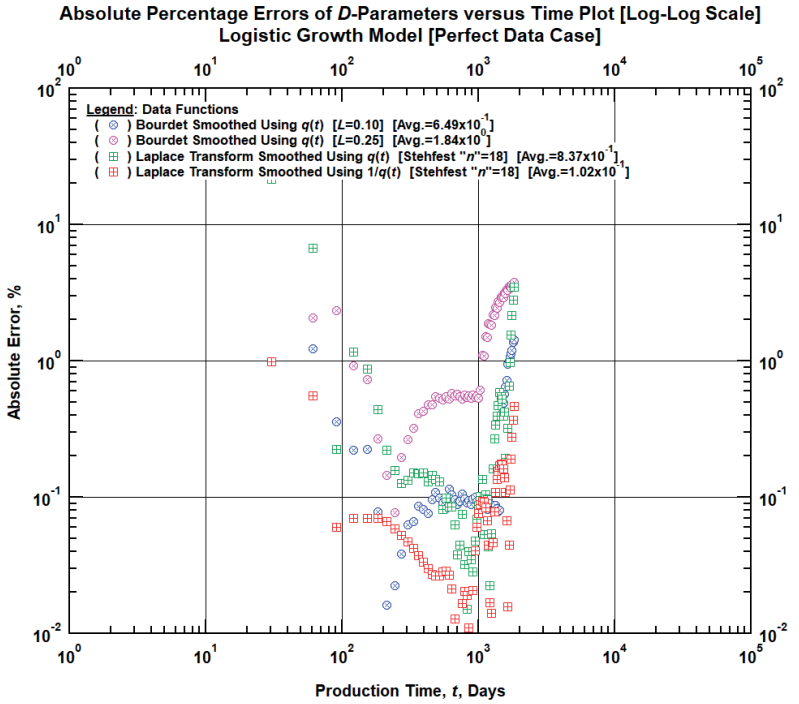

Figure D-12.4 — Comparison Plot of the Absolute Percentage Errors of the Bourdet-Derived *D*-Parameters and Laplace Transform Smoothed *D*-Parameters using Rate and Reciprocal of Rate Functions as the Basis Functions Versus Time [Logistic Growth Model (Perfect Data Case)].

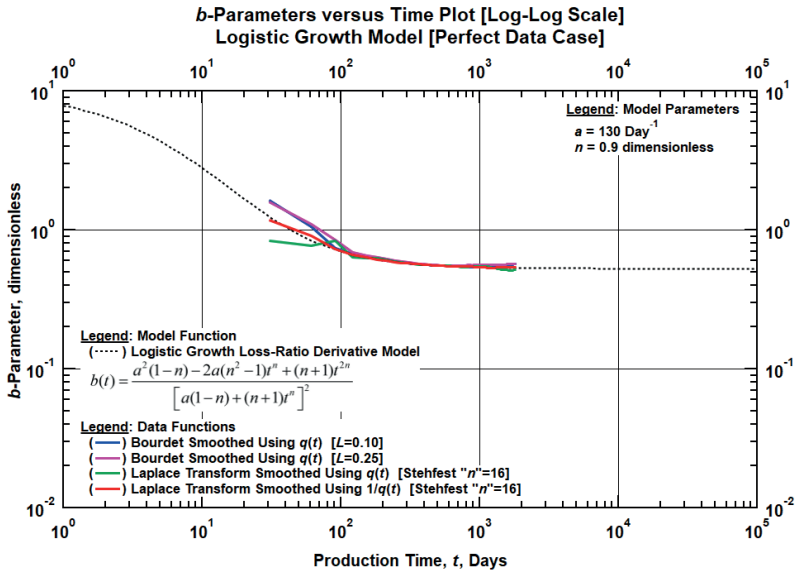

Figure D-12.5 — Comparison Plot of the Modelled *b*-Parameters, Bourdet-Derived *b*-Parameters, and Laplace Transform Smoothed *b*-Parameters using Rate and Reciprocal of Rate as the Basis Functions Versus Time [Logistic Growth Model (Perfect Data Case)].

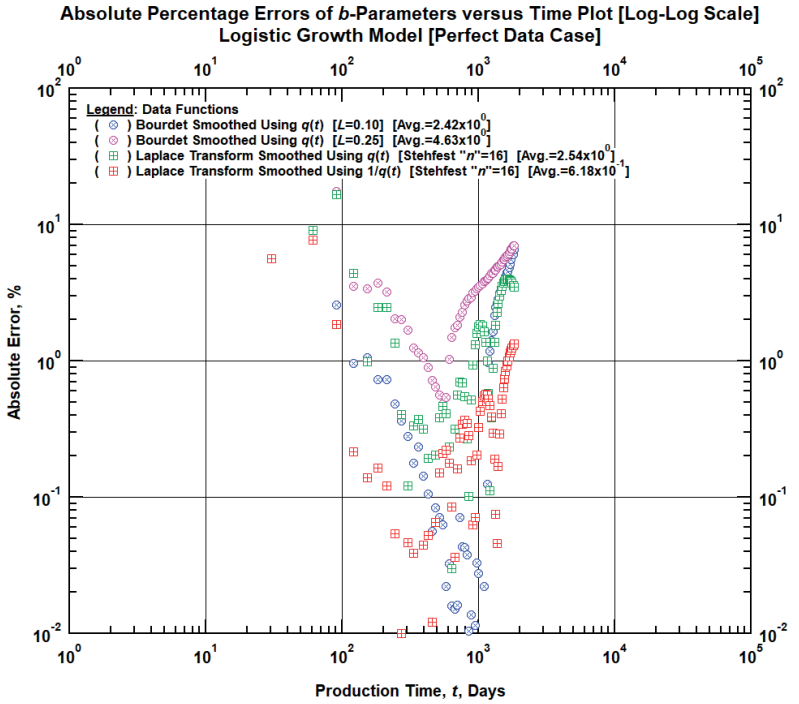

Figure D-12.6 — Comparison Plot of the Absolute Percentage Errors of the Bourdet-Derived *b*-Parameters and Laplace Transform Smoothed *b*-Parameters using Rate and Reciprocal of Rate as the Basis Functions versus Time [Logistic Growth Model (Perfect Data Case)].

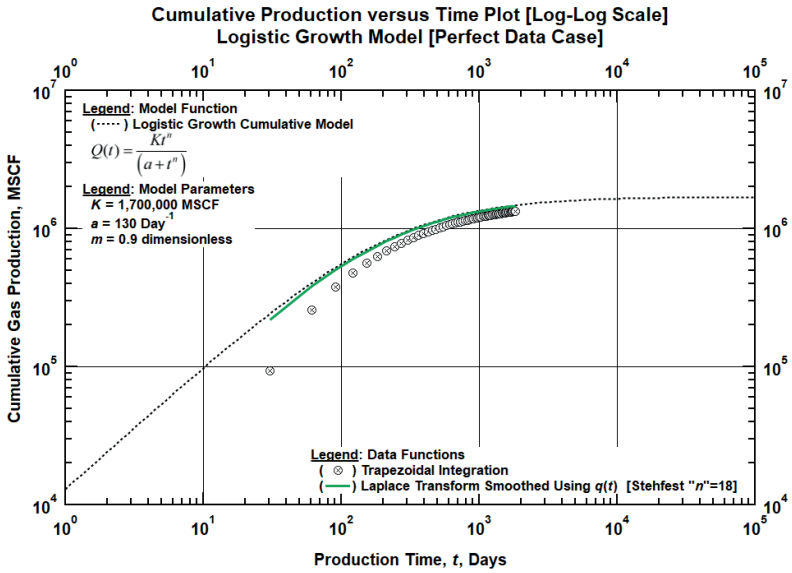

Figure D-12.7 — Comparison Plot of the Modelled Cumulative Production, Trapezoidal-Integrated Cumulative Production, and Laplace Transform Smoothed Cumulative Production using Rate as Basis Function versus Time [Logistic Growth Model (Perfect Data Case)].

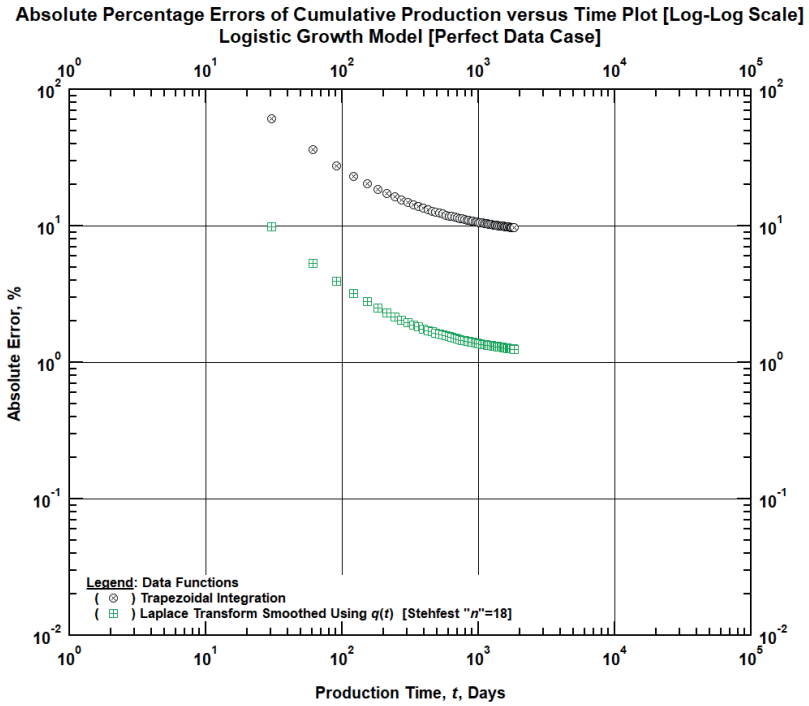

Figure D-12.8 — Comparison Plot of the Absolute Percentage Errors of Trapezoidal-Integrated Cumulative Production and Laplace Transform Smoothed Cumulative Production using Rate as Basis Function versus Time [Logistic Growth Model (Perfect Data Case)].

Table D-12 — Input Parameters for Logistic Growth Model (Perfect Data Set) Case

Basis Function: Time-Rate Data

Laplace Smoothed Functions	**Rate & Cum. Production**	**D-Parameter**	**b-Parameter**
Basis Functions	$q(t)$	$q(t)$	$1/D(t)$
Numerical Laplace Transform Parameters			
LHS Extrapolation Type (NP1)	Log-Linear	Log-Linear	Log-Log
RHS Extrapolation Type (NP3)	Log-Linear	Log-Linear	Straight Line
LHS Regression Range (lL)	0.35	0.35	0.87
RHS Regression Range (lR)	0.01	0.01	0.43
Numerical Laplace Inversion Parameter			
Stehfest "n" Parameter	18	18	16

Basis Function: Time-Reciprocal of Rate Data

Laplace Smoothed Functions	**Rate**	**D-Parameter**	**b-Parameter**
Basis Functions	$1/q(t)$	$1/q(t)$	$1/D(t)$
Numerical Laplace Transform Parameters			
LHS Extrapolation Type (NP1)	Straight Line	Straight Line	Log-Log
RHS Extrapolation Type (NP3)	Log-Log	Log-Log	Straight Line
LHS Regression Range (lL)	0.35	0.35	0.87
RHS Regression Range (lR)	0.01	0.01	0.22
Numerical Laplace Inversion Parameter			
Stehfest "n" Parameter	18	18	16

D.13 Logistic Growth Model (Noisy Data Case)

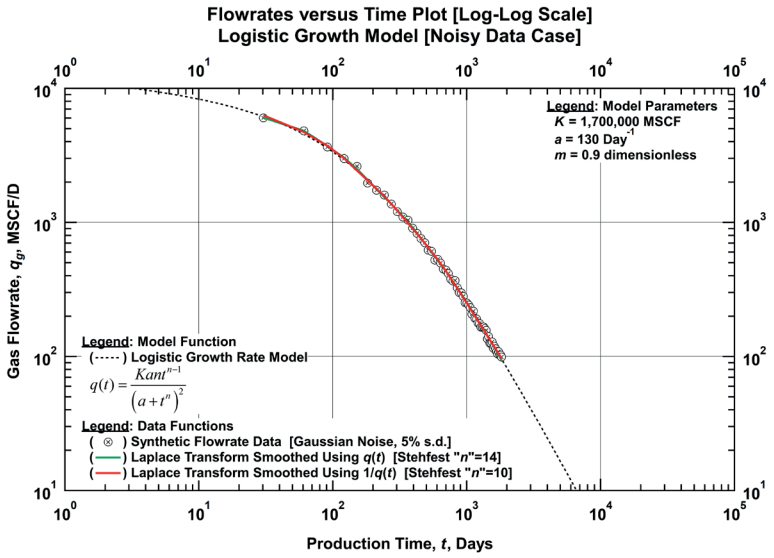

Figure D-13.1 — Comparison Plot of the Modelled Flowrate, Synthetic Flowrate, and Laplace Transform Smoothed Flowrates using Rate and Reciprocal of Rate as the Basis Functions Versus Time [Logistic Growth Model (Noisy Data Case)].

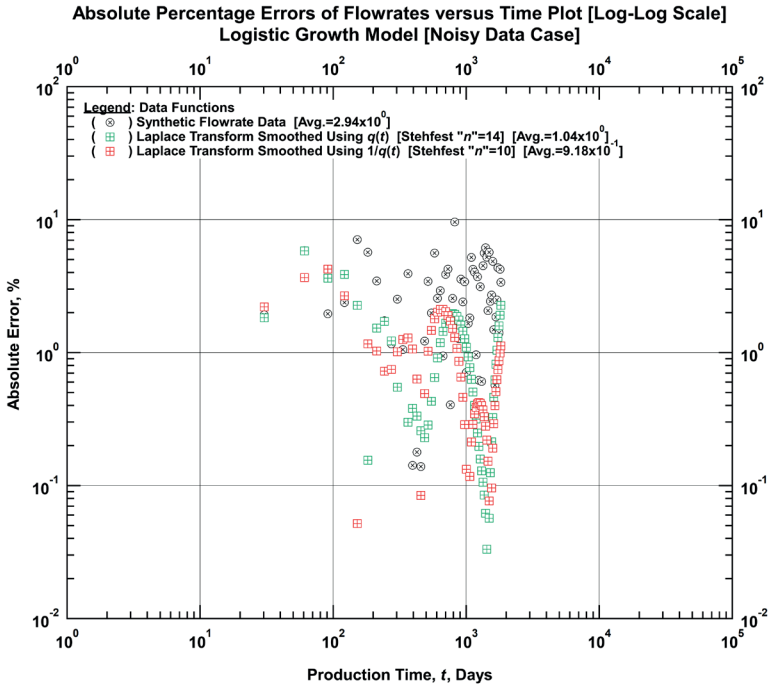

Figure D-13.2 — Comparison Plot of the Absolute Percentage Errors of the Synthetic Flowrate and Laplace Transform Smoothed Flowrates using Rate and Reciprocal of Rate as the Basis Functions Versus Time [Logistic Growth Model (Noisy Data Case)].

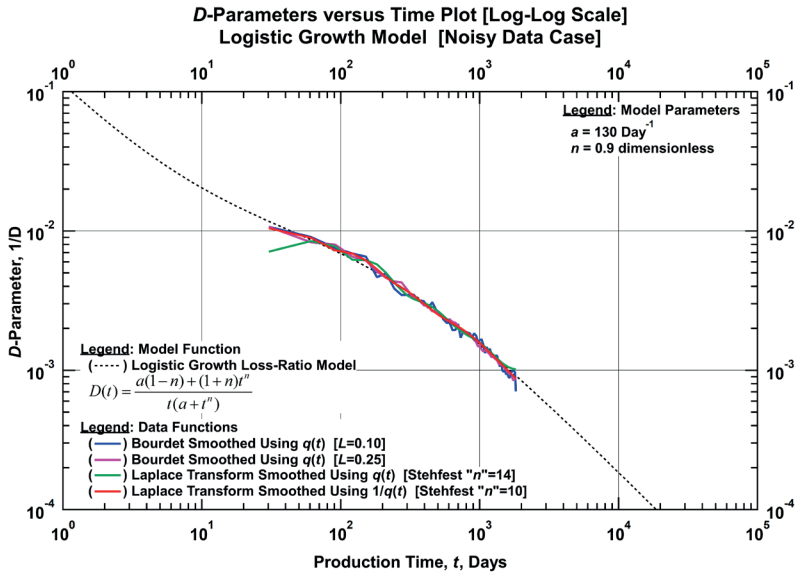

Figure D-13.3 — Comparison Plot of the Modelled *D*-Parameters, Bourdet-Derived *D*-Parameters, and Laplace Transform Smoothed *D*-Parameters using Rate and Reciprocal of Rate as the Basis Functions Versus Time Logistic Growth Model (Noisy Data Case)].

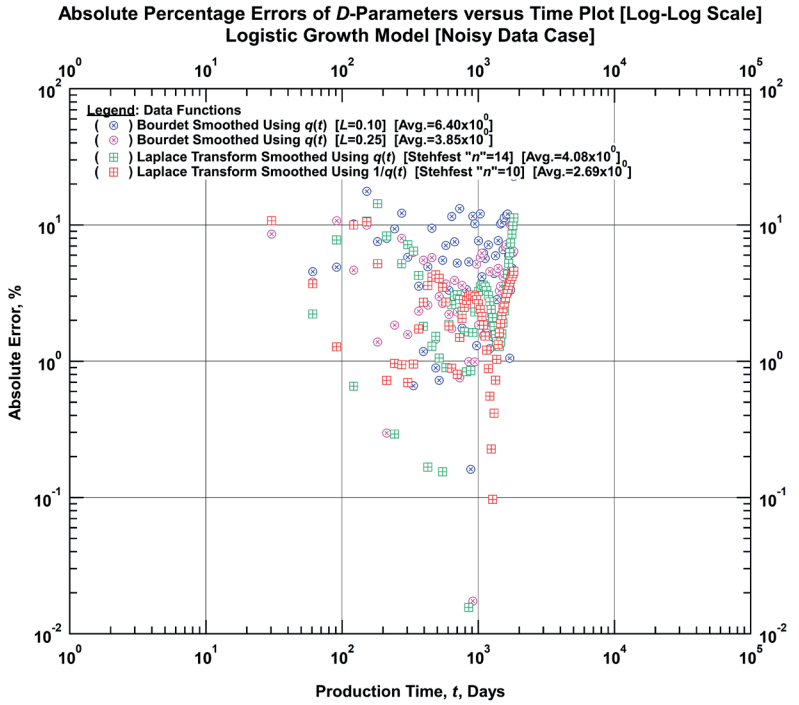

Figure D-13.4 — Comparison Plot of the Absolute Percentage Errors of the Bourdet-Derived *D*-Parameters and Laplace Transform Smoothed *D*-Parameters using Rate and Reciprocal of Rate Functions as the Basis Functions Versus Time [Logistic Growth Model (Noisy Data Case)].

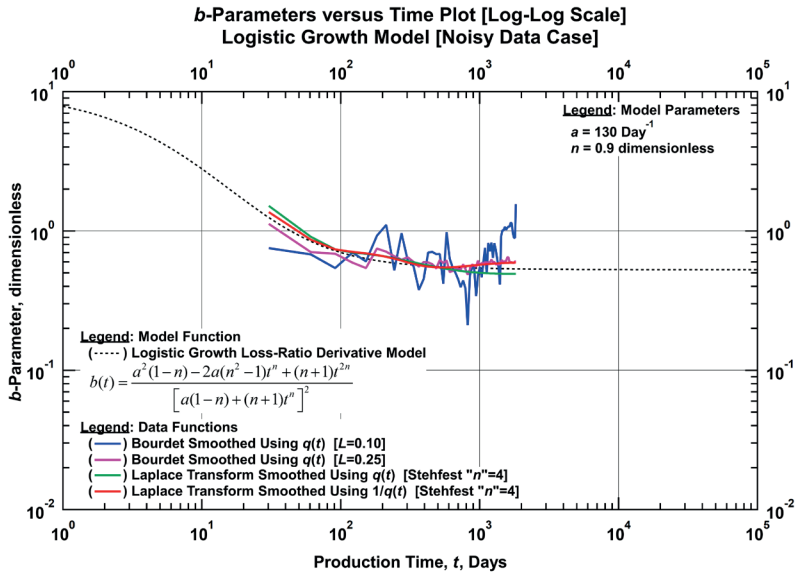

Figure D-13.5 — Comparison Plot of the Modelled *b*-Parameters, Bourdet-Derived *b*-Parameters, and Laplace Transform Smoothed *b*-Parameters using Rate and Reciprocal of Rate as the Basis Functions Versus Time [Logistic Growth Model (Noisy Data Case)].

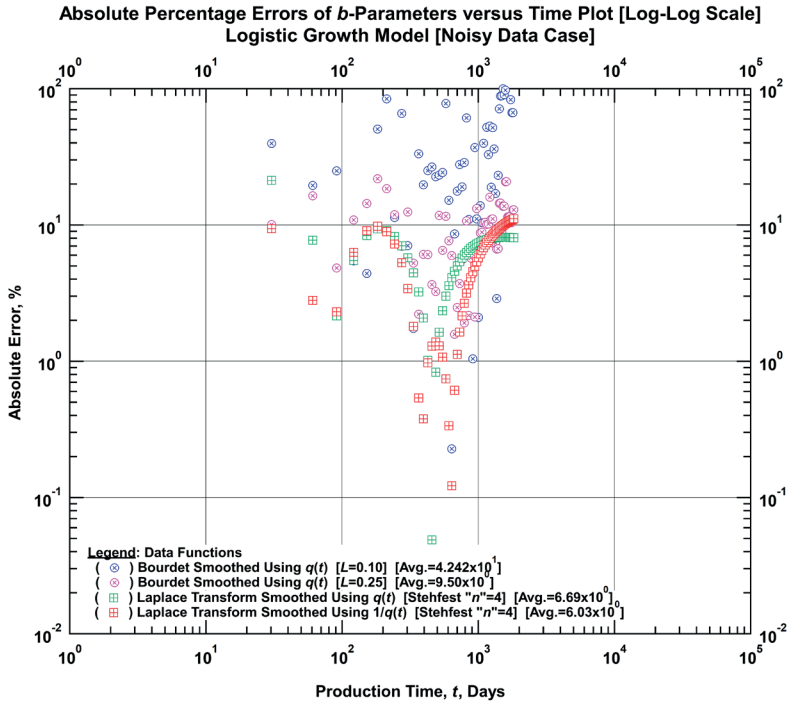

Figure D-13.6 — Comparison Plot of the Absolute Percentage Errors of the Bourdet-Derived *b*-Parameters and Laplace Transform Smoothed *b*-Parameters using Rate and Reciprocal of Rate as the Basis Functions versus Time [Logistic Growth Model (Noisy Data Case)].

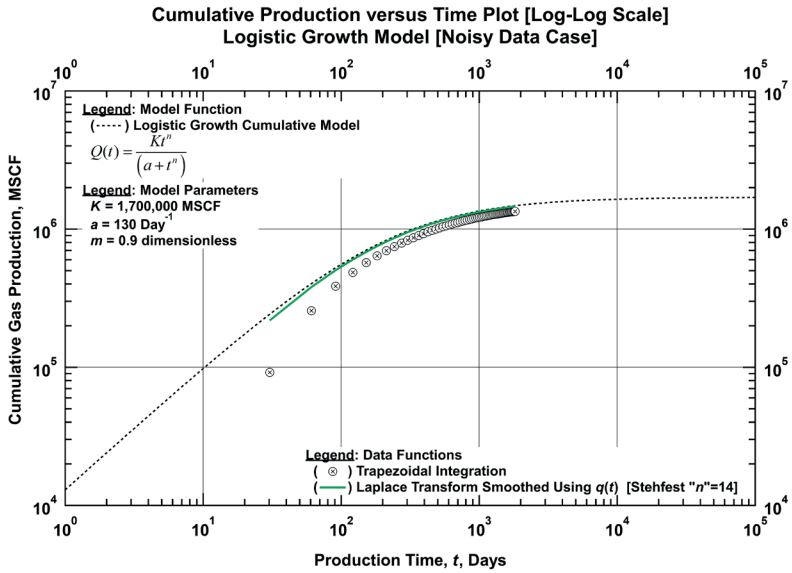

Figure D-13.7 — Comparison Plot of the Modelled Cumulative Production, Trapezoidal-Integrated Cumulative Production, and Laplace Transform Smoothed Cumulative Production using Rate as Basis Function versus Time [Logistic Growth Model (Noisy Data Case)].

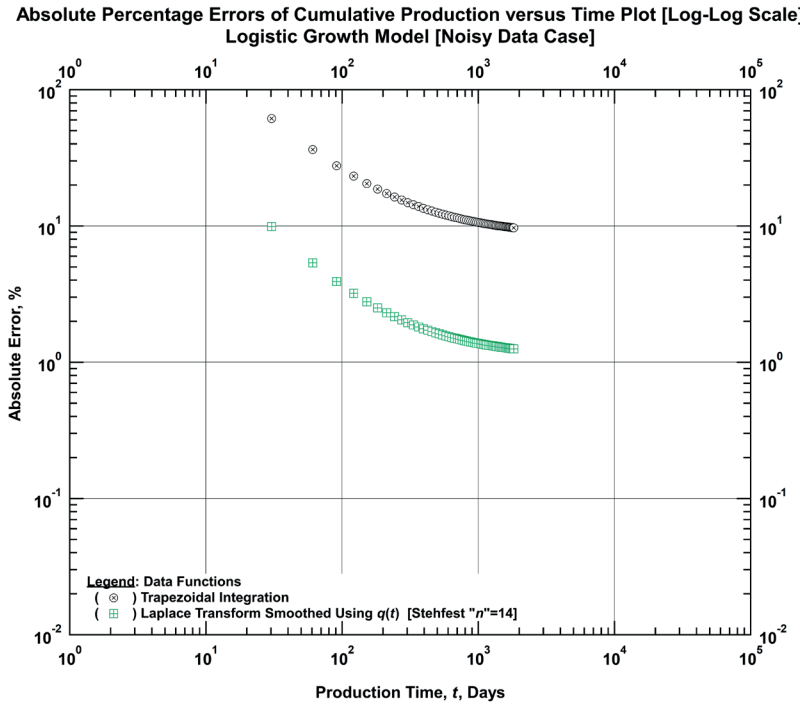

Figure D-13.8 — Comparison Plot of the Absolute Percentage Errors of Trapezoidal-Integrated Cumulative Production and Laplace Transform Smoothed Cumulative Production using Rate as Basis Function versus Time [Logistic Growth Model (Noisy Data Case)].

Table D-13 — Input Parameters for Logistic Growth Model (Noisy Data Set) Case.

Basis Function: Time-Rate Data

Laplace Smoothed Functions	**Rate & Cum. Production**	**D-Parameter**	**b-Parameter**
Basis Functions	$q(t)$	$q(t)$	$1/D(t)$
Numerical Laplace Transform Parameters			
LHS Extrapolation Type (NP1)	Log-Linear	Log-Linear	Log-Log
RHS Extrapolation Type (NP3)	Log-Linear	Linear-Log	Straight Line
LHS Regression Range (lL)	0.43	0.43	1.74
RHS Regression Range (lR)	0.22	0.22	0.87
Numerical Laplace Inversion Parameter			
Stehfest "n" Parameter	14	14	4

Basis Function: Time-Reciprocal of Rate Data

Laplace Smoothed Functions	**Rate**	**D-Parameter**	**b-Parameter**
Basis Functions	$1/q(t)$	$1/q(t)$	$1/D(t)$
Numerical Laplace Transform Parameters			
LHS Extrapolation Type (NP1)	Straight Line	Straight Line	Log-Log
RHS Extrapolation Type (NP3)	Log-Log	Log-Log	Straight Line
LHS Regression Range (lL)	0.65	0.65	1.30
RHS Regression Range (lR)	0.43	0.43	0.43
Numerical Laplace Inversion Parameter			
Stehfest "n" Parameter	10	10	4

APPENDIX E

METHOD VALIDATION WITH ACTUAL FIELD TIME-RATE DATA

The actual field datasets include:

- Field Example 1: East Texas Gas Well (SPE 84287)
- Field Example 2: Fractured Gas Well (SPE 132352)
- Field Example 3: Fractured Gas Well (SPE 132352)
- Field Example 4: Fractured Gas Well (SPE 132352)

E.1 Field Example 1: East Texas Gas Well (SPE 84287)

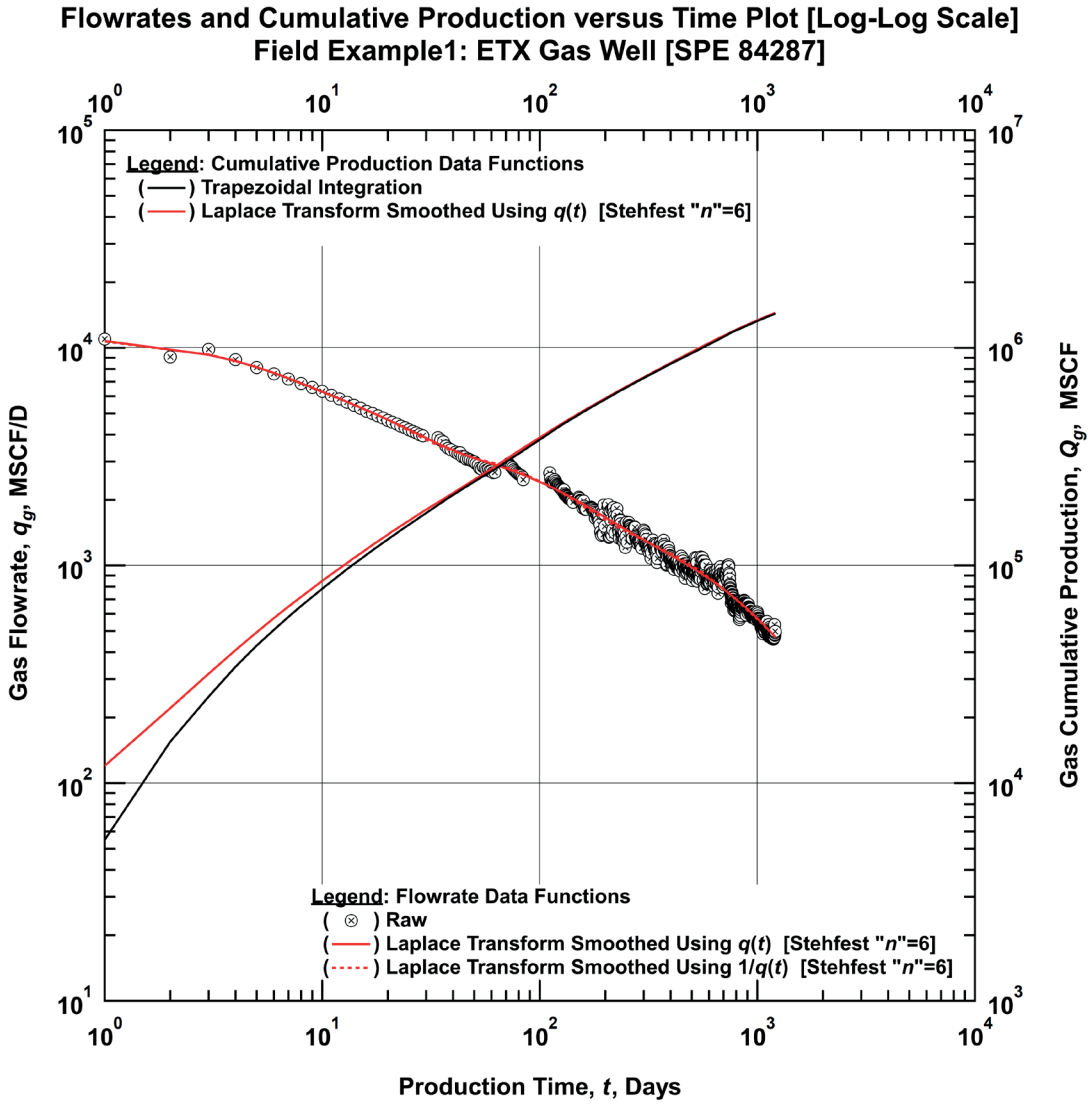

Figure E-1.1 — Comparison Plot of Raw and Laplace Transform Smoothed Flowrates and Cumulative Production Using a Selected Stehfest "*n*" Value Versus Time [Field Example 1: East Texas Gas Well (SPE 84287)] [Log-Log Plot]

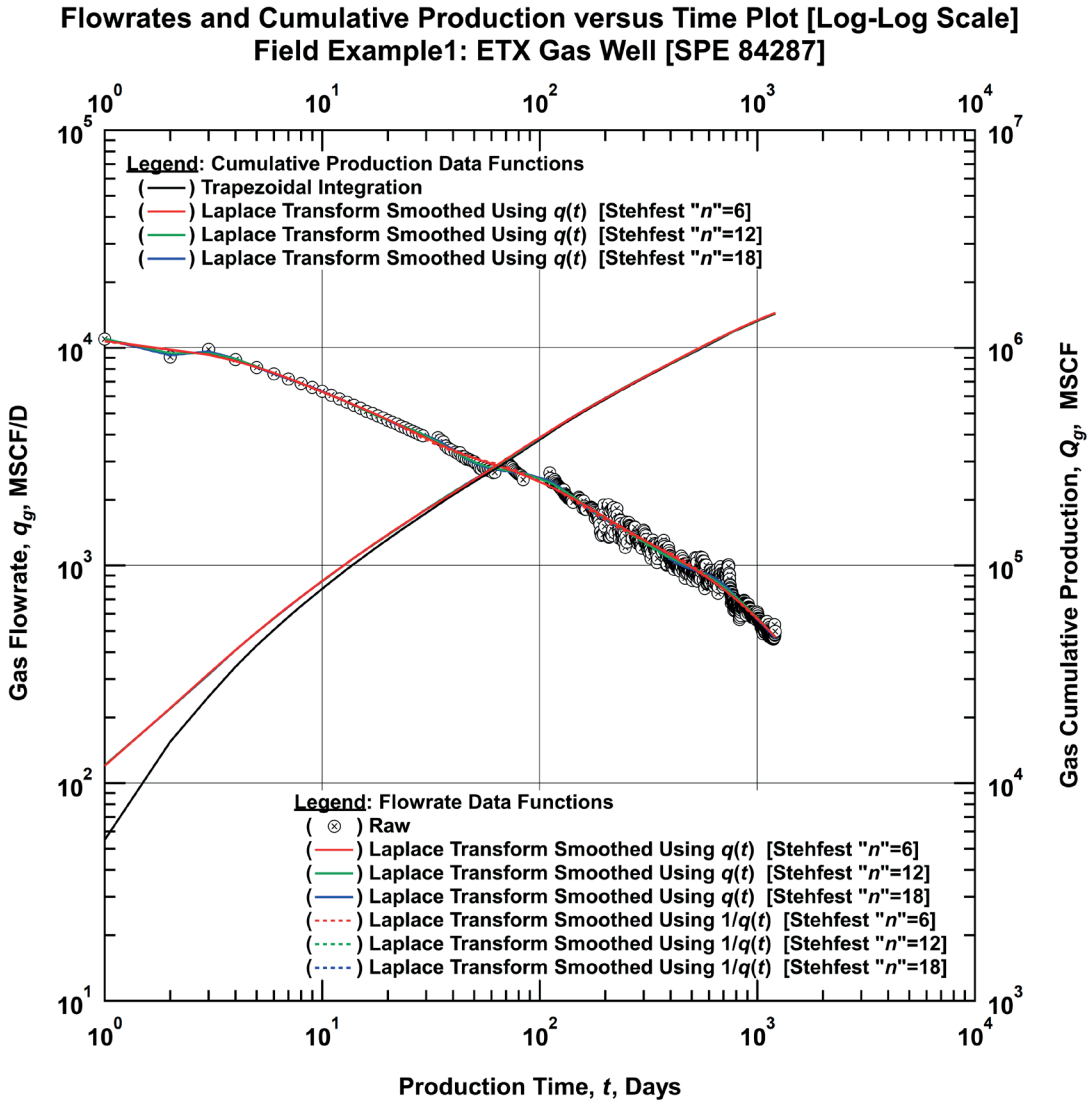

Figure E-1.2 — Comparison Plot of Raw and Laplace Transform Smoothed Flowrates and Cumulative Production Using Various Stehfest "*n*" Values Versus Time [Field Example 1: East Texas Gas Well (SPE 84287)] [Log-Log Plot]

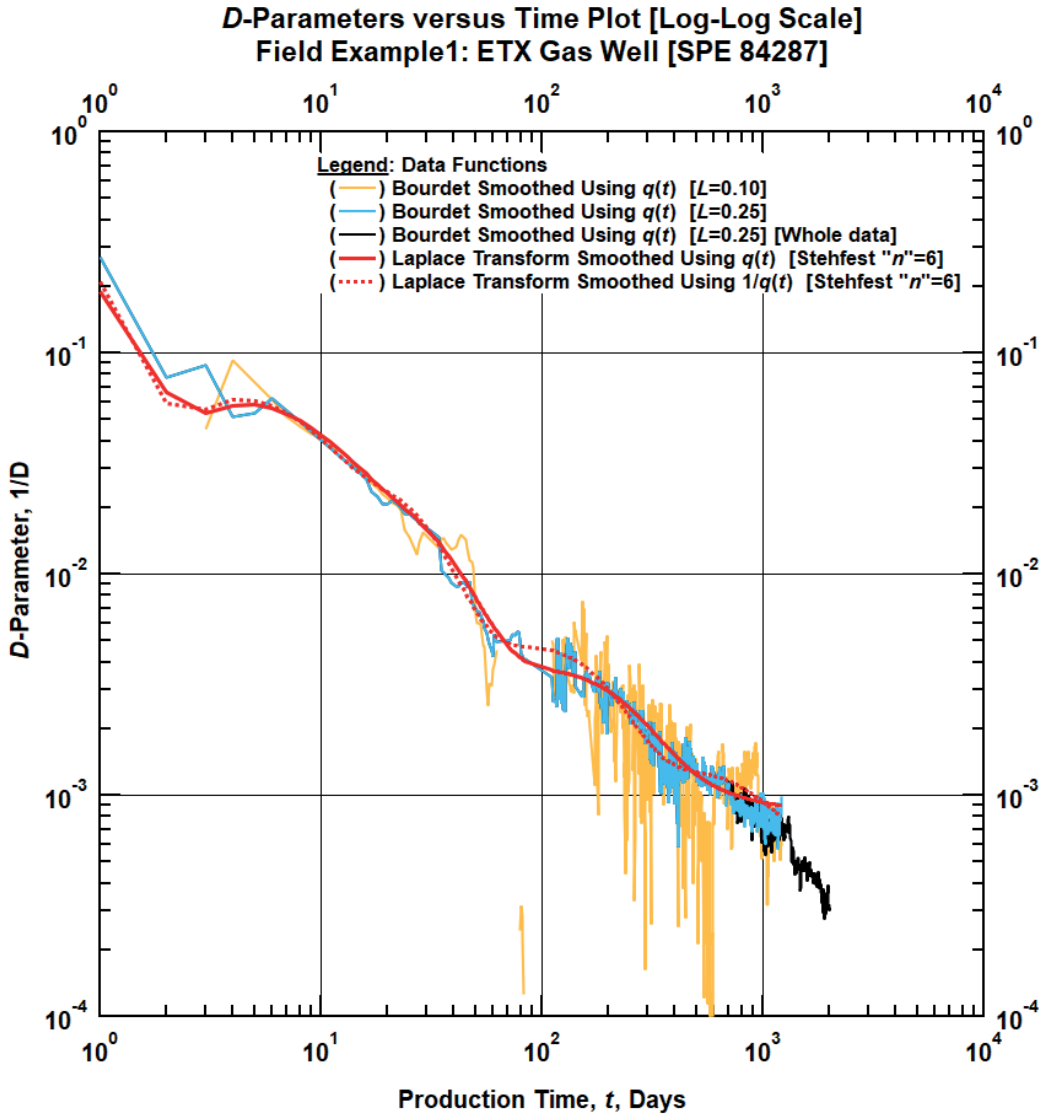

Figure E-1.3 — Comparison Plot of Bourdet Derived and Laplace Transform Smoothed *D*-Parameters Using a Selected Stehfest "*n*" Value Versus Time [Field Example 1: East Texas Gas Well (SPE 84287)] [Log-Log Plot]

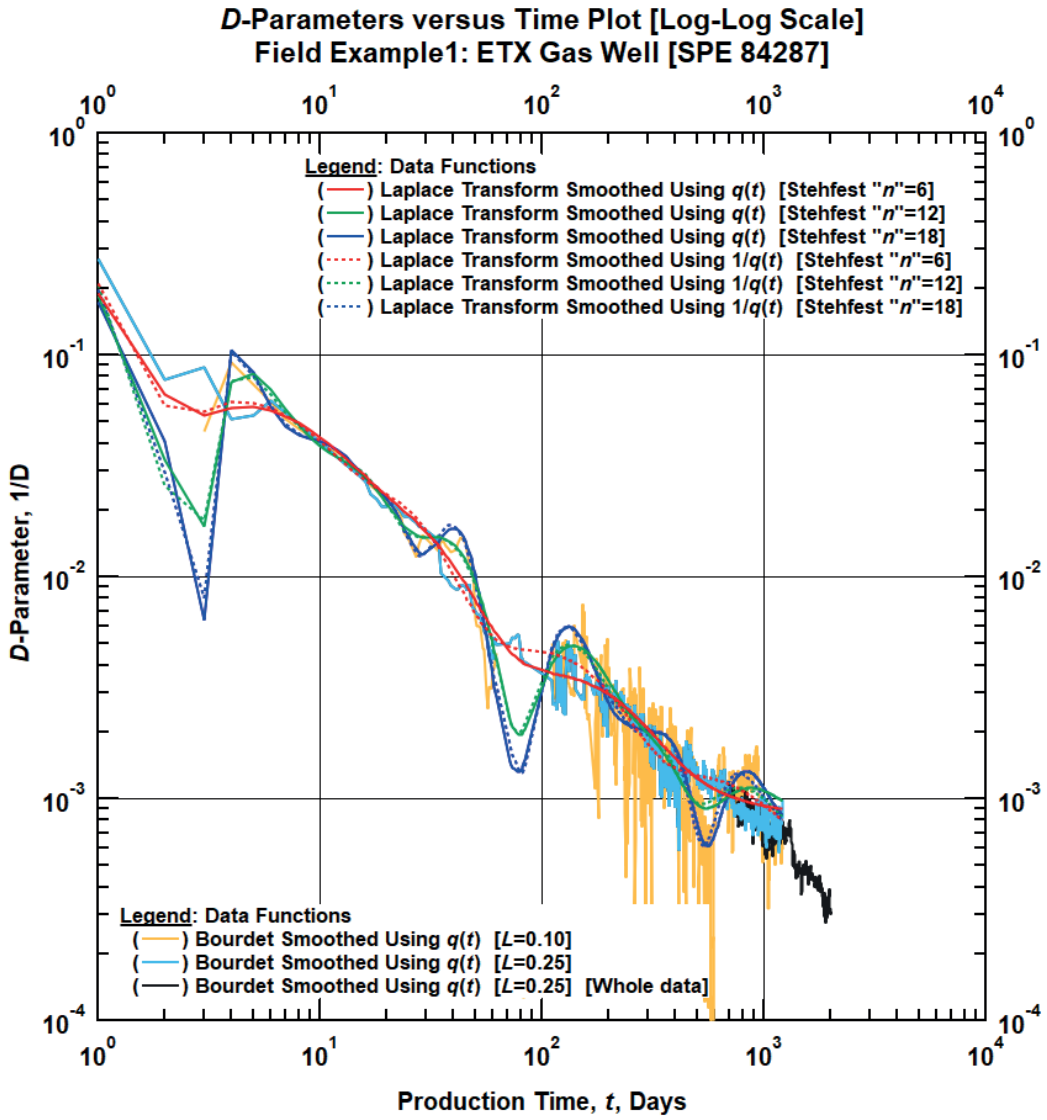

Figure E-1.4 — Comparison Plot of Bourdet Derived and Laplace Transform Smoothed *D*-Parameters Using Various Stehfest "*n*" Values Versus Time [Field Example 1: East Texas Gas Well (SPE 84287)] [Log-Log Plot]

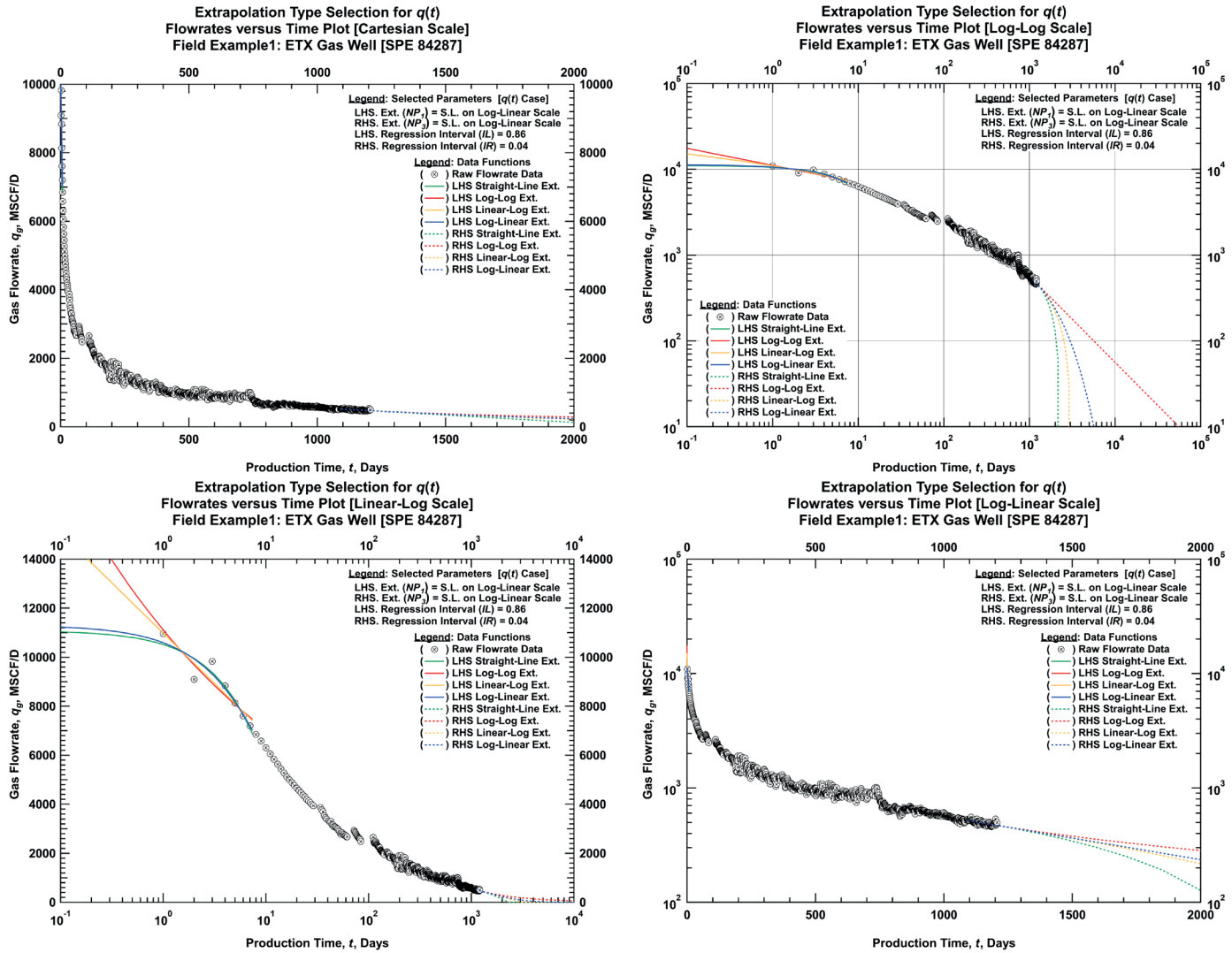

Figure E-1.5 — Plots for Extrapolation Type Selection of Flowrate Data [Field Example 1: East Texas Gas Well (SPE 84287)]

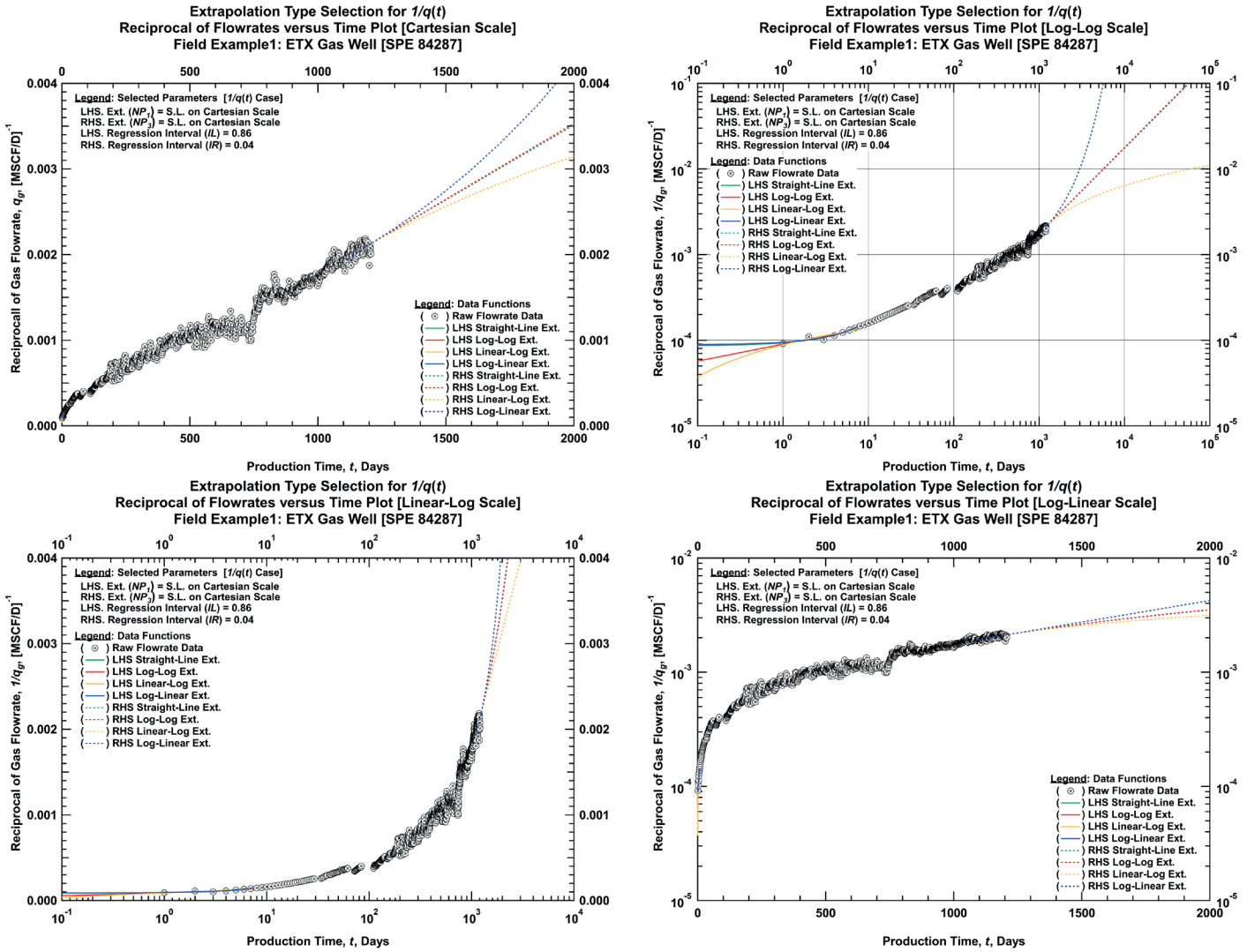

Figure E-1.6 — Plots for Extrapolation Type Selection of the Reciprocal of Flowrate Data [Field Example 1: East Texas Gas Well (SPE 84287)]

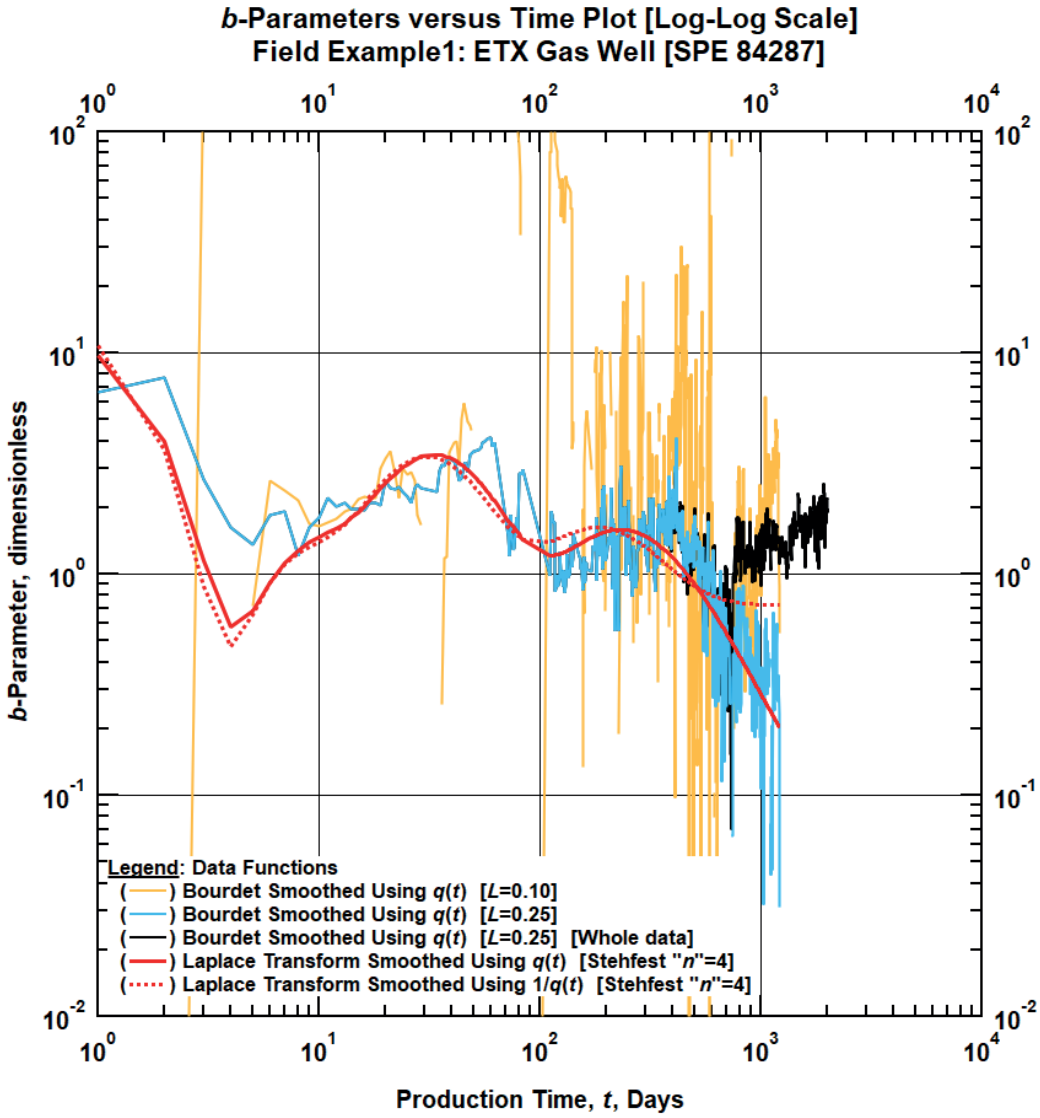

Figure E-1.7 — Comparison Plot of Bourdet Derived and Laplace Transform Smoothed *b*-Parameters Using a Selected Stehfest "*n*" Value Versus Time [Field Example 1: East Texas Gas Well (SPE 84287)] [Log-Log Plot]

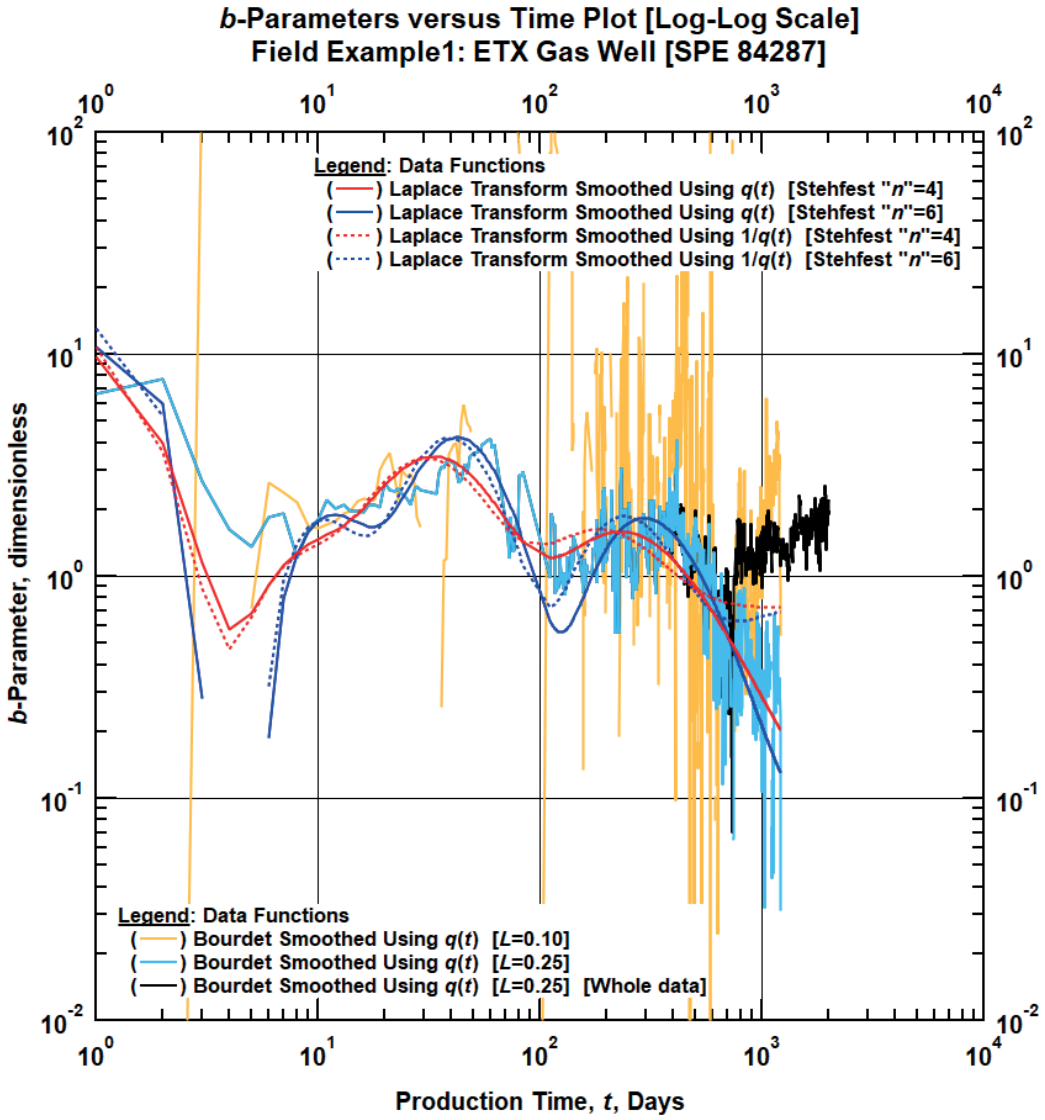

Figure E-1.8 — Comparison Plot of Bourdet Derived and Laplace Transform Smoothed *b*-Parameters Using Various Stehfest "*n*" Values Versus Time [Field Example 1: East Texas Gas Well (SPE 84287)] [Log-Log Plot]

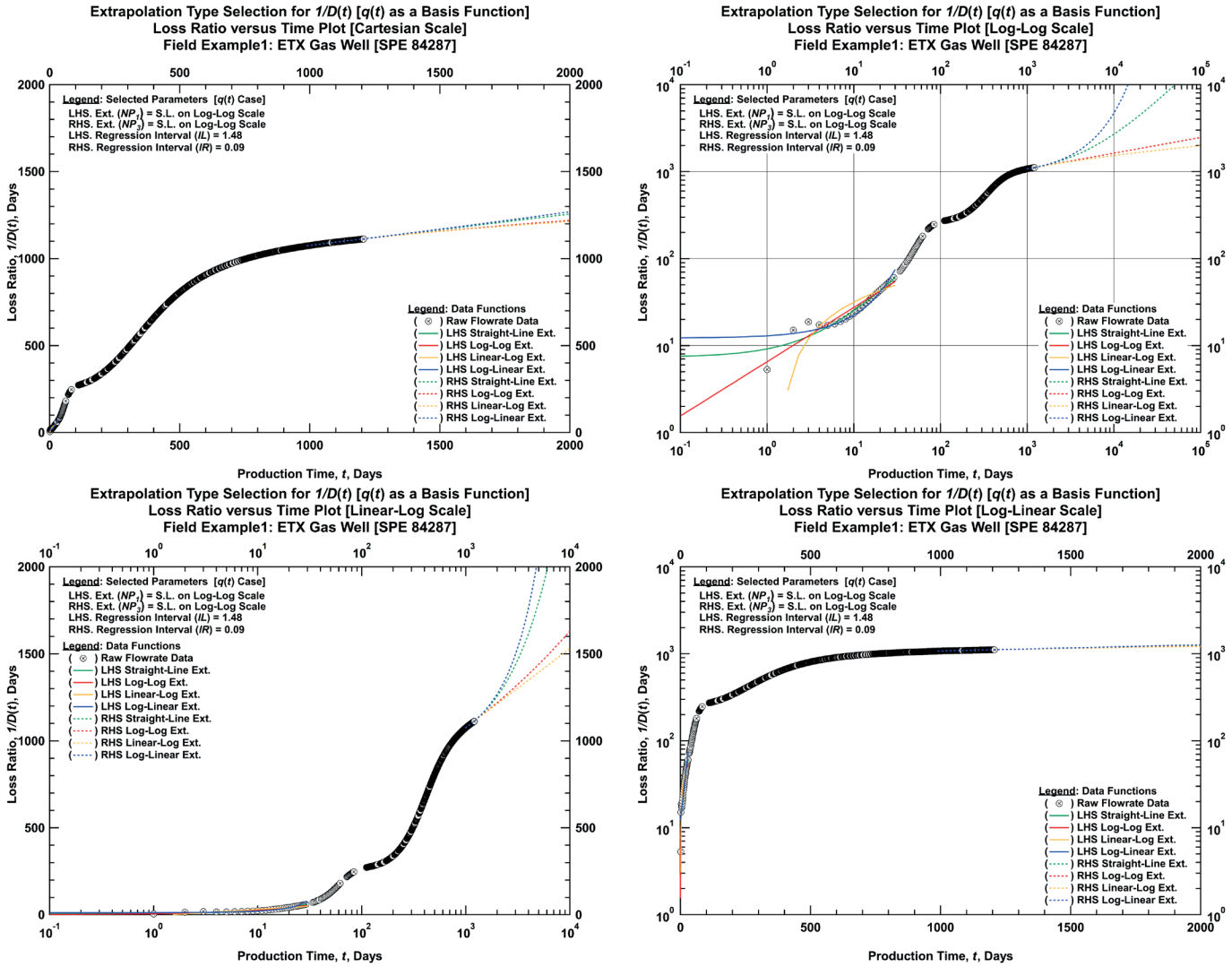

Figure E-1.9 — Plots for Extrapolation Type Selection of Loss-Ratio Data Function Computed Using Flowrate Data as the Basis Function [Field Example 1: East Texas Gas Well (SPE 84287)]

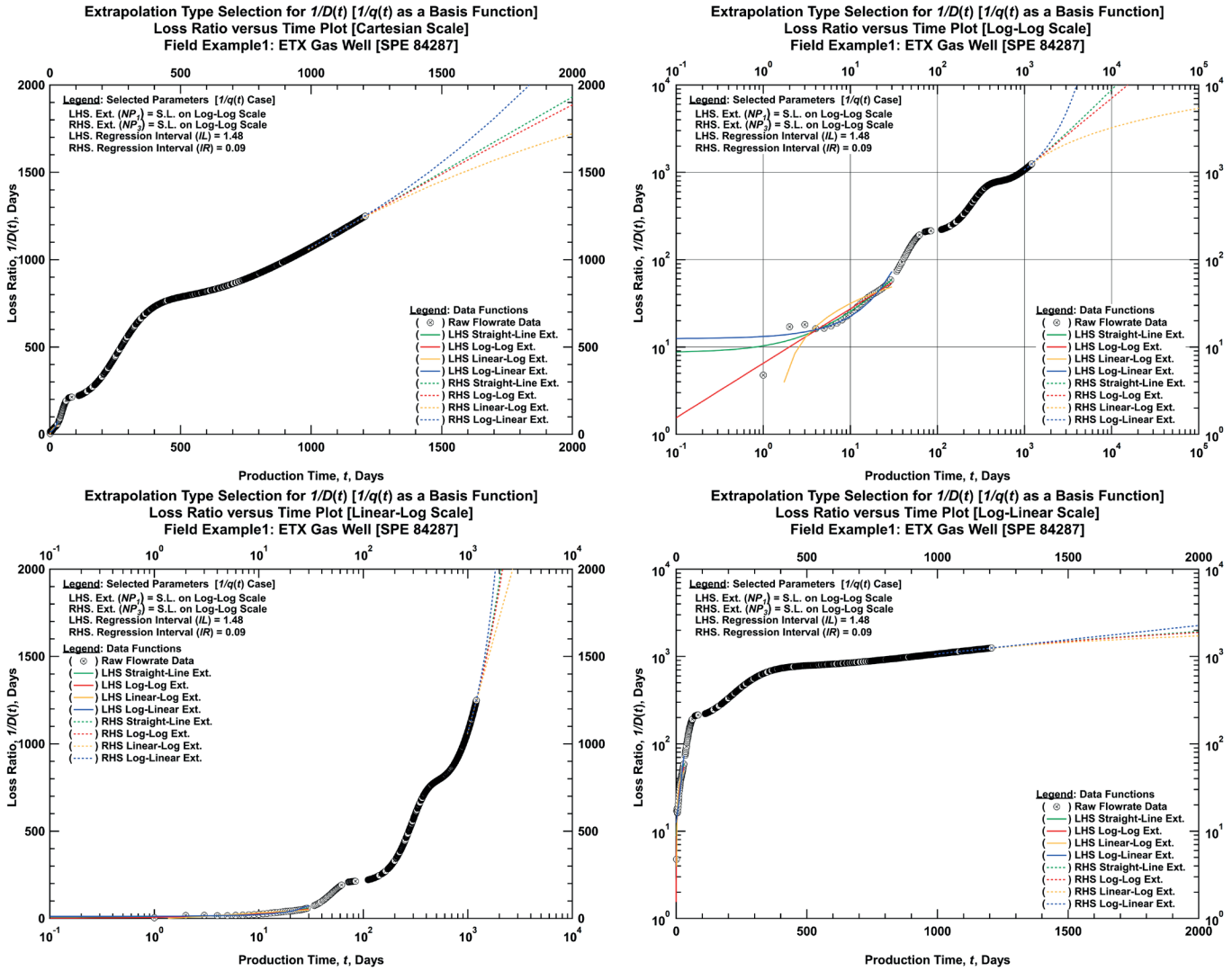

Figure E-1.10 — Plots for Extrapolation Type Selection of Loss-Ratio Data Function Computed Using the Reciprocal of Flowrate Data as the Basis Function [Field Example 1: East Texas Gas Well (SPE 84287)]

E.2 Field Example 2: Fractured Gas Well (SPE 132352)

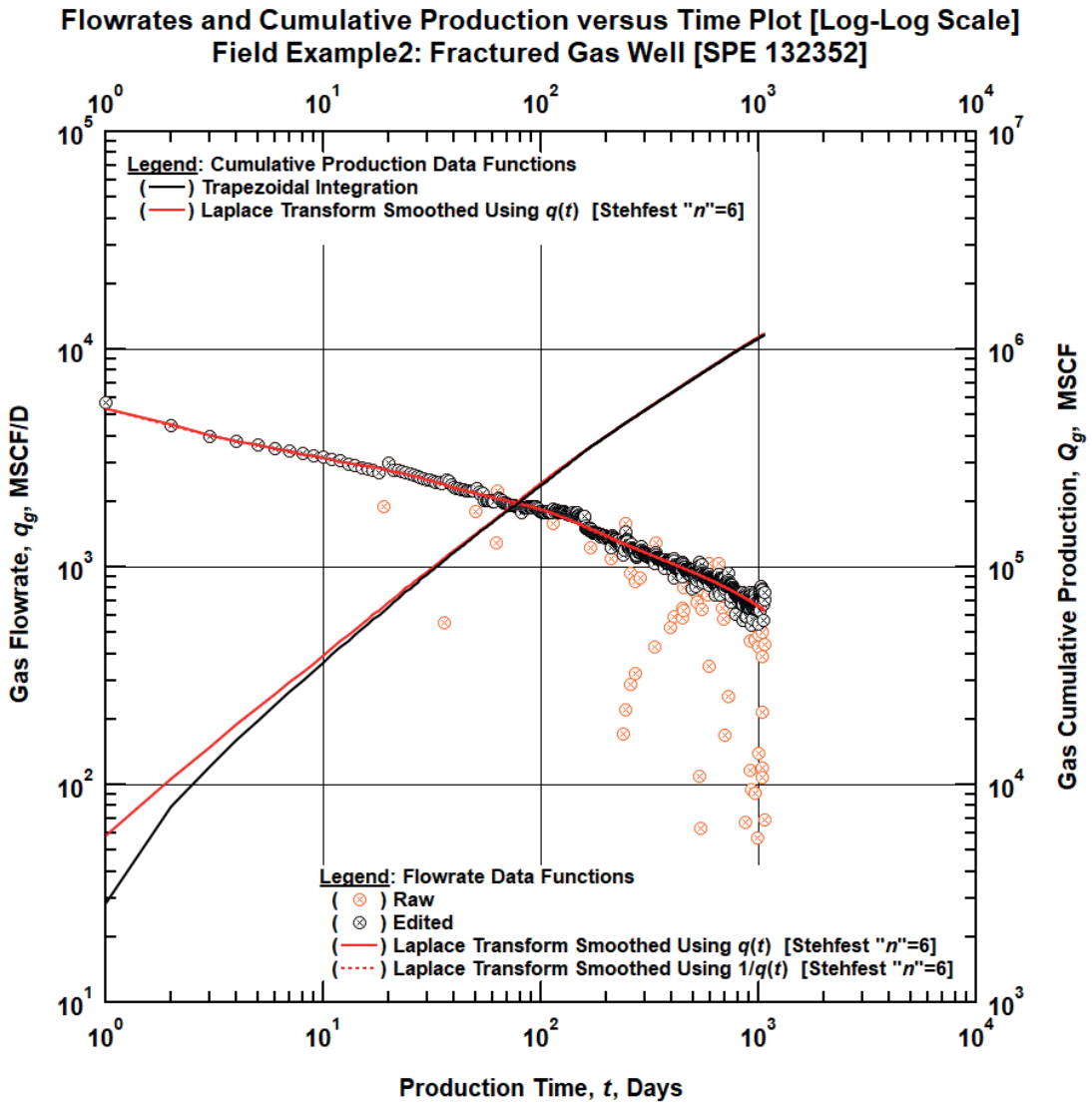

Figure E-2.1 — Comparison Plot of Raw and Laplace Transform Smoothed Flowrates and Cumulative Production Using a Selected Stehfest "*n*" Value Versus Time [Field Example 2: Fractured Gas Well (SPE 132352)] [Log-Log Plot]

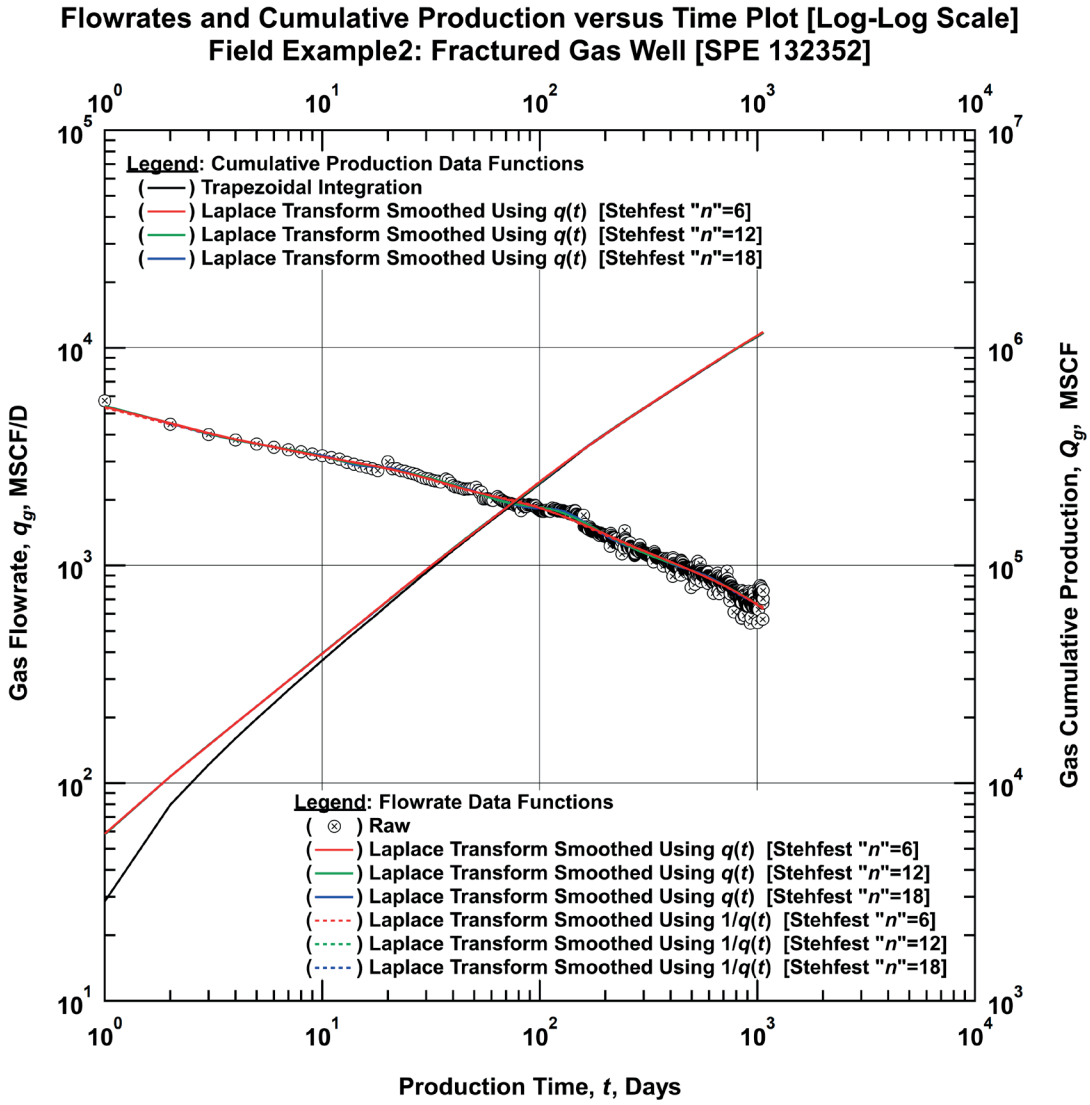

Figure E-2.2 — Comparison Plot of Raw and Laplace Transform Smoothed Flowrates and Cumulative Production Using Various Stehfest "*n*" Values Versus Time [Field Example 2: Fractured Gas Well (SPE 132352)] [Log-Log Plot]

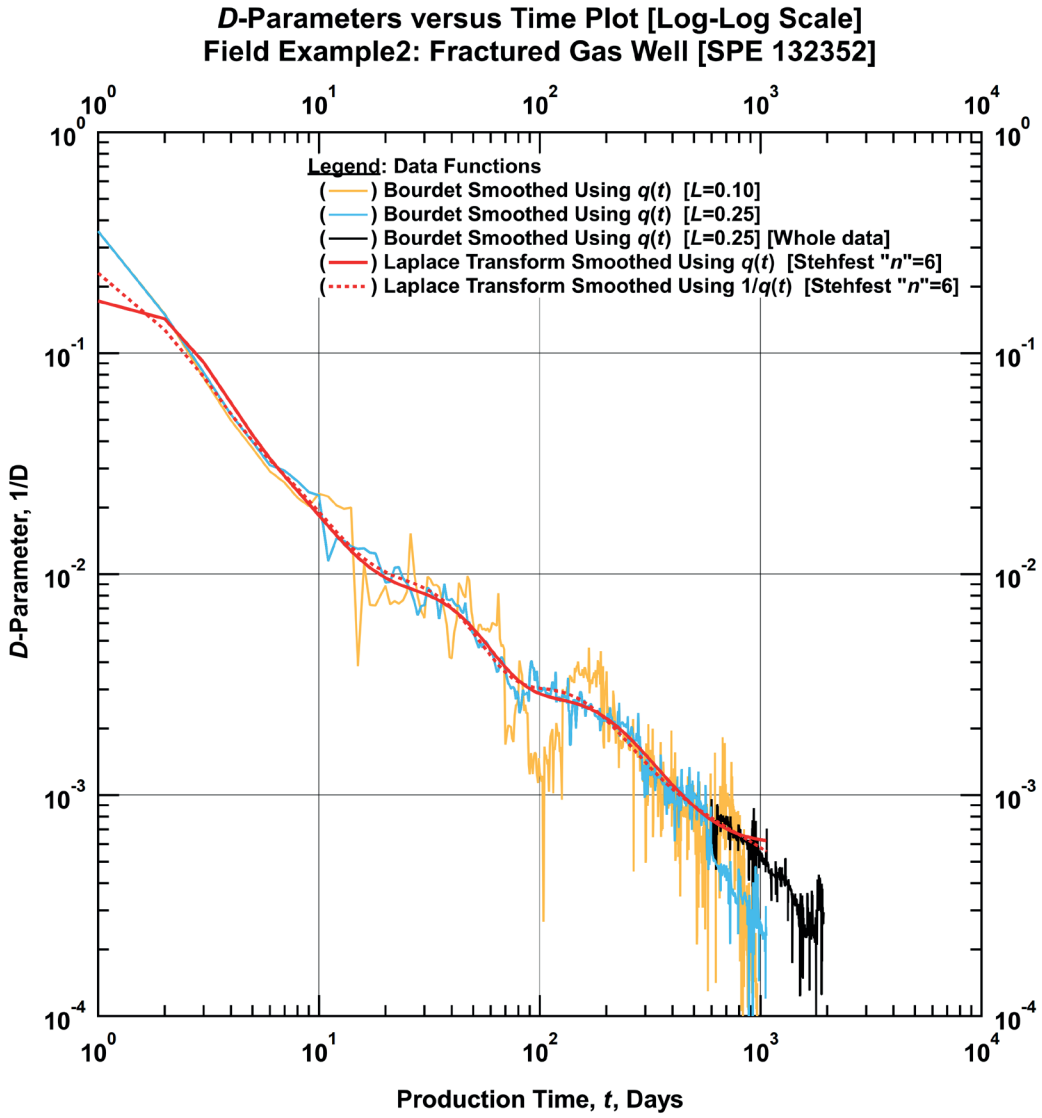

Figure E-2.3 — Comparison Plot of Bourdet Derived and Laplace Transform Smoothed *D*-Parameters Using a Selected Stehfest "*n*" Value Versus Time [Field Example 2: Fractured Gas Well (SPE 132352)] [Log-Log Plot]

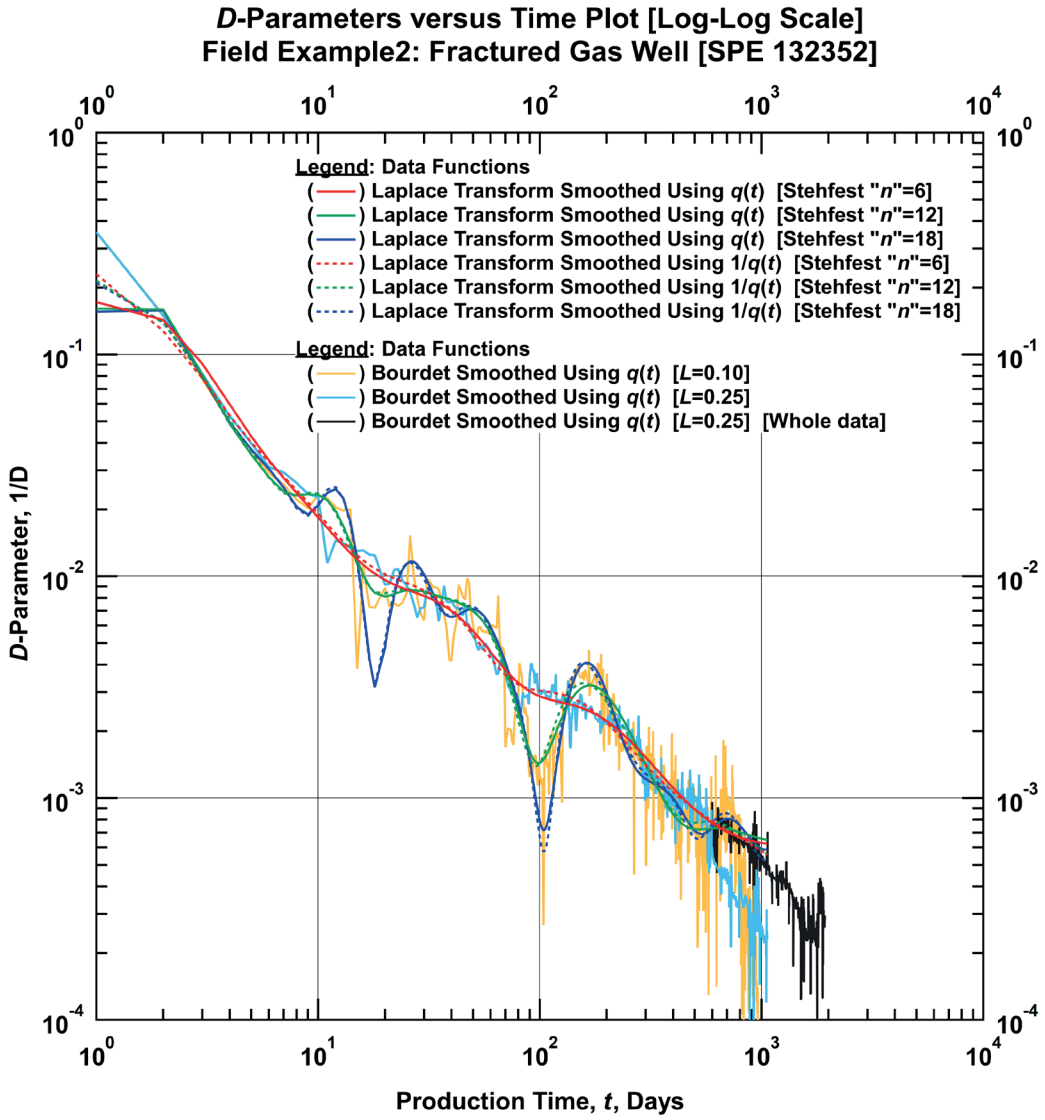

Figure E-2.4 — Comparison Plot of Bourdet Derived and Laplace Transform Smoothed *D*-Parameters Using Various Stehfest "*n*" Values Versus Time [Field Example 2: Fractured Gas Well (SPE 132352)] [Log-Log Plot]

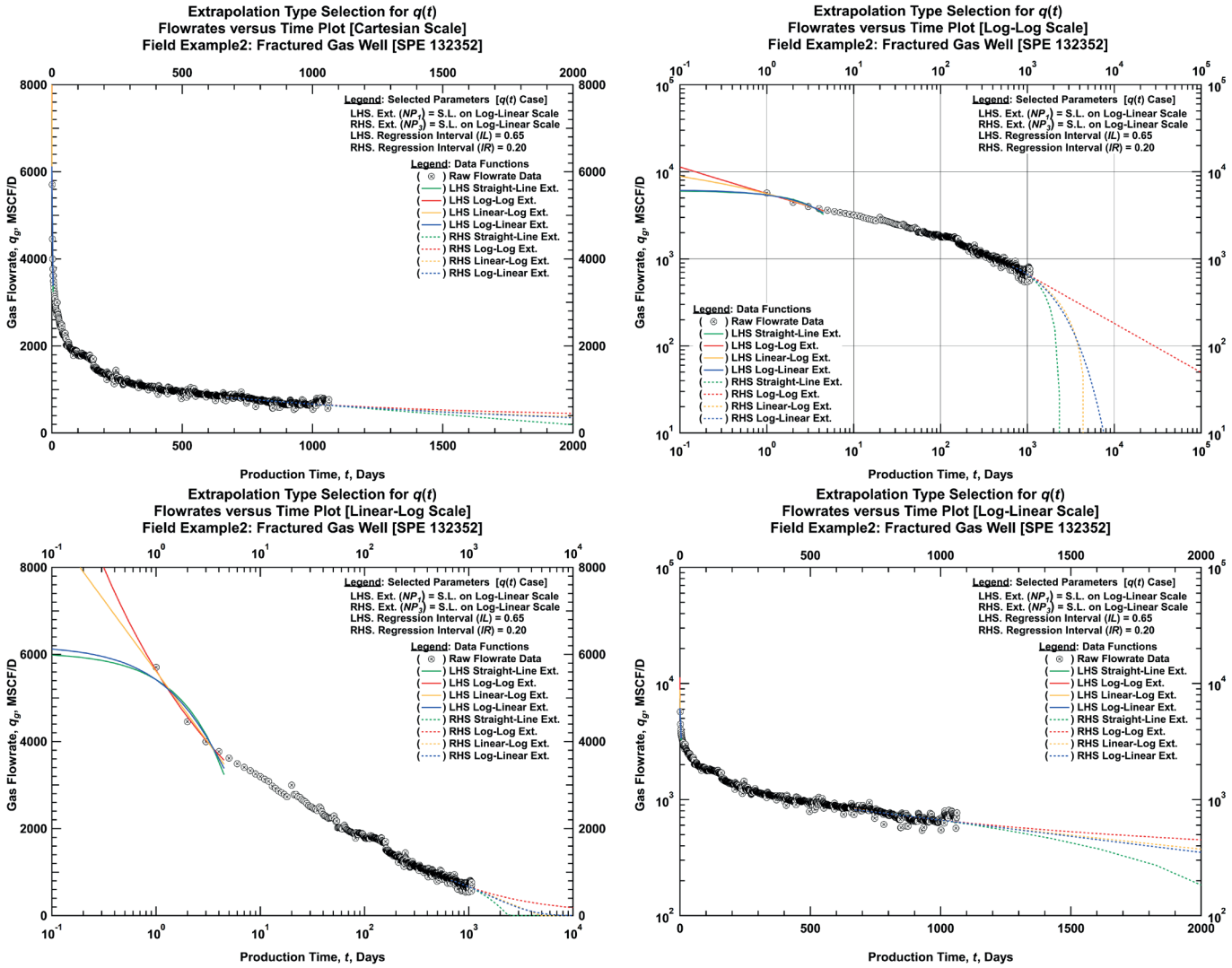

Figure E-2.5 — Plots for Extrapolation Type Selection of Flowrate Data [Field Example 2: Fractured Gas Well (SPE 132352)]

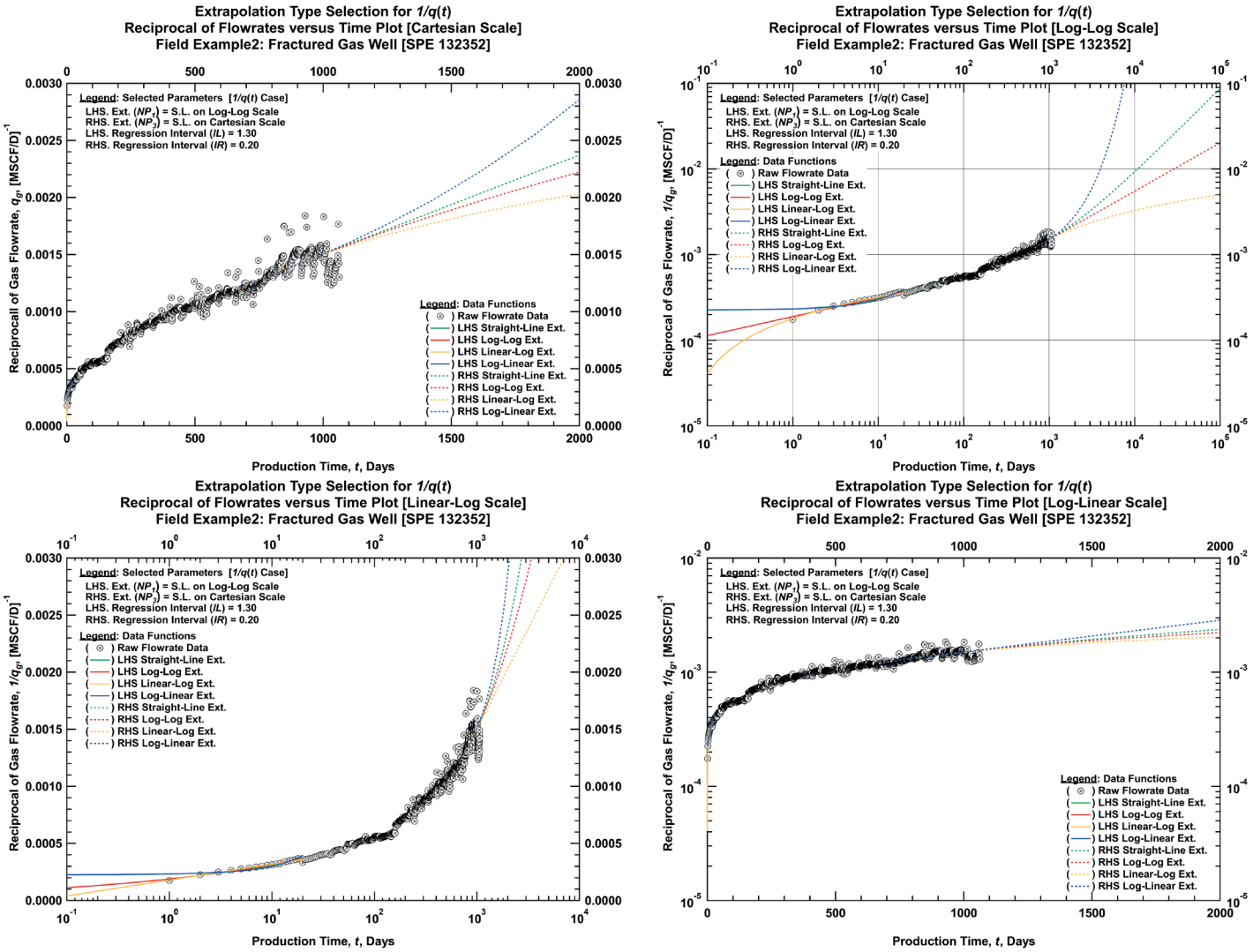

Figure E-2.6 — Plots for Extrapolation Type Selection of the Reciprocal of Flowrate Data [Field Example 2: Fractured Gas Well (SPE 132352)]

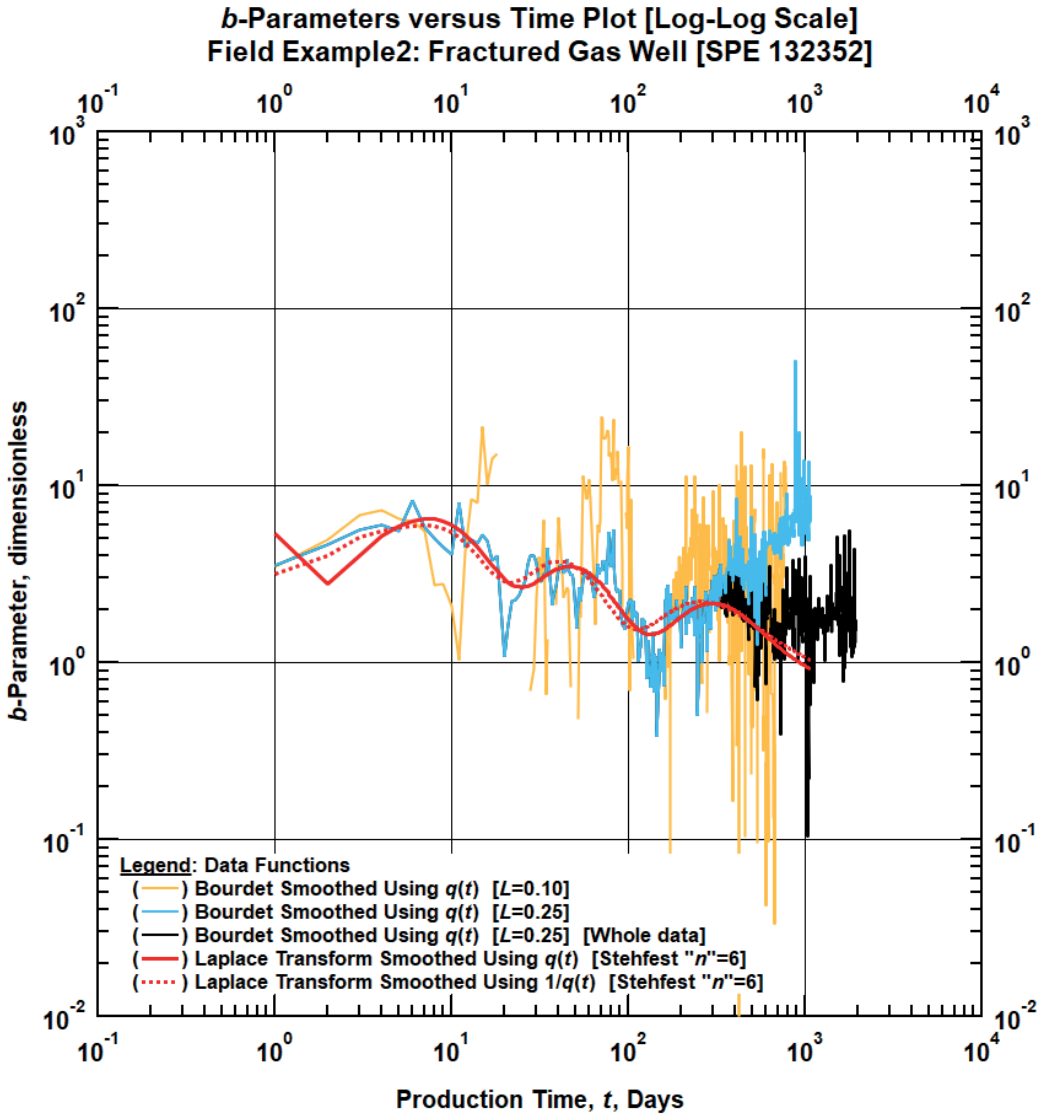

Figure E-2.7 — Comparison Plot of Bourdet Derived and Laplace Transform Smoothed *b*-Parameters Using a Selected Stehfest "*n*" Value Versus Time [Field Example 2: Fractured Gas Well (SPE 132352)] [Log-Log Plot]

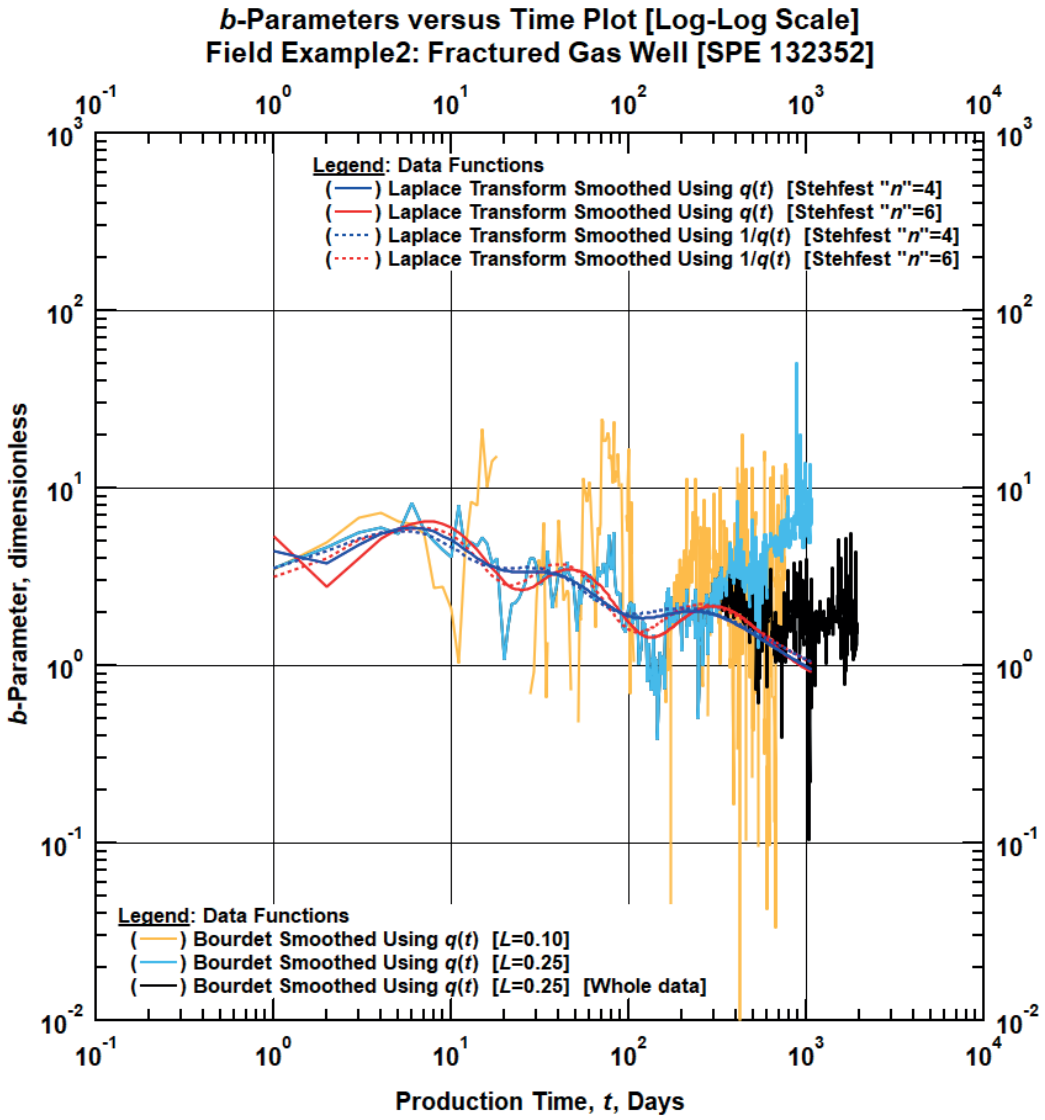

Figure E-2.8 — Comparison Plot of Bourdet Derived and Laplace Transform Smoothed *b*-Parameters Using Various Stehfest "*n*" Values Versus Time [Field Example 2: Fractured Gas Well (SPE 132352)] [Log-Log Plot]

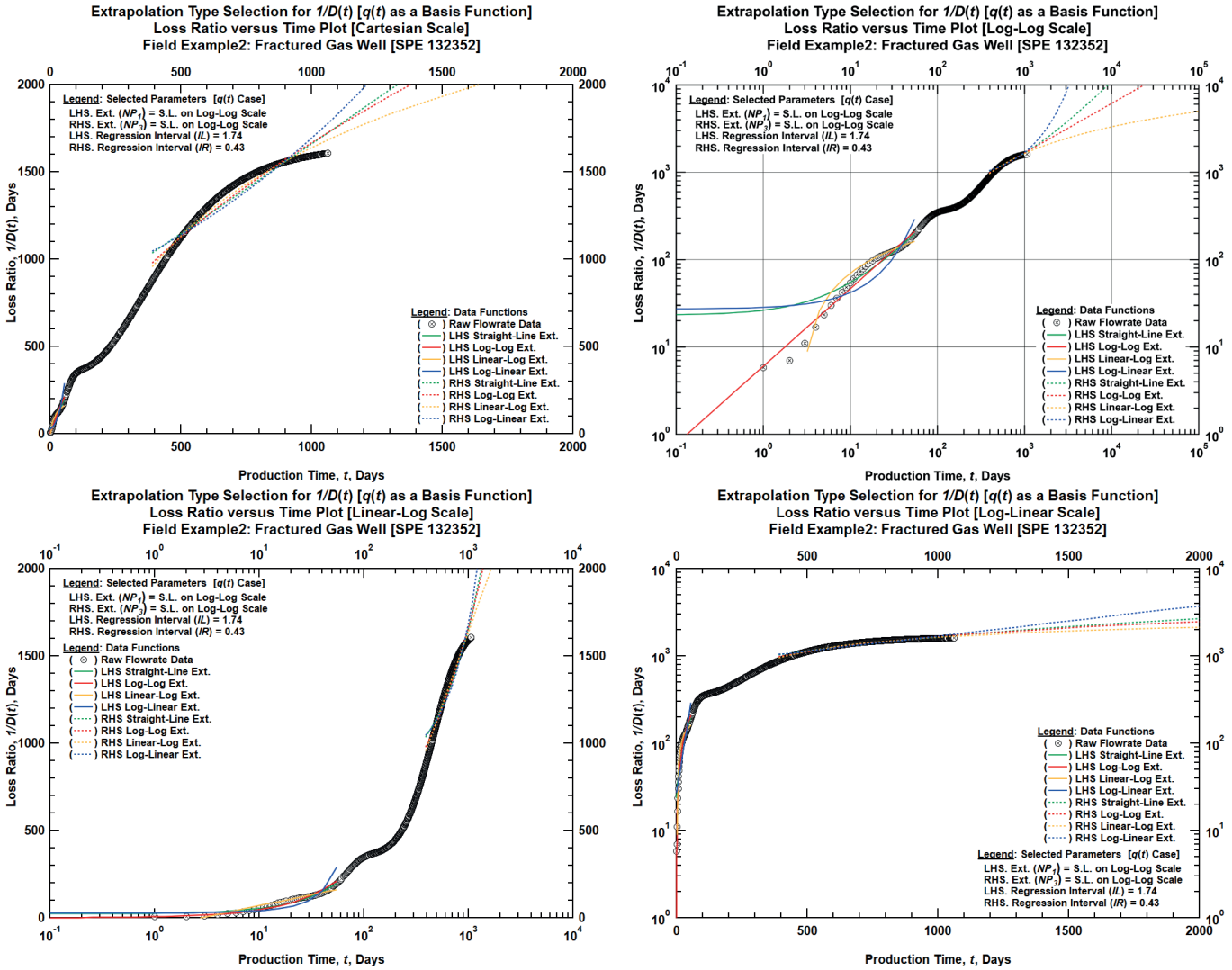

Figure E-2.9 — Plots for Extrapolation Type Selection of Loss-Ratio Data Function Computed Using Flowrate Data as the Basis Function [Field Example 2: Fractured Gas Well (SPE 132352)]

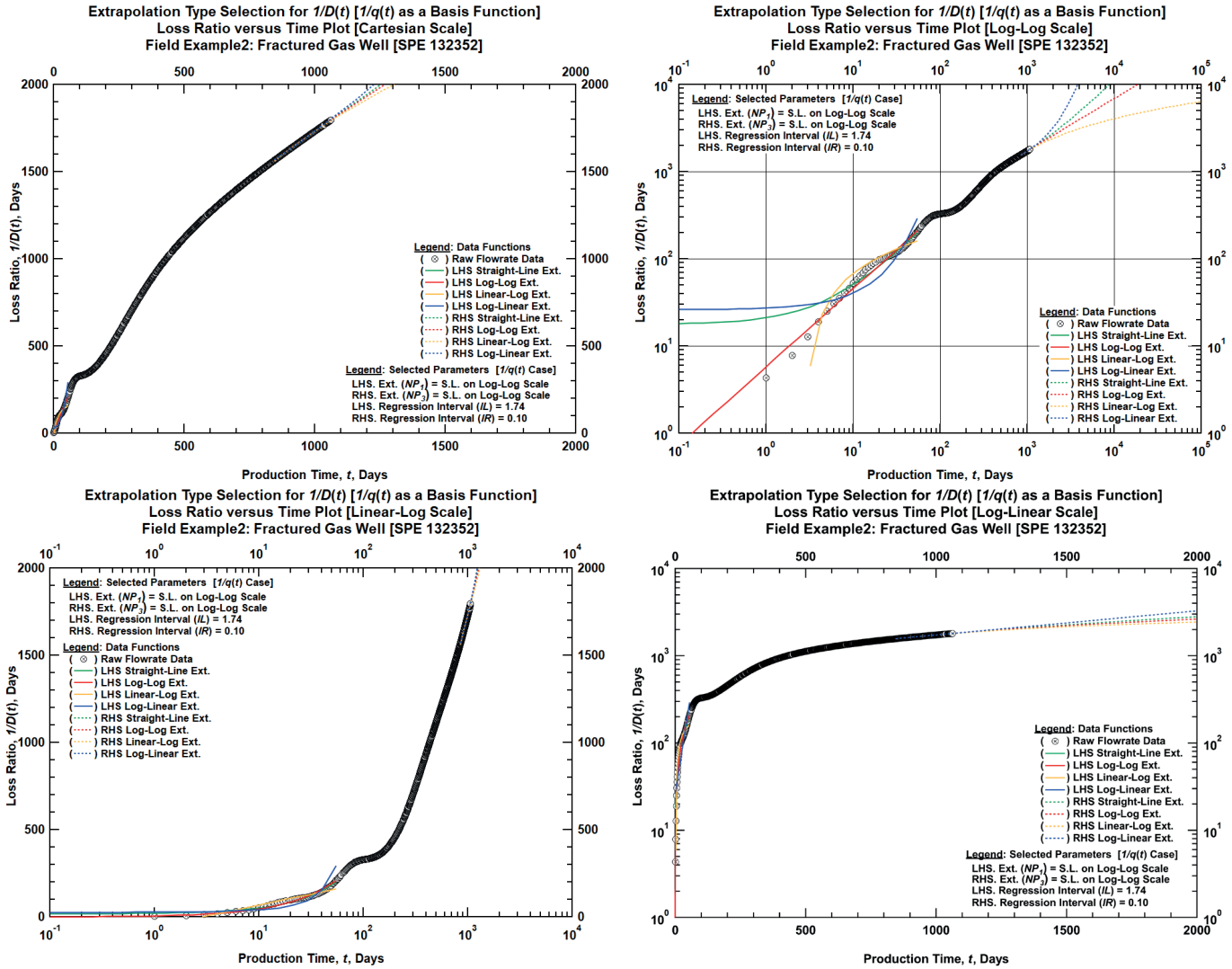

Figure E-2.10 — Plots for Extrapolation Type Selection of Loss-Ratio Data Function Computed Using the Reciprocal of Flowrate Data as the Basis Function [Field Example 2: Fractured Gas Well (SPE 132352)]

E.3 Field Example 3: Fractured Gas Well (SPE 132352)

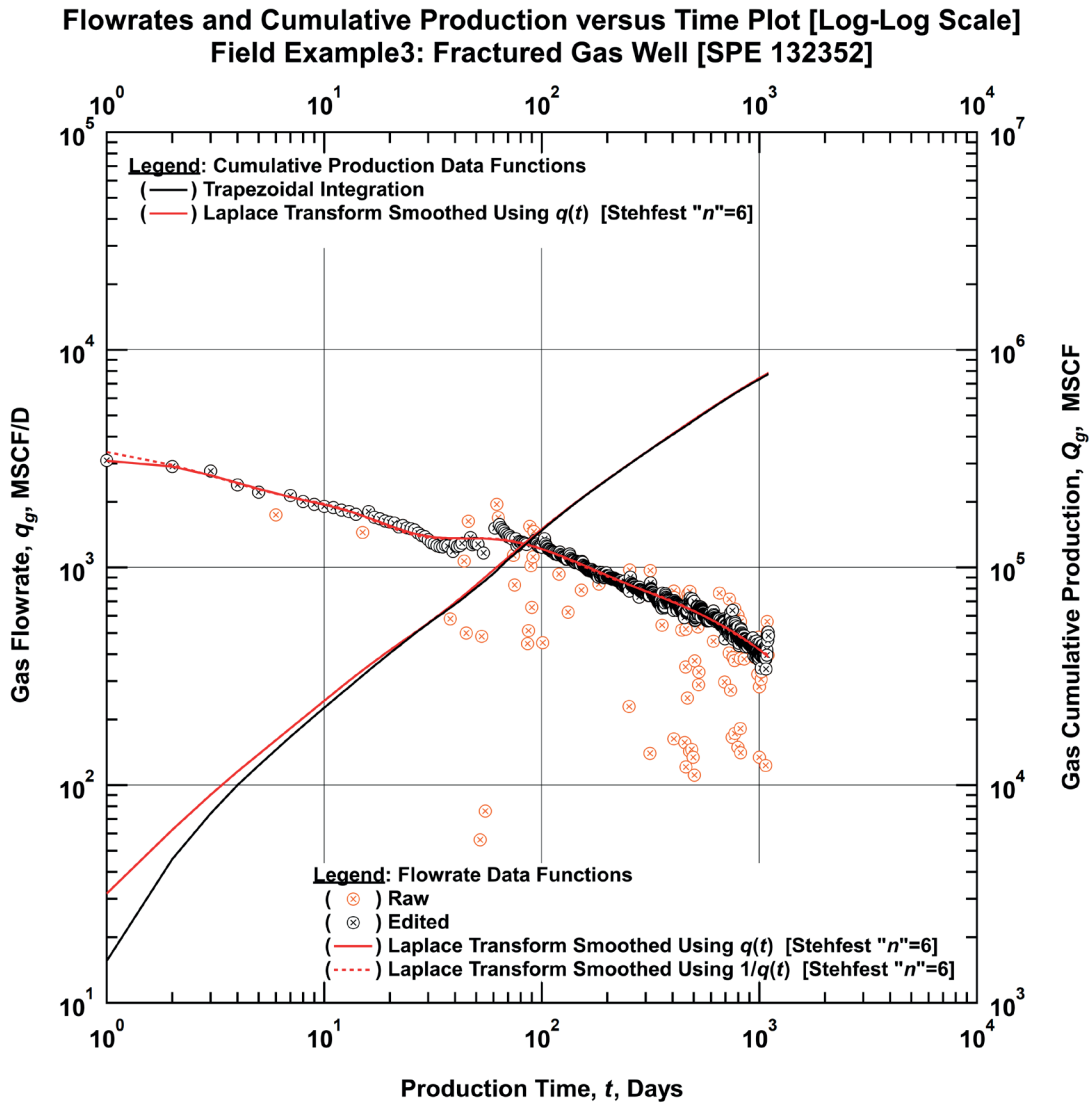

Figure E-3.1 — Comparison Plot of Raw and Laplace Transform Smoothed Flowrates and Cumulative Production Using a Selected Stehfest "*n*" Value Versus Time [Field Example 3: Fractured Gas Well (SPE 132352)] [Log-Log Plot]

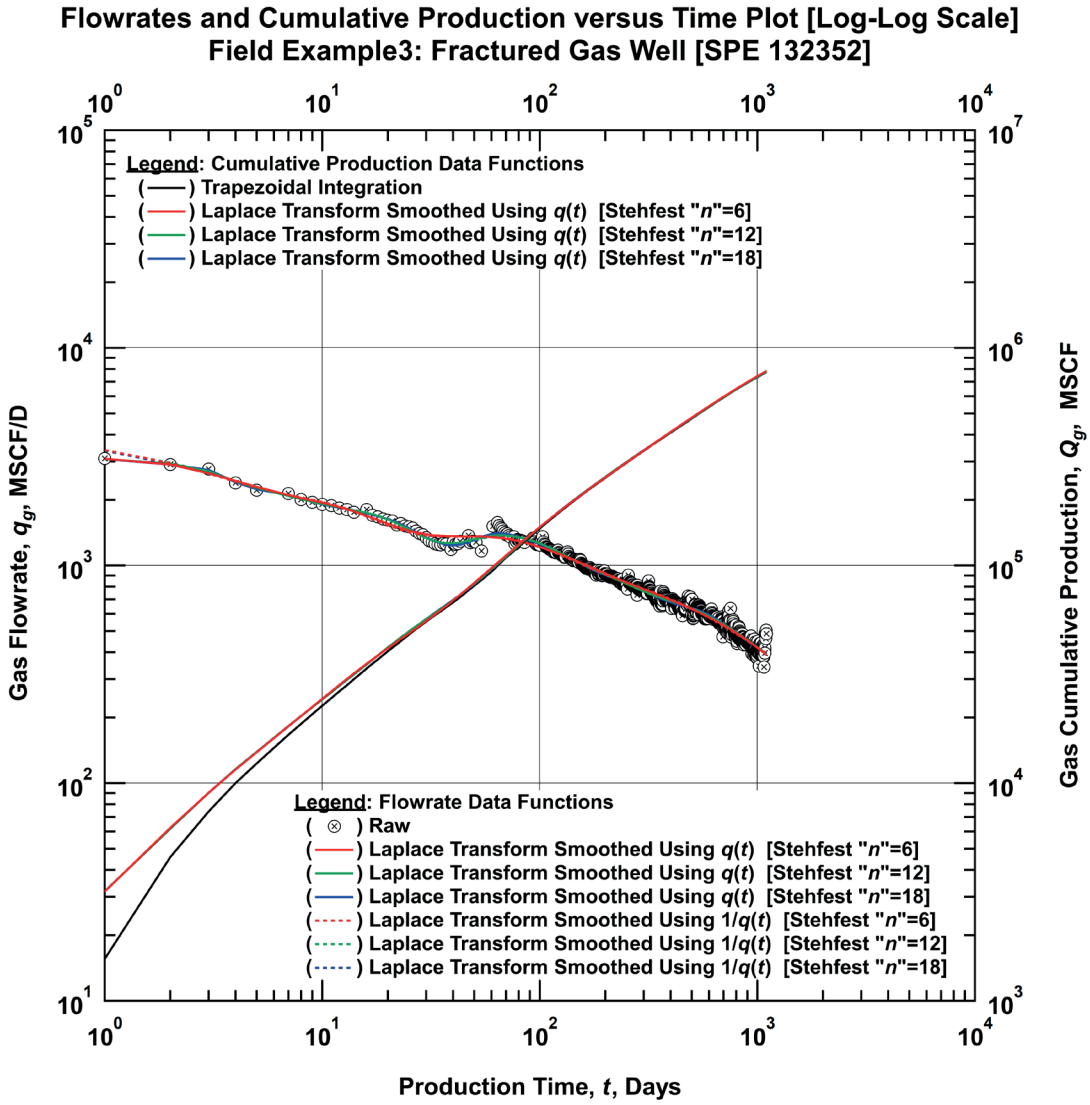

Figure E-3.2 — Comparison Plot of Raw and Laplace Transform Smoothed Flowrates and Cumulative Production Using Various Stehfest "*n*" Values Versus Time [Field Example 3: Fractured Gas Well (SPE 132352)] [Log-Log Plot]

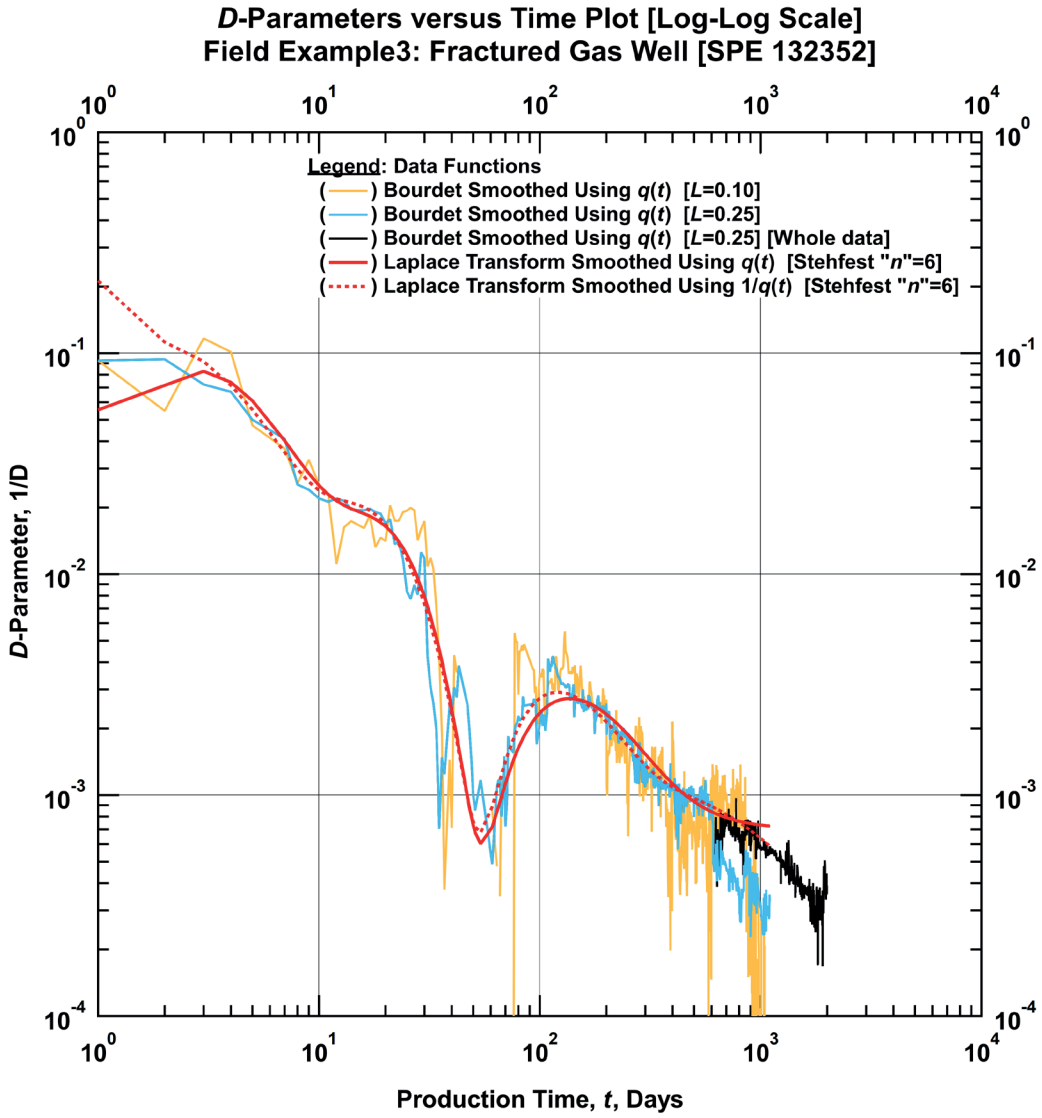

Figure E-3.3 — Comparison Plot of Bourdet Derived and Laplace Transform Smoothed *D*-Parameters Using a Selected Stehfest "*n*" Value Versus Time [Field Example 3: Fractured Gas Well (SPE 132352)] [Log-Log Plot]

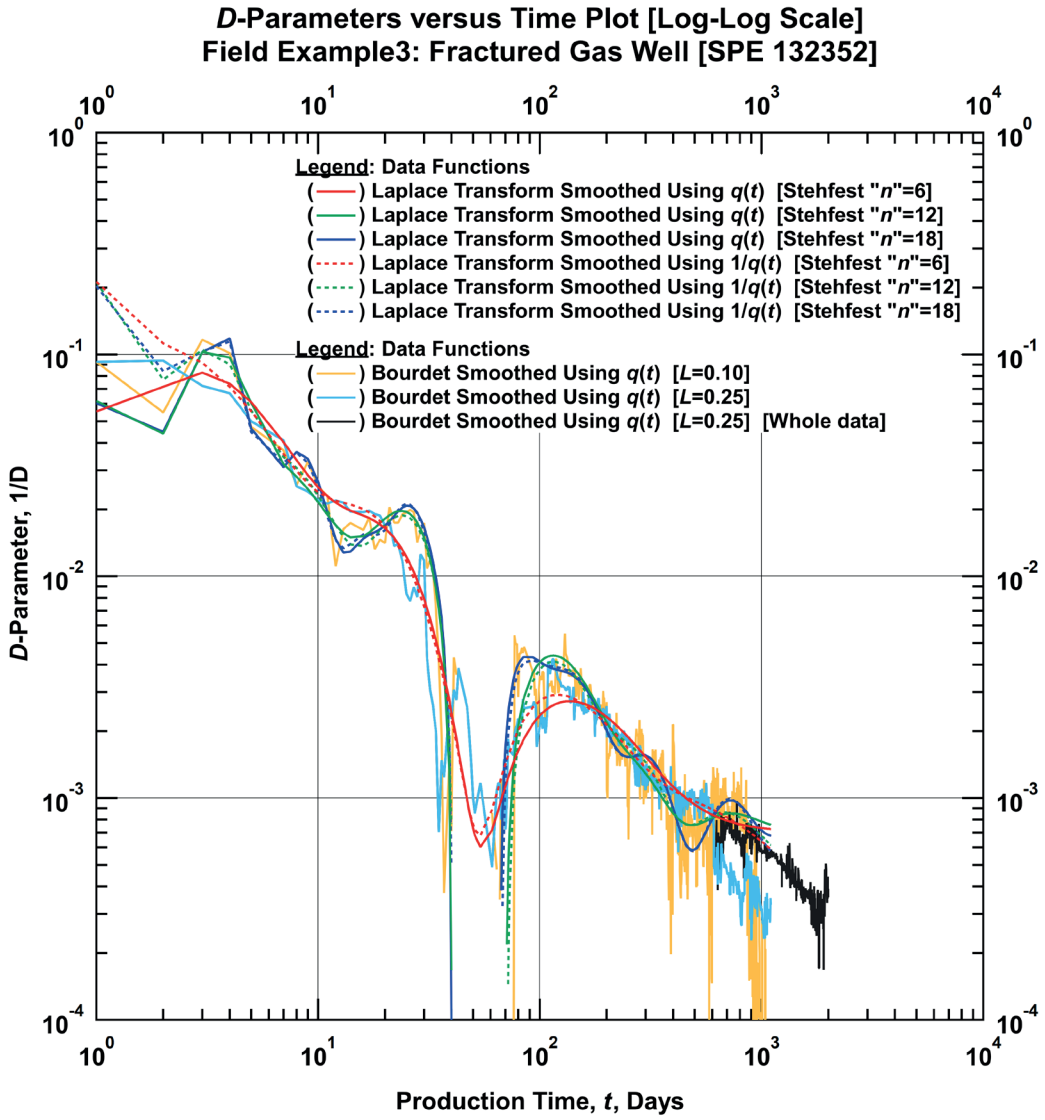

Figure E-3.4 — Comparison Plot of Bourdet Derived and Laplace Transform Smoothed *D*-Parameters Using Various Stehfest "*n*" Values Versus Time [Field Example 3: Fractured Gas Well (SPE 132352)] [Log-Log Plot]

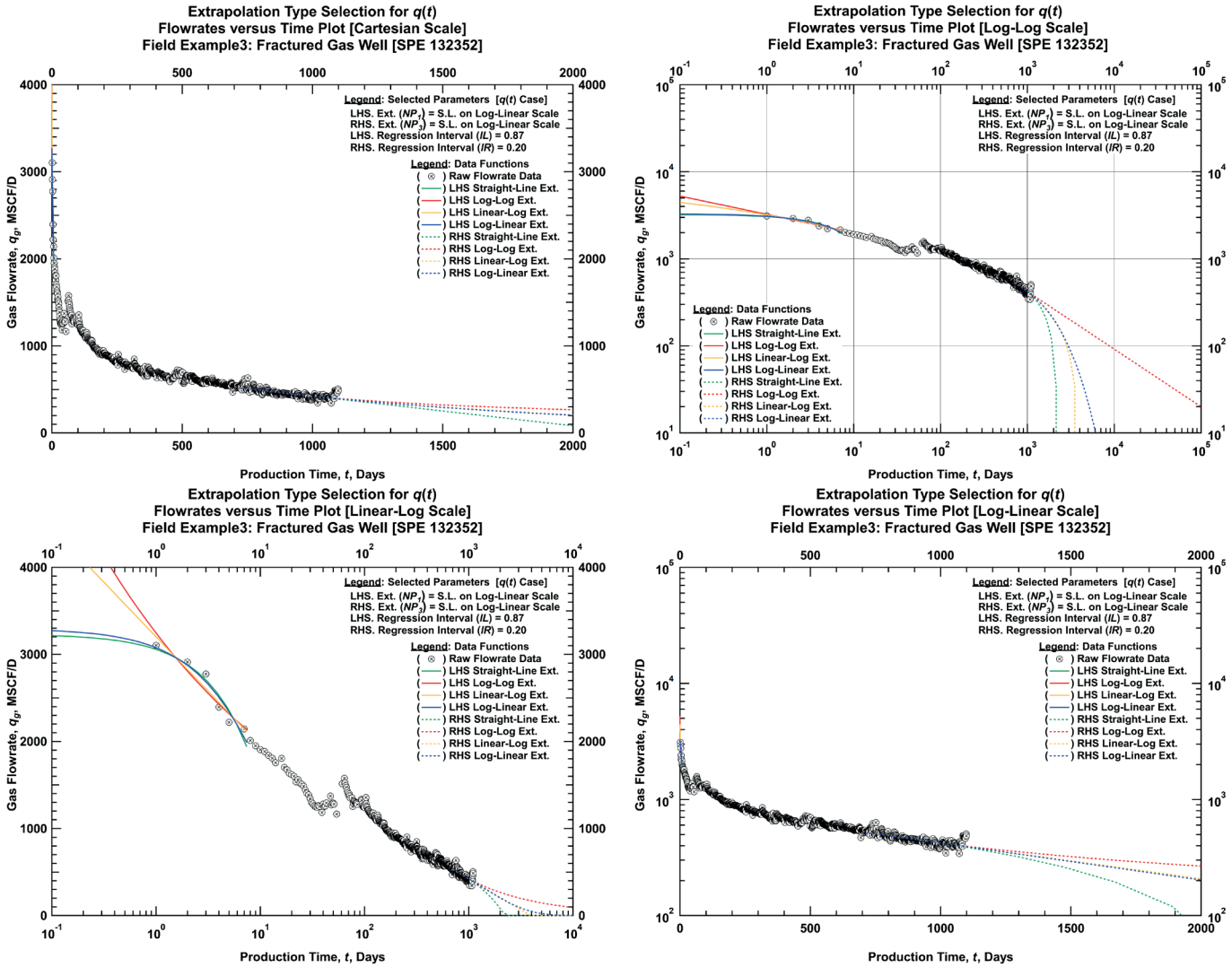

Figure E-3.5 — Plots for Extrapolation Type Selection of Flowrate Data [Field Example 3: Fractured Gas Well (SPE 132352)]

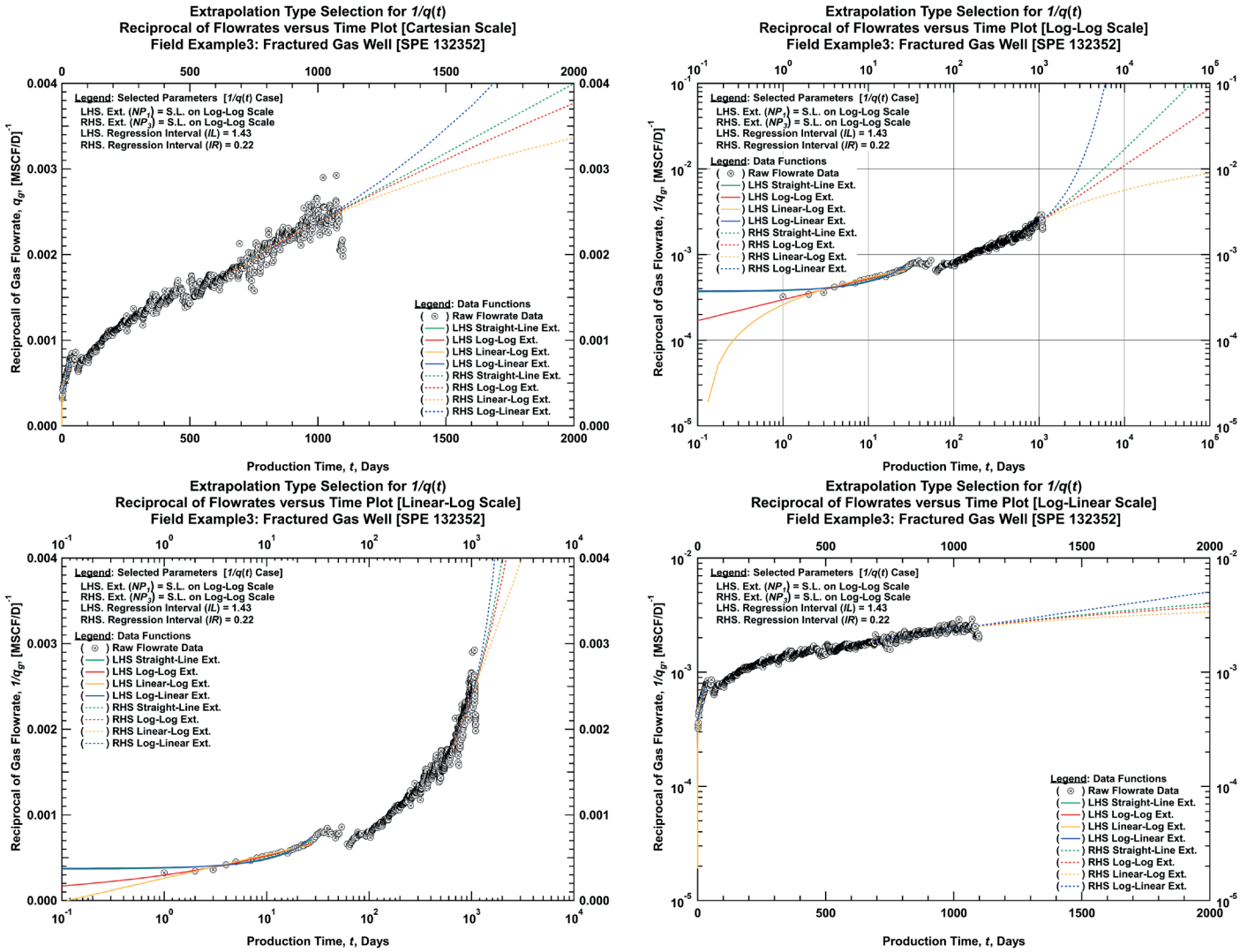

Figure E-3.6 — Plots for Extrapolation Type Selection of the Reciprocal of Flowrate Data [Field Example 3: Fractured Gas Well (SPE 132352)]

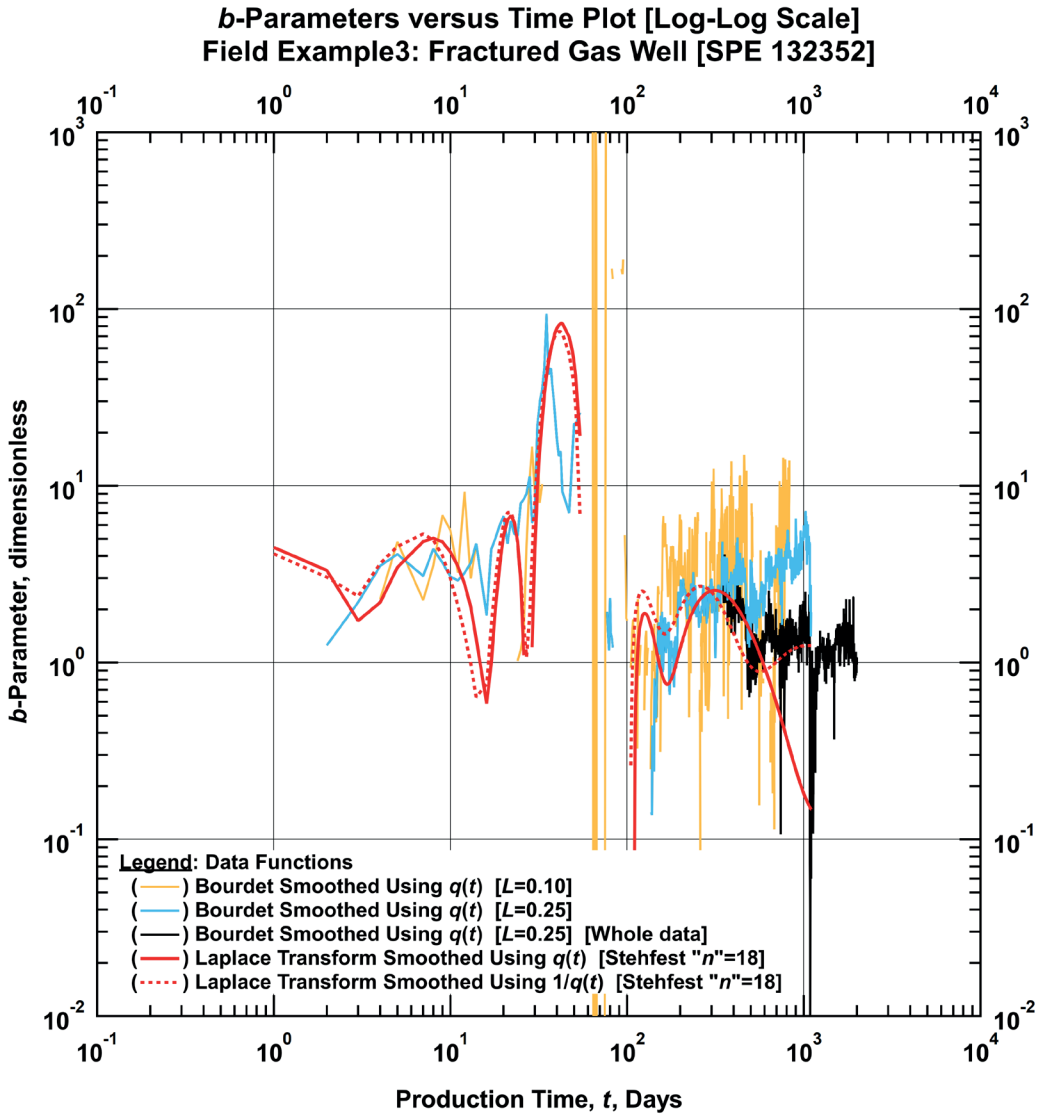

Figure E-3.7 — Comparison Plot of Bourdet Derived and Laplace Transform Smoothed *b*-Parameters Using a Selected Stehfest "*n*" Value Versus Time [Field Example 3: Fractured Gas Well (SPE 132352)] [Log-Log Plot]

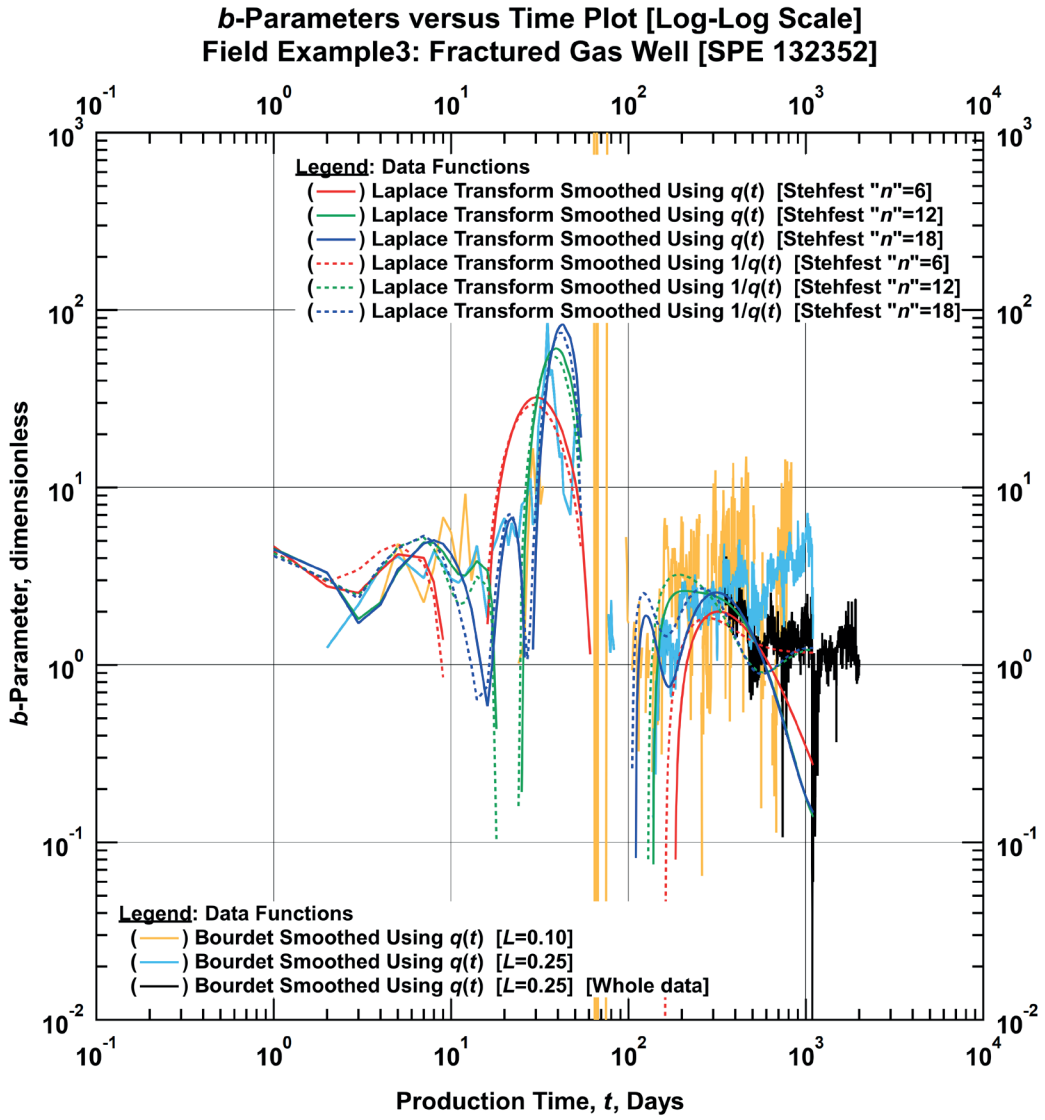

Figure E-3.8 — Comparison Plot of Bourdet Derived and Laplace Transform Smoothed *b*-Parameters Using Various Stehfest "*n*" Values Versus Time [Field Example 3: Fractured Gas Well (SPE 132352)] [Log-Log Plot]

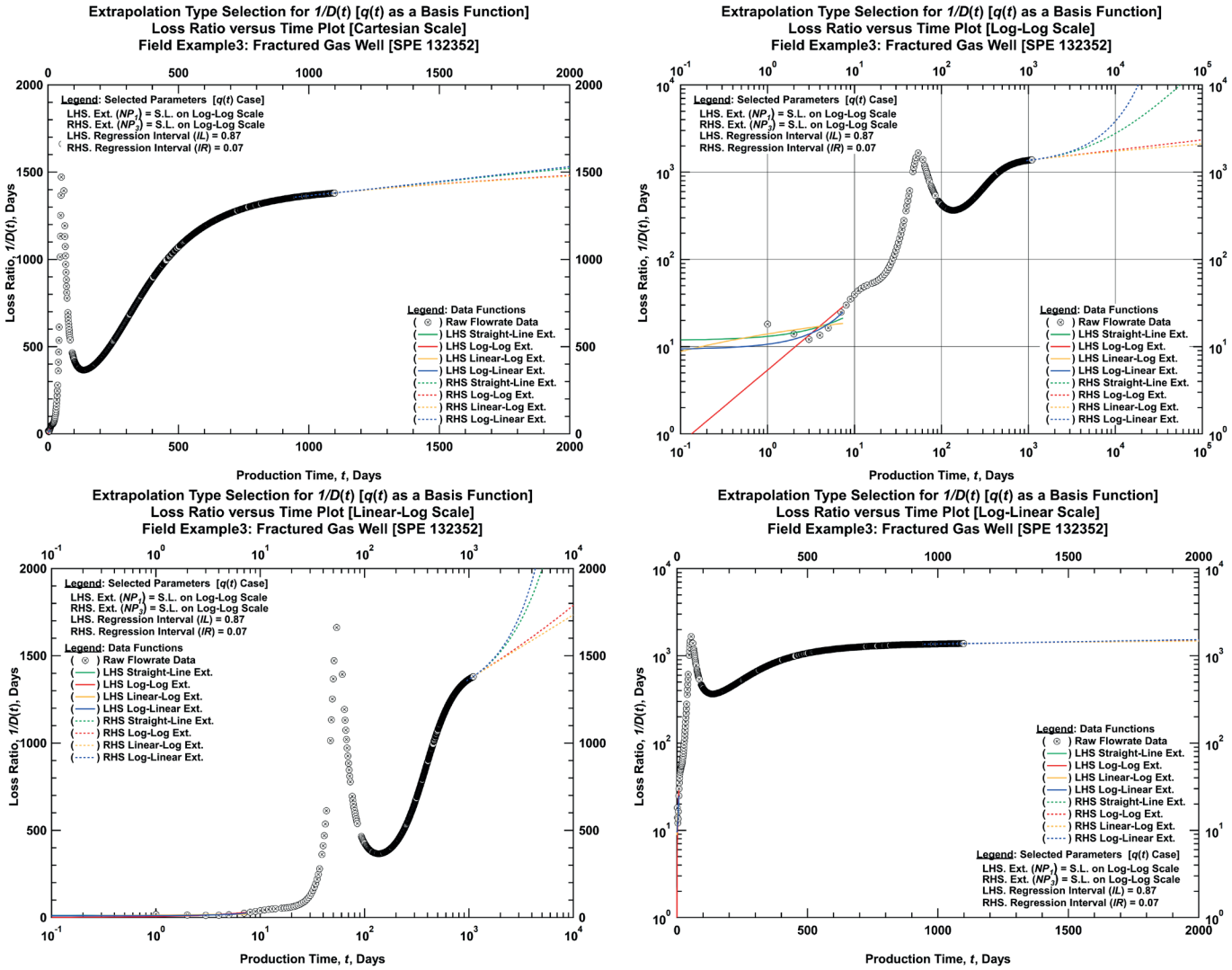

Figure E-3.9 — Plots for Extrapolation Type Selection of Loss-Ratio Data Function Computed Using Flowrate Data as the Basis Function [Field Example 3: Fractured Gas Well (SPE 132352)]

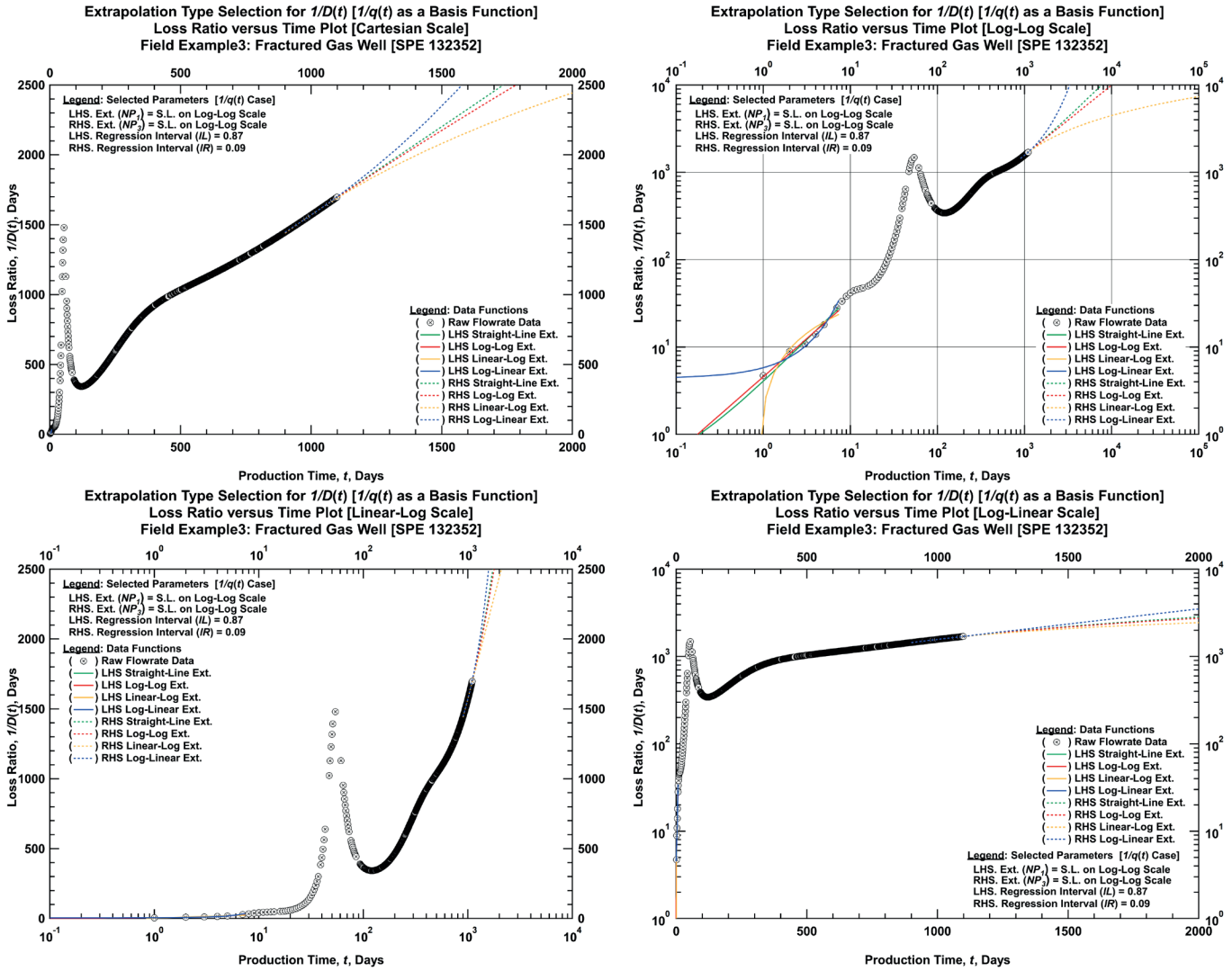

Figure E-3.10 — Plots for Extrapolation Type Selection of Loss-Ratio Data Function Computed Using the Reciprocal of Flowrate Data as the Basis Function [Field Example 3: Fractured Gas Well (SPE 132352)]

E.4 Field Example 4: Fractured Gas Well (SPE 132352)

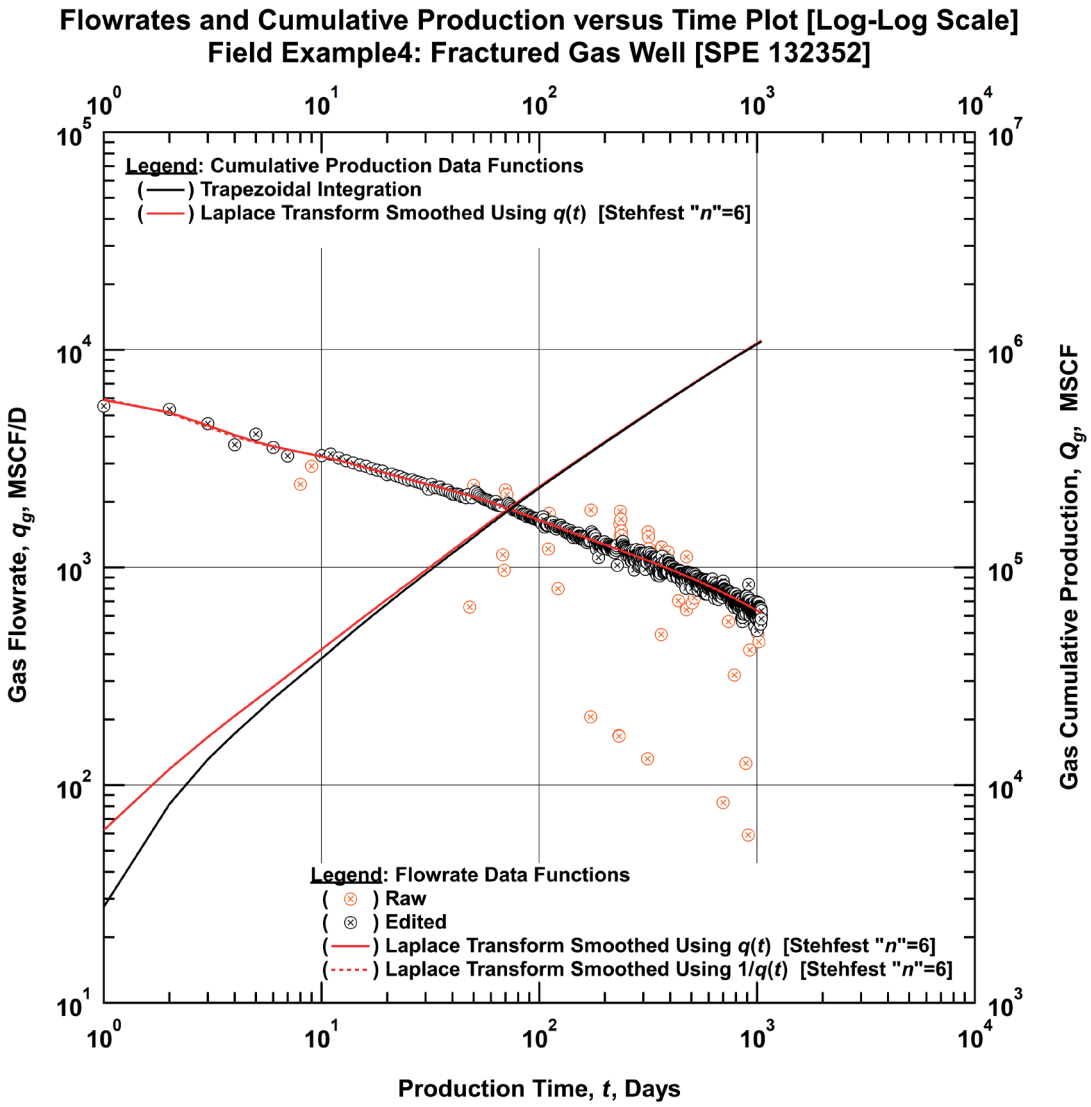

Figure E-4.1 — Comparison Plot of Raw and Laplace Transform Smoothed Flowrates and Cumulative Production Using a Selected Stehfest "*n*" Value Versus Time [Field Example 4: Fractured Gas Well (SPE 132352)] [Log-Log Plot]

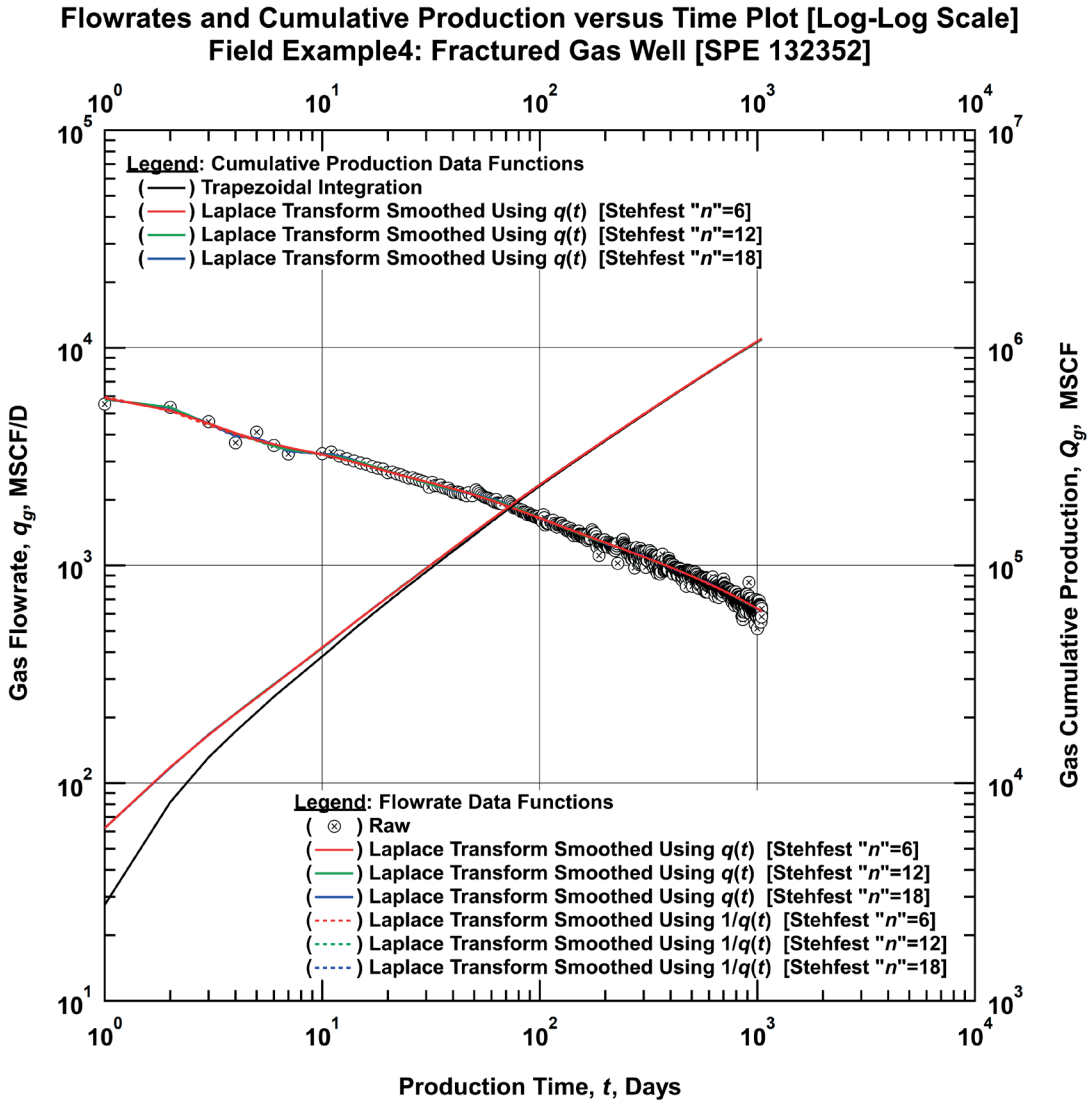

Figure E-4.2 — Comparison Plot of Raw and Laplace Transform Smoothed Flowrates and Cumulative Production Using Various Stehfest "*n*" Values Versus Time [Field Example 4: Fractured Gas Well (SPE 132352)] [Log-Log Plot]

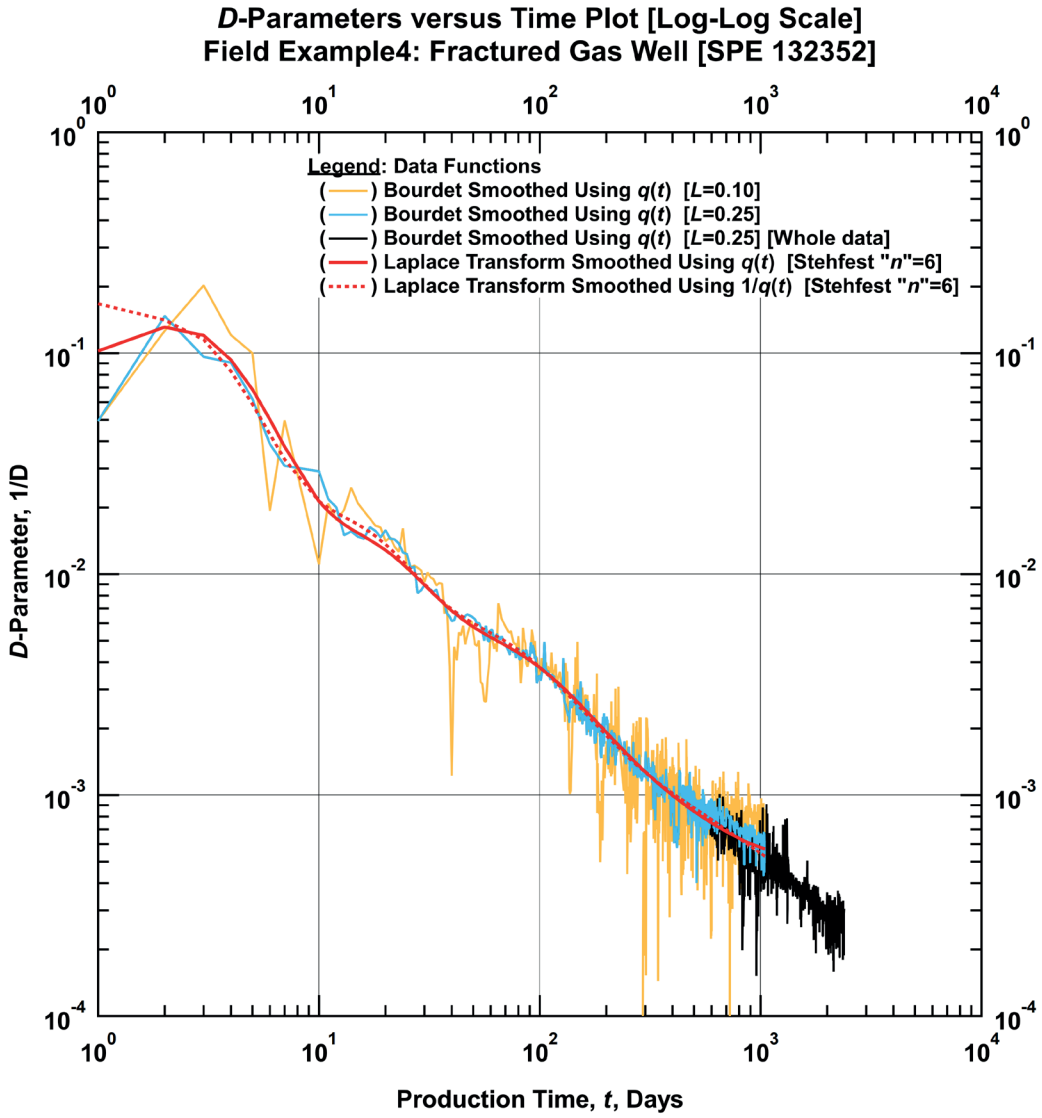

Figure E-4.3 — Comparison Plot of Bourdet Derived and Laplace Transform Smoothed *D*-Parameters Using a Selected Stehfest "*n*" Value Versus Time [Field Example 4: Fractured Gas Well (SPE 132352)] [Log-Log Plot]

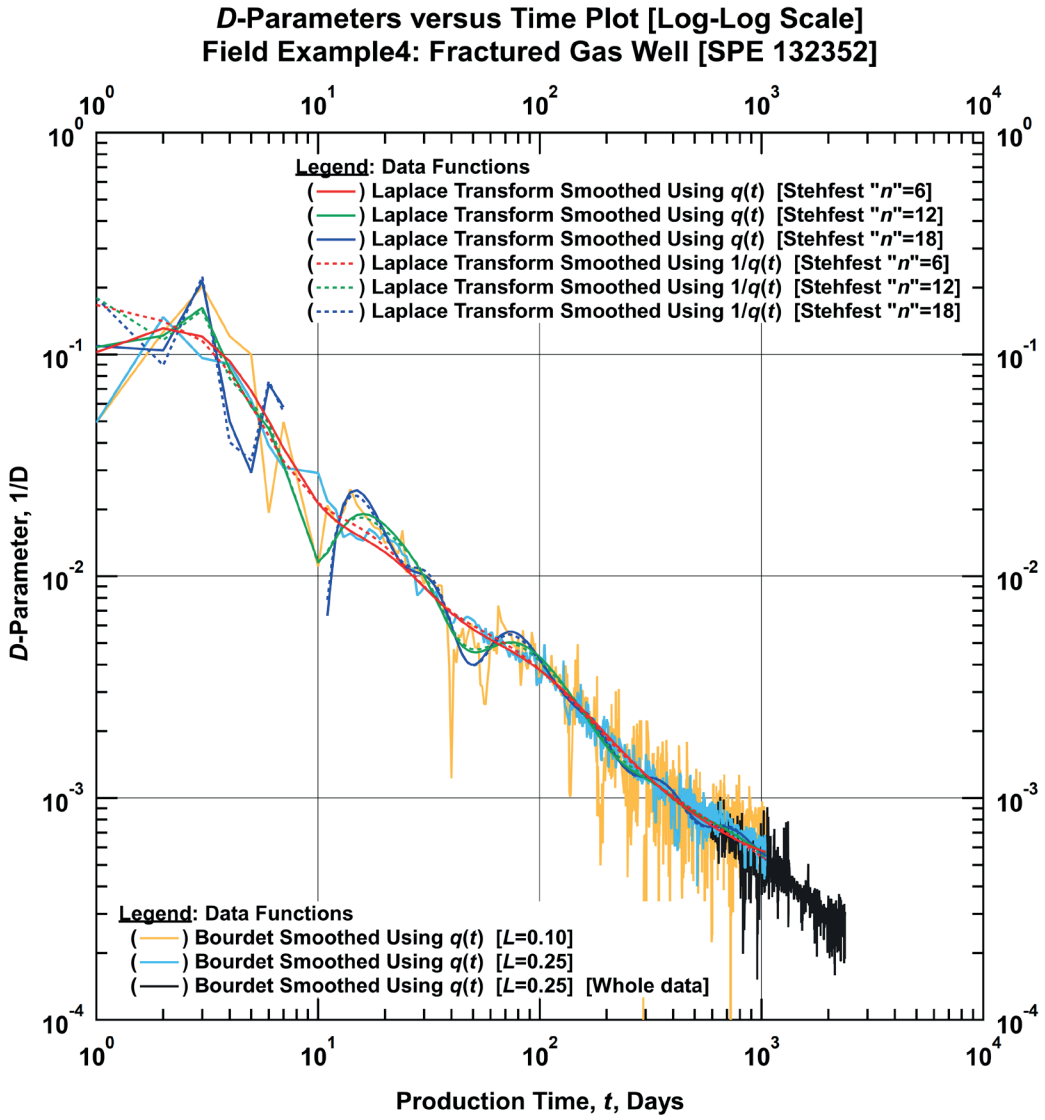

Figure E-4.4 — Comparison Plot of Bourdet Derived and Laplace Transform Smoothed *D*-Parameters Using Various Stehfest "*n*" Values Versus Time [Field Example 4: Fractured Gas Well (SPE 132352)] [Log-Log Plot]

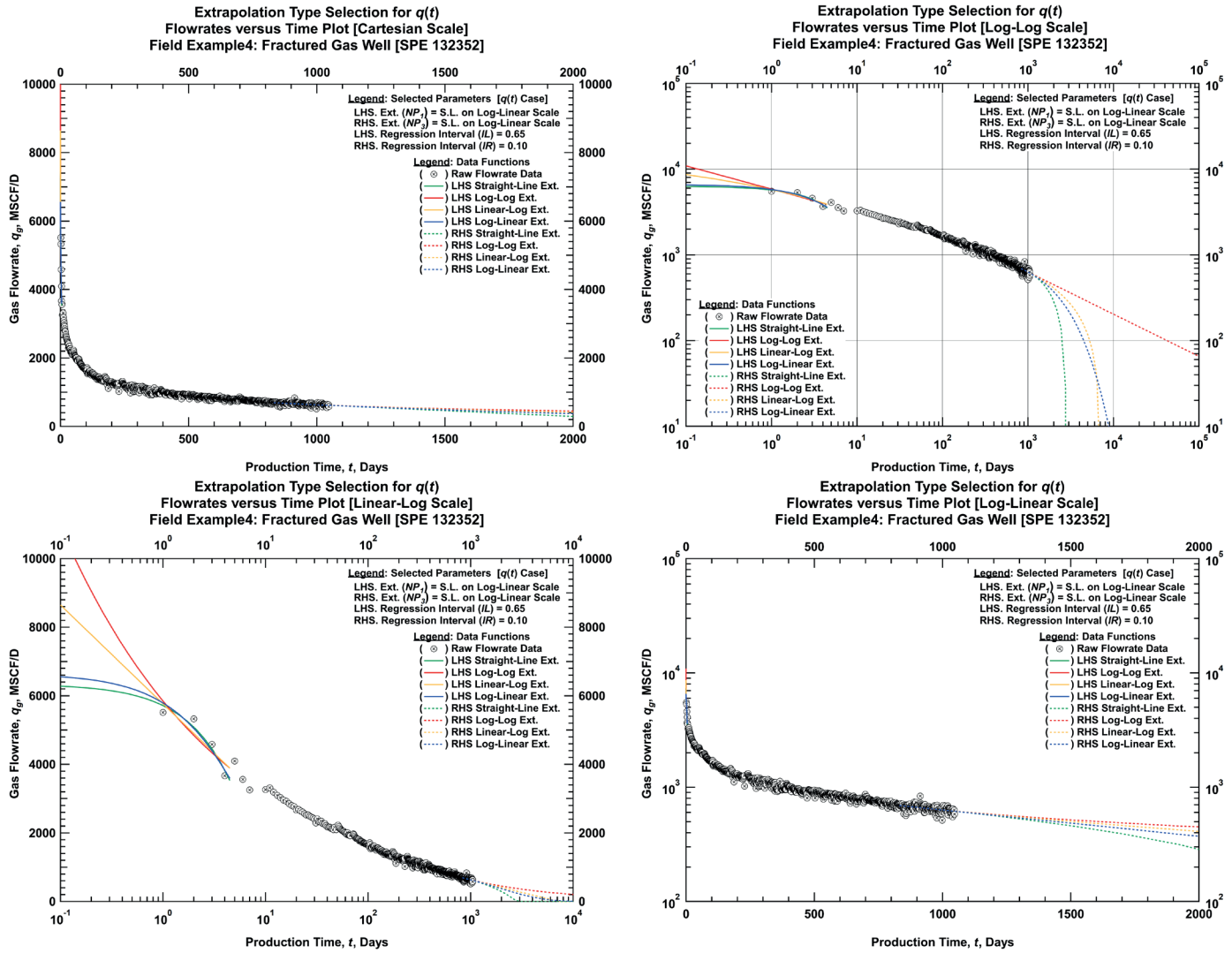

Figure E-4.5 — Plots for Extrapolation Type Selection of Flowrate Data [Field Example 4: Fractured Gas Well (SPE 132352)]

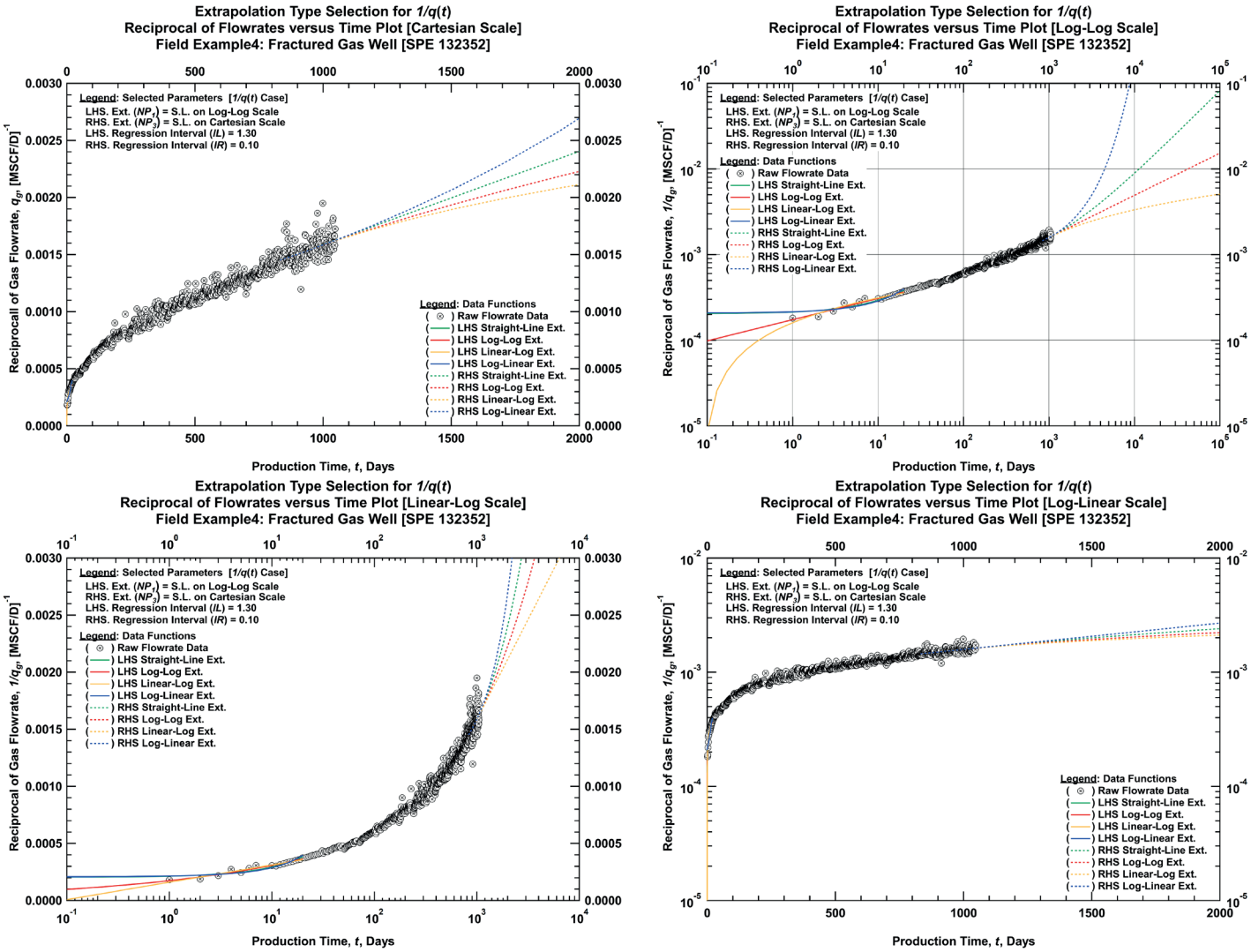

Figure E-4.6 — Plots for Extrapolation Type Selection of the Reciprocal of Flowrate Data [Field Example 4: Fractured Gas Well (SPE 132352)]

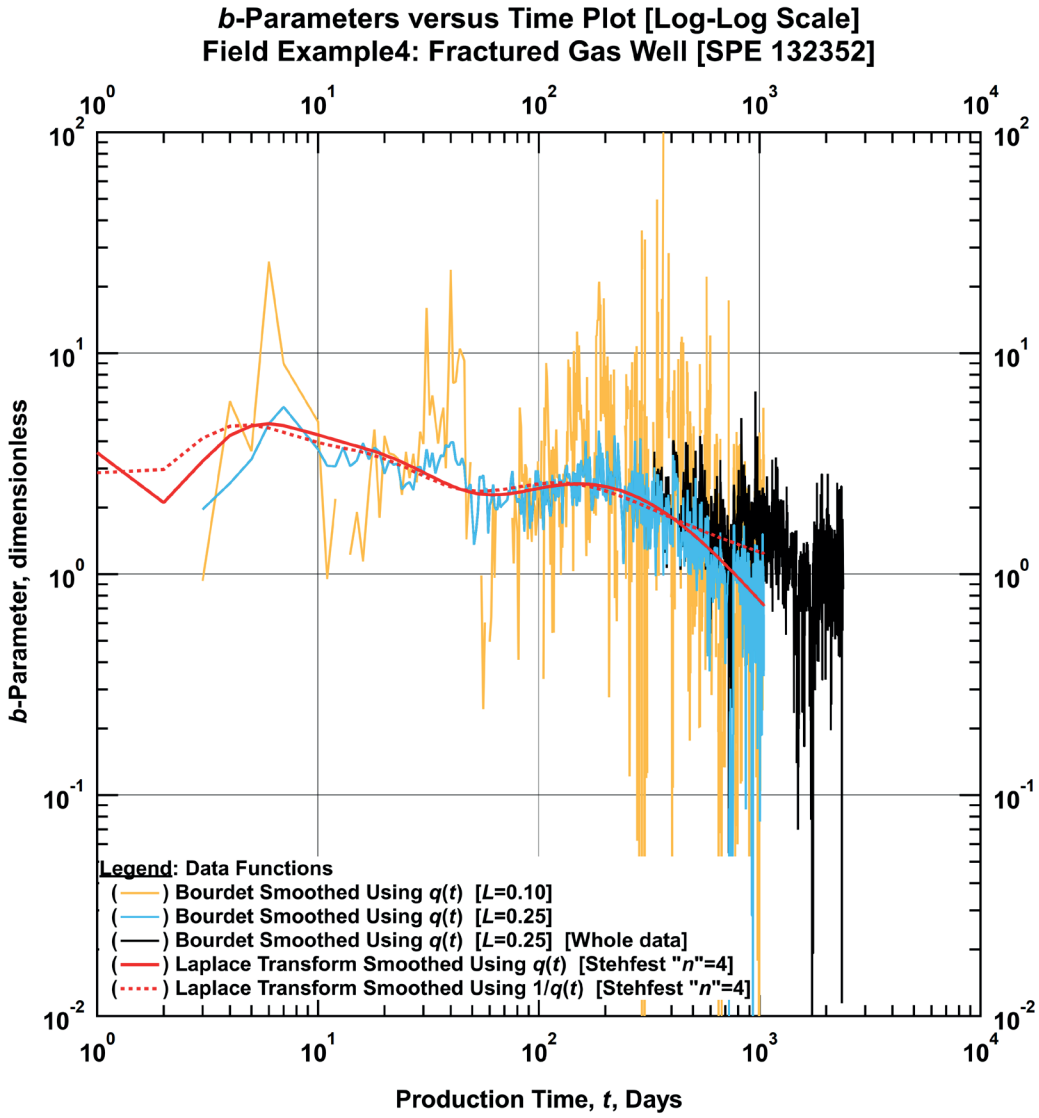

Figure E-4.7 — Comparison Plot of Bourdet Derived and Laplace Transform Smoothed *b*-Parameters Using a Selected Stehfest "*n*" Value Versus Time [Field Example 4: Fractured Gas Well (SPE 132352)] [Log-Log Plot]

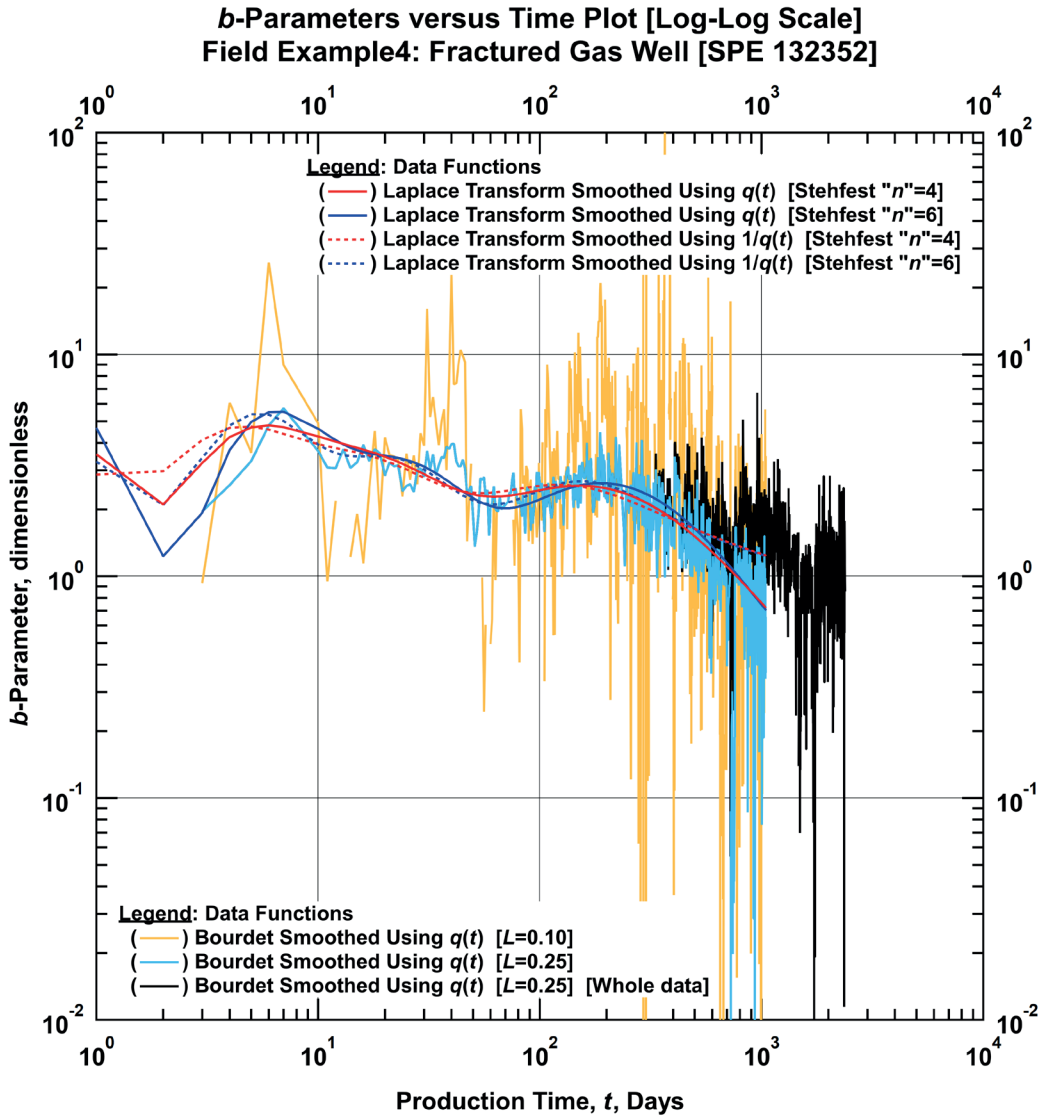

Figure E-4.8 — Comparison Plot of Bourdet Derived and Laplace Transform Smoothed *b*-Parameters Using Various Stehfest "*n*" Values Versus Time [Field Example 4: Fractured Gas Well (SPE 132352)] [Log-Log Plot]

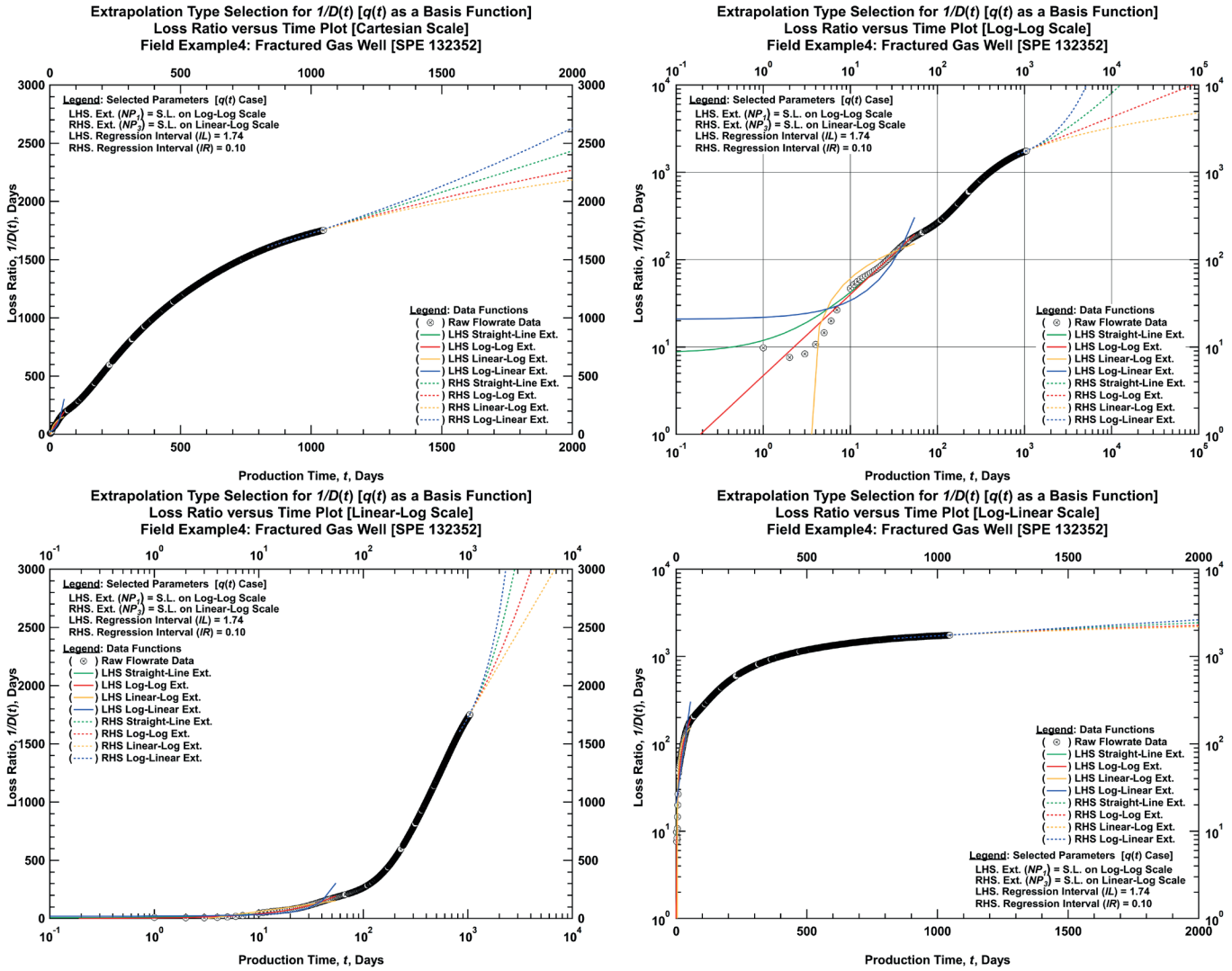

Figure E-4.9 — Plots for Extrapolation Type Selection of Loss-Ratio Data Function Computed Using Flowrate Data as the Basis Function [Field Example 4: Fractured Gas Well (SPE 132352)]

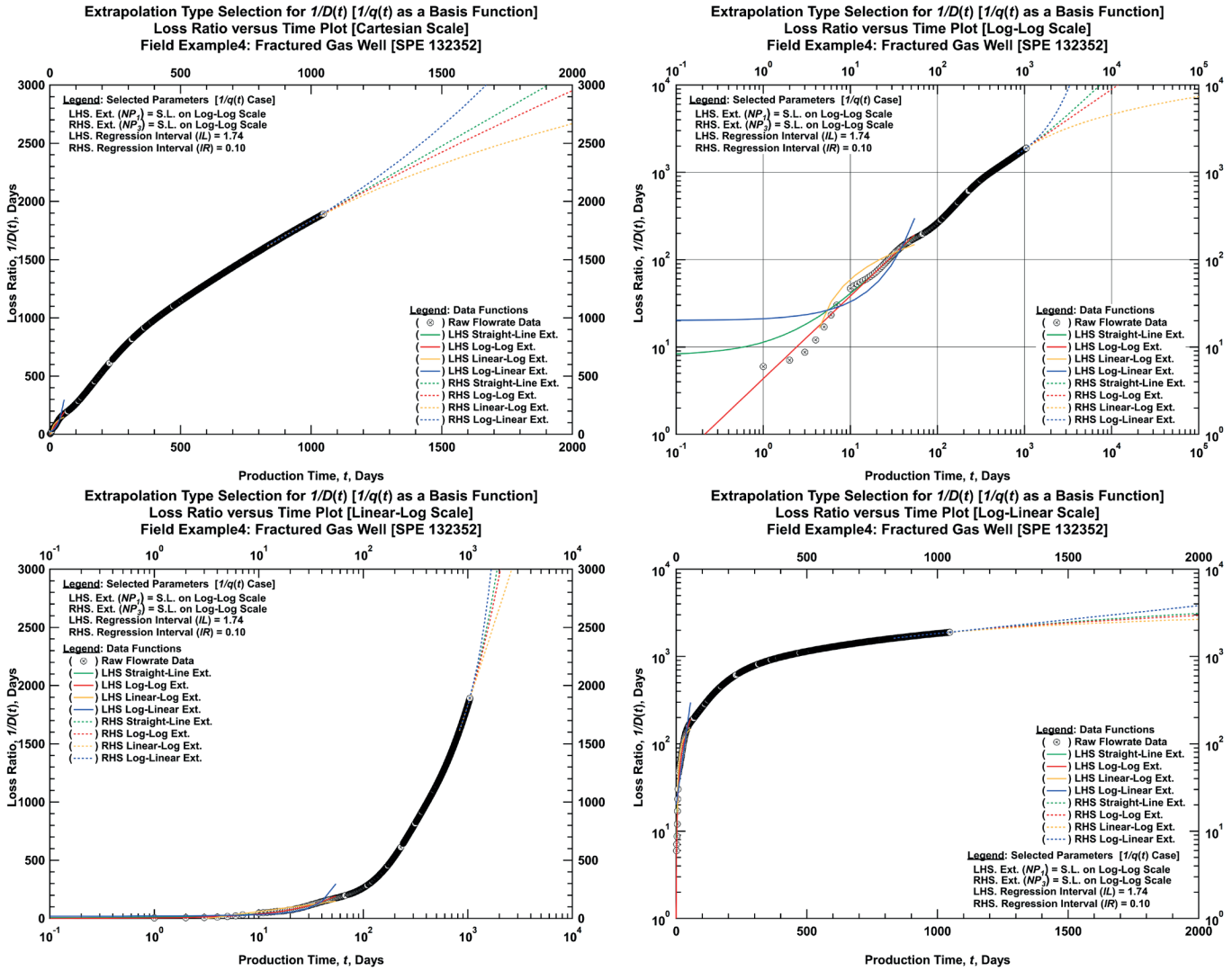

Figure E-4.10 — Plots for Extrapolation Type Selection of Loss-Ratio Data Function Computed Using the Reciprocal of Flowrate Data as the Basis Function [Field Example 4: Fractured Gas Well (SPE 132352)]